A WAVELET PACKET TRANSFORM-BASED TECHNIQUE FOR THREE PHASE POWER TRANSFORMER PROTECTION

SALEH A.M. SALEH

A Wavelet Packet Transform-Based Technique for Three Phase Power Transformer Protection

By

© Saleh A. M. Saleh, B.Eng.

A thesis submitted to the School of Graduate
Studies in partial fulfillment of the
Requirements for the degree of
Master of Engineering

Faculty of Engineering and Applied Science

Memorial University of Newfoundland

July 2003

St.John's Newfoundland Canada

To

My Parents

Brothers and Sisters

and all my Friends

Abstract

The protection of power transformers has been always a challenge due to the problem of distinguishing between the magnetizing inrush and different internal fault currents. There have been many proposed techniques to carry out the protection of power transformers. These techniques are based on the harmonic content of the differential current, transformer equivalent circuit, voltage and flux restraint, pattern recognition using trained artificial neural network, etc. These techniques have either limitation or some assumptions to validate their performance that may affect their reliability, speed of operation, complexity of the required computations, validity under transformer parameters changes and/or change in type of core material. In this work, a wavelet packet transform based algorithm for differential protection of three phase power transformers is developed, implemented and tested on-line for two different three phase power transformers using DS1102 digital signal processing board. The wavelet packet transform based algorithm is used to detect and classify various disturbances, in particular, the magnetizing inrush and internal fault currents with neither a harmonic analysis nor any dependency on the power transformer parameters, ratings, loading conditions and/or winding configurations. Wavelet transforms can create a multi resolution analysis, where the frequency contents of the analyzed signal are divided into octal bands beginning from the highest frequency component, ending with the lowest one and preserving the time location of these frequency components. This analysis is carried out using a cascaded filter banks associated with the selected mother wavelet and the number of levels of resolution. Both optimal mother wavelet and number of levels of resolution can be selected using the minimum description length criteria, that is based on the minimum entropy calculations. Applying any form of wavelet transforms produces details, which are related to high frequency compo-

nents, as well as approximations, which are related to low frequency components at each level of resolution. In the case of applying the wavelet packet transform, the details are downsampled by 2 and filtered with the same filter bank at each level of resolution. An experimental setup is developed for collecting various differential currents waveforms for purposes of selecting the optimal mother wavelet and the number of levels of resolutions as well as off-line testings. The Daubechies ($db4$) mother wavelet with two levels of resolution are found to be optimal in providing adequate information to discriminate the magnetizing inrush current from internal fault currents. The proposed algorithm is tested off-line using Matlab on a data collected from a three-phase core type power transformer. An experimental setup is developed to accommodate the on-line testings, which are carried out on two different power transformers. The results of these tests show no difference in its ability to distinguish between the different magnetizing inrush and various internal fault currents. Also, the on-line testing results are consistent with those obtained from off-line testings in terms of reliability, accuracy, speed of response and applicability.

Acknowledgments

I would like to express my gratitude and thanks to my supervisor Dr. M. A. Rahman who suggested this as my research topic, provided me with complete freedom to try ideas and be essentially self-directed. Also, for the financial support he provided me during my masters degree study. I also wish to thank the Faculty of Engineering and Applied Science and Memorial University of Newfoundland, for providing much needed laboratory space, equipment, and technical services to take this project from idea to implementation.

Special thanks and appreciations are expressed to my brother Omar and sister Lubna for their great encouragement and support. I would like to thank my colleagues Shu, Casey, Jai, Max, my roomates Pouria and Mahmood, and my best friend Iyad for their support, help and useful suggestions.

Financial support from the National Sciences and Engineering Research Council of Canada (NSERC) is greatly appreciated.

Contents

List of Figures

List of Tables

Chapter 1

Introduction

1.1 General

Power transformers play a very important role in modern power systems, which is basically connecting different zones operated on different voltage levels. The continuous growth in demand for electric energy has resulted in larger power systems spreading over wide geographical areas with higher capacity of power generation and distribution. Such a trend of operating these systems has increased the concerns about both the stability and reliability. To improve the stability and reliability, more attention is paid to the protection systems and the functionality of protection apparatus. Although, ideal protection systems will never eliminate the faults, abnormal conditions or any other undesired modes of operation, which may affect both the stability and reliability from taking place, well-designed, coordinated and effective protection systems may reduce the impact of any fault or other catastrophic conditions on the whole power system. One of the key components of any protection apparatus is the protective relay, which has a main task of taking a prompt action against any undesired condition that may affect the operation of the power system or parts of the power system by isolating only the

directly affected parts, while maintaining as much unaffected parts or elements in service as possible. The actual isolation of the affected parts or elements is carried out by circuit breakers that are commanded by protective relays. Efficient and well-designed protective relays should meet the basic design criteria, which are: simplicity, speed, selectivity, economics and reliability [1]. Simplicity in designing a relay makes the implementation, installation, replacement and maintenance more easy. In addition, simplicity in design makes the desired relay more practical and acceptable to be manufactured. Speed of response when the relay is required to act is of great importance, so that the damage of the affected parts or elements can be minimized and system stability can be ensured. It is worth mentioning that the speed of a relay is measured in terms of cycles or mili-seconds (ms). The Westinghouse Company. classifies any relay capable of operating in less than three cycles based on 60 Hz systems (50 ms), as a high speed relay [1]. Selectivity guarantees the switching of the minimum number of isolated parts or elements in case of a relay operation. Economics, as in any case of design yields the maximum desired function with optimum cost. In the case of a relay, it is desired to achieve an effective protection with a minimum cost. Reliability consists of two factors namely dependability and security. The dependability concerns about the correct action when the relay is required to function, while security ensures the capability of the relay to avoid mal-function under any normal or predicted abnormal conditions. Both factors of reliability are critically important, since mal-function of a relay under disturbing conditions may aggravate the impact of the disturbance on the whole operation of the power system. Unfortunately, dependability and security appear to counter each other, thus for practical designs, some compromises between the two factors are needed.

Protective relaying techniques applied in power systems can be categorized as:

1. Electromechanical Relays

2. Solid-State or Static Relays

3. Programmable Relays

4. Computer-Based Relays

The electromechanical relays were developed as the first protection apparatus in early 1900s and still in service for different protection purposes in various types of power utilities. Electromechanical relays have four major types, which are:i) magnetic attraction, ii) magnetic induction, iii) D'Arsonval and iv) thermal. The development of solid-state semiconductor switches in late 1950s, had made it possible to apply these switches in protection apparatus. Solid-state relays have inherent advantages over traditional electromechanical relays, such as higher speed of operation, more reliability, easier installation and replacement, smaller size, more sensitivity, less burden to current transformers, less maintenance, etc.. Due to these advantages, many electromechanical-based protection apparatus have been replaced by solid-state-based protection apparatus. Microprocessor-based relays are the latest development of protective relays that began to appear in 1980s, as a result of the rapid development in digital technology. The basic operation of a microprocessor-based relay includes sampling of an analog input, digitizing the input samples and storing the digitized data for further processing using a certain algorithm. The latest types are computer-based multi-function relays. This type of protective relays has many advantages over the other conventional relays. Some of these advantages are:

- Improved Relay Performance: Changing the operating characteristics of a relay will make it possible to improve speed, sensitivity and selectivity. This feature of programmable and computer-based relays is due to the ease in modifying the algorithm to meet various complex operating conditions.

- Reliability: The self-checking feature in this type of relays improves both the dependability and security. Moreover, the practical compromises between the two factors can be adjusted more effectively.

- Size: Due to the rapid advancement in integrated circuits technology and the ability of manufacturing sophisticated generations of microprocessors, it is possible to realize compact protective relays.

- Flexibility: This is one of the most attractive features of microprocessor-based protective relays. Since the relaying functions are implemented through software, any necessary modifications can be easily done in the software itself. In addition, some of the needed functions by protective schemes can be realized through software rather than hardware; filtering, comparisons, and sampling are very simple examples of such functions [1, 2].

Three phase power transformer protection is of critical importance to ensure stable and reliable power transfer to various bulk loads. The protection of this particular key element of power system has been always a challenging problem for protection engineers. The major problem in this context is the magnetizing inrush current, which flows through the power transformer when switched on, and in many cases is indistinguishable from internal fault current resulting in a mal-operation of the protective relays [1]. Differential protection scheme is quite popular in transformer protection, as it is used to identify the internal fault currents of three phase power transformers, where the current rises up to about 10 times the normal operating current [3]. Fault current can be used to trigger the protective relays to avoid more damage in power system due to the flow of high currents under fault conditions.

There are many operating protective relays applied for power transformer protection purposes. In this area, research continues with an objective of imple-

menting more accurate, reliable, sensitive and economic protective relay for power transformer protection purposes. The following section gives an overview of the operating techniques applied in power transformer protection.

1.2 Literature Review of Differential Relaying in Power Transformer Protection

The design of a protective relay to be applied for power transformer protection must consider the magnetizing inrush current. It is very important to have an insight into this phenomenon in power transformers. Therefore, modeling and simulation of the magnetizing inrush current is an essential step for designing programmable and computer-based differential protective relays. Many research works have been conducted with different approaches and methods to model inrush current. Specht [4] has developed formula and curves to determine the magnetizing inrush current for single phase power transformers.

Blume, *et al.* [5] used an experimental approach mainly depending on the physical dimension and the flux densities in a power transformer to model the magnetizing inrush current. They were able to develop an analytical tool to determine the average magnetizing inrush current. Finzi and Mutschler [6] have developed an iterative technique to solve a time integral equation for the magnetizing inrush current, but still the accuracy of the solution is not high and some approximations are used.

Sonnemann, *et al.* [7] tried to generalize the analysis of the magnetizing inrush current in single-phase power transformers to include the mutual inductances between phases in three-phase power transformers. In 1980s, with the availability of digital technology, researchers began to employ the digital techniques to determine and model the magnetizing inrush current.

Rahman, *et al.* [3] used the relationships provided by Specht to generate magnetizing inrush data with some practical assumptions to use this generated data for testing algorithms of differential protection. Rahman and Gangopadhey [3] were the first to generalize the simulation and modeling of magnetizing inrush current for three-phase power transformers with the sequence impedance and mutual inductances taken into account. The obtained current waveforms were close to the current waveforms obtained experimentally.

The magnetizing inrush current represents one pattern of electromagnetic transients any transformer may experience. The design of an effective differential protective relay for power transformers, has to consider more electromagnetic transients at both high and low frequencies due to magnetic inrushes, lightning and subharmonics generated by the power electronic components used to control the power flow in other parts of the power system. The aforementioned conditions are just examples of such transient currents that may flow through power transformers. The response of power transformer to such transient currents can be simulated if an accurate model is developed. There are many considerations when modeling the magnetizing inrush current or modeling the transformer itself. Such models include nonlinearity of the flux with current, skin and proximity effects, the effects of high frequency electromagnetic transients, leakage and mutual inductances and capacitances as well as hysteresis and eddy current effects [2]. There are many transformer models based on both the time and frequency domains. The recent works included models based on duality principle, models based on field measurements, models based on frequency response and models based on combining two or more of these models [8]. Leon and Semylen [9–11] have developed a model for three-phase power transformer based on turn-to-turn inductances and capacitances, and modeled the iron core as a nonlinear inductance. The solution of the state equations was obtained iteratively considering the resistance as a constant

in the final reduction of the model. The model is not accurate to simulate the response of the three-phase power transformer in case of low frequency signals, while for high frequency electromagnetic transients, this model is invalid. Vaessen and Hanique [8] presented a model of transformer based on frequency response, which considers an active coupling between the iron core and transformer windings. However, this model assumes linearity over a wide range of frequencies and assumes the active coupling is dependent on the primary current. Saleh and Rahman [12] have developed a model for power transformer based on employing a wavelet filter bank with its analysis and synthesis sides. This model presents the primary windings as a two stage analysis side and the secondary windings as a two stage synthesis side of a wavelet filter bank, while the iron core is modeled as an additional weighted stage of the analysis side. The model accurately simulated different cases of inrush and normal current and high frequency electromagnetic transients , and the simulation results were very close to the experimental results.

The frequency analysis of various transformer currents has shown that second harmonic has a significant amount in the magnetizing inrush current. This feature has led to the development of a differential relay that uses the second harmonic to restraint the relay action during transformer energizing. In addition, the ratio of the second harmonic to the fundamental harmonic has been used to distinguish the magnetizing inrush current from different internal fault currents in power transformers. However, in some cases the inrush current is so sever that it is not distinguished from the internal fault currents using the second harmonic ratio technique. In spite of various limitations of the second harmonic ratio technique, it is still the most commonly used technique for power transformer differential protection [1]. Many operating differential relays are replacing their conventional electromechanical or solid-state relays with digital relays due to their advantages over the other conventional types of relays.

1.2.1 Conventional electromechanical and solid-state differential relays

The basic structure of a differential relay for power transformer protection is known as the unbiased differential relay [1]. This protective relay is very sensitive to any unbalance of the current transformer (CT) and/or CT saturation, and sometimes to the sever unbalanced loads connected to the power transformer. The unbiased relay can not be prevented from initiating a false trip under the above mentioned unbalanced currents conditions. To improve the reliability of the unbiased relay, two restraining coils are used with one operating coil. This structure is known as percentage differential relay. Both the unbiased and percentage differential relays have the same principle of operation, except for the percentage one, the through-currents produce restraint that is proportional to the amount of the flowing and inrush currents, while internal fault currents produce a differential current enough to activate the operating coil. False trip still can be initiated under magnetizing inrush current even with the existence of the restraint coils [1,2]. Many research works were conducted to develop techniques to avoid false trip due to magnetizing inrush currents. Among these techniques, the delay in the relay component technique, which is obtained by a slow-speed induction-disk type relay that has high current and long time settings. Temporary desensitizing the relaying component for a fixed interval of time, is another technique to improve the reliability of the differential relays. The desensitizing is usually controlled by a voltage relay operated through a potential transformer (PT) [1]. Prior to the introduction of high speed coordinated relays, the induction-disk relays with a suitable time delay to outlast the magnetizing inrush current were sufficient. As the capacity of power systems grows and the number of generating units increase, it has become mandatory to use high speed relays due to stability considerations. These conditions are a result of high exciting currents that flow through power transformers during

switching. Normal unbiased or percentage differential relays can not guarantee the proper response in such critical protection schemes. One of the major developments in differential protection is the application of the harmonic restraint in differential relays [1]. The magnetizing inrush current contains significant amount of both the second and fifth harmonics. The harmonic restraint relay was introduced in 1938 [1]. The simple structure of this type of differential relays contains two filters, one of them is to extract the fundamental component of the current flowing in the operating coil, and the other one is to extract the second harmonic in the current. The extracted second harmonic is used to restrain the relay in case of inrush current [1, 3]. The early implementations of this differential relay used analog elements and L-C tuned circuits. This type of relays is detailed in [1].

Kennedy and Hayward [13] conducted more spectra analysis on both the magnetizing inrush and internal fault currents in order to improve the performance of the harmonic restraint differential relay used in power transformer protection. They suggested to use more harmonics to restrain the relay during energizing the power transformer. This modification was aimed to decrease the effect of saturation in power transformer and/or the current transformers on the operation of the relay. The employment of the second harmonic only to restrain the relay could be efficient in the case of typical magnetizing inrush currents, but still saturation under heavy fault currents might affect the reliability of this modified differential relay. On the other hand, the employment of the third harmonic to improve the reliability against the saturation of the transformers might not be able to distinguish between the internal fault and the magnetizing inrush currents. This condition could arise out of heavy internal fault, where the harmonics extracted could be enough to restrain the relay from functioning. In [13], authors suggested settings for a designed differential relay with this multi-harmonic restraints technique. The Westinghouse HDD type relay with harmonic restraint [1] has been

widely applied for power transformer protection and considered a high speed sensitive differential relay. This relay was operated mainly from current transformers and does not need any auxiliary desensitizing units or potential transformers. The Westinghouse HDD type is basically a percentage differential relay with harmonic restraint obtained using two filters. To avoid the critical failure of the HDD relay under sever internal faults, an over-current unit without any restraint was used for this task. This over-current unit has a time setting longer than that corresponds to the maximum inrush current. Westinghouse has developed a new version of HDD type relay known as BDD [14]. The BDD type relay is smaller in size and less dependent on the current transformer (CT) characteristics. Sharp and Glassburn [15] developed a high-speed harmonic restraint differential relay for multi-windings power transformers, which was capable of distinguishing between the magnetizing inrush and internal fault currents. This relay was composed of differential and harmonic restraint units with ratio-matching taps added on each unit to compensate for the main current-transformer ratio mismatches. This differential relay responded properly to the cases of inrush and internal faults. Moreover, it was capable of proper response during under-frequency conditions [15]. Einval and Linders [16] presented a three-phase differential relay with harmonic restraint for multiple windings power transformers. This relay simplified the frequency tuned circuits with an improved procedure to determine the harmonic contents in the applied differential current. Also, this relay was considered a high-speed relay, since it could respond to internal faults in less than two cycles and with sever internal faults, it was able to respond in less than one cycle.

1.2.2 Computer-based differential relays

The first detailed digital relay was presented in early 1970s, which was applied for fault protection. This digital relay was introduced by Rockfeller [17],with the

description of its operation and the needed digital computer in the sub-station to carry out the relaying function. Mann and Morrison [18, 19] presented a transmission line computer-based protection scheme, which was implemented as a joint project between Pacific Gas and Electric Co. and Westinghouse Electric Co. In early 1980s, computer-based relays began to replace the conventional electromechanical and solid-state based relays and due to the fast developments in digital technology. Most of the operating computer-based relays employ algorithms to carry out the harmonic analysis of differential current using digital signal processing techniques. Among these algorithms Walash Functions, Discrete Fourier Transform (DFT), Least-Square Method, Harr Functions, Kalman filtering, etc. [20]. All the previous mentioned algorithms were used to realize one objective, which is a fast and accurate extraction of the first, second and sometimes the fifth harmonics in the samples of the differential current.

Sykes and Morrison [21] used two recursive filters to extract the fundamental and the second harmonic components in the differential current samples. The discrimination between different internal faults and magnetizing inrush currents was based on the output of these two filters, and as a result the trip signal was initiated. This relay was tested off-line on a simulated data for both the magnetizing inrush and fault currents. It was implemented using IBM 350/60 computer, and the code was written in FORTRAN IV, which was applicable to single-phase power transformers. The main advantage of this relay was the simplicity, while the major drawbacks are the long time for response and undetermined applicability in three-phase power transformers.

Malik, *et al.* [22] developed an algorithm called the cross-correlation algorithm, which is very similar to Discrete Fourier Transform (DFT). This algorithm included evaluation of the odd and even functions of any harmonic components existed in the differential current. To decrease the response time of this relay, the

sine and cosine basis functions were replaced by odd and even square-pulse basis functions. This decreased the calculation time but decreased the accuracy of the whole algorithm as well. Once both the fundamental component and the second harmonic were calculated, the ratio of the second harmonic to the fundamental was compared to a threshold value. If the ratio exceeded the threshold, a magnetizing inrush was declared, otherwise a trip signal indicating an internal fault is initiated. This algorithm was tested off-line on a simulated data for magnetizing inrush and internal fault currents, but it was not tested on a real power transformer. For the off-line testing, the response time was within 1/2 to 3/4 cycle based on 60 Hz systems.

Sheweitzer, *et al.* [23] simplified the arithmetic operations (mainly the multiplication and division) needed to realize the filtering functions and used finite impulse response (FIR) filters. These FIR with coefficients +1 or -1 during one cycle time period, were used to evaluate at least four Fourier odd and even coefficients for both the fundamental component and the second harmonic present in the samples of the differential current. This algorithm was tested off-line with a FORTRAN IV language code on simulated magnetizing inrush and fault currents. The algorithm sampled the differential current at a sampling rate of 8 samples per cycle with a response time of about one cycle based on 60 Hz system. The FIR algorithm was implemented by Larson, *et al.* [24] to protect a 500 VA power transformer using a Motorola MC 6800 microprocessor. The fault was detected in about 1.25 to 1.5 cycles based on 60 Hz system.

Ramamoorty [25] introduced the Fourier Transform approach to extract different harmonic components in either the current or the voltage from fault data. Throp and Phadke [26] introduced the application of Discrete Fourier Transform (DFT) for power transformer protection. This algorithm was tested on transformer model and generated data with sampling rate of 12 samples per cycle. The

response of this algorithm for faults was found to be about one cycle. Rahman and Dash [27] used the rectangular transform, which was based on calculating Fourier odd and even coefficients. The algorithm has a significant accuracy. Also, since the calculations included only addition and subtraction, this algorithm was fast. It was tested off-line using PDP-11/60 computer on a simulated transformer data. Moreover, it was implemented for on-line testing using Intel 8085 microprocessor on a three-phase, 400 V, 60 Hz laboratory transformer with a sampling rate of 12 samples per cycle.

Horton [28] and Rahman and Jayasurya [29] employed Walsh functions to compute the fundamental component and second harmonic components in the differential current samples. The Walash functions are viewed as a squared up sine and cosine functions that take +1 or -1 only. The sign changes at instant n, if n is a power of 1/2. The calculation of Walsh functions is simple and does not take a long time. Since there exists a relation between Fourier coefficients and Walsh coefficients, Fourier coefficients can be derived from Walsh coefficients [29]. The Walsh functions algorithm was tested off-line on a digitally simulated magnetizing inrush and internal fault currents. Also, it was implemented for on-line testing using Intel 8085 microprocessor with a sampling rate of 12 samples per cycle. The response time was found to be less than one cycle.

Fakruddin, *et al.* [30] employed the Harr Functions to carry out the harmonic extraction, through which the needed sine and cosine components of any harmonic in the differential current can be determined using the Harr-Fourier relationship [30]. This algorithm uses a combined second and fifth harmonic magnitude to compare with the magnitude of the fundamental component, and upon the result, a trip signal is initiated. This algorithm included complicated calculations, and as a result, the response time is longer than the DFT algorithm [2].

Murty and Smolinski [31] developed a digital relaying algorithm using five-

state Kalman filter. This algorithm used the second harmonic component in the differential current to diagnose the magnetizing inrush current. This relay was implemented using TM320 digital signal processor and tested on-line on a three-phase power transformer [31]. This implemented relay responded for the case of internal fault with the first sample of the differential current in about half a cycle, while with 12^{th} or 13^{th} samples, it responded in about one cycle. The Kalman filter algorithm has no provision for higher order harmonics, which may affect the diagnosis of the magnetizing inrush current. Later, Murty and Smolinski [32] extended the Kalman filter from five to seven states to include the fifth harmonic. The extended Kalman filter algorithm used the percentage differential relay and over-excitation characteristics to restrain the relay. The relay responded to the fault occurrence at the first sample of the differential current in about a cycle, and for the fault taking place at the 13^{th} or the 14^{th} sample of the differential current in longer time. Moreover, this relay used a threshold for the second harmonic to fundamental component ratio of 25%, that is considered high for the modern power transformers, where the low-loss amorphous core material is used. On the other hand, lowering the threshold value would increase the needed computations resulting in longer response time. Also, the obtained Kalman filter coefficients depend on the used transformer model [32], which indicates that for each transformer, the coefficients need to be calculated.

Degens [33] used the least square curve-fitting method to determine the ratio of the second harmonic to the fundamental component of the differential current to identify the magnetizing inrush current. This method of power transformer protection is based on the assumption of unknown time constant of the DC component of the magnetizing inrush current, and the existence of only five harmonic components in the magnetizing inrush current. A threshold of 12.5% was used to compare the ratio of the second harmonic to the fundamental component in order

to declare either a magnetizing inrush current or an internal fault. The response time in the case of an internal fault was about two cycles. The least square method was extended further by Degens [34] through implementing a digital filter using a microprocessor to speed up the trip signal. For the case of sever fault, the response time varied between 1/3 to 2/3 of a cycle, whereas in the case of traditional faults or winding faults , response was obtained in about two cycles.

Rahman, *et al.* [35] developed a weighted least-square method for differential protection of power transformer. The development in this method was the use of the root mean square error (RMSE) criterion to select the harmonic order, data window length, weighting matrix and sampling rate. This algorithm needs many cases of magnetizing inrush and internal fault currents to obtain the optimal weighting factor. Also, this algorithm is dependent on the transformer model.

Sachdev and Sidhu [36] also used the least square method in differential protection of power transformers. The hardware and software for this relay are given in details in reference [36]. This algorithm is implemented and tested on-line on a laboratory 15 kVA, 2540/480 V,Δ-Y three-phase power transformer. The response time for most of the internal faults was about one and half cycles, and as the level of faults was lowered, the response time went longer.

Linhua, *et al.* [37] designed three all-zeros filters to extract the fundamental, second harmonic and fifth harmonic components present in the differential current. Also, they introduced two performance indicies in order to make a quantitative comparison between different algorithms. These two indicies were the number of needed computations and the logarithm of the ratio of the undesired frequency components to the desired frequency components. In addition, they employed a voltage restraint depending on the fact that voltage will decrease under fault conditions, so as to replace the harmonic restraint and to avoid a false tripping under magnetizing inrush current conditions. The authors improved the voltage

restraint method and used two measured voltages and the rated voltage of the power transformer. This relay is quite simple and fast. However, its cost is higher and more dependent on the potential transformers. Both the voltage restraint and improved voltage restraint relays were tested off-line, but they were not tested on-line.

Hermanto, *et al.* [38] presented a detail design of a stand-alone prototype differential relay. The protection functions of this relay included percentage differential relay with the second harmonic to restrain the relay during the magnetizing inrush current and the fifth harmonic to restrain during over excitation conditions. This relay was implemented using TMS320E15 digital signal processor with sampling of 16 samples per cycle, and tested on-line on a three-phase 5 k VA, 230/550-575-600 V, Δ-Y laboratory power transformer. The response time of this relay was within one cycle based on 60 Hz system. However, this relay had a limited sensitivity to ground fault, and the used chebychev anti-aliasing filter created a time delay due to complex computations [38].

Habib and Martin [39] presented a comparative analysis of various algorithms for computer-based power transformer protection. The analysis is based on problem of differential protection and detection of excitation-current. Also, they defined two performance indicies based on both time and frequency. The comparative analysis recommended Discrete Fourier Transform (DFT) as the best algorithm for implementing computer-based relays.

Rahman and Jayasurya [40] carried out a comprehensive comparative study, which included six different algorithms for computer-based differential relays. Fourier Analysis, Rectangular Transform, Walsh Functions, Finite Impulse Response, Haar Functions and Least Square curve fitting were covered by this comparative study. Rahman and Jayasurya [40] also recommended DFT as the most efficient algorithm for implementing computer-based power transformer differen-

tial protection.

1.2.3 Modern technology relaying algorithms

The use of harmonic restraint including second or higher harmonics to avoid false tripping signals under magnetizing inrush current or over excitation conditions has been widely used in differential protection of power transformers. However, the new technology applied in other parts of power system such as parallel capacitance for adjusting phase angle, flexible ac transmission systems (FACTS) devices to control the power flow, power electronic converter to improve the power quality, etc., has produced differential currents under internal fault conditions with considerable amount of harmonic components, in particular, the second harmonic. In addition, the employment of new low-loss amorphous core material in modern power transformers may produce magnetizing inrush current with lower amount of second harmonic component [41]. Also, the existing protection schemes are sensitive to CT saturation. These aspects adversely affect the operation of the differential protective relays with harmonic restraint. Therefore, the modern designs of power transformer protection tend to deviate from employing the harmonic restraint technique or the harmonic ratio to identify the type of current flowing through a power transformer. Some of the recently developed algorithms, which did not use the harmonic restraint technique, used phase current, voltages, pattern recognition and/or electromagnetic power transformer models, to avoid mal-operation under non-fault conditions.

Sachdev, *et al.*[42, 43] introduced an algorithm that was based on calculating the primary phase voltage using the measured values of the quantized phase voltage and current samples and some parameters of the power transformer like the primary and secondary leakage inductances and mutual flux. The calculated primary voltage was compared to the measured one and the difference (error) was

obtained. If the error value is located in the fault region of the relay characteristic curve, the value is one, otherwise it is zero.

Gangopadyay [44] carried out extensive analysis of differential protection of power transformer. Also, he modeled the magnetizing inrush current using digital computer, and the simulation data was very close to the actual magnetizing inrush current. In addition, Rahman applied the Walsh Functions to evaluate the second harmonic instead of using the sine and cosine coefficients so as to reduce the needed computations.

Zaman and Rahman [45] presented an artificial neural network (ANN)-based technique that was basically dependent on designing a two layer ANN and train it for many cases of magnetizing inrush, different internal faults and over excitation currents. The algorithm was implemented using DS-1102 digital signal processing board (DSP), where the code was written in C language, compiled using Texas Instrument (TI) compiler and then downloaded to the DSP board. The ANN algorithm was both tested off-line and on-line on a three-phase 5 kVA, 230/550-575-600 V Δ-Y laboratory power transformer. The relay was able to distinguish between the magnetizing inrush and internal fault currents, and in case of internal fault, the trip signal was initiated in almost 1/2 a cycle based on 60 Hz system. However, the training of the ANN needs a lot of data representing many cases of faults and magnetizing inrush currents, which indicates a large required memory, if the ANN is to be designed with additional hidden layers to accommodate complex operating conditions. Moreover, the training of the ANN may need updating if the power transformer is changed.

The existing techniques of differential protection of power transformers depend on harmonic analysis of the differential current, mainly on the second harmonic to identify the type of the flowing current through the power transformer. On the other hand, modern techniques have used pattern recognition through building

ANN algorithms. However, the training of the ANN and the needed memory to accommodate all different cases needed for training and the extra memory needed in case of increasing the number of hidden layers may affect both the simplicity and the cost of the relay. Moreover, the ANN needs to be trained for each case of application for its own specifications. Pattern recognition can be a powerful tool to identify the type of current in power transformer protection, but more sophisticated signal processing techniques are needed.

The nature of any electromagnetic transient that is likely to occur in power systems is of short duration, non-periodic and with impulse superimposed [46]. The traditional tools of analyzing the frequency components of such transients like the Fourier analysis assume periodicity. Even for the windowed version of such tools, the analysis may not provide all the needed information due to the non-periodic nature and the loss of time location of the extracted frequencies. Any electromagnetic transient with the aforementioned natures can be viewed as a signal composed of different frequency components that may not fall in linear frequency divisions, that is, not only integer multiples of the fundamental frequency. Although, a detailed review of the existing mathematical tools used in power transformer protection is provided in the previous section, these tools are based on the Fourier analysis and the decomposition of the current waveforms into harmonic components. These waveforms have mostly periodic nature for the case of fault currents, but dc offsets are created in the cases of magnetizing inrush currents. The fast Fourier transform has been found to be the most effective for real-time differential protection schemes of power transformers.

Another new alternative mathematical tool known as wavelet analysis has been recently delegated, particularly in signal processing, pattern recognition and disturbance classification areas. It is becoming quite evident that wavelet transforms can handle both periodic and non-periodic signals with relative ease; it may be

used for the precise and efficient protection of the modern power transformers against transients, complex faults and magnetizing inrush currents.

Wavelets and wavelet transforms (WT) have recently emerged as a powerful tool for signal processing in board fields of applications including power systems. The applications in power systems include detection and classification of electromagnetic transients, power system protection, fault location and analysis of partial discharge phenomenon in gas isolated switchgear (GIS) [47, 48]. There are several papers presenting different aspects of applying wavelet analysis in power quality assessment [48–51]. The reported papers for power transformer protection provide simulations of the WT technique. There has been no on-line testing results for the WT technique so far, which implies that there is still a wide scope of research in this area.

The reported papers on applying wavelet transform in power system protection are mainly deal with the application of the WTs on a simulated data of different faults and transients currents [52]. Youssef [53] developed a four levels of resolution wavelet transform-based scheme to distinguish between magnetizing inrush and external fault currents. The scheme was simulated using Mathworks/MATLAB on data obtained from the electromagnetic transient program (EMTP), and provided simulation results. The scheme showed very fast distinguishing capabilities, less computational burden and high reliability. However, it was neither tested on data obtained from a real power transformer nor tested on a real power transformer. Pandy and Satish [54] developed a multiresolution signal decomposition (MSD) method using discrete wavelet transform (DWT) to detect the internal faults during impulse testing of three phase power transformers. The method was simulated using Mathworks/MATLAB on a data representing the neutral current obtained form a real power transformer. The results showed fast and accurate detection of the faults during the impulse test. The method was tested off-line for

typical internal faults ,but it was not tested on-line for the conditions of a practical impulse testing. The previous works of the application of wavelet transform in differential protection of power transformers have not been implemented for the on-line testing yet, which indicates that there is ample scope of innovation and development of a real-time wavelet based relay for differential protection of power transformers.

1.3 Objective of This Thesis

There exist many digital techniques for differential protection of power transformers, most of them are based on second and/or fifth harmonic restraint principle. Others are based on voltage restraint principle and ANN techniques. However, there have been reported works indicating that some internal faults might have significant amount of second, fifth and higher harmonic components enough to prevent the relay from proper functioning. In addition, the employment of the low-loss amorphous core material in modern power transformers that can produce lower harmonic contents in the magnetizing inrush current, would make the application of the harmonic restraint principle even more complex. On the other hand, the voltage restraint principle is dependent on the parameters of the transformer, where these might be subject to change under different operating conditions. The use of ANN requires training data for different cases including several magnetizing inrush and internal fault currents that need a large memory affecting the cost of the relay. Moreover, increasing the number of hidden layers to increase the reliability of the relaying algorithm may affect the speed of operation. The proposed work of this thesis is an attempt to develop a differential protection scheme using wavelet packet transform (WPT), which has shown to exhibit many superior features of analyzing non-stationary signals arising out of complex frequency-time

relations, mainly non-periodic signals [46], in particular in electromagnetic transient detection and process of image-edge detection. Some of its advantages over other analysis techniques like DFT include time information and realising non-stationary signals comprising of both low and high frequency components through using a variable length window. In addition, WPT can be implemented through a multiresolution analysis (MA) providing higher frequency resolution and poor time location at low frequencies. Reciprocally, it is able to provide poor frequency resolution and accurate time location at high frequencies [49].

The problem of distinguishing between the magnetizing inrush and internal fault currents can be considered as a problem of disturbance detection and classification with non-stationary nature of the processed signals. Thus, the WPT technique seems to be adequate for developing a sophisticated solution for this particular problem. The effective and efficient implementation of the WPT technique requires a proper selection of a mother wavelet. A new procedure has been developed for selecting the mother wavelet and the optimal number of levels of resolution necessary to create the WPT known as the minimum description length (MDL) data [55]. A dedicated WPT with two levels of resolution has been created, and the coefficients of the needed wavelet filter bank to construct the desired MA has been obtained. The WPT-based algorithm has been tested both off-line and on-line, and provided satisfactory results in terms of speed, accuracy, computational burden, independence of transformer or CT parameters, memory size and reliability. The algorithm of WPT is implemented on-line with computer codes written in Turbo C, compiled using Texas Instrument compiler and downloaded to DSpace DS-1102 digital signal processor. Various operating conditions on two different power transformers are investigated in this work including magnetizing inrush, internal fault and through-fault currents.

1.4 Outline of the Thesis

Chapter 2 describes the basic principle of three-phase power transformer differential protection. The magnetizing inrush phenomenon and the various factors that should be considered when designing digital differential relay for power transformer differential protection. Also, two examples of differential protective relays are presented, one is based on the harmonic analysis, while the other is based on pattern recognition approach. In Chapter 3, the wavelets and wavelet transforms are introduced, including the wavelet packet transform. Also, the selection of the mother wavelet and the optimal number of levels of resolution using minimum description length (MDL) data criterion are presented. Chapter 4 contains the experimental setup and data acquisition procedure for different power transformer differential currents. Moreover, it contains the results of the off-line testings. Also, chapter 4 provides the application of the MDL criterion to select both the optimal mother wavelet and the number of levels of resolution. Chapter 5 presents the real-time implementation of the WPT algorithm using the selected mother wavelet and the number of levels of resolution along with details of the on-line testing experimental setup. The tests procedures and on-line test results for a 5 kVA, three-phase, core type, step up power transformer are provided for different conditions of loading and energizing. The WPT algorithm with the same experimental setup is tested on a 2 kVA, multi tap, three-phase, step down power transformer, mainly to test the general applicability of the proposed algorithm. The results for different faults under different loading and energizing conditions are provided in chapter 6. Finally, the thesis is summarized and concluded in Chapter 7 and the main contributions and future scope of this work are discussed.

Chapter 2

Fundamentals of Differential Protection in Power Transformers

Power transformers are considered one of the most essential elements in modern power systems. The structure of such an element provides ruggedness that tends to make it reliable under normal operating conditions. However, internal faults can produce high currents with transient components that flow through the windings and the iron core causing saturation in the iron core. Such conditions violate the reliable features and can cause sever damages in both the faulty transformer and other parts of the power system. The sequence of an internal fault leads to more damages and critical impacts if immediate and proper action against the fault is not initiated.

Differential current can provide quite significant information about the nature of the current flowing through power transformer windings. Such informations may include frequency contents, transient nature, periodicity, non-periodicity and frequency-time relations (stationary or non-stationary nature). There are many factors that should be considered when attempting to design differential protection for power transformers such as magnetizing inrush current, over-excitation and CT

saturation. In the following sections, these factors are described. Then the basic differential relaying principles with typical operating examples are described. Two techniques for digital differential relaying are presented in this chapter. These techniques are: a conventional wide spread harmonic restraint technique and a modern pattern recognition technique, that is implemented using an artificial neural network (ANN).

2.1 Magnetizing Inrush Phenomenon in Power Transformers

The main challenge in power transformer protection is to avoid false trip action under the magnetizing inrush current, i.e. the ability of the relaying algorithm to distinguish different magnetizing inrush currents from internal faults, external faults and normal currents. The magnetizing inrush current can not be easily predicted and as a result, the characteristics of this type of current are very complex and difficult to handle. Magnetizing inrush current is dependent on many factors including the instant of connecting the supply to the power transformer, the residual flux, the type of winding connection (self and mutual inductances), core type material and the type of relation between current and voltage. Moreover, such characteristics change from single-phase to three-phase or single winding to multi windings. The following subsections illustrate the magnetizing inrush phenomenon in both single-phase and three-phase power transformers [44, 45].

2.1.1 Magnetizing inrush current in single phase power transformers

When a transformer is connected to a supply voltage under no-load steady-state conditions, an exciting current flows through the primary windings producing sufficient flux to induce a back EMF opposite to the applied voltage. This process is known as the energization of the power transformer. The flux level reaches 1.6 Tesla (T) for a primary current of about 1% of the rated current. If the flux level reaches 2 T , the iron core gets saturated and high current is required to produce that flux level [1,2,44]. The flux usually remains in the iron core after the transformer is de-energized, which is known as the residual flux. Thus, each time the transformer is energized a transient saturation of the core and the residual flux takes place resulting in a high inrush current. The exciting current is also known as the magnetizing inrush current that lags the applied voltage by 90°. Also, the magnitude of this current depends on instant of energizing, magnitude, polarity of the applied voltage and the rate of change of the applied voltage. Figure 2.1 shows the relation between the applied voltage and the exciting current as a functions of time. It is clear that the flux is proportional to the rate of change of the applied voltage, also, if the instant of switching the supply voltage is at the positive zero going position, the phase shift ϕ between the applied voltage and the flux will be 90°, as shown in Figure 2.1(b). The worst conditions for excitation current is when the supply voltage (sinusoidal) is switched on at zero voltage with positive rate of change, and the residual flux is at its minimum possible value [3]. If B_r is the flux density of the residual flux and B_m is the peak value of the magnetic flux density $B(t)$, the magnetic flux will have its maximum value when ($\phi = 90°$) as shown in Figure 2.2 and when the residual flux is zero. The needed exciting current to produce this amount of flux can be determined using the magnetizing curve shown in Figure 2.3 [25, 44].

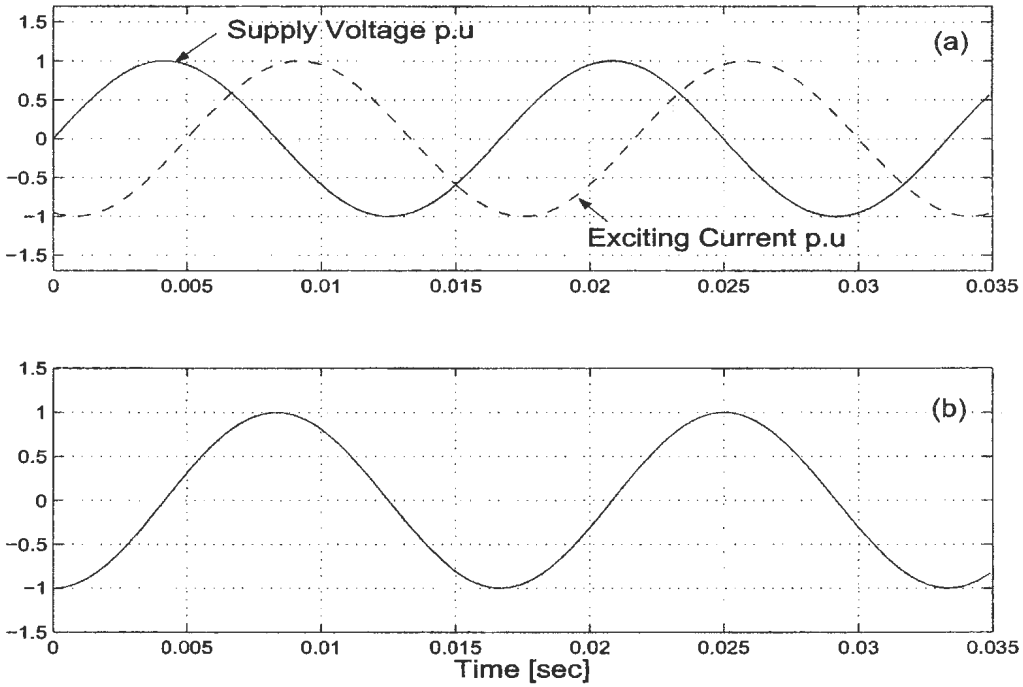

Figure 2.1: The phase shift between applied voltage and magnetic flux, (a) the applied voltage and the exciting current and (b) the magnetic flux without residual flux

The instantaneous magnetic flux density can be expressed mathematically as [2]:

$$B(t) = -B_m cos(\omega t) + B_m + B_r \tag{2.1}$$

The iron core gets saturated when the magnetic flux density reaches a certain value. Let B_s be the flux density enough to saturate the iron core. The instant when the flux density $B(t)$ equals B_s, can be determined on the flux curve from equation (2.1), let the instant on the flux curve $\omega t = \theta$ given as [2]

$$B_s = -B_m cos(\theta) + B_m + B_r \tag{2.2}$$

$$\theta = cos^{-1}\left[\frac{B_m + B_r - B_s}{B_m}\right] \tag{2.3}$$

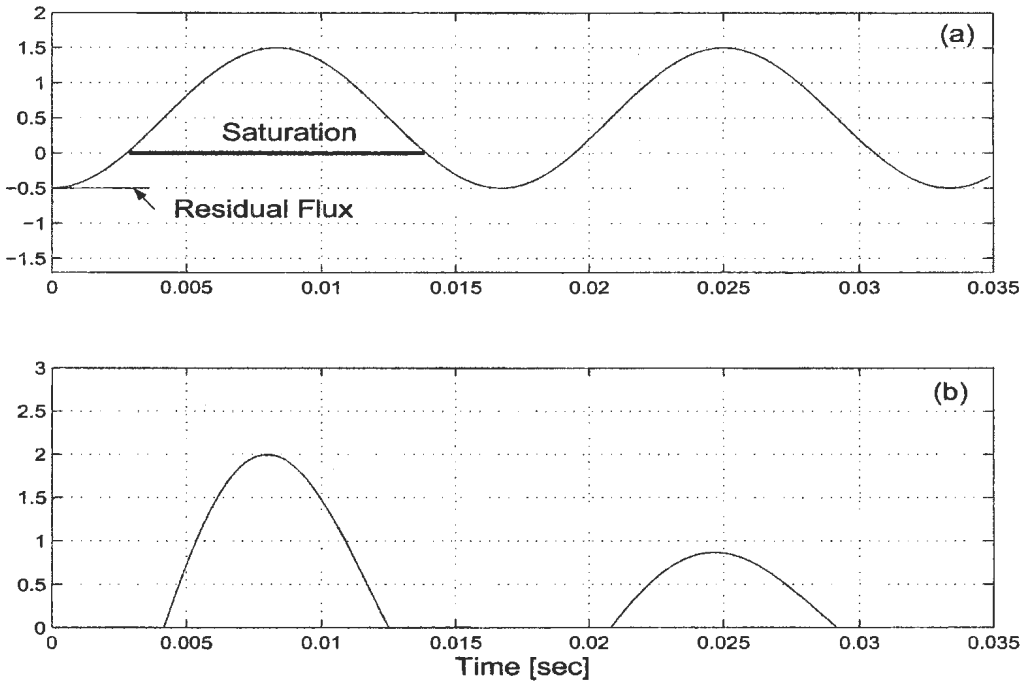

Figure 2.2: The effect of core saturation on exciting current, (a) the magnetic flux with residual flux and (b) the exciting current (inrush)

The angular position θ on the flux curve is known as the saturation angle. The maximum duration of each cycle of the magnetizing inrush current is given as [3]

$$\gamma = 2(180^\circ - \theta) \tag{2.4}$$

The angle γ increases as the magnitude of the inrush current decreases [3]. Figure 2.2 (b) shows computer simulation of the magnetizing inrush current in a single phase power transformer.

2.1.2 Magnetizing inrush current in three-phase power transformers

The analysis of inrush phenomenon in three-phase power transformers must include the mutual interaction of flux between the three phases, which complicates

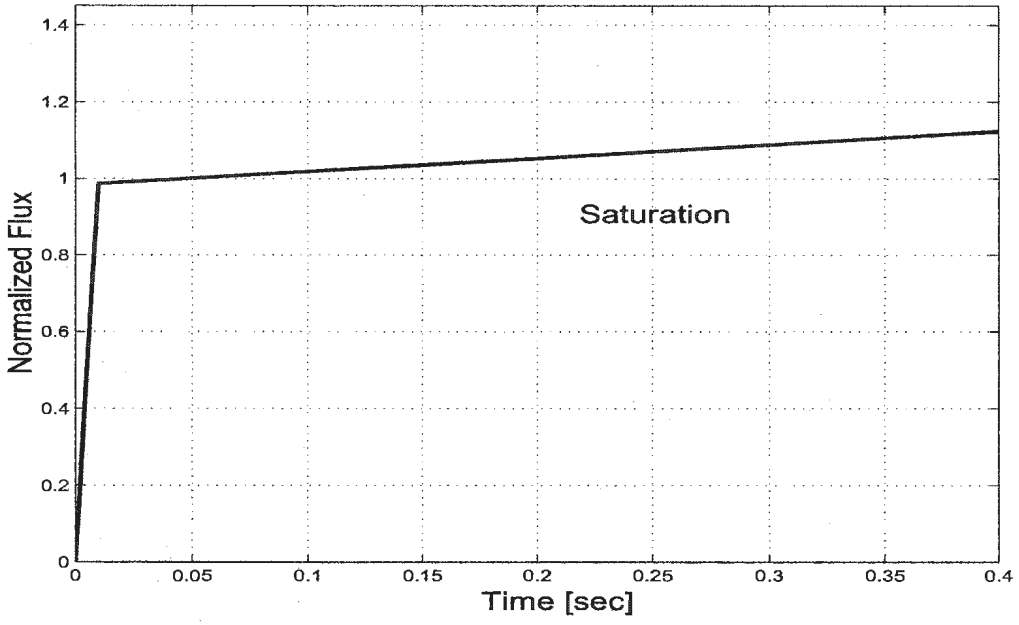

Figure 2.3: The magnetic saturation curve

this phenomenon. The core of a three-phase power transformer has a magnetic flux which is a combination of the three phase fluxes. Additional factors that also affect the magnetizing inrush current in three-phase power transformers, may include the type of connection and the level of residual flux. Y-Δ connected power transformer banks have a circulating current in Δ side, which has an effect on the three phase currents, as a result, it affects the flux in the iron core. It is worth mentioning that, the residual flux may not be the same in all the limbs of the power transformer bank, causing some phases to get saturated before others. This difference in residual flux in the three phases will increase the reluctance seen by the limbs with lower residual flux resulting in a higher magnetizing inrush current [2, 3]. In the case of Δ-Y connected power transformers, there is no circulating current and the transformer in this case can be considered as three single-phase power transformers. The magnetic flux in this type of power transformers is produced by the three phase fluxes and the residual flux. In general, the magnetizing inrush current in three-phase power transformers has a quite high magnitude that

may become as high as a typical internal fault current magnitude [3, 44]. Figures 2.4-2.6 show the effects of different residual flux on the magnetic flux and the magnetizing inrush currents in the three phases.

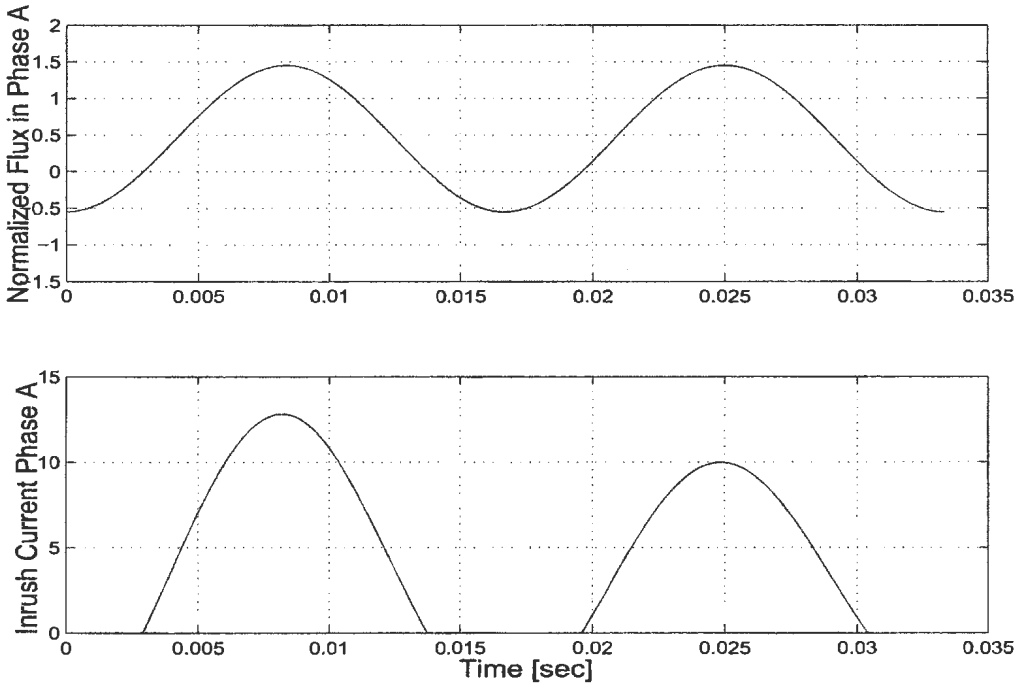

Figure 2.4: Magnetic Flux and Exciting current in Phase (a)

2.1.3 Over-excitation

The steady state magnetic flux density has a normal operating range, but certain changes in the operating conditions may produce magnetic flux density higher than the normal range. Such operating conditions that may cause the magnetic flux density to exceed its normal range include external faults causing high currents to flow through power transformers, over-voltage, decrease in the supply frequency and/or mal-operation of tap-changing service [44, 45]. All the aforementioned conditions cause high currents with transient components to flow through power

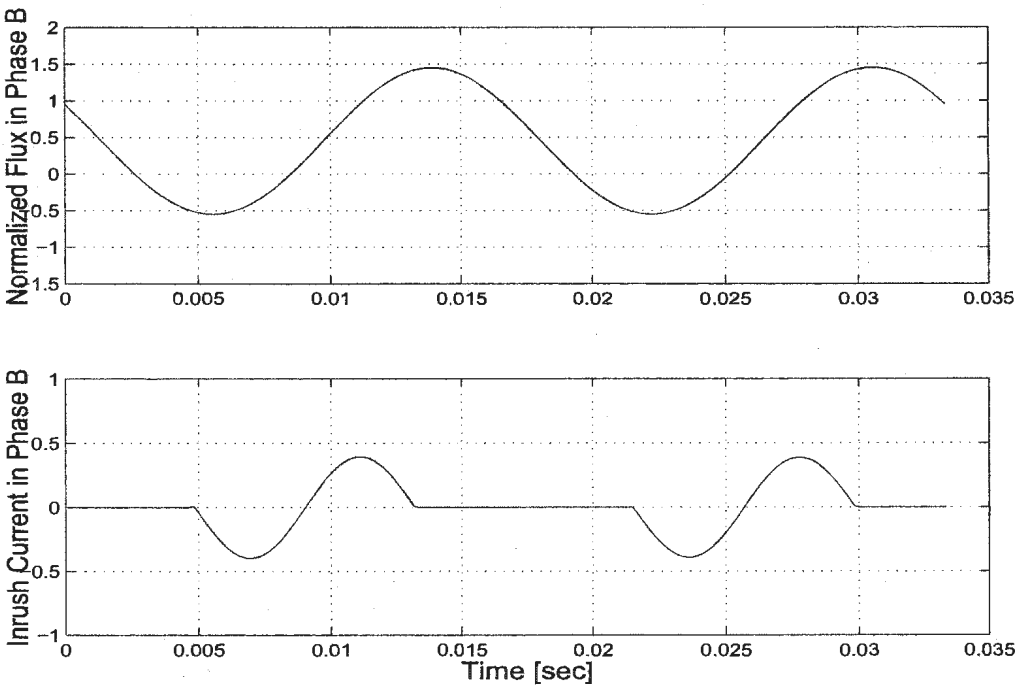

Figure 2.5: Magnetic Flux and Exciting current in Phase (b)

transformers that can be categorized in some severe situations as fault currents. The transient nature of the currents involved in over-exciting conditions may be enough to initiate a trip signal by conventional harmonic restraint differential relays.

2.1.4 Current transformer saturation

Current transformers are essential instruments needed for practical implementation of different protection apparatus, where the fault and inrush currents, usually of high magnitudes, can be transformed to a suitable level for the relaying parts and for data acquisition instruments. When faults take place in power transformers, high magnitude currents flow through the primary side of CTs with slow-decaying large dc components causing saturation. The fault and CT saturation affect the current flowing in the secondary side of the CT producing spill conse-

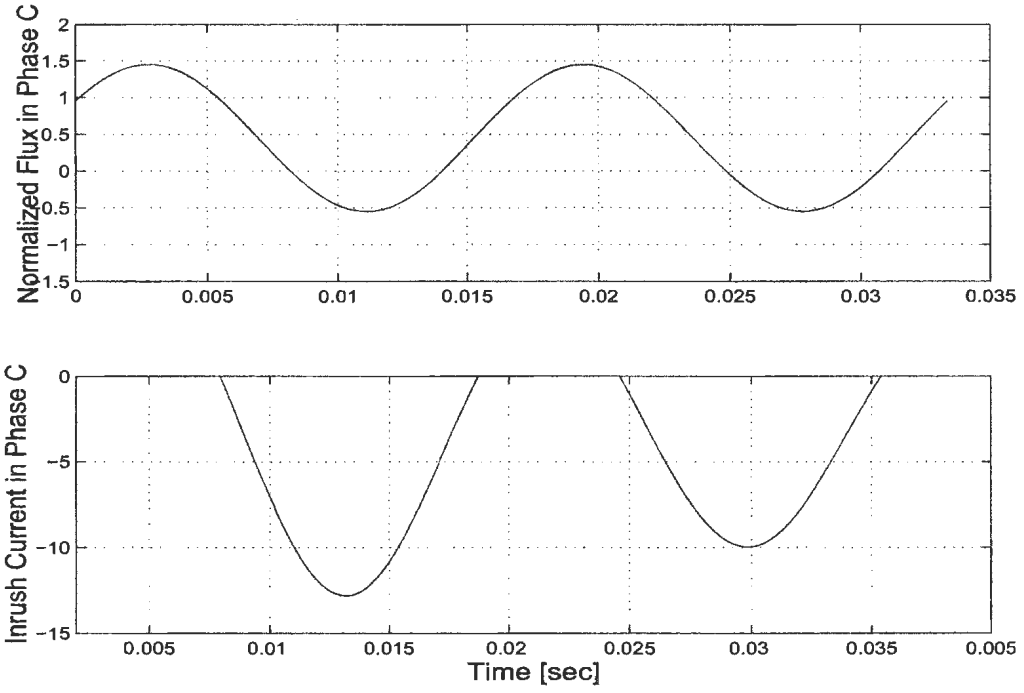

Figure 2.6: Magnetic Flux and Exciting in Phase (c)

quent differential current to flow through the protective relay. Many other factors can cause CT saturation, such as voltage level, turns ratio, mismatch of CTs, etc. The percentage differential relays are designed to minimize the probability of relay mal-operation due to current transformers saturation [45].

2.2 Basic Principles of Differential Protection

The fundamental function of a differential relay for power transformer protection includes converting the primary and the secondary per phase currents into a common base for comparison purposes. These per phase currents can not be converted directly, rather, they have to be stepped down first using current transformers(CTs). The desired current is measured if the CTs are connected with the matching polarities. In steady-state conditions, the differential current is very small that is less than 5% of the full load current of the power transformer.

However, under transient conditions (magnetizing inrush, internal faults or severe over-excitation) differential current rises up to 10-20 times the steady-state differential current value [2].

In three-phase power transformers, the connection of the CTs is dependent on the connection of the power transformer windings. For Δ-Y or Y-Δ transformer banks, the CTs are connected in opposite order. For example, in Δ-Y transformer banks, the CTs of the primary are connected in Y, while the CTs of the secondary are connected in Δ. Such opposite order in connecting the CTs is made to block the zero-sequence current in line currents and to account for the 30° phase shift introduced by Δ-Y or Y-Δ connections of the transformer windings. The primary ratings of current transformers should match the rated primary and secondary currents of the power transformer. Figure 2.7 shows the difference between correct and incorrect connections of CTs.

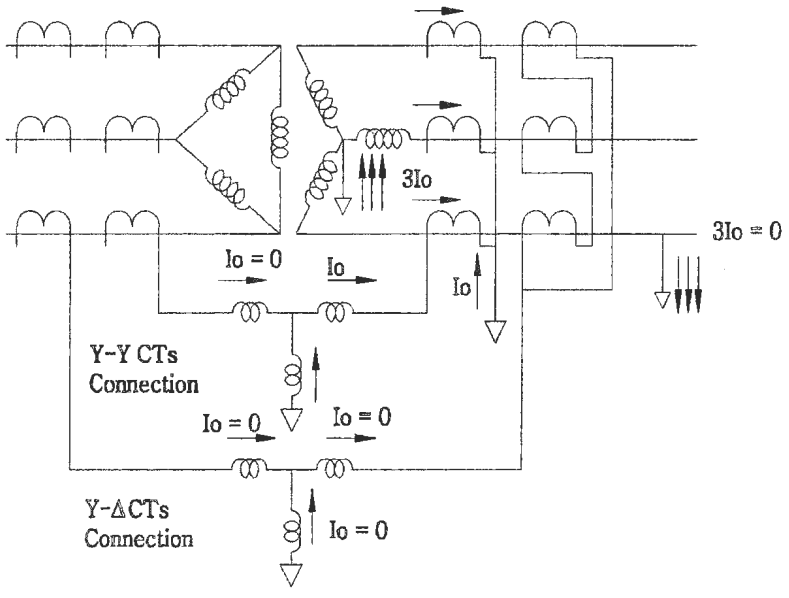

Figure 2.7: Transformer CTs Connection for a Δ-Y Transformer Bank, with Two Possibilities Y-Y and Y-Δ

If the protection is implemented for a power transformer with on-line tap-changer, special attention must be paid to incorporate the bias feature if the low-fault settings and high speed functioning are required.

The simplest design of a differential relay is the unbiased differential relay shown in Figure 2.8. If the CTs on both sides of the power transformers are considered identical.Therefore, the differential current under steady-state is ideally zero or very small and can be neglected. When an internal fault takes place, the difference between currents will not remain negligible and a differential current will flow through the operating coil causing a trip signal to be initiated. The unbiased relay does not have high reliability, since a differential current may flow through the operating coil due to the saturation characteristics of CT and/or highly unbalanced loads. To reduce the effect of CT characteristics on the operation of the unbiased relay, a modified design has been proposed known as the percentage differential relay. The proposed modification is simply to employ two restraining coils in order to allow certain percentage of the differential current to flow through the operating coil without relay operation. This percentage differential current can be caused by CT characteristics, unbalanced load currents or CT saturation under heavy external faults. A small percentage of bias is effective to avoid relay mal-function under current transformer errors, protective circuit asymmetry and normal magnetizing inrush currents of the protected power transformer. In case of protecting tap-changer transformers, higher percentages are required to prevent relay mal-operation under significant imbalance currents of the protected transformer. The magnetizing inrush current has a peak value about 10 times the rated current after energizing the transformer. If such a high amplitude current flows through the normal percentage differential relay, it becomes enough to operate the relay and a trip signal may be initiated. This mal-operation makes the percentage bias relay insufficient to ensure high reliable operation.

One of the most used techniques to deal effectively with high magnetizing inrush currents is the harmonic restraint principle, as shown in Figure 2.8. Many

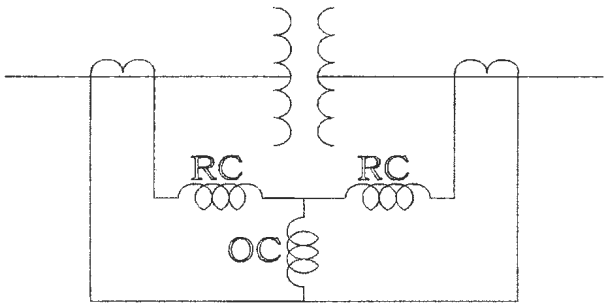

Figure 2.8: A percentage Differential Relay with Restraining Coils

research works have been conducted to analyze both the magnetizing inrush and internal fault currents in power transformers. It has been found that the magnetizing inrush current contains a significant amount of the second, fifth and higher harmonics that are higher than the internal or normal currents. The harmonic restraint relay has been implemented even before the introduction of the digital relays. The simplest design of this type of differential relays employs two filters, one of them is responsible of extracting the fundamental component of the differential current and allow it to flow through the operating coil. The second filter is responsible of extracting the other harmonic components of the differential current and allow them to flow through the restraining coils. Early designs of this relay used simple L-C tuned circuits. The structure of this type of relay is shown in Figure 2.9. A typical harmonic restraint variable percentage differential relay [1] uses two L-C analog filters, where one of these filters is responsible for passing the second harmonic to the restraint coil (RC) to block the relay from operation under currents containing high second harmonic component, which is likely to be

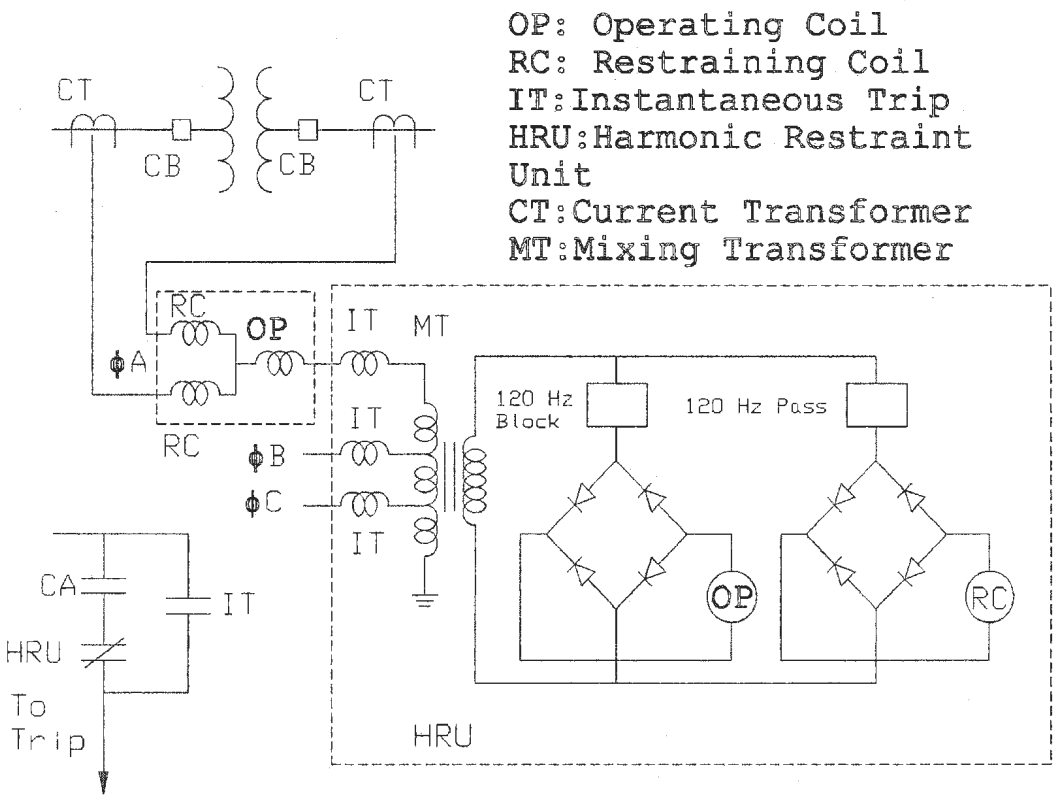

Figure 2.9: Typical Harmonic Restrained Percentage Differential relay [1]

magnetizing inrush current. The other filter is responsible for blocking the second harmonic from flowing through the operating coil (OC) of the protective relay, while passing the fundamental and other harmonic components, which usually exist in internal fault currents to activate the relay when there are such currents. It is worth mentioning that this type of differential relays contains a mixing transformer to combine the three differential currents flowing out of the differential circuit [1]. The analog filters are being generally replaced by digital filters due to their inherent advantages like design flexibility, high reliability, accuracy and high speed response.

2.3 Digital Differential Protective Relays

Modern protective differential relays are implemented digitally where the relaying functions are realized through software rather than hardware. The software relaying functions use algorithms mainly to carry out a harmonic analysis. As mentioned in Chapter 1, Discrete Fourier Transform (DFT) was found to be the optimal algorithm for implementing digital harmonic restraint differential relay for power transformer protection. Other principles had been used like pattern recognition realized through Artificial Neural Network (ANN) algorithm, flux and voltage restraints, transformer parameters during the final reduction, etc. [2,25,45]. In the following subsection the DFT algorithm is illustrated along with its implementation and an example of a harmonic restraint differential relay.

2.3.1 Discrete Fourier Transform

Ramamoorthy proposed the DFT approach [25], which states that the fundamental component of a voltage or current signals can be obtained by correlating a stored samples of reference basis functions (sine and cosine functions). This approach is basically developed from the Fourier series. In general, any periodic signal $f(t)$ with finite number of discontinuities over an interval of $[0, T]$ can be decomposed to its sine and cosine components as.

$$f(t) = \frac{a_0}{2} \sum_{k=1}^{\infty} C_k cos(k\omega t) + S_k sin(k\omega t) \tag{2.5}$$

where

$$\frac{a_0}{2} = \frac{1}{T} \int_0^T f(t)dt \tag{2.6}$$

$$S_k = \frac{2}{T} \int_0^T f(t) sin(k\omega t)dt \tag{2.7}$$

$$C_k = \frac{2}{T} \int_0^T f(t) cos(k\omega t)dt \tag{2.8}$$

a_0 is the average value or the dc component present in $f(t)$, and S_k, C_k are the sine and cosine coefficients of the different frequencies present in $f(t)$, respectively. In case of non-periodic signals (like the currents with transient components for protection purposes), the windowed DFT is used. If the signal is sampled with sampling interval of Δt, such that there are $N/\Delta t$ samples per cycle, then the DFT basis function coefficients can be represented as.

$$S_k = \frac{2}{N}\sum_{n=1}^{N-1} x[n] sin\left(\frac{2\pi kn}{N}\right) \tag{2.9}$$

$$C_k = \frac{2}{N}\sum_{n=1}^{N-1} x[n] cos\left(\frac{2\pi kn}{N}\right) \tag{2.10}$$

The Fourier harmonic coefficients can be expressed as.

$$F_k = \sqrt{S_k^2 + C_k^2} \tag{2.11}$$

where F_k is the kth harmonic Fourier coefficient, $k = 1, 2, ..., N$ and $x[n]$ is the sampled sequence of the continuous signal $f(t)$.

2.3.2 Implementing DFT algorithm for transformer protection

The DFT is one of the best methods to extract the frequency components of any periodic signal. Also for the non-periodic signals the windowed DFT can be used. The sine and cosine coefficients of DFT can be modeled as coefficients of a discrete frequency selective-filter. In the application of DFT for power transformer protection, three filters are being used to extract the fundamental, second and fifth harmonics, i.e to evaluate F_1, F_2, F_5. These coefficients have been used to identify magnetizing inrush, over-exciting and internal fault currents according to their ratios. If the ratio F_2/F_1 is higher than 17.7%, magnetizing current is

decleared, while a trip signal indicating an internal fault is initiated if the ratio falls below 17.7%. The ratio F_5/F_1 is employed to distinguish between over-exciting and internal fault currents. If the ratio F_5/F_1 is higher than 24.2% the relay is restrained and over-exciting current is decleared, otherwise it declears an internal fault.

In power transformer protection, accurate and quick distinguish between magnetizing inrush and internal fault currents is still a challenge. The DFT is one of the most applied algorithms in digital percentage harmonic restraint differential relays. However, modern transformers with low-loss amorphous core materials are able to produce magnetizing inrush currents with low second harmonic component, which complicates the application of DFT algorithm. Moreover, DFT algorithm is powerful tool for extracting the integer-multiples of the fundamental frequency in periodic signals, and other frequency components (non-integer-multiples) will either be attenuated or they will not affect the evaluation of Fourier harmonic coefficients.

2.3.3 Pattern recognition using artificial neural network (ANN) technique

There have been many research works on applications of neural networks, in particular, for pattern recognition applications. ANN has an advantage in this context, which is the non-algorithmic parallel distributed architecture for information processing. For power transformer protection, the problem can be formulated as current pattern recognition [2]. In the case of implementing the ANN technique, first, the case has to be stated, that is to formulate the inputs and outputs to the neural network, second, the network has to be trained for these inputs and the desired outputs. The network is trained to give input-output patterns when there is an input propagating from the input layer to the processing (hidden) layer and

finally to the output layer. The processing or hidden layer consists of processing units, each of them receives a net sum from the input layer and then the net sum is passed through the unit itself with its transfer function. For a given input pattern $X_p = [X_{p1}, X_{p2}, ..., X_{pN}]$, the input to the jth processing unit in the hidden layer is given as [45]

$$sum^h_{pj} = \sum_{i=1}^{N} W^h_{ji} X_{pi} + B^h_j \tag{2.12}$$

where the subscript p and subscript h refers to pattern and hidden layer respectively, W^h_{ji} are the weights associated with the connection between the input layer and the hidden layer and B^h_j are the biases associated with the input layer neuron. The output of this processing unit in the hidden layer is just applying the transfer function of that particular unit to the net-sum sum^h_{pj} as [2, 45]

$$I_{pj} = f^h(sum^h_{pj}) \tag{2.13}$$

The output of the hidden layer propagates towards the output layer, where the output of the k^{th} processing unit of the output layer is given as [45]

$$sum^o_{pk} = \sum_{j=1}^{L} W^o_{kj} I_{pj} + B^o_k \tag{2.14}$$

where the subscript o refers to the output layer, W^o_{kj} are the weights associated with the connections between the hidden layer and the output layer and B^o_k are the biases associated with the hidden layer neurons. The final output is obtained when the output layer net-sum sum^o_{pk} is passed through the transfer function of the k^{th} processing unit of the output layer given as [2, 45]

$$O_{pk} = f^o(sum^o_{pk}) \tag{2.15}$$

This output O_{pk} is compared to the desired output T_{pk} and depending on the error the weight of each connection and the bias of each processing unit are updated. To update the weights and biases, delta rule is employed and a cost function can be defined as [2, 45]

$$E_p = \frac{1}{2}\sum_k (T_{pk} - O_{pk})^2 \tag{2.16}$$

The objective of training the ANN is to minimize the cost function. Steepest descent method is used stating that the changes in weight and biases are proportional to negative the rate of change of the cost function that is given as [45].

$$\Delta_p W^o_{kj} \propto -\frac{\delta E_p}{\delta W^o_{kj}} \tag{2.17}$$

where δ is called the error terms of layers. The final relation for the update is stated in terms of equality instead of proportionality as

$$\Delta_p W^o_{kj} = \eta \delta^o_{pk} I_{pj} \tag{2.18}$$

Equation 2.18 is for one layer (output layer) and it should be generalized for all layers. The constant η is called the learning rate and is chosen by trial and error. The value of η can show the learning process, high values can indicate fast learning, while small values indicate slow learning process.

When this technique is applied for differential protection, the inputs are the samples of the three-phase differential currents. The ANN was trained using data obtained from the transformer to be protected. All the possible types of currents including many magnetizing inrush currents (loaded, unloaded and different switching angles), internal faults (loaded and unloaded), normal current and overexcitation currents. Then this data is windowed by a 16 samples window. Each sample is converted to its absolute value and compared with a predefined threshold

depending on the full load current of the protected transformer. If the absolute value of the current sample is below the threshold, then the sample is turned into '0', otherwise it is given a value of '1'. Then each pattern becomes 16-bit binary number, among the possible ($2^{16} = 65536$) different combinations, the inrush and fault currents would not have taken the same possible combinations [2]. Finally some redundant data are removed resulting in magnetizing inrush nd internal fault currents patterns only. These patterns are compared each time there is a differential current. Once the input and target vectors are ready, the ANN is trained with specific momentum and adaptive learning rate [2, 44].

Training the ANN makes it ready for testing, and when this technique is implemented using DSP DS1102 board, the results were quite good in terms of speed of operation, that is, the fault is identified with almost '0.6' cycle based on 60 Hz systems. In [45], there is a detail design of an ANN based differential relay. However, this technique needs a lot of data files to train the ANN, and considering accuracy, the number of hidden layers must be increased to improve the accuracy, more memory is needed to accommodate the weights and biases for the new layers, and as a result, many trials are needed to determine the learning rate, so as to improve the functionality of the ANN. Moreover, this technique is dependent on the currents flowing to recognize the pattern, and a threshold is defined based on the normal full-load current which may be not equal to the operating current.

2.3.4 Signal processing using wavelet functions

The recent development of wavelets and wavelet transforms as powerful tools for processing non-periodic and non-stationary signals provides a new opportunity for accurate and quick analysis of the frequencies present in any signal. Distinguish between magnetizing inrush and internal fault currents can be considered a disturbance detection and classification problem, where wavelet transforms seem to

provide a good solution. In the next chapter, a close insight of wavelet families, types and characteristics, companion scaling function, wavelet transforms including continuous, discrete and the wavelet packet transforms are introduced. Also, the concept of multireolution analysis along with the needed filter banks are provided. In addition, the minimum description length (MDL) data criteria to select both the optimal mother wavelet and number of levels of resolutions is illustrated.

Chapter 3

Wavelets and Wavelet Transforms

Signal processing is a very important topic, and the search for proper techniques is one of the most attractive areas of research in a board band of applications like communication systems, control systems, power systems, etc. There are many working techniques including Fourier transforms, Laplace transform and Z-transform. These techniques work well when the processed signal satisfies certain conditions such as finite energy, periodicity, stationarity and finite number of discontinuities [46, 47]. In processing any signal, it is desirable and often necessary to apply a frequency-time based analysis techniques in an attempt to extract all the frequency components including the transient components present in the processed signal, in addition, to preserve their location in time. This in turn can help in identifying the phenomenon producing signals with such frequency-time characteristics. Signal processing has many applications in power systems. Voltage stability, power systems dynamic stability, fault detection, protective relaying systems and power quality assessment are just few examples that show the need for accurate and efficient techniques of signal representation [52]. In general, signal processing is needed in conditions involving disturbances that affect the stable operating conditions, and since the power system elements have oscillatory

nature, these disturbances are likely to contain transient components. Typical transients that may take place in power systems are of non-periodic nature with both high-frequency oscillations and very short-duration impulses superimposed on the much lower frequency components of the signal (usually current and/or voltage are considered). Such characteristics create a problem for the traditional techniques to process these signals, and the need for a technique to overcome the limitations of the traditional techniques becomes more mandatory. Wavelets with their characteristics and capabilities of processing signals with complex frequency-time relations seem to be a proper solution for problems including processing such signals.

This chapter provides a detailed view of the wavelets, scaling functions and the different types of wavelet transforms. Also, it introduces the multiresolution analysis along with conditions of implementing this analysis, and the concept of quadrature mirror filter banks. Finally, it shows a method for selecting both the optimal mother wavelet and the number of levels of resolution.The following section introduces wavelets, their types and characteristics.

3.1 Wavelets and Wavelet Functions

A wavelet is a "little" wave in the sense of having short duration with finite energy and fast decaying behavior in time. In addition, wavelets have an oscillating feature that comes along with the location in time and frequency. These basic transient features of any wavelet make wavelets highly adequate for signals representation [46]. Some wavelets (*Mother Wavelet*) $\psi(t)$, have a companion function called the *scaling function* $\phi(t)$, which is responsible for generating all the basis functions needed to represent any signal, i.e. to either decompose or reconstruct any signal. The scaling function has the following properties [56].

- compact support, which indicates that the value of scaling function is zero outside the interval of support $[t_0, t_s]$ of the mother wavelet, that is ($\phi(t) = 0$ for $t \notin [t_0, t_s]$)

- averaging which guarantees an average value of the scaling function to be '1' over the region of support

$$\int_{t_0}^{t_s} \phi(t)dt = 1 \tag{3.1}$$

- orthogonality, which ensures the orthogonality property of all the translates of $\phi(t)$, or $\phi(t - m_1)$ are orthogonal to $\phi(t - m_2)$ where $m_1, m_2 \in Z$

- regularity which guarantees that constant and linear functions can be regenerated by $\phi(t)$ and its translates

The term "Mother" implies that functions with different region of support that are used in the transformation process are derived from one main function. The region of support is defined as an interval $[t_0, t_s]$ of the smallest length outside of which, the mother wavelet ψ(t) vanishes identically.

A basis of a vector space V is a set of linearly independent vectors, such that any vector λ in V can be written as a linear combination of these basis vectors. There may be more than one basis for a vector space. However, all of them have the same number of vectors, and this number is known as the *dimension* of the vector space. For example in four-dimensional space, the basis will have four vectors as [56].

$$\lambda = \sum_{k=1}^{4} c_\lambda^k b_k \tag{3.2}$$

where c_λ^k are the corresponding coefficients and b_k are basis vectors of space V. This concept, given in terms of vectors, can easily be generalized to functions by replacing the basis vectors b_k with basis functions $\phi_k(t)$, and the vector λ

with a function $f(t)$. These basis functions may be polynomials or any other type of functions - in case of Fourier transform, the basis functions are complex exponentials. The expression of any function $f(t)$ in space V using the basis functions can be stated as [56].

$$f(t) = \sum_k c_f^k \phi_k(t) \tag{3.3}$$

Any wavelet has a number of vanishing points (m), and its scaling function (if exists) should have the capability of generating polynomials of degree (p) such that $p \leq m$. A level of resolution refers to one translation of the mother wavelet frequency band. Such translation will produce an other wavelet, which is a shifted scaled copy of the wavelet in the previous level of resolution. The new generated wavelet is known as *Daughter Wavelet* . At each level, where a daughter wavelet can be generated, the scaling function related to the mother wavelet generates the basis functions of that level. This property is given as [53].

$$\phi_{j,k}(t) = 2^{-j/2}\phi(2^j t - k); j, k \in Z \tag{3.4}$$

where j is the level of resolution and k is the dimension of the function space at level j [53]. The relation between the generated wavelet at level j, and the mother wavelet is given as [53].

$$\psi_{j,k}(t) = 2^{-j/2}\psi\left(\frac{t - 2^j k}{2^j}\right); j, k \in Z \tag{3.5}$$

There are different types of wavelets whose qualities vary according to several criteria. The main criteria are [56, 59].

1. The support of ψ or $\hat{\psi}$ (its dual wavelet) and ϕ or $\hat{\phi}$ (the scaling function related to the dual wavelet) guarantees the speed of convergence to

zero of these functions ($\psi(t)$ and $\phi(t)$ or $\hat{\psi}(t)$ and $\hat{\phi}(t)$) when the time t or the frequency f goes to infinity, which quantifies both time and frequency localizations

2. The number of vanishing points for ψ or for ϕ (if it exists), which is useful for compression purposes

3. The regularity, which is useful for getting nice features, like smoothness of the reconstructed signal or image, and for the estimated function in a nonlinear regression analysis

Wavelets can be classified into two main types, orthogonal and non-orthogonal. The next subsections give an explanation of the main properties of each type.

3.1.1 Orthogonal wavelets

Orthogonal wavelets are the wavelets with a scaling function $\phi(t)$ capable of generating orthogonal basis functions at each level of resolution. These basis functions created through shifting by integers and dilation by 2^j, are orthogonal to the mother wavelet $\psi(t)$. The orthogonal wavelets have to meet the orthogonality conditions, which are given as [53–55]:

- Inner-product of the mother wavelet with itself is unity

$$\int_{-\infty}^{\infty} \psi(t)\psi(t)dt = 1 \tag{3.6}$$

- Inner products of mother wavelet and any other basis function are zero

$$\int_{-\infty}^{\infty} \psi(t)\phi_j(t)dt = 0 \tag{3.7}$$

There are several examples of orthogonal wavelets including *Daubechies family, Meyer, Coiflet, B − splines biorthogonal wavelets* and *Symlet* [59]. Orthogonal wavelets are more popular in different applications including image processing, disturbance detection and classification, denoising, etc., due to [56, 59]:

- Perfect representation of a signal without redundancy
- Good for compression, relatively simple and numerically stable
- Each coefficient is computed with a single scalar product

The Daubechies wavelet family is the best example of orthogonal wavelets. These wavelets (a part from the Haar wavelet) do not have linear phase, and they have problems at the edges of signals (the start and end points of signals), and the boundaries of the interval of support, since the analysis requires that the signal is defined outside the region of support. Traditionally, this problem has been solved by zero-padding, wrap-around or reflection, but all of these options impose a particular choice, which degrades the wavelet decomposition at the edges of the signal [47, 48]. Figure.3.1 (a) shows the Daubechies $(db4)$ wavelet and Figure.3.1 (b) shows the Symlet $(sym4)$ wavelet.

In case of biorthogonal wavelets, which use spline wavelet function $\psi_{j,m}(t)$ at level j and shifted by $m/2^j$ and $\hat{\psi_{j,m}}(t)$ as dual for $\psi_{j,m}(t)$ wavelets, the number of vanishing points is maximized for a given extent of their support. The spline function candidates for building biorthogonal wavelets have to satisfy the following condition given as [56, 57, 59]

$$\left\langle \psi_{j,m}(t), \hat{\psi_{j,m}}(t) \right\rangle = \delta(j - j')\delta(m - m') \tag{3.8}$$

One of the most interesting properties of biorthogonal wavelets is that, all the generated basis functions are compactly supported at all levels of resolution.

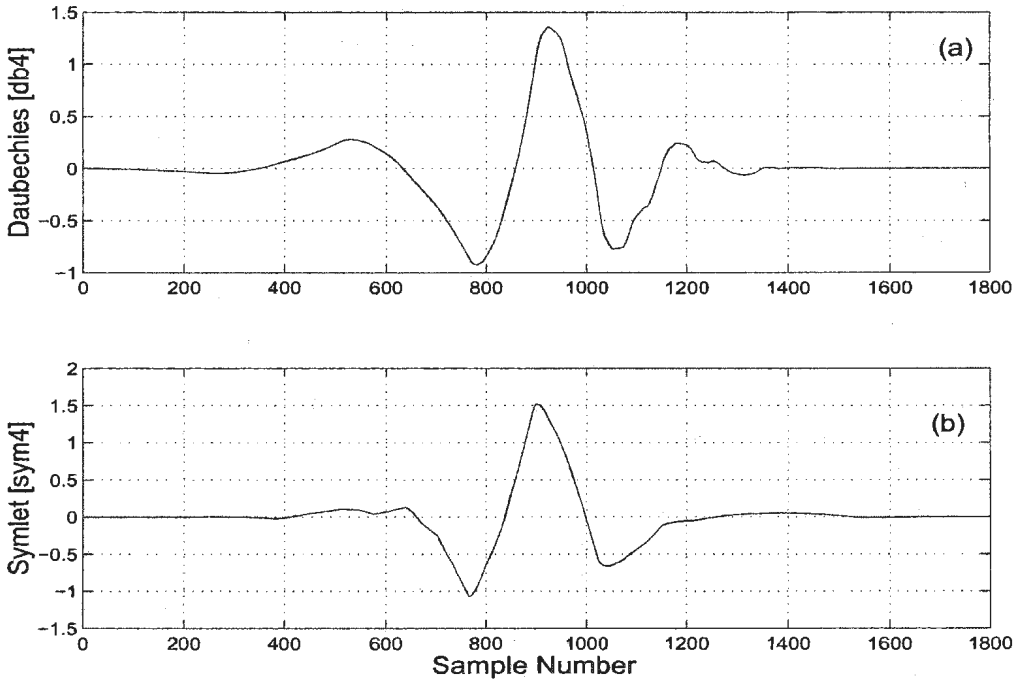

Figure 3.1: Orthogonal Mother wavelets (a) the Daubechies [db4] wavelet and (b) the Symlet [sym4] wavelet

3.1.2 Non-orthogonal wavelets

Some wavelets have a scaling function which generates basis functions that are not polynomials, or some wavelets don't have a scaling functions (like Morlet wavelet). Such wavelets are categorized as nonorthogonal wavelets [56]. Nonorthogonal wavelets also known as *Crude wavelets*, which include *Gaussian Wavelets (Gaus)*, *Morlet*, *Mexican Hat (mexihat)*, *Complex Gaussian wavelets*, *complex Morlet wavelets*, *complex Shannon wavelets*, *complex frequency B − spline wavelets* [59].

The main properties of the nonorthogonal wavelets include the following: (*i*) some of the non-orthogonal wavelets do not have a scaling function ϕ, (*ii*) the analysis is not orthogonal and (*iii*) the mother wavelet ψ and its bases are not compactly supported and the reconstruction property is not insured. It is worth

mentioning that for the wavelets which do not have a scaling function, the analysis is carried out using wavelet bases [58].

The main difference between orthogonal and non-orthogonal wavelets, is that non-orthogonal wavelet systems provide a good balance between regularity and reduced support, while the orthogonal wavelets are more symmetric and smooth. Also, they must be truncated to achieve finite support [57]. However, non-orthogonal wavelets have complicated algorithms to carry out the wavelet analysis. Figure. 3.2 (a) shows the Morlet wavelet and Figure.3.1 (b) shows the MaxicanHat ($mexhat4$) wavelet

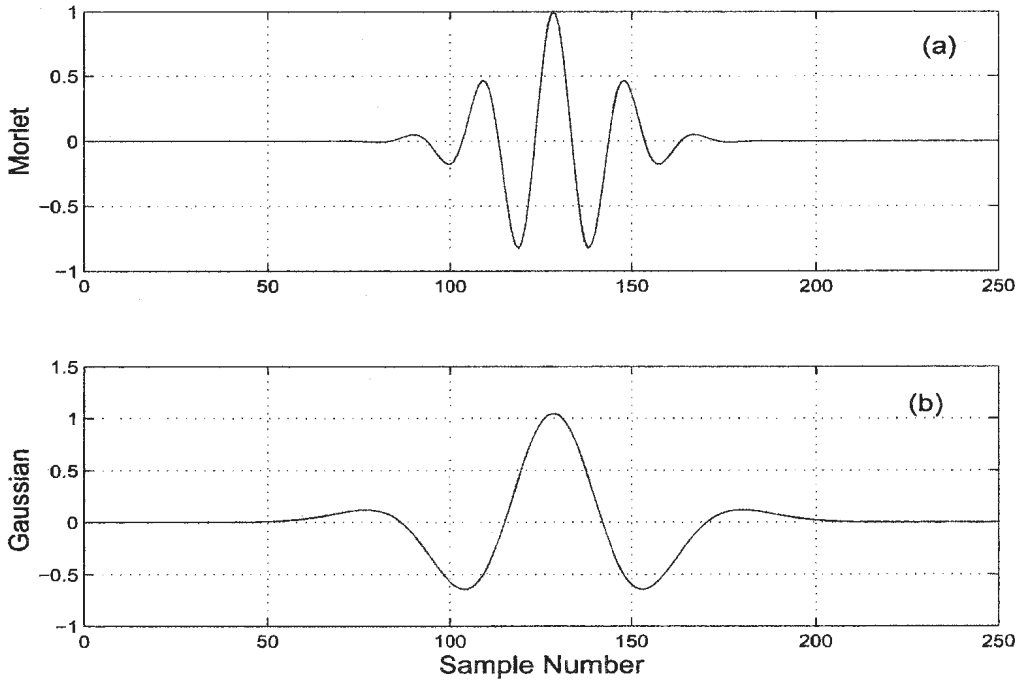

Figure 3.2: Nonorthogonal Mother wavelets, (a) the Morlet wavelet and (b) the Mexican Hat wavelet

3.2 Wavelet Transforms

The wavelet transform procedures are carried out to adopt a wavelet prototype function (the mother wavelet) to the processed signal. Temporal analysis is performed with a contracted high-frequency version of the mother wavelet, while frequency analysis is performed with a dilated, low-frequency version of the mother wavelet. The original signal or function can be represented in terms of a wavelet expansion (using coefficients in a linear combination of a set of basis functions generated by the scaling function). In general, wavelet transform provides the time and frequency information simultaneously; hence, giving a frequency-time representation of the processed signal through passing the time-domain signal from various high pass and low pass filters, which filters out either high frequency or low frequency portions of the processed signal. This procedure is repeated and every time some portion of the signal corresponding to some frequency is being removed from the signal.

The wavelet transforms like any other transform can be applied to both continuous and discrete signals. In the following subsections, the different forms of wavelet transforms along with their mathematical forms are introduced .

3.2.1 Continuous wavelet transform

The continuous wavelet transform (CWT) was developed as an alternative approach to the short time Fourier transform (STFT) to overcome the resolution problem. The wavelet analysis is done in a similar way to the STFT analysis, in the sense that the signal is multiplied by a function, *the mother wavelet*, similar to the window function in the STFT, and the transform is computed separately for different segments of the time-domain signal. However, there are two main differences between the STFT and the CWT [56].

- The Fourier transforms of the windowed signals are not taken, and therefore single peak will be seen corresponding to a sinusoid, i.e., negative frequencies are not computed.

- The width of the window is changed as the transform is computed for every single spectral component, which is probably the most significant characteristic of the wavelet transform, while the window width is fixed in the case of STFT.

The continuous wavelet transform of a continuous signal $x(t)$ using the mother wavelet $\psi(t)$ is defined as [53].

$$CWT_x^{\psi} = \Psi_x^{\psi}(a,b) = \frac{1}{\sqrt{|a|}} \int x(t)\psi\left(\frac{t-b}{a}\right) dt \tag{3.9}$$

As seen in equation (3.9) , the transformed signal is a function of two variables, namely a that represents the scale factor and b which represents the translation. The translation is related to the location of the window, as the window is shifted through the signal. This term, obviously, corresponds to time information in the transform domain. The parameter scale in the wavelet transform is similar to the scale used in geographical maps, where high scales correspond to a non-detailed global view (of the signal), and low scales correspond to a detailed view. Similarly, in terms of frequency, low frequencies (high scales) correspond to a global information of a signal (that usually spans the entire signal), whereas high frequencies (low scales) correspond to a detailed information of a hidden pattern in the signal (that usually lasts a relatively short time). Scaling, as a mathematical operation, either dilates or compresses a signal. Larger scales correspond to dilated (or stretched out) signals and small scales correspond to compressed signals. However, in the definition of the wavelet transform, the scaling term is used in the denominator, and therefore, the opposite of the above statements holds, i.e., scales $a > 1$ dilates

the signals whereas scales $a < 1$, compresses the signal. This interpretation of scale will be used throughout this thesis.

All the windows used are the dilated (or compressed) and shifted versions of the mother wavelet. Once the mother wavelet is selected the computation starts with $a = 1$ and the continuous wavelet transform is computed for all values of a, which may be smaller and/or larger than 1. However, depending on the signal, a complete transform is usually not necessary. For practical purposes, the signals are usually band limited, and therefore, computation of the transform for a limited interval of scales is usually adequate. For convenience, the procedure will start from scale $a = 1$ and will continue for increasing values of a, i.e., the analysis will start from highest frequency component in the time-domain signal and proceed towards low frequencies. This first value of a corresponds to the most compressed wavelet, and as the value of a is increased, the wavelet will dilate. The wavelet is placed at the beginning of the signal at the point which corresponds to time $(t = 0)$. The wavelet function at scale 1 is multiplied by the signal and then integrated over the region of support. The result of the integration is then multiplied by the constant number $1/\sqrt{|a|}$. This multiplication is for energy normalization purposes so that the transformed signal will have the same energy at every scale. The final result is the value of the transformation, i.e., the value of the continuous wavelet transform at time $(t = 0)$ and scale $a = 1$. In other words, it is the value that corresponds to the point $b = 0$, $a = 1$ in the frequency-time plane.

The wavelet at scale $a = 1$ is then shifted towards the right by b to the location t = b , and the above equation is computed to get the transform value at t = b , $a = 1$ in the frequency-time plane. This procedure is repeated until the wavelet reaches the end of the signal. One row of points on the time-scale plane for the scale $a = 1$ is now completed. Then, a is increased by a small value. Since it is a continuous transform, both b and a must be incremented continuously . Figure 3.3

shows a hierarchy of a wavelet transform for fixed translation and variable scaling for $j = 0, 1, 2$ (the scale $a = 2^{-j}$) and $b = 0$ (the translation) producing $\psi_{j,0}$, using the Daubechies [*db*4] mother wavelet [59].

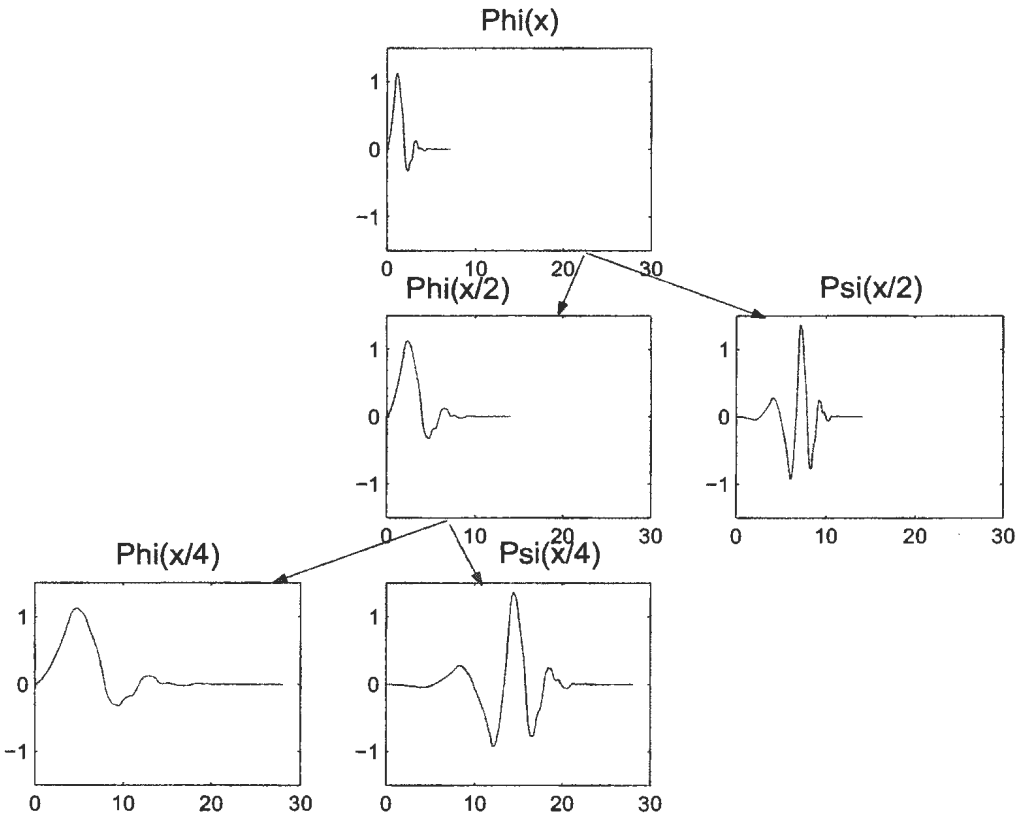

Figure 3.3: The Two-Level Wavelet Transform Using Daubechies [*db*4] Wavelet

If this transform needs to be computed by a computer, then both parameters are increased by a sufficiently small step size. Every computation for a given value of a fills the corresponding single row of the time-scale plane. When the process is completed for all desired values of a, the continuous wavelet transform of the signal has been calculated. The definition of the CWT shows that the wavelet transform is a measure of similarity between the wavelet bases (daughter wavelets) and the processed signal itself. Here the similarity is in the sense of similar frequency content. The calculated CWT coefficients refer to the closeness

of the signal to the wavelet at the current scale (level of resolution). If the signal has a major component of the frequency corresponding to the current scale, then the daughter wavelet (the window function) at the current scale will be similar or close to the signal at that particular location where this frequency component occurs. Therefore, the CWT coefficient computed at this point in the time-scale plane will be a relatively large number.

3.2.2 Discrete wavelet transform

The main idea of the discrete wavelet transform (DWT) is the same as it is in the CWT, a time-scale representation of a digital signal using digital filtering techniques. The continuous wavelet transform was computed by changing the scale of the analysis window, shifting the window in time, multiplying by the signal, and integrating over the region of support of the mother wavelet. In the discrete case, filters of different cutoff frequencies are used to analyze the signal at different scales. The signal is passed through a series of high pass filters to analyze the high frequencies, and through a series of low pass filters to analyze the low frequencies. The resolution of the signal, which is a measure of the amount of detail information in the signal, is changed by the filtering operations, and the scale is changed by downsampling operations. Downsampling a signal corresponds to reduce the sampling rate, or remove some of the samples of the signal. For example, downsampling by two refers to dropping every other sample of the signal. Downsampling by a factor n reduces the number of samples in the signal n times [53, 54].

The procedure starts with passing the signal (sequence of data) $x[n]$ through a half band digital lowpass filter with impulse response $g[n]$ and a half band digital highpass filter with impulse response $h[n]$. Filtering a signal corresponds to the mathematical operation of convolution of the signal with the impulse response of

the filter. The convolution operation in discrete time is defined as [56]

$$x[n] * G[n] = \sum_{k=-\infty}^{\infty} x[k]G[n-k] \tag{3.10}$$

where $G[n]$ is the impulse response of a filter or any other time-invariant system. The unit of the frequency is of a particular importance in this transform. In discrete signals, frequency is expressed in terms of radians. Accordingly, the sampling frequency of the signal is equal to 2π radians in terms of radian frequency. Therefore, the highest frequency component that exists in a signal will be π radians, if the signal is sampled at Nyquist rate (which is twice the maximum frequency that exists in the signal); that is, the Nyquist rate corresponds to π rad/s in the discrete frequency domain [55]. The DWT analyzes the signal at different frequency bands with different resolutions by decomposing the signal into a coarse approximation and detail information. The DWT employs two sets of functions, called scaling functions and wavelet functions, which are associated with low pass and highpass filters, respectively. The original signal $x[n]$ is first passed through a halfband highpass filter $h[n]$ and a lowpass filter $g[n]$ [46, 47]. One important property of the discrete wavelet transform is the relationship between the impulse responses of the highpass and lowpass filters and they are not independent of each other, rather they are related by the following expression [46]

$$h[L-1-n] = (-1)^n g[n] \tag{3.11}$$

where L is the filter length (dimension). The two filters are odd index alternately reversed versions of each other. Lowpass to highpass conversion is provided by the $(-1)^n$ term. Filters satisfying this condition are commonly used in signal processing, and they are known as the *Quadrature Mirror Filters* (QMF) bank. This filter bank structure is illustrated later in this chapter.

After the filtering, half of the samples can be eliminated according to the Nyquists rule, since the signal now has the highest frequency of π /2 radians instead of π . The signal can therefore be downsampled by 2, simply by discarding every other sample. This constitutes one level of decomposition and can mathematically be expressed as [54]:

$$d1[n] = \sum_k x[k]h[2n-k] \tag{3.12}$$

$$a1[n] = \sum_k x[k]g[2n-k] \tag{3.13}$$

where $d[n]$ is the output of the halfband highpass filter known as *details* and '1' refers to the first level of resolution, and $a[n]$ is the output of the halfband lowpass filter known as *approximations* and '1' refers to the first level of resolution as well. The frequencies that are most prominent in the original signal will appear as high amplitudes in that region of the DWT signal which includes those particular frequencies. The difference of this transform from the Fourier transform is that the time localization of these frequencies will not be lost [46, 48]. However, the time localization will have a resolution that depends on which level they appear. If the main information of the signal lies in high frequencies, as it happens most often, the time localization of these frequencies will be more precise, since they are characterized by more number of samples. If the main information lies only at very low frequencies, the time localization will not be very precise, since few samples are used to express signal at these frequencies. This procedure in effect offers a good time resolution at high frequencies, and good frequency resolution at low frequencies [56]. The DWT has a decomposition tree shown in Figure 3.4 that employs the halfband highpass filters H and halfband lowpass filters G as basic steps in the decomposition process.

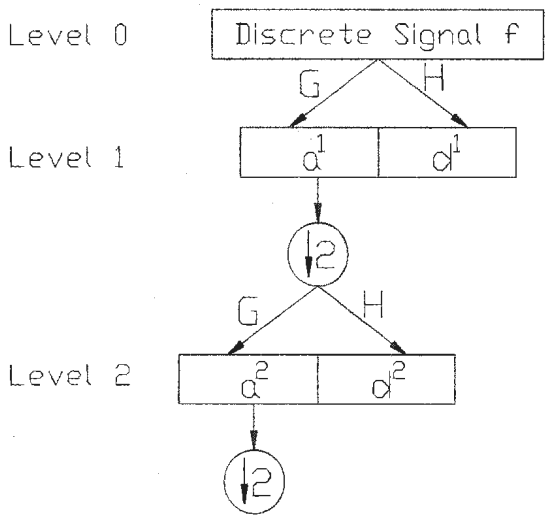

Figure 3.4: Decomposition of The signal $f[n]$ by DWT

3.2.3 Wavelet packet transform

The wavelet Packet Transform (WPT) is a generalized version of the discrete wavelet transform in a way that each level of resolution (also known as *octave*) j consists of 2^j boxes, generated by a tree of lowpass and highpass filter operations. Therefore, the frequency bandwidth of a box decreases with growing octave number. In other words, with increasing octave number the frequency resolution becomes higher while the time resolution is reduced. Starting with the signal $x[n]$ with length N, the first level decomposition will produce $d^1[N/2]$ and $a^1[N/2]$ as the discrete wavelet transform. The second level decomposition will produce four subbands due to the decomposition of both $d^1[N/2]$ and $a^1[N/2]$ using the same set of filters in the case of DWT or the same mother wavelet in case of CWT. These four subbands are $aa^2[N/4]$, $ad^2[N/4]$, $da^2[N/4]$ and $dd^2[N/4]$. Thus the ordinary discrete wavelet decomposition is a subtree of the wavelet packet decomposition. The main advantage of WPT over both the CWT and DWT is better, more ac-

curate and more detailed representation of the decomposed signals. Also, wavelet packet basis functions are localized in time offering better signal approximation and decomposition. These basis functions are generated from one base function at scale s, oscillation c and location b given as [54]

$$w_{s,c,b} = 2^{j/2} W_c \left(2^{-j}(n-b)\right) \tag{3.14}$$

In wavelet packet analysis, a signal $f[n]$ is represented as a sum of orthogonal wavelet packet basis functions $w_{s,c,b}$ at different scale s, oscillation c and location b given as [54]

$$f[n] = \sum_s \sum_c \sum_b w_{s,c,b} W_{s,c,b}[n] \tag{3.15}$$

The most recent application of WPT is in pattern recognition, particularly in transient detection that is much simpler task than the generalized pattern recognition case. This task can be achieved using matched filters, whose coefficients are determined from wavelet bases, which can provide the least entropy. On the other hand, WPT has many applications mainly in image processing, denoising and edge detection [54]. The WPT has a decomposition tree shown in Fig. 3.5 that employs the DWT as part of its general decomposition process [54, 57].

3.3 Multiresolution Analysis

Multiresolution analysis (MRA) and wavelet transforms (WT) are new frequency-time analysis tools that have been developed in recent years, and they are widely used in digital signal processing (DSP) applications. These approaches make sense especially when the signal at hand has high frequency components for short durations and low frequency components for long durations. A function or a signal

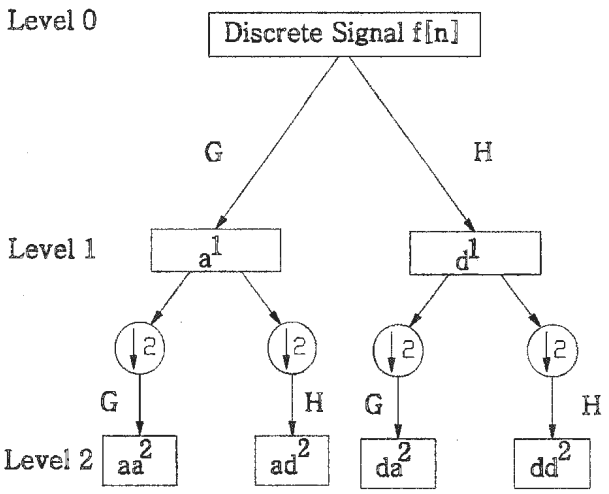

Figure 3.5: Decomposition of the signal $f[n]$ by WPT

can be viewed as a composition of a smooth background (approximations $a(t)$) and fluctuations (details $d(t)$) on top of it. The distinction between the smooth part and the details is determined by the resolution, that is, by the scale below which the details of a signal can not be discerned. At a given resolution, a signal is approximated by ignoring all fluctuations below that scale. At each stage of the increase in resolution, finer details are added to the coarser description, providing a successively better approximation to the signal. Eventually, when the resolution goes to infinity, we recover the exact signal. The above approach to this kind of description can be made more precise by considering a signal $f(t)$ composed as [56, 57].

$$f(t) = \sum_{j=1}^{\infty} a_j(t) + \sum_{j=1}^{\infty} d_j(t) \tag{3.16}$$

The effective implementation of multiresolution analysis has four requirements given as [55–57].

1. The multiresolution analysis involves a decomposition of the function space

into a sequence of subspaces, and each subspace must be contained in the higher subspaces. This requirement implies that a new level of resolution can be created by dilating the mother wavelet without any loss of information in the decomposed signal, and also to ensure orthogonality of the basis functions at all levels of resolutions.

2. As the resolution gets coarser and coarser, more and more details are removed in such a way that as $j \rightarrow \infty$, only a constant frequency component remains

3. All the spaces V_j are scaled versions of the central space V_0, that is, if $x(t)$ does not contain any fluctuations (transient components)at scales smaller than $1/2^j$, then $x(2t)$ will not contain any fluctuations at scale smaller than $1/2^{j+1}$

4. If the signal $x(t) \in V_0$ and do all its integer shifts $x(t-m)$, then all the subspaces V_j are shift-invariance. Conditions 3 and 4 deal with the dilation and translation of signals, and both imply that if $x(t) \in V_0$, then $x(2^j t - m) \in V_j$

The requirements of the multiresolution analysis ensure the ability of the scaling function $\phi(t)$ to generate orthogonal basis functions at each level of resolution.

In the case of the continuous wavelet transform, the MRA is implemented through the correlation between the mother wavelet at different scales and the signal with the scale (or the frequency) being used as a measure of similarity. In DWT case, filters of different cutoff frequencies are used to analyze the signal at different scales. The signal is passed through a series of high pass filters to analyze the high frequencies, and it is passed through a series of low pass filters to analyze the low frequencies. As was stated before, the cascade filtering of the signal at different scales produces details (output of high pass filters) and

approximations (the output of low pass filters). Such a structure can perform a multiresolution analysis (MRA). The case of DWT implies that digital filters are used, and downsampling is used to change the frequency band at each resolution j. The next subsection illustrates the digital filtering procedure in implementing MRA for the case of discrete wavelet transform.

3.3.1 Quadrature mirror filter banks

An orthonormal wavelet basis function of $L^2(R)$ is formed by dilating and translating the mother wavelet $\psi[n]$ given as [54]

$$\psi_{j,k}[n] = 2^{-j/2}\psi[2^{-j}n - k]; j, k \in Z \tag{3.17}$$

The mother wavelet usually has m vanishing points and satisfies the following two-scale difference equation given as [54]

$$\psi[n] = \sqrt{2}\sum_{k=0}^{L-1} h_k \psi[2n - k] \tag{3.18}$$

The companion scaling function $\phi[n]$ for the mother wavelet $\psi[n]$ can generate a set of orthonormal compactly supported basis functions in $L^2(R)$ as well, which are given as [54]

$$\phi_{j,k}[n] = 2^{-j/2}\phi[2^{-j}n - k]; j, k \in Z \tag{3.19}$$

Based on the fact that scaling function property of having an average of '1' over the region of support, it satisfies a two-scale difference equation given as [54]

$$\phi[n] = \sqrt{2}\sum_{k=0}^{L-1} g_k \phi[2n - k] \tag{3.20}$$

Since both the wavelet bases and the basis functions satisfy the requirements needed to form a MRA, then the discrete wavelet analysis is a MRA. On the other

hand, the two coefficient sets h_k and g_k have the same finite length L for a certain wavelet bases, where L is related to the number of vanishing points of $\psi[n]$. For example, $L = 2m$ for the case of Daubechies wavelet family. The MRA is basically decomposing a signal to transients details and fine approximations depending on the similarity to the used wavelet at each level of resolution, then the coefficients h_k and g_k represent filter set coefficients. On the assumption that transients represent the high frequency components in the signal, the set $\{h_k\}_{k=0,1,2,...,L-1}$ represents a highpass filtering function and $\{g_k\}_{k=0,1,2,...,L-1}$ represents a lowpass filtering function. This filter set is known as *Quadrature Mirror Filter (QMF)* banks. The coefficients h_k and g_k are not independent of each other, rather they are related by the relation given as [54, 57].

$$h_k = (-1)^k g_{L-k}; k = 0, 1, 2, ..., L-1 \tag{3.21}$$

These particular digital filter structures allow signals to be divided into frequency sub-bands and decimated without any loss of information. The main advantages of this filter bank are [47, 48]

- The localization of quantization noise into the frequency sub-bands that prevents noise interference between the bands
- The enabling of bit resource allocation to the frequency sub-bands signals according to certain spectral criteria
- Since both $H_k(j\omega)$ and $G_k(j\omega)$ have linear phase, the system introduces no phase distortion

The basic process of QMF filtering is designed to overcome the effect of non ideal transition-band and stop-bands filtering. The non-zero signal energy in the transition and stop bands is reflected back into the pass-band. The interpolation

process at the receiver usually causes aliasing in conventional filter banks. This aliasing is eliminated in QMF banks during reconstruction of the signal, thus allowing accurate reconstruction. In addition, in the QMF banks each filter is described using a minimal set of parameters which are directly related to the zeros of the filter. This property permits to construct filters with any preassigned set of zeros in the stopband. In particular, filters are constructed such that for each fixed order, the maximally flat filters are generated by wavelets that have maximum number of vanishing points (like biorthogonal and orthogonal wavelets) [47, 58, 59]. Moreover, the QMF banks have a specified minimum stopband attenuation of the composite magnitude-frequency response, in other words, they have minimum stopband attenuation for the individual filters in the QMF banks. The QMF banks still have real coefficients and almost linear phase even with a mother wavelet that is asymmetric [59]. In this context, the orthogonal wavelets are capable of constructing finite impulse response (FIR) filters [47]. Figure 3.6 shows the structure of a typical two stages QMF filter bank for both analysis and synthesis.

3.4 Selection of the Mother Wavelet

The most attractive features of the wavelet theory over other signal processing theories are the multiresolution analysis and the frequency-time localization. The wavelet analysis admits a nonuniform bandwidths, such that the bandwidth is higher at higher frequencies, making it possible to implement the wavelet analysis through different levels of decimation in a filter bank. The wavelet basis functions are generated by dilating and shifting the mother wavelet $\psi(t)$. The wavelet function is not unique and its design can be related to the design of a power symmetric FIR lowpass filter. Obviously, different mother wavelets are capable

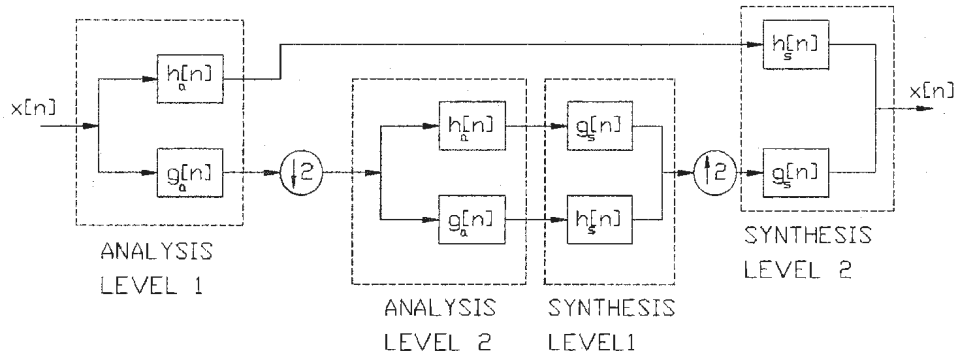

Figure 3.6: Two Level Typical Analysis-Synthesis Quadrature Mirror Filter Bank

of producing different FIR filters. However, appropriate selection of the mother wavelet for signal representation can maximize the advantages of this technique. Different wavelets are suitable for different signals representation or approximation [60]. If the selected wavelet function contains enough information about the signal, then the multiresolution analysis will be simplified in terms of the required number of levels and the computational complexity [54, 60].

The key for optimal wavelet function selection lies in the appropriate parametrization and the adequate performance measure, in addition to the accurate interpretation of the physical phenomenon [60]. A particular setup for the problem of selecting the mother wavelet can be defined as the selection of orthonormal discrete basis function with compact support, which helps in implementing the wavelet transform using digital computers. Such compactness provides means of isolation and detection of signals at certain region, which has proved useful in many applications of signal processing [54, 56, 59].

3.4.1 Best-basis selection

The best-basis function selection allows optimal signal representation and minimize the required number of levels of resolution, resulting in less computational efforts. The determination of the best-basis functions or the wavelet coefficients, namely the details and approximations are to be calculated to a desired level depending on the nature of the signal being represented. Then the entropy can be used to measure the efficiency of these basis functions. The entropy of a signal $x[n] = [x_0, x_1, ..., x_{N-1}]$ is defined as [54].

$$H(x) = -\sum_{n}^{N-1} |x_n|^2 \, log \, |x_n|^2 \tag{3.22}$$

The best-basis or the wavelet coefficients are those capable of providing the minimum entropy or maximum information for their distribution [54, 60]. To determine the optimal number of levels of resolution, the entropy is evaluated at each level, when there is a new level j such that [54].

$$H(x)_j \geq H(x)_{j-1} \tag{3.23}$$

then the level j is redundant and can be omitted, this indicates that the multiresolution analysis up to level $j-1$ is enough to represent the signal $x[n]$ [54].

3.4.2 Minimum description length criterion

The minimum description length (MDL) criterion is an approach to select the optimal number of wavelet coefficients to be retained for the signal reconstruction. The MDL method is free from any parameter settings or thresholding, which makes it adequate for data compression and denoising applications [54, 58, 60]. The algorithm for this approach is basically picking a function known as MDL(k, n)

index defined for a signal $x[n]$ as [54] .

$$MDL_x(k,j) = min\left\{\frac{3}{2}log(N) + \frac{N}{2}log\left\|\alpha_{x,j}^{\sim} - \alpha_{x,j}^{(k)}\right\|^2\right\} \tag{3.24}$$

where $0 \leq k < N$ which represents the length of the signal $x[n]$, $1 \leq j < M$ the total number of wavelet filters (levels of resolution) used for the decomposition of the signal $x[n]$, $\alpha_{x,j}^{\sim} = W_{x,j}x[n]$ denotes to the vector of decomposition coefficients of $x[n]$ up to level j, $\alpha_{x,j}^{(k)} = \Theta^{(k)}W_{x,j}x[n]$ denotes to the vector that contains k non-zero elements and $\Theta^{(k)}$ is the hard-thresholding operation that keeps the k largest elements of $\alpha_{x,j}^{\sim}$ in absolute value intact and set all other elements to zero [54]. The vectors $\alpha_{x,j}^{\sim}$ and $\alpha_{x,j}^{(k)}$ have to be normalized by $\|\alpha_{x,j}^{\sim}\|$ so that the magnitude of each coefficient in $\alpha_{x,j}^{\sim}$ and $\alpha_{x,j}^{(k)}$ vectors is strictly less than 1. The first term of the MDL index represents the penalty function that is increasing linearly with the number of the retained wavelet coefficients k, while the second term describes the logarithmic energy residual between $\alpha_{x,j}^{\sim}$ and $\alpha_{x,j}^{(k)}$. It should be noted that the residual energy decreases as k increases. The number of coefficients k for which the MDL function reaches its minimum value, is considered as an optimal one. The wavelet filters can be optimized using the MDL criterion as well. It should be noted that a wavelet filter which is optimal for a signal, is not necessarily the best for another type of signals [54, 60].

The application of the MDL for the case WPT is employed for transformer protection with real data from the protected transformer, along with the selection of the optimal mother wavelet are provided in the next chapter. The off-line testings using the selected mother wavelet and the optimal number of levels of resolution are also provided in chapter 4.

Chapter 4

Data Acquisition and Mother Wavelet Selection

This chapter provides an overview of the experimental setup for data acquisition to test the wavelet packet based-technique. The collected data are mainly used for off-line testings and for applying the minimum description length (MDL) criterion to select the mother wavelet, and also to determine the optimal number of levels of resolution needed to identify the type of currents flowing through the power transformer. The selection of the mother wavelet may be done using simulated data, but the actual data is necessary for accurate selection. Moreover, the sampling imperfections (like jumps which may be considered as transients) should be taken into consideration when optimizing the number of the needed levels of resolutions. Therefore, reliable and real data are needed for accurate application of the MDL. The selection of a mother wavelet $\psi(t)$ is based on selecting a mother wavelet, out of available orthogonal or nonorthogonal mother wavelets, which has the minimum MDL index. Once the mother wavelet is selected, the optimal number of levels of resolution can be determined.

The experimental setup for data acquisition, transformer connection with cur-

rent transformers, sampling the differential current and the interface with the PC are explained first. Then, the procedure for applying the MDL criterion on the collected data both to select the mother wavelet and to determine the optimal number of levels of resolution is provided. Finally, the selected mother wavelet for the wavelet packet transform along with the optimal number of levels of resolution are tested off-line using *Mathworks* / MATLAB on the collected data from one of the two protected three-phase power transformers.

4.1 Experimental Setup and Data Acquisition

One of the initial and important steps in this work is to setup the protected transformer with all the necessary instrumentations to accurately collect the needed data. The needed data consist mainly of different magnetizing inrush (loaded, unloaded and for different switching angles) and internal fault currents (both primary and secondary phase to ground, phase to phase and three phase). The collected data are to be employed for selecting both the mother wavelet and the optimal number of levels of resolution. In addition, they are to be used for off-line testings of the proposed wavelet packet-based protection technique. In this work, a 5 kVA, 230/550-575-600 V, Δ-Y, core type, 60Hz three-phase laboratory prototype power transformer and a 2kVA, 127-220/31.8-42-63.5 V, Δ-Y, 50Hz, multi-tap three-phase power transformer are to be protected. However, all the data are collected from the core type 5 kVA power transformer. The experimental setup is shown in Figure 4.1. As mentioned in chapter 1, the current transformers (CTs) are connected in an opposite order to the power transformer winding connection, to step down both the primary and the secondary currents. Three identical CTs are connected in Y on the Δ connected primary side of power transformer, while another three identical CTs are connected in Δ on the Y-connected secondary side

of the power transformer. The ratios of the primary side CTs and the secondary side CTs are chosen in a manner that guarantees a negligible value (approximately zero) of the differential current under steady-state operating conditions. The differential current is measured at point 'Q' in Figure 4.1 in all the data acquisitions throughout all steps in this work. The differential current is collected using Tektronics 2212 storage digital oscilloscope, which samples the data at sampling rate (f_s) of 10 kHz. In the following subsections the different types of current data collections are explained along with the data collection procedure.

4.1.1 Magnetizing inrush current data acquisition

Magnetizing inrush current depends on many factors, such as, the residual magnetisim, loading conditions of power transformer and the switching angle γ. These aforementioned factors can vary the waveform of the magnetizing inrush current, thus, the effect of these factors has to be considered when acquiring different magnetizing inrush currents data. To acquire the data for magnetizing inrush current, the power transformer is energized at random (different values of γ) for both the loaded and the unloaded conditions. For the loaded conditions throughout this work, a three-phase Y-connected resistive and inductive loads are used.

The current waveform obtained from the secondary side of the CTs as in Figure 4.1, using current probes, is stored in the digital oscilloscope after being sampled, then downloaded to a personal computer (PC) through a serial bus. The software package *Grab* 2212 is used to download the collected waveforms from the oscilloscope, and convert them to data files for further processing. For each case of acquiring a current waveform, three identical TRIAC switches provide a contact between the voltage source and the power transformer. These TRIAC switches are controlled by a triggering circuit constructed mainly from pulse-generator IC's (555 timers), which is activated by a single push-button switch. The circuit dia-

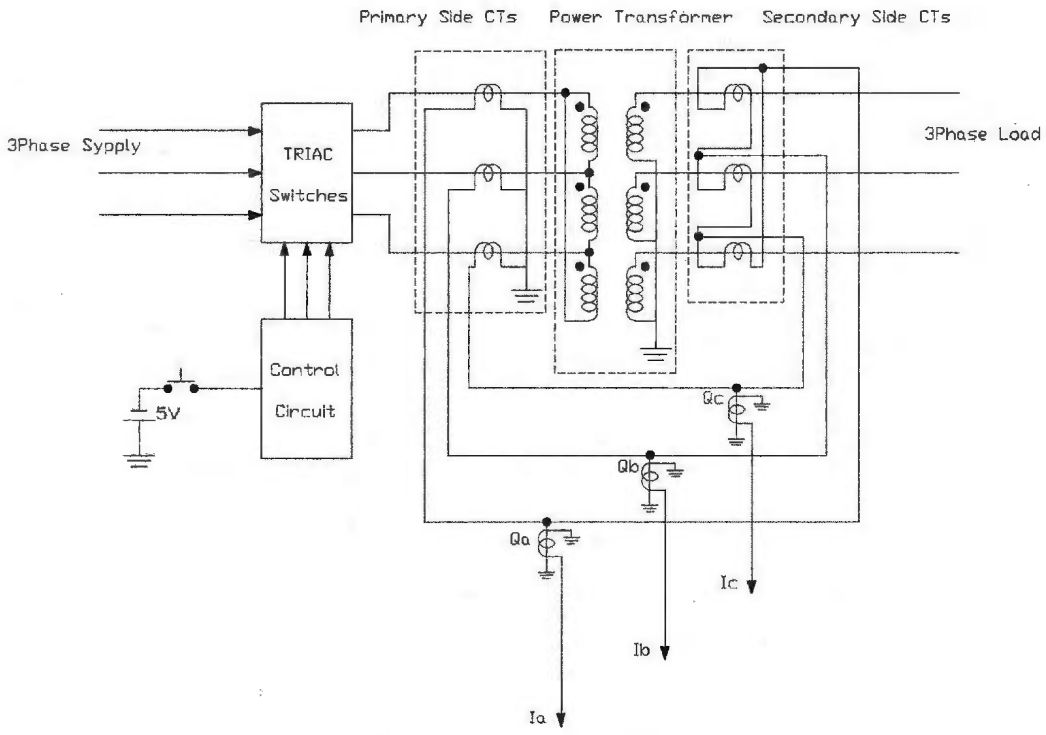

Figure 4.1: Experimental Setup for Data Acquisition

gram is shown in Figure 4.2. The contact is made for a short time (almost 5 cycles based on 60 Hz systems) such that the data files would have a reasonable size.

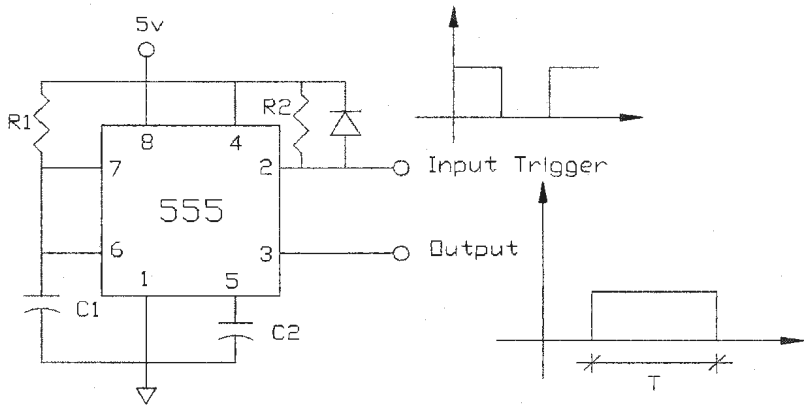

Figure 4.2: The Triggering Circuit Connection, R1= 100 kΩ, C1= 1 μF, R2=10kΩ, C2=0.01 μF and T=1.1R1C1= 0.1 sec

4.1.2 Internal fault currents data

There are large number of different types of internal faults that a power transformer may experience. Different faults may occur either before or after energizing the power transformer, or with both load and no-load conditions. The different internal faults considered for data acquisition in this work include:

1. Primary side faults:

    - single phase to ground fault unloaded and before energization
    - single phase to ground fault unloaded and after energization
    - single phase to ground fault loaded and before energization
    - single phase to ground fault loaded and after energization

- phase to phase fault loaded and before energization
- phase to phase fault loaded and after energization

2. Secondary side faults:

   - single phase to ground fault loaded and after energization
   - between taps loaded and after energization
   - between taps loaded and before energization
   - phase to phase fault loaded and after energization
   - three-phase to ground fault loaded and after energization

For each case of the collected current waveforms, the data are stored in a separate file for further processing. In all the collected internal fault currents data, the duration of the fault was ensured to be less than 5 cycles to prevent any damage of power transformer windings or other instruments. Also, the supply line voltage was set to 50 V to reduce the fault current so as to avoid any damage to the power transformer. In addition, high fault currents may cause CT saturation, but still this effect has to be considered for reliable differential relay testing.

It should be noted that in case of normal or through-fault currents, the power transformer was energized before the data was collected.

In the next chapter, the experimental setup for the on-line testings, which is very close to the setup for data acquisition, along with more cases of internal fault currents, will be detailed.

4.2 The Selection of the Mother Wavelet and the Optimal Number of Levels of Resolution

At this stage, the data files are ready and they can be used for selecting both the mother wavelet and the optimal number of levels of resolution. As mentioned in chapter 3, the mother wavelet can be selected from many known wavelets both of orthogonal and nonorthogonal types. In the next subsections, the MDL criterion is applied on the collected data, initially to select the mother wavelet. Once the mother wavelet is selected, the MDL criterion is applied again to determine the optimal number of levels of resolution using the selected mother wavelet.

4.2.1 Selecting the mother wavelet

There are several known wavelets including the orthogonal wavelets (Daubechies family, Coiflet family, Meyer and Symlet family), biorthogonal wavelets (mainly the B-spline biorthogonal wavelet family) and the nonorthogonal wavelets (Morlet, Gaussian and Mexican Hat). According to equation (3.24), the MDL index is calculated after the wavelet coefficients are determined. The wavelet coefficients can be determined using the following relation [51, 53, 56]

$$\alpha = W_\psi x[n] \tag{4.1}$$

where, W_ψ is an orthogonal square matrix contains the row basis vectors. the row basis vectors are specified by numbers known as wavelet and scaling filter coefficients generated according to the mother wavelet ψ. In other words, the elements of the square matrix W_ψ are the coefficients of the discrete wavelet series. The elements of W_ψ can then be determined by discretizing the continuous wavelet transform CWT. In this work, the elements of W_ψ are determined using

the *Mathworks* MATLAB/Wavelet Toolbox for each candidate mother wavelet. When the matrix W_ψ is ready for all the candidate mother wavelets, the MDL criterion can be applied to the collected data with each of the candidate mother wavelets using equation (3.24). The candidate mother wavelets for this work are:

- Orthogonal Wavelet Families
    1. Daubechies ($db4$)
    2. Coiflet ($coif4$)
    3. Symlet ($Sym4$)
    4. B-Spline ($bior2.2$)
    5. Meyer
- Nonorthogonal Wavelet Families
    1. Morlet
    2. Gaussian ($gaus4$)

The MDL is applied for each candidate mother wavelet with three types of collected data, which are normal full load current representing a through-fault current, primary single phase-to-ground fault and unloaded magnetizing inrush currents. The coefficients are calculated up to the second level of resolution for each candidate wavelet. The results of evaluating the MDL index for the normal current data are provided in Table 4.1.

The evaluations of the MDL index for the unloaded magnetizing inrush current data are provided in Table 4.2

The evaluations of the MDL index for the primary side single phase-to-ground fault current data are provided in Table 4.3

Tables 4.1 through 4.3 show the MDL index evaluated for the three types of real data representing three different current waveforms. The evaluation of the MDL

Mother Wavelet	MDL(1)	MDL(2)
*coif*4	6.4993	6.5010
*db*4	5.7926	6.4153
*sym*4	5.9773	6.4357
*bior*2.2	6.3351	6.3897
Morlet	6.4410	6.5064
*gaus*4	6.5973	6.2569
Meyer	6.2313	6.1491

Table 4.1: Two Levels MDL Index Evaluations for Normal Current Data

Mother Wavelet	MDL(1)	MDL(2)
*coif*4	6.7977	6.7702
*db*4	6.5349	6.7488
*sym*4	6.5953	6.7564
*bior*2.2	6.7433	6.7511
Morlet	6.7847	6.7900
*gaus*4	6.8185	6.6858
Meyer	6.6985	6.6617

Table 4.2: Two Levels MDL Index Evaluations for Unloaded Magnetizing Inrush Current Data

indices shows that the Daubechies wavelet family has the smallest MDL indices for the three types of current data. Moreover, the MDL indices for the second level of resolution also are small, but not the smallest for the three tested current data. Based on the first level MDL index, the Daubechies mother wavelet can be employed to carry out a MRA with the highest degree of similarity between the approximations and the original signal [54]. In other words, the approximations can contain most of the information about the signal when moving from a lower level of resolution to a higher one. The Daubechies mother wavelet is selected to be employed in all the wavelet transforms needed for both the off-line and the on-line testing of the proposed algorithm.

Mother Wavelet	MDL(1)	MDL(2)
$coif4$	6.5680	6.5848
$db4$	5.8842	6.5044
$sym4$	6.0645	6.5187
$bior2.2$	6.4018	6.4639
$Morlet$	6.5082	6.5973
$gaus4$	6.6579	6.3949
$Meyer$	6.3036	6.2246

Table 4.3: Two Levels MDL Index Evaluations for Primary Side Single Phase-to-Ground Fault Current Data

4.2.2 The optimal number of levels of resolution

The optimal number of levels of resolution indicates the minimum number of changing the scale during the MRA without violating the synthesis of the decomposed signal. The number of levels can provide information about the signal frequency components, or the nature of the high frequency components superimposed on a signal. This condition for the minimum number of scaling has an effect on the computations to decompose the signal, and can provide the ability to realize the MRA. The determination of the optimal number of levels of resolution can be done using the MDL criterion, once the mother wavelet is selected. As mentioned in chapter 3, the MDL criterion states that the optimal level of resolution j is reached when $\text{MDL}(j) \leq \text{MDL}(j+1)$. Applying this criterion on the same current data that are used to select the mother wavelet using the selected mother wavelet up to the 4^{th} level of resolution, gives the MDL indecies as provided in Table 4.4.

From the values of the MDL index, the first levels have the lowest values. These low values of MDL(1) are due to to the jumps of the data at the switching instant and some missing data. Thus, MDL(1) may not provide accurate indication. However, evaluating the MDL index at the second and higher levels of

Current Data	MDL(1)	MDL(2)	MDL(3)	MDL(4)
Normal	5.7926	6.4153	6.8642	7.5342
Unloaded Inrush	6.5349	6.7488	7.0649	7.6231
Primary Side SPG Fault	5.8842	6.5044	7.0045	7.3569

Table 4.4: Four Levels MDL Index Evaluations Using Daubechies Mother Wavelet ($db4$)

resolution will always include more detailed representation of the signal. It is to be noted that, at higher levels the values of MDL index tend to decrease (MDL(2) $\leq$ MDL(3) $\leq$ MDL(4)). According to Table 4.4, the second level of resolution is selected as the optimal level of resolution for the wavelet packet-based differential relay algorithm. Figures 4.3 through 4.8 provide the time location diagrams of the wavelet packet coefficients representing first level details (d^1), and both second level details (da^2) and (dd^2) for different current data using the selected mother wavelet. These figures clearly show the existence of the (dd^2) in all cases of internal fault currents data, and its absence in both cases of magnetizing inrush and normal current data.

These diagrams give the basic approach of applying the WPT in power transformer protection, where the needed informations can be obtained from the second level details dd^2. This information can be thought of as signatures, which are able to provide accurate and reliable diagnosis of the differential current. In other words, such information provide the basic step in constructing the desired disturbance classifier.

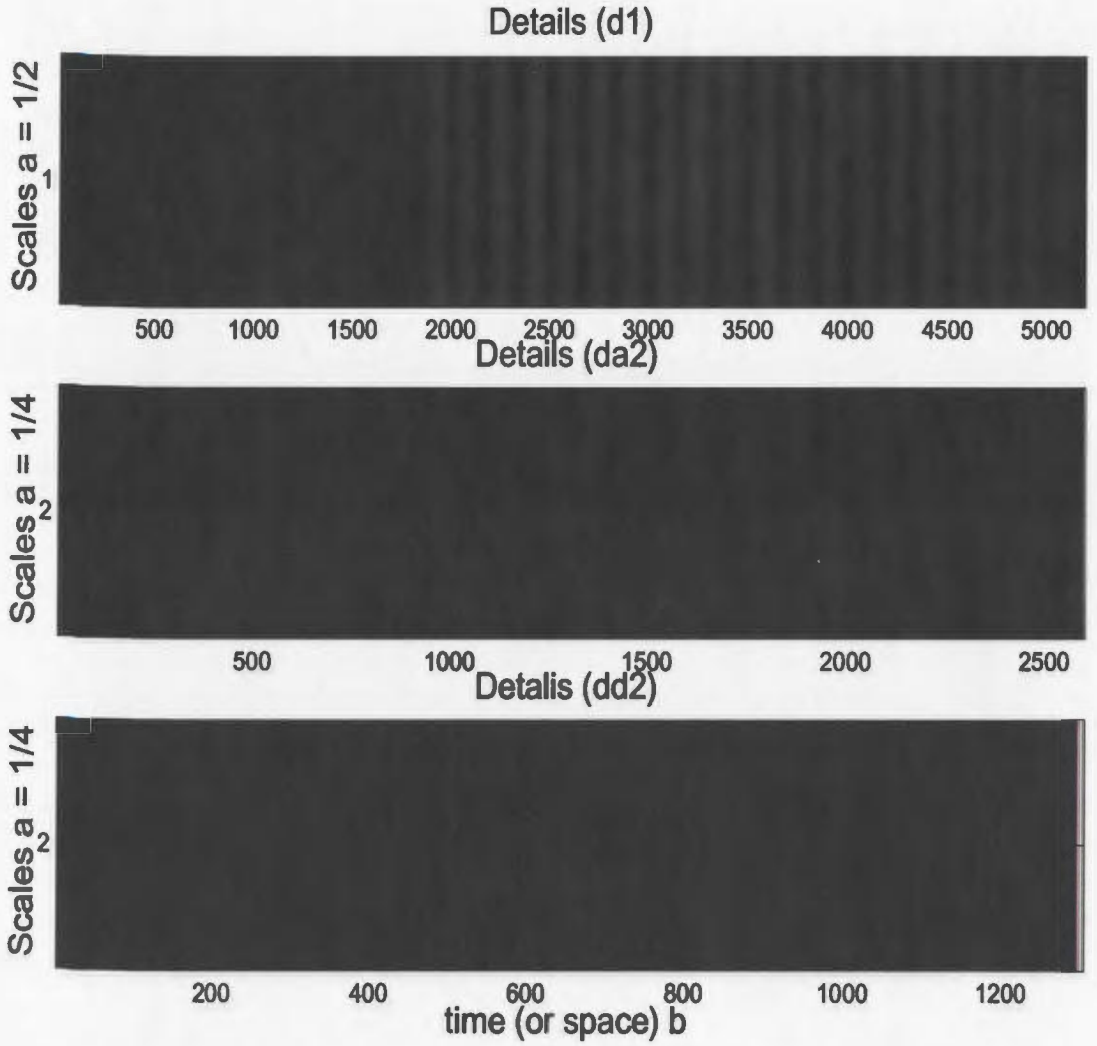

Figure 4.3: Two Level Evaluation of the Wavelet Packet Coefficients for the Normal Current (Resistive Load) Using ($db4$) Mother Wavelet

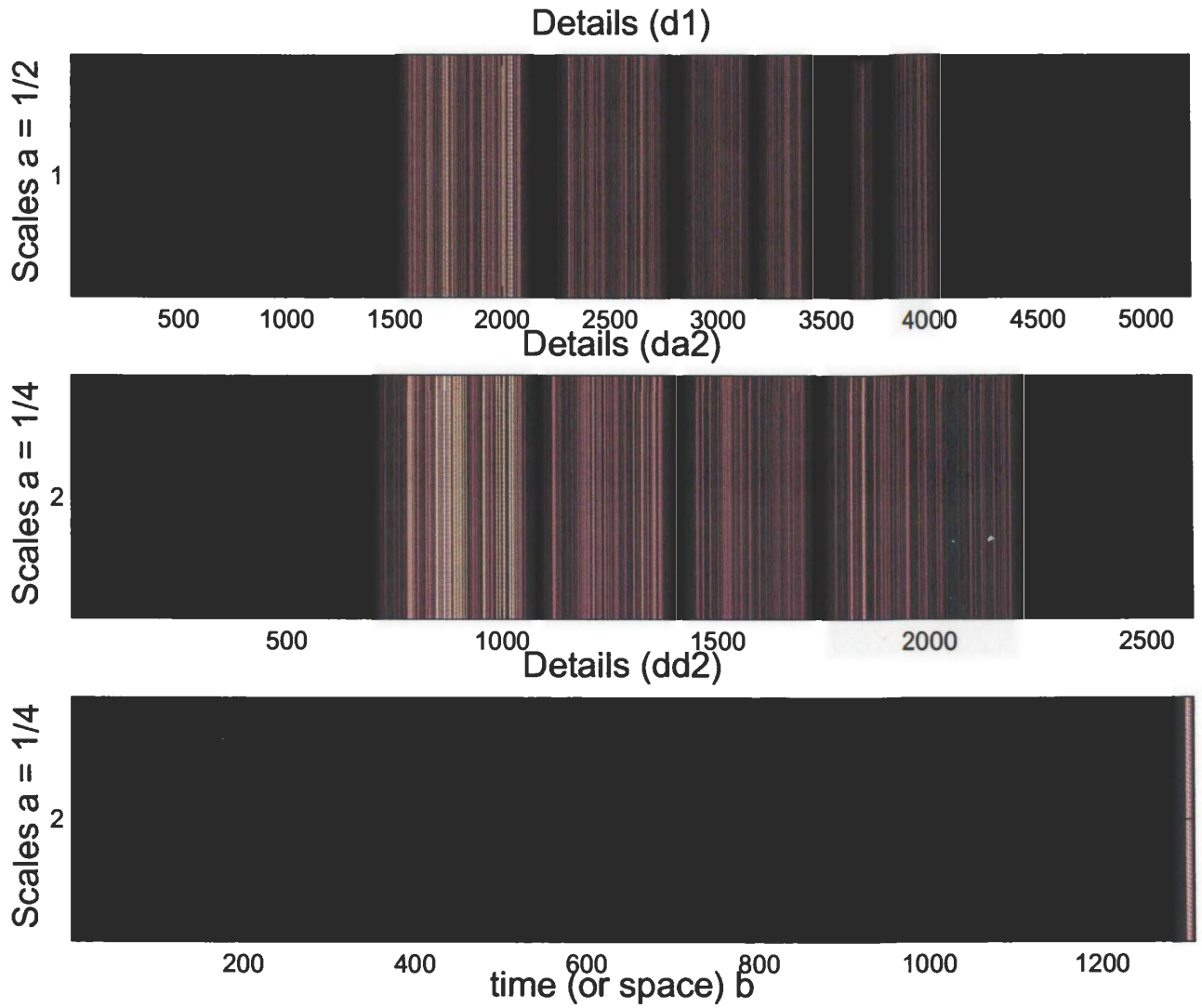

Figure 4.4: Two Level Evaluation of the Wavelet Packet Coefficients for the Unloaded Magnetizing Inrush Current Using ($db4$) Mother Wavelet

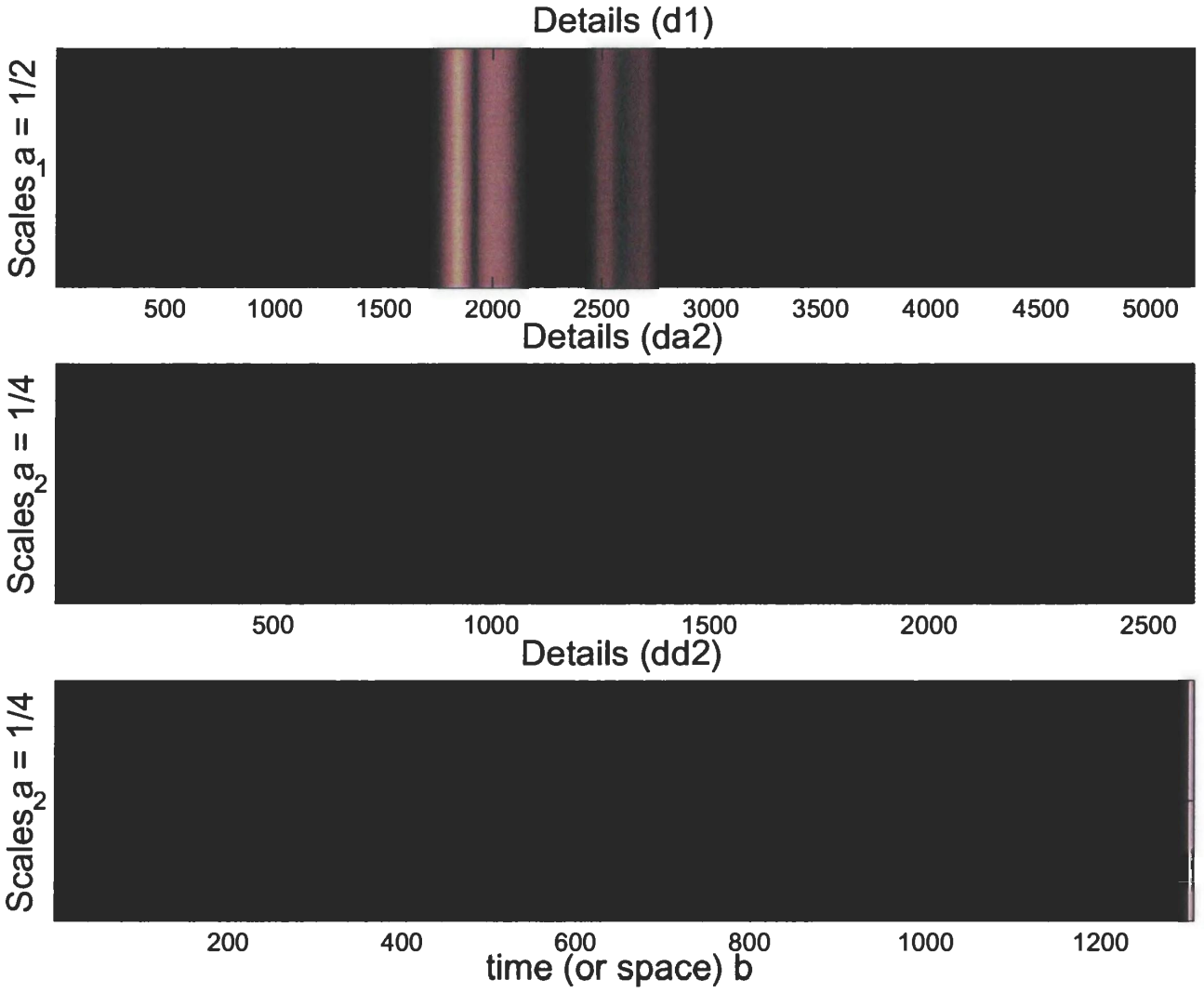

Figure 4.5: Two Level Evaluation of the Wavelet Packet Coefficients for the Loaded Magnetizing Inrush Current (Resistive Load) Using ($db4$) Mother Wavelet

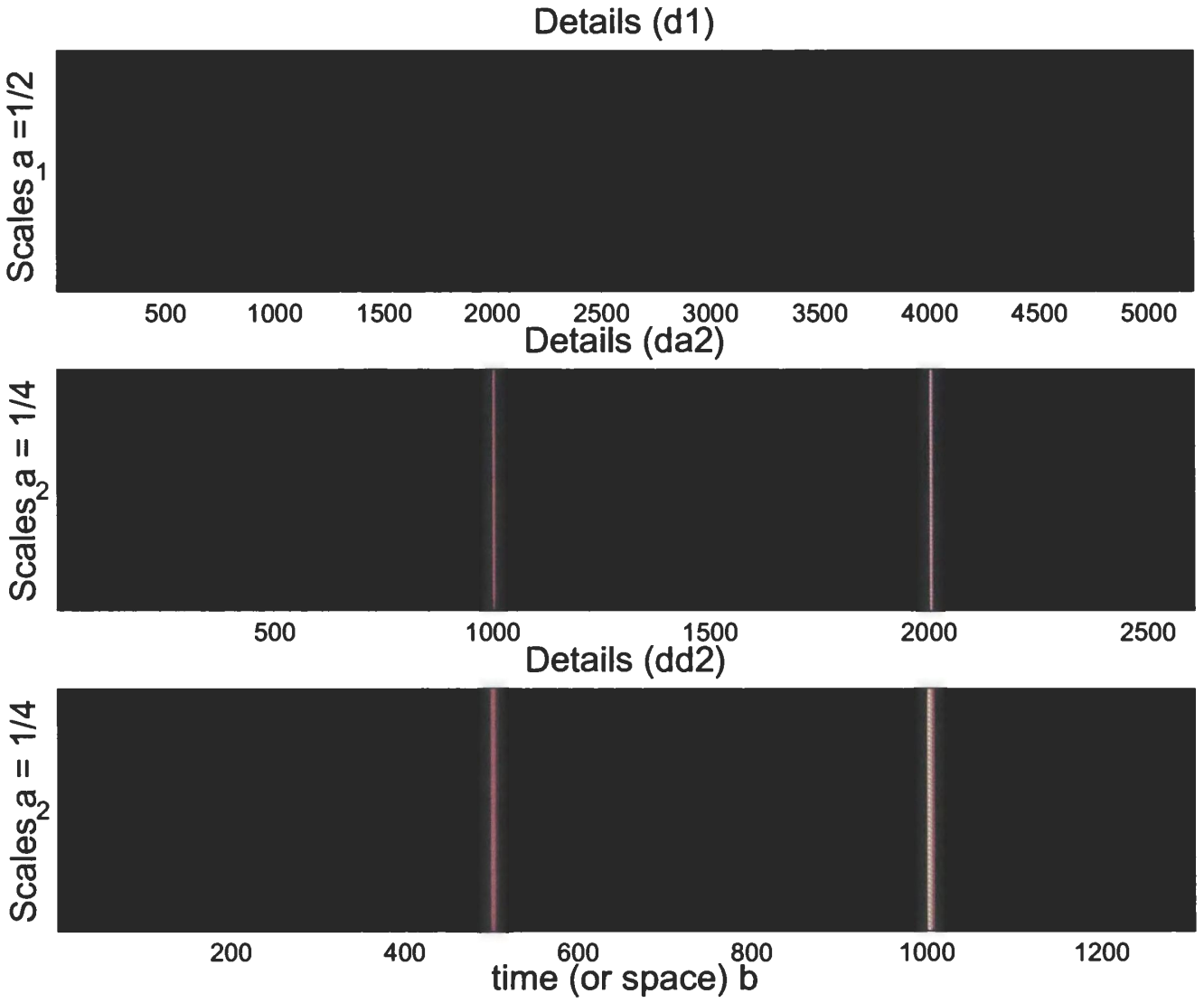

Figure 4.6: Two Level Evaluation of the Wavelet Packet Coefficients for the Primary Side Phase to Phase Fault Current Using ($db4$) Mother Wavelet

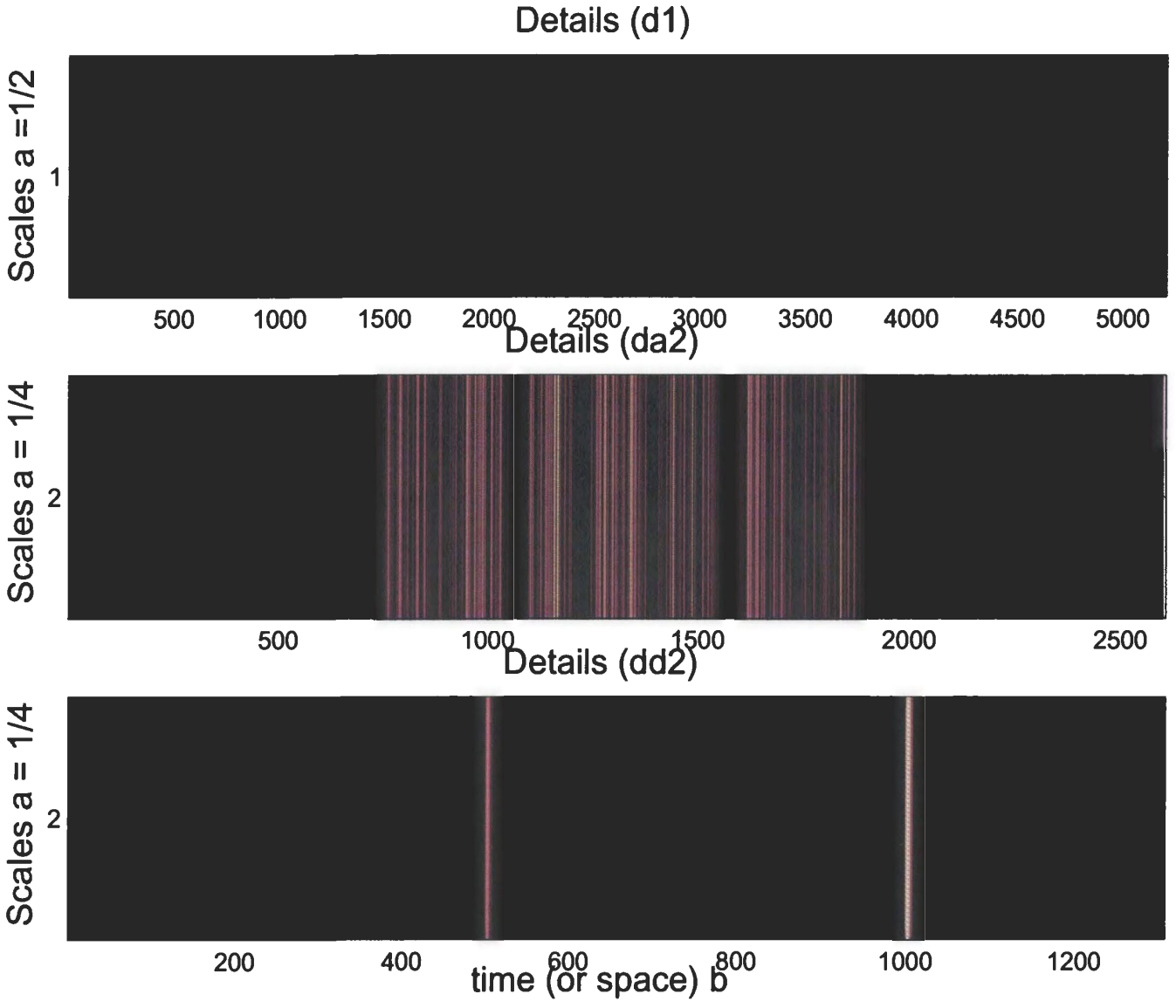

Figure 4.7: Two Level Evaluation of the Wavelet Packet Coefficients for the Secondary Side Loaded Phase to Phase Fault Current (Resistive Load) Using ($db4$) Mother Wavelet

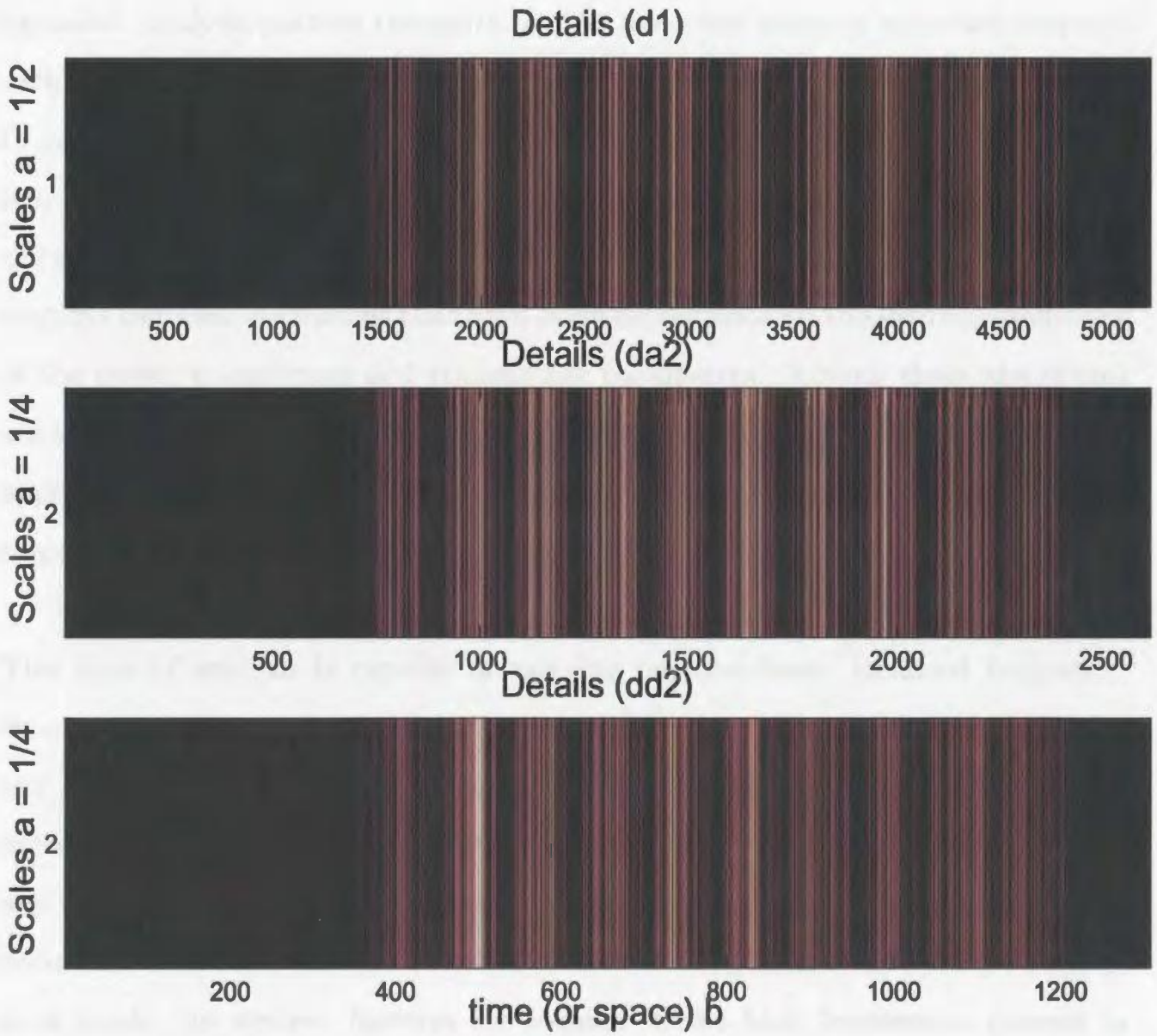

Figure 4.8: Two Level Evaluation of the Wavelet Packet Coefficients for the Primary Side Unloaded Three-Phase to Ground Fault Current Using (*db*4) Mother Wavelet

4.3 The Proposed Disturbance Detector and Classifier

The current approaches of power transformer protection are mainly dependent on harmonic analysis pattern recognition. The harmonic analysis approach employs various algorithms to calculate the 2^{nd} harmonic and some times the 5^{th} harmonic. In general, these algorithms are based on Fourier analysis, which applies a linear non-localized frequency subdivision. In addition, the Fourier analysis requires the signals to have periodicity and stationarity. The pattern recognition approach employs different algorithms that have large dependence on the loading conditions of the power transformer and transformer parameters. Among these algorithms are the ANN, fuzzy logic and voltage and flux restraints. The pattern recognition approach requires a lot of data for training and large memory, as a result, the response is not fast enough.

The proposed WPT approach employs an MRA using localized basis functions. This type of analysis is capable of carrying out non-linear localized frequency-time analysis. In addition, it does not require any pre-defined thresholds for any disturbance detection and classification. The sub-band frequency structure extracted using the MRA can provide the needed features to detect and classify any disturbance a power transformer may experience. The disturbances likely to occur in power transformers are with transient components that decays quickly, as a result, the desired features are located in the high frequencies present in the differential current. The proposed WPT algorithm is to construct the high frequency sub-bands such that the disturbances can be detected and classified. The previous section showed that both the magnetizing inrush and normal (through-fault) currents have zero valued coefficients in the second level highest frequency sub-band.

The WPT algorithm is shown in the following flow chart for a three-phase power transformer case. The algorithm is basically implementing a two levels of resolution WPT and checking for the values of the highest frequency sub-band in the second level whether it is zero or not.

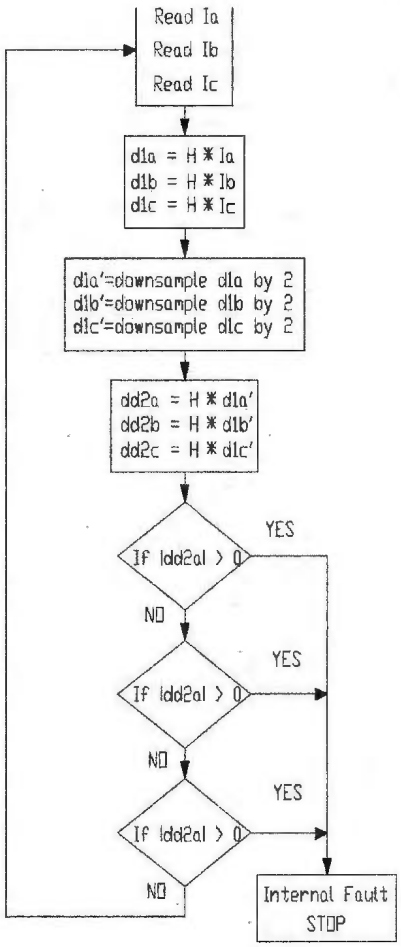

Figure 4.9: The Flowchart of the Proposed WPT Algorithm

4.3.1 Implementing the Wavelet Packet Transform

As mentioned in Chapter 3, the wavelet packet transform (WPT) is a direct expansion of the conventional discrete wavelet transforms (DWT). The needed signatures to identify the type of current or to recognize the current pattern flowing in the power transformer can be obtained by feature extraction technique. The feature extraction technique is simply done by taking the wavelet packet transform of the differential current samples for an optimal number of levels of resolution, where the WPT coefficient corresponding to high energy will be presented in the next level of resolution. In addition, important features for signal classification are characterized by local information in both time and frequency domains. This fact is true particularly for signals with transient components. Thus, the frequency-time relationship implying the localization of all frequencies in time provides an effective settings for extracting different features of the analyzed disturbance. The extraction of these features can provide an efficient tool for recognizing and classifying the investigated disturbance. This feature of the WPT will provide the second level of resolution only with the frequency components which contains information about the type of the differential current. Using this technique, each current will have certain frequency components present in the second level of resolution, which provides an identification tool for any current flowing through the transformer.

The frequency components can be extracted from the details (outputs of high pass filters). In WPT, there are two types of details at each level of resolution, first type is provided by high pass filtering the approximations of the previous level of resolution (da^j), and the other type is provided by high pass filtering the details of the previous level of resolution (dd^j). The (dd^j) details contain frequency components with more or less the shortest duration and highest transient components. The evaluation of the WPT coefficients in the second level of resolution

provides an accurate and effective classification tool for the disturbances in power transformer case. The values of these coefficients are zero for all cases of normal and magnetizing inrush currents, while these coefficients have a value other than zero for all the cases of internal fault currents.

The flowchart of the WPT algorithm is shown in Figure 4.9 using the coefficients of both the high pass filters and low pass filters obtained from the selected mother wavelet (Daubechies). The filters coefficients are given as [59]

$$\{h_8\} = \left\{ \begin{array}{cccccccc} -0.23 & 0.72 & -0.63 & -0.03 & 0.19 & 0.03 & -0.03 & -0.01 \end{array} \right\} \quad (4.2)$$

$$\{g_8\} = \left\{ \begin{array}{cccccccc} -0.01 & 0.03 & 0.03 & -0.19 & -0.03 & 0.63 & 0.72 & 0.230 \end{array} \right\} \quad (4.3)$$

4.4 Off-Line Testing of Wavelet Packet-Based Algorithm

At this stage, the mother wavelet has been selected as the Daubechies ($db4$). Moreover, the optimal number of levels of resolution has been determined as 2. The algorithm is ready to be tested on the data collected from the three-phase 5 kVA core type power transformer. The desired off-line testing will include different magnetizing inrush currents, different internal fault currents and normal operating current. Figure 4.10 shows the case of normal current data, that was taken long after the energization of the power transformer. This current represents a through-fault case and it is clear that WPT algorithm has responded accurately by keeping the status of the trip signal unchanged. Figure 4.11 shows the case of unloaded magnetizing inrush current and again the WPT algorithm has identified the inrush current and a trip signal status is not changed. Figure 4.12 shows the case of loaded magnetizing inrush current and it is clear that the WPT algorithm identified it and again no change in the status of the trip signal. Many fault currents data

were collected. Figure 4.13 shows a primary side loaded phase to phase fault that happened long after the power transformer was energized, and it is clear that the WPT algorithm is capable of identifying the fault in less than quarter a cycle and the status of the trip signal is changed. Figure 4.14 shows the three-phase to ground unloaded fault occurred before the transformer was energized, and the WPT responded by initiating a trip signal in less than quarter a cycle based on 60Hz system. Figure 4.15 shows the case of secondary single phase to ground fault with load before energizing the transformer and the response of the WPT which is capable of recognizing the fault case and initiating a trip signal in less than quarter a cycle (within 2-3 ms) based on a 60 Hz system.

Although many current data were collected and tested off-line, some of the results representing different patterns with major different frequency components were shown in the previous section. The off-line testings have demonstrated quite encouraging results, where different currents flowing through the power transformer were identified in less than quarter a cycle. In all the cases of fault currents, the trip signal declaring a fault was initiated in less than quarter a cycle regardless of the existence of the magnetizing inrush effect in some cases. The WPT algorithm has provided high accuracy, small computational burden and powerful capability of identifying the type of current signatures. The next stage of this work is to test the WPT algorithm on-line, which will be detailed in the next two chapters. The experimental setup for the on-line testings, the realization of the WPT algorithm and all cases of currents that may flow through a power transformer will be provided in the next two chapters for two different three-phase power transformers.

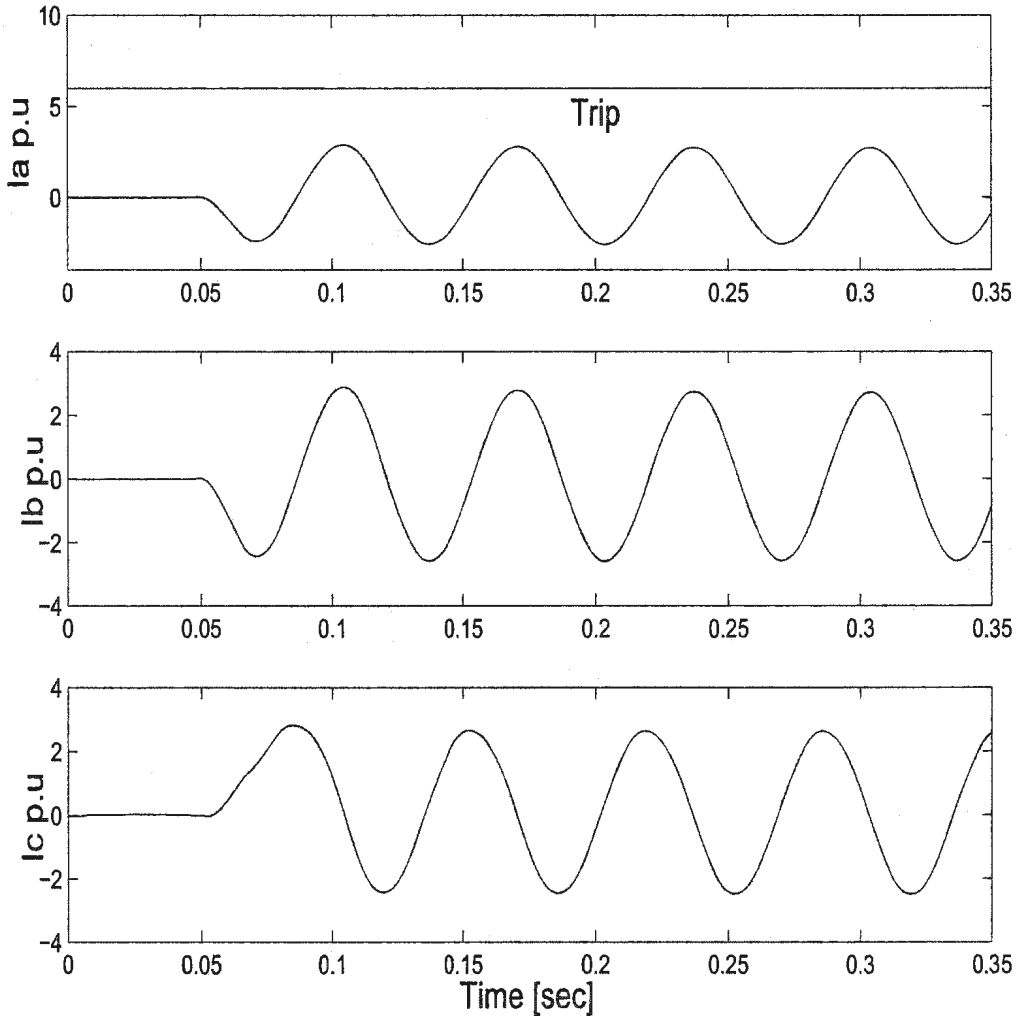

Figure 4.10: The Three-Phase Currents for the Case of Normal Load Current After the Transformer Has Been Energized and the WPT Response Signal

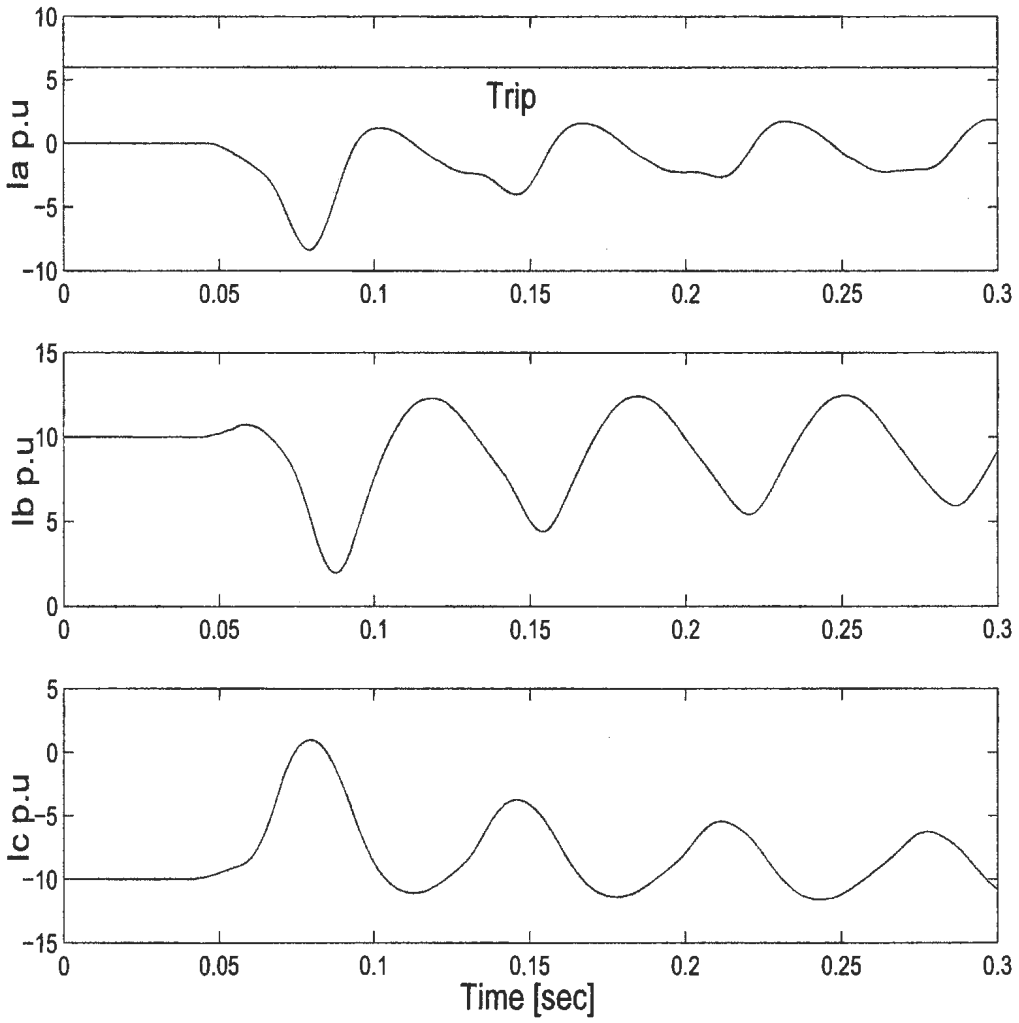

Figure 4.11: The Three-Phase Currents for the Case of Unloaded Magnetizing Inrush Current and the WPT Response Signal

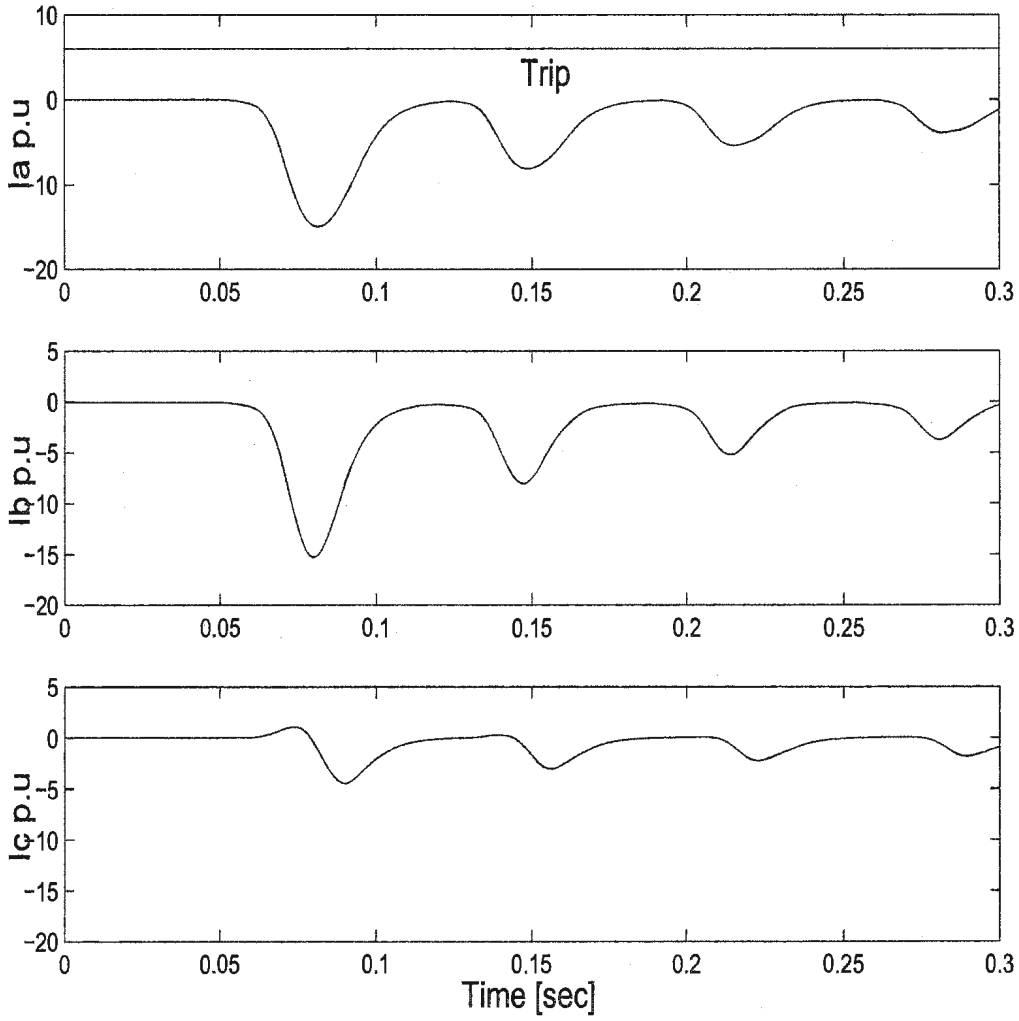

Figure 4.12: The Three-Phase Currents for the Case of Loaded Magnetizing Inrush Current and the WPT Response Signal

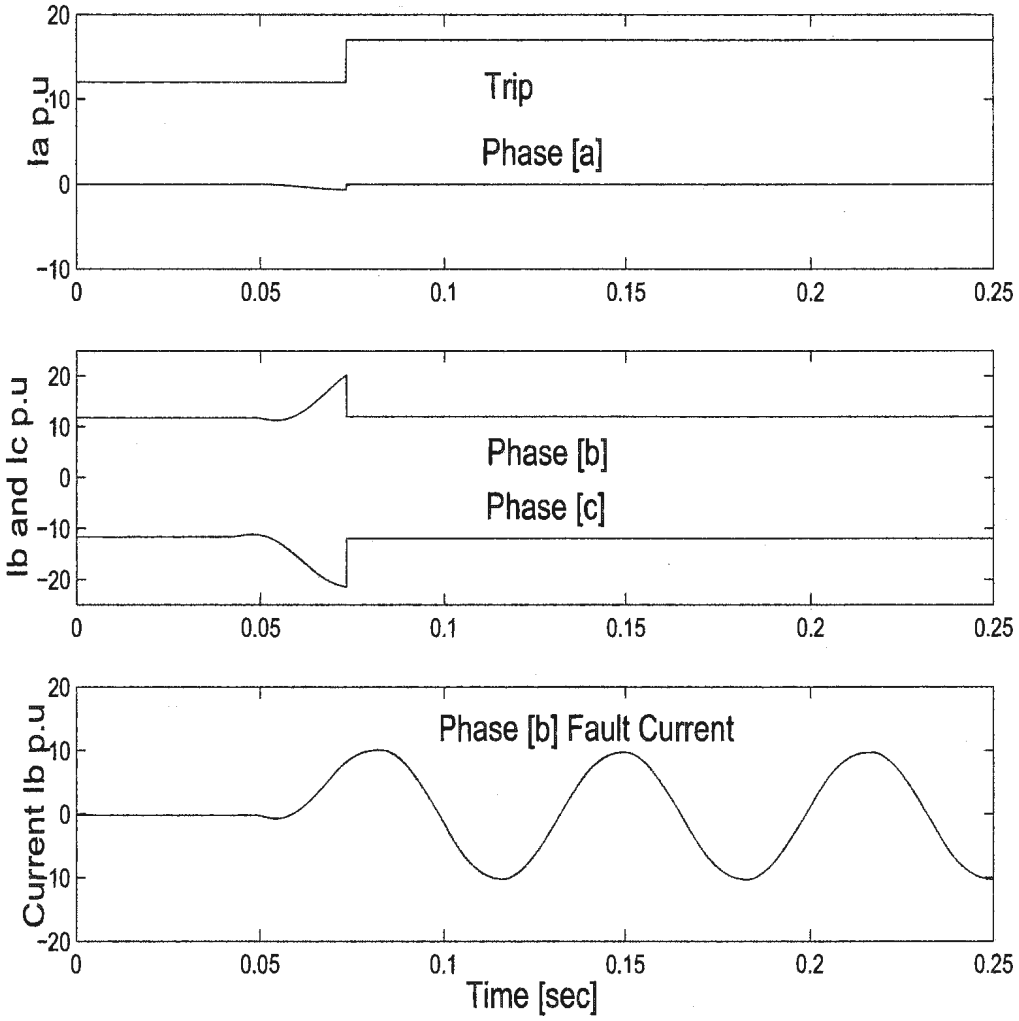

Figure 4.13: The Three-Phase Currents for the Case of Primary Loaded Phase to Phase Fault Current Before Energization and the WPT Response Signal

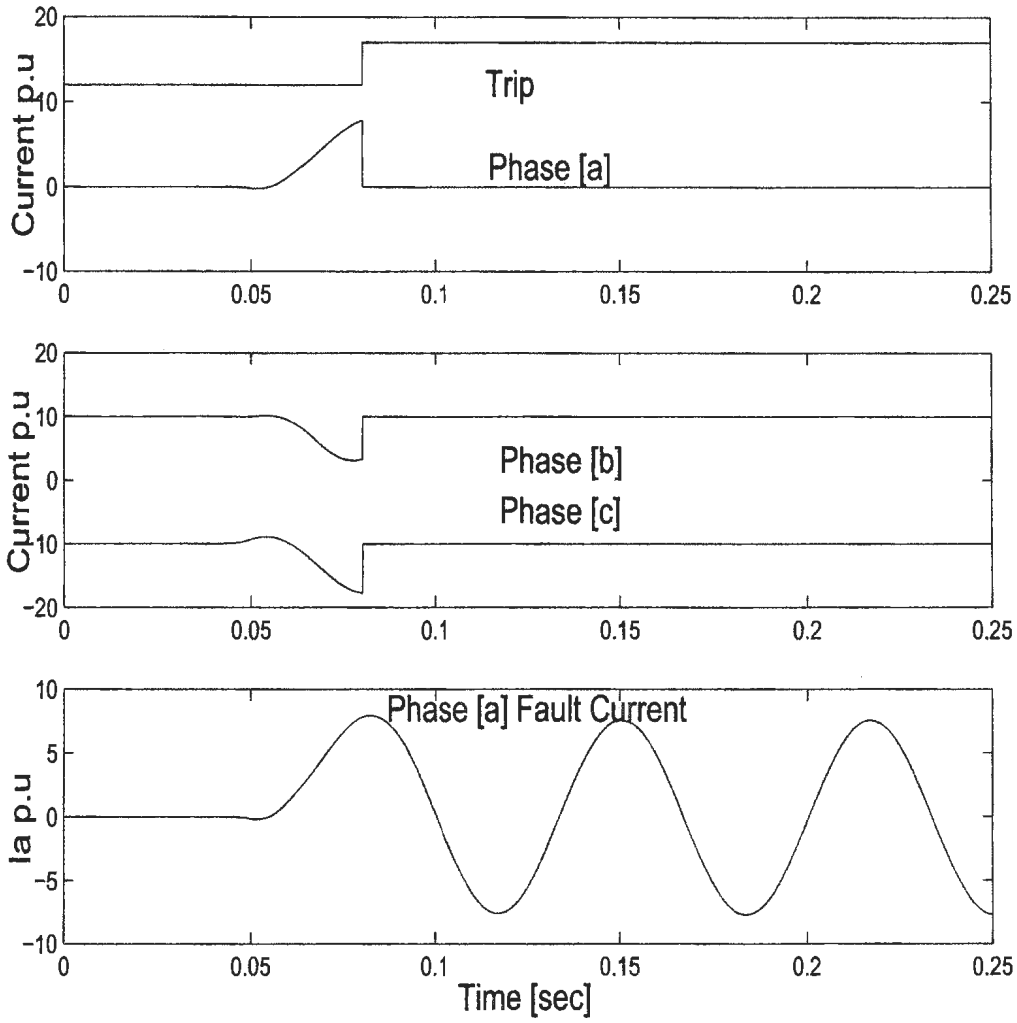

Figure 4.14: The Three Phase Currents for the Case of Unloaded Secondary Three-Phase to Ground Fault Current After Energization and the WPT Response Signal

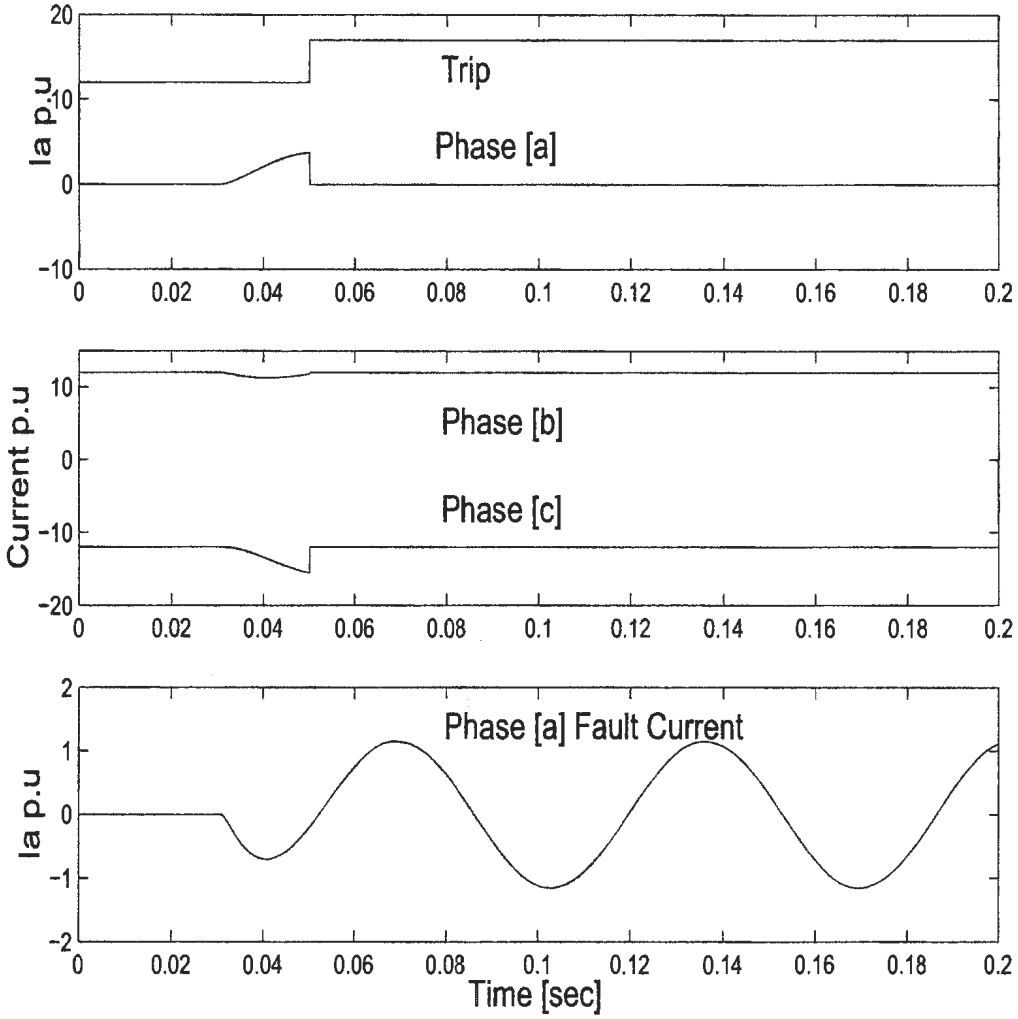

Figure 4.15: The Three Phase Currents for the Case of Secondary Loaded Single Phase to Ground Fault Current Before Energization and the WPT Response Signal

Chapter 5

On-Line Testing of the Wavelet Packet-Based Algorithm

The simulations of the wavelet packet transform (WPT)-based protection technique in chapter 4 showed encouraging results, where all the different types of currents flowing through the power transformer were accurately identified. The on-line testing of the proposed technique is an integral part of this work. The first step required to test the technique on line is the development of an experimental setup, will includes both hardware and software components. The hardware includes in addition to the setup used for data acquisition presented in chapter 4, the connection of the interface with the *dSpace Digital Signal Processor* (DSP) board model DS1102, which is responsible for executing the WPT algorithm and initiating the trip signal (WPT response signal). Moreover, another set of TRIAC switches is needed to carry out the disconnection of the supply voltage in case of any fault. Finally, the software part is required for implementing the WPT-based algorithm. Prior to providing the complete setup to be used for the on-line testing, a typical digital relaying scheme is illustrated in the following section, then the detailed experimental setup is described, and finally, the on-line test results

for different types of currents that may flow through a power transformer are provided.

5.1 A Typical Digital Relaying Scheme

A stand alone digital relay has two main parts; the first is the hardware and the second one is the software. The functional block diagram representing a typical digital relay is shown in Figure 5.1. The hardware usually has the following features [38, 42–45].

1. Data acquisition capability, where current and/or voltage data are required depending on the relaying algorithm. Therefore, current transformers (CTs) and/or potential transformers (PTs) are included with suitable turns ratios.

2. In some cases, the analog inputs have to be low pass filtered before sampling to avoid aliasing due to transient components superimposed on the desired analog input.

3. The sampling frequency must satisfy the Nyquist rate, such that, the sampling frequency must be greater than or equal to twice the highest frequency component of the sampled signal. Moreover, when considering the sampling frequency, it should be noted that the sampling frequency should not be so high to avoid overflow of the computations within the digital signal processor.

For the case of implementing a wavelet packet transform, a multiresolution analysis is involved, which has downsampling operations, which creates more concerns about selecting the sampling frequency. However, for the case of on-line testing the sampling rate was selected to be 10 kHz.

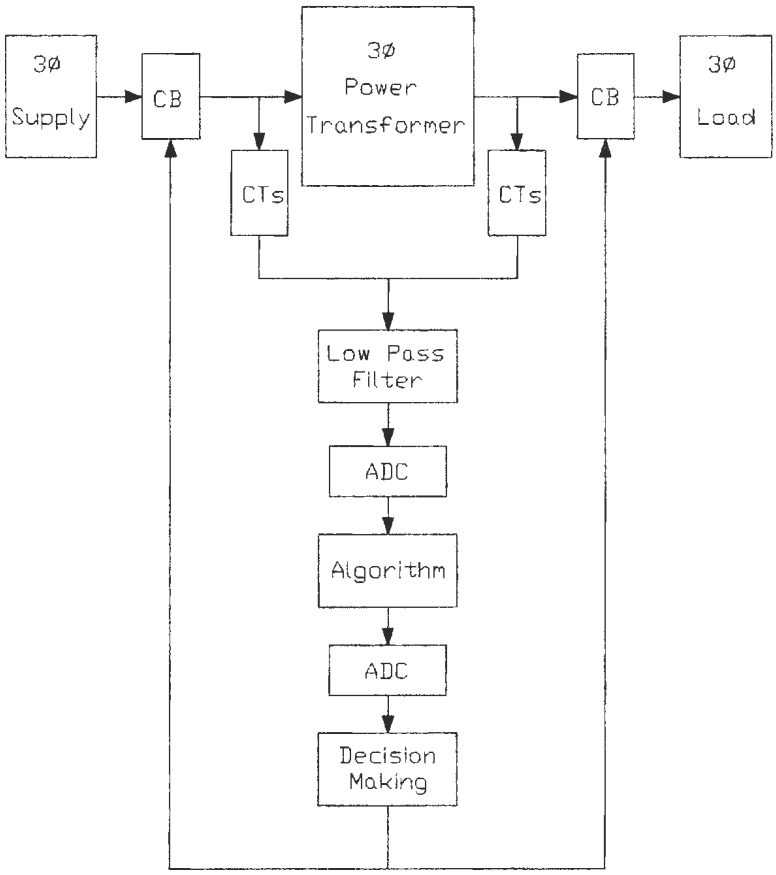

Figure 5.1: Functional Block Diagram of a Typical Digital Relaying Scheme

5.2 Experimental Setup for On-line Testings

As mentioned in chapter 4 and recalling the functional capabilities any digital relay should have, the experimental setup developed for data acquisition can be the basic setup for on-line testings. However, additional hardware has to be connected. The DSP DS-1102 has to carry out the computations and send a trip signal in the case of any internal fault. This trip signal (WPT response signal) can be responsible for removing the trigger signal of another set of TRIAC switches connected in series with the power transformer. Also, for the case of testing the proposed technique on conditions of loaded faults, a TRIAC switch is to added in series with the fault connection. Figure 5.2 shows the complete experimental setup for on-line testings.

5.3 Real Time Implementation of the Wavelet Packet Transform

The WPT-based algorithm is tested on a 5 kVA, Δ-Y, 230/550-575-600 V, 60Hz, core type three-phase prototype laboratory power transformer and on a 2kVA, Δ-Y, 127-220/31.8-42-63.5 V, 50Hz, multi-tap three-phase power transformer. In this chapter, the test results for the 5 kVA core type power transformer are provided, while the test results of the 2 kVA multi-tap power transformer are provided in the next chapter. The complete relaying scheme consists of both the hardware and software. The processing of the differential current is done by the WPT algorithm using the DSP board DS-1102. A program written in Turbo C language is developed for this purpose, where the the wavelet packet transform (WPT) is applied to the samples of the differential current using the selected mother wavelet (Daubechies *db*4), then the details are downsampled by 2 and the WPT is applied

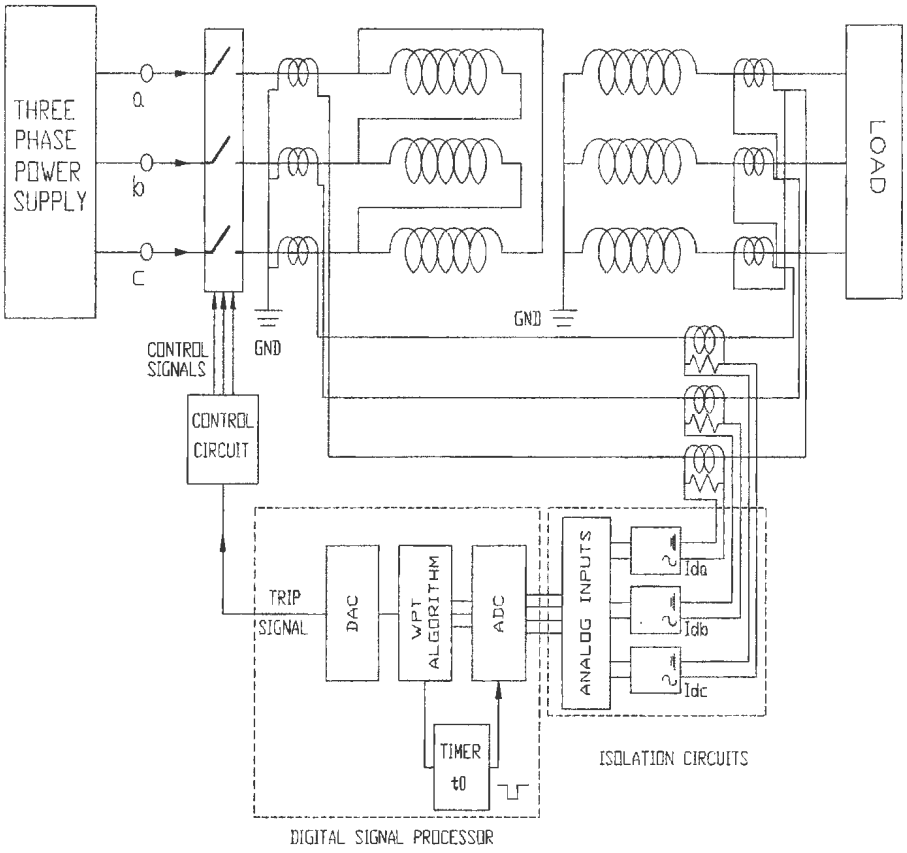

Figure 5.2: Experimental setup for on-line testing on the core type power transformer

again. Finally, the second level details are checked to identify the current type. Figure 5.3 shows the block diagram of the proposed WPT algorithm.

When the DSP DS-1102 is started, it continuously samples the differential current at a sampling frequency of 10 kHz using a built-in analog-to-digital converter (ADC). The samples of differential current are sent to the memory of the DSP board by the host PC. The samples of the three phase differential currents are squared and summed into one sample, then they are placed in a circular buffer of size 16 and stored in a vector x of length 16 such that the previous 16^{th} sample is automatically dropped off the buffer and the vector x is updated. Each time a new sample is read from the ADC port, a discrete 16-sample circular convolution is applied to the samples vector with the high pass filter coefficients described in chapter 4. The high pass filtering produces first level details, and those details are downsampled by 2 to perform the frequency scaling step. Finally a discrete 8-sample circular convolution is applied again with the same filter coefficients. The second discrete circular convolution operation produces the second level details. Their absolute values are compared to zero to identify the type of the current pattern flowing in the power transformer. If the absolute values of the second level details exceed zero, then a fault is declared and a trip signal is initiated. The trip signal can be taken from the digital to analog converter (DAC) port. Figure 5.3 shows the flowchart of the WPT-based algorithm.

5.4 On-line Test Results

One of the most attractive features of Wavelet transforms is the reduced computational burden [47, 54, 57]. To achieve more reduction in computational burden for the power transformer protection application, the three-phase differential current samples are prepared using an unbiased method [2, 45], where the samples

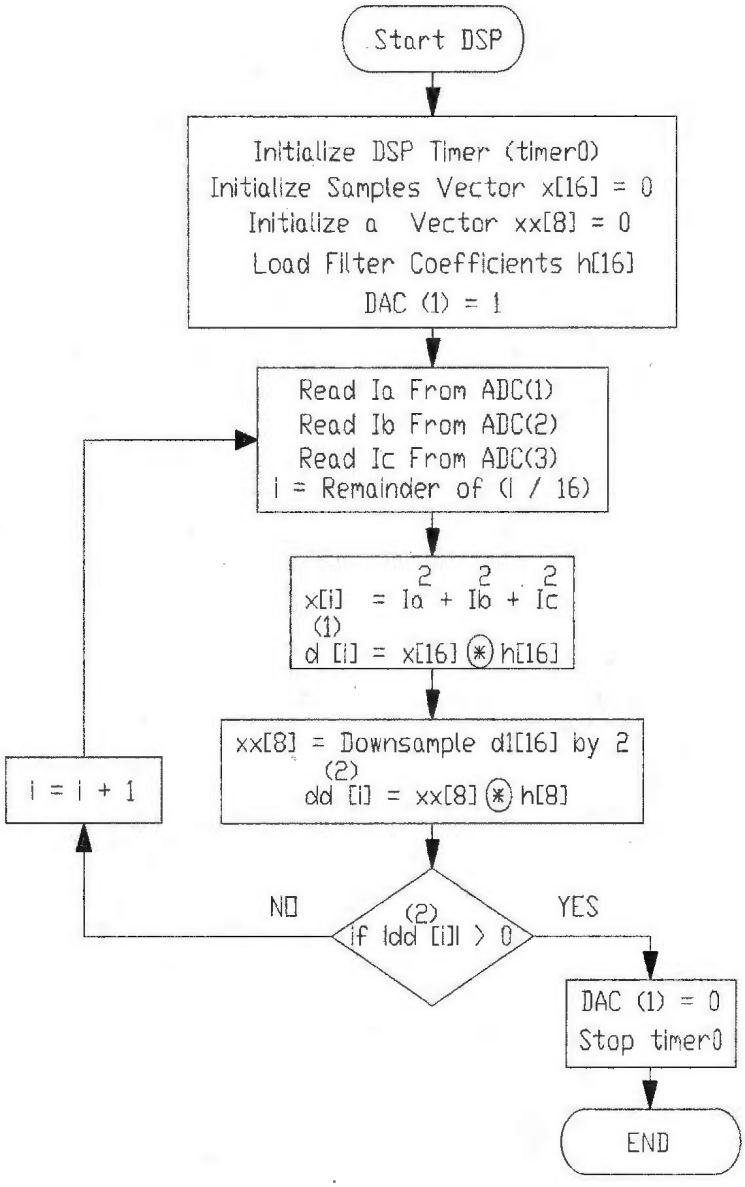

Figure 5.3: Flowchart of Implementing the Wavelet Packet-Based Algorithm

of the three phases are squared and summed to produce one vector of samples $x[n]$, which will be processed by the wavelet packet transform (WPT). Although, there are other methods to prepare the samples for application of the WPT, such as applying the WPT to three vectors representing the three phases differential current samples. These methods increase the computational burden and affect the sampling frequency. Both methods were tested, and the unbiased method was found to have less computational burden and it will be used for all the on-line testings through out this work.

5.4.1 Magnetizing inrush current

The magnetizing inrush currents tested in this work included many cases with a random switching to test for both the positive and negative inrush currents for the following conditions:

1. no-load condition
2. loaded conditions
    - balanced resistive load
    - unbalanced resistive load
    - balanced R-L load
    - unbalanced R-L load

Many tests were carried out for the aforementioned cases, and the WPT-based protection algorithm never generated a trip signal. Sample results are provided in Figures 5.4 and 5.5. The results of other test results for cases of balanced and unbalanced (R-L) and resistive loads are provided in Appendix A1. It was found from all these figures that even with a high differential current magnitude, the WPT is capable of recognizing it as a non-fault condition. In all these Figures, no

trip signal is initiated, as shown with the three-phase differential currents. It is worth mentioning that during hundreds of random switchings of the transformer, neither the direction nor the shape of the magnetizing inrush current waveforms are predictable. However, both the direction and the shape of the magnetizing inrush current did not affect the ability of the WPT to recognize the magnetizing inrush current. The magnetizing inrush current waveforms for the loaded conditions usually have a quite different shape from those for the unloaded cases. Moreover, the (R-L) load cases are not the same as the resistive loaded cases. Nevertheless, the WPT had no problem recognizing them as magnetizing inrush currents, and the trip signal remained high ensuring no false trip of the circuit breaker in all tests that were carried out. It should be noted that the faults outside the CT zones of each phase of the protected power transformer are considered as through-fault currents. Thus, no trip signal was initiated for any fault outside the CT zones.

5.4.2 Internal fault currents

Many internal faults are investigated as an integral part of this work to test the WPT-based algorithm response for different faults under conditions of loading and energizing. All the fault tests were performed for the following four combinations **(i)** for fault occurrence without a load before energizing,**(ii)** without a load after energizing, **(iii)** with a load before energizing and **(iv)** with a load after energizing. All the fault tests were performed by connecting the two points involved in the considered fault. Four conditions were tested for fault occurrence without a load before energizing, without a load after energizing, with a load before energizing and with a load after energizing. These different fault conditions were tested for each phase of the three phases on both the primary side and the secondary side of the power transformer. The results showed that the fault is distinguished and the trip signal is initiated in less than quarter a cycle based on 60 Hz system in

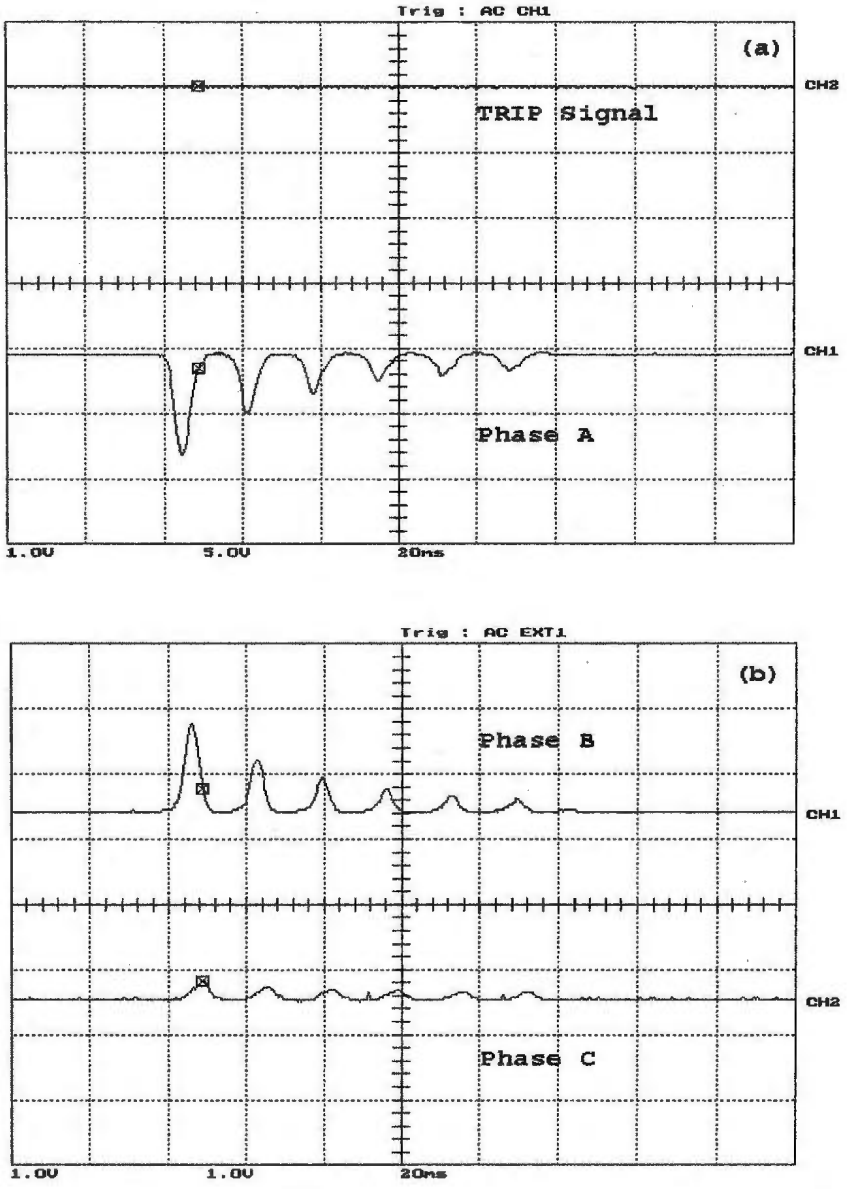

Figure 5.4: Unloaded magnetizing inrush current, (a) the WPT response and phase A differential current,(b) phase B and phase C differential currents. Y-scale is 1 Div. = 11.67 A

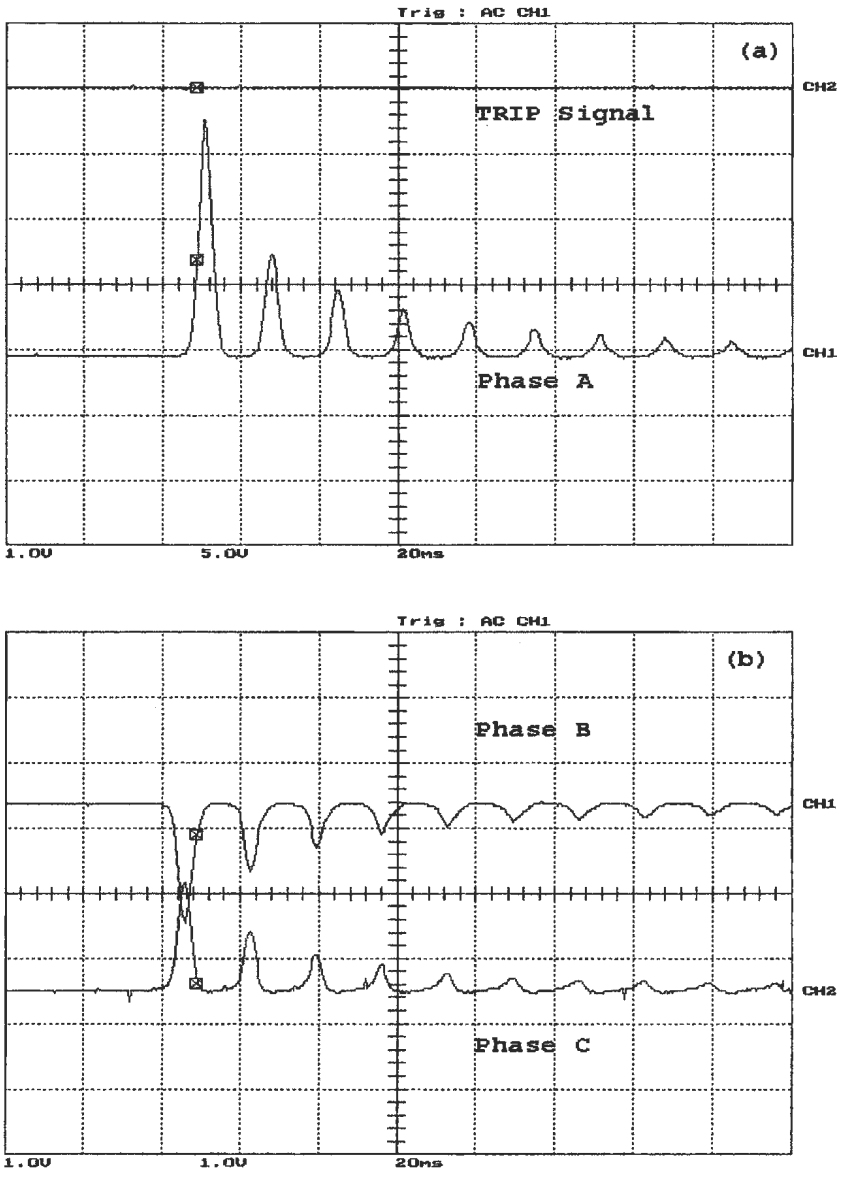

Figure 5.5: Unloaded magnetizing inrush current, (a) the WPT response and phase A differential current, (b) phase B and phase C differential currents. Y-scale is 1 Div. = 11.67 A

all cases.

Single phase to ground fault

The single phase to ground fault test was carried out by connecting one phase to the ground under different conditions including before energization without a load, before energization with a load, after energization without a load and after energization with a load on both the primary and the secondary sides of the power transformer for each phase. It is worth mentioning that in all cases of loaded conditions, a balanced (R-L) load of Z=20 + j11.9129 Ω/phase is used. Figures 5.6 through 5.13 show the test results of the single phase to ground fault took place on phase A. The test results for both phases B and C are provided in Appendix A2. These figures show the differential current in the three phases as well as the WPT trip signal. In all the tests carried out, the fault was identified and the trip signal was initiated in less than quarter a cycle based on 60 Hz system.

1- Primary side faults

Figure 5.6 shows the primary side phase A to ground fault occurring before energizing the power transformer without a load. The results of the same type of fault occurring after energizing the power transformer without a load are shown in Figure 5.7. When the balanced inductive load is connected on the secondary side of the power transformer, the result of the phase A to ground fault on the primary side occurring before energizing the power transformer is shown in Figure 5.8. When the phase A to ground occurred on the primary side after energizing the power transformer for the same loading condition, the result is shown in Figure 5.9.

2- Secondary side faults

Figure 5.10 shows phase A to ground fault on the secondary side before energizing the power transformer without connecting the load. The result when the same type of fault occurred after energizing the power transformer with out the load is

shown in Figure 5.11. The condition of phase A to ground fault with the load connected occurring before energizing the transformer is shown in Figure 5.12. Figure 5.13 shows the same type of fault occurred after energizing the power transformer with the inductive load connected.

Phase to phase fault

Tests for this fault were carried out by connecting two phases for the four aforementioned conditions of energization and loading on primary and on secondary sides of the power transformer for the three phases. Figures 5.14 through 5.21 show the phase A to phase B fault, while the remaining results for phase A with phase C and phase B with phase C are provided in Appendix A3. In all these figures, the differential three-phase current and the WPT trip signal are shown. Again the WPT identified the fault and initiated a trip signal in less than quarter a cycle.

1- Primary side faults

When phase A to phase B fault occurred before energizing the power transformer without load, the result is shown in Figure 5.14. Figure 5.15 shows the result of the same type of fault occurring after energizing the power transformer. For the case of connecting an inductive load, Figure 5.16 shows the results when the same fault occurred before energizing the power transformer. Figure 5.17 shows the case when the fault occurred after the power transformer is energized with a load.

2- Secondary side faults

For the case of phase A to phase B fault occurring before energizing the power transformer without a load, the result is shown in Figure 5.18. When the same type of fault occurred after the power transformer had been energized, the result is shown in Figure 5.19. The result of connecting an inductive load while the fault takes place before energizing the power transformer is shown in Figure 5.20. Fig-

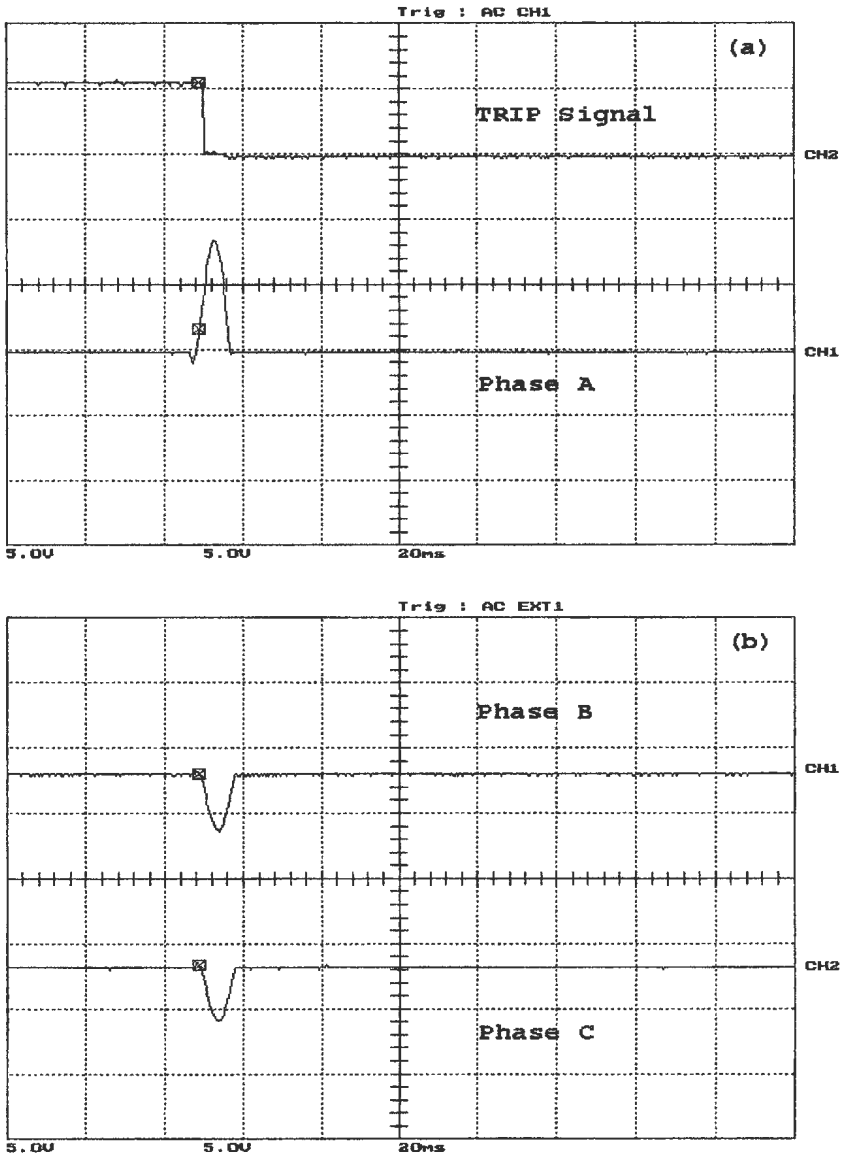

Figure 5.7: Unloaded phase A to ground fault, occurred after energization on the primary side, (a) the WPT response and phase A differential current,(b) phase B and phase C differential currents. Y-scale is 1 Div. = 11.67 A

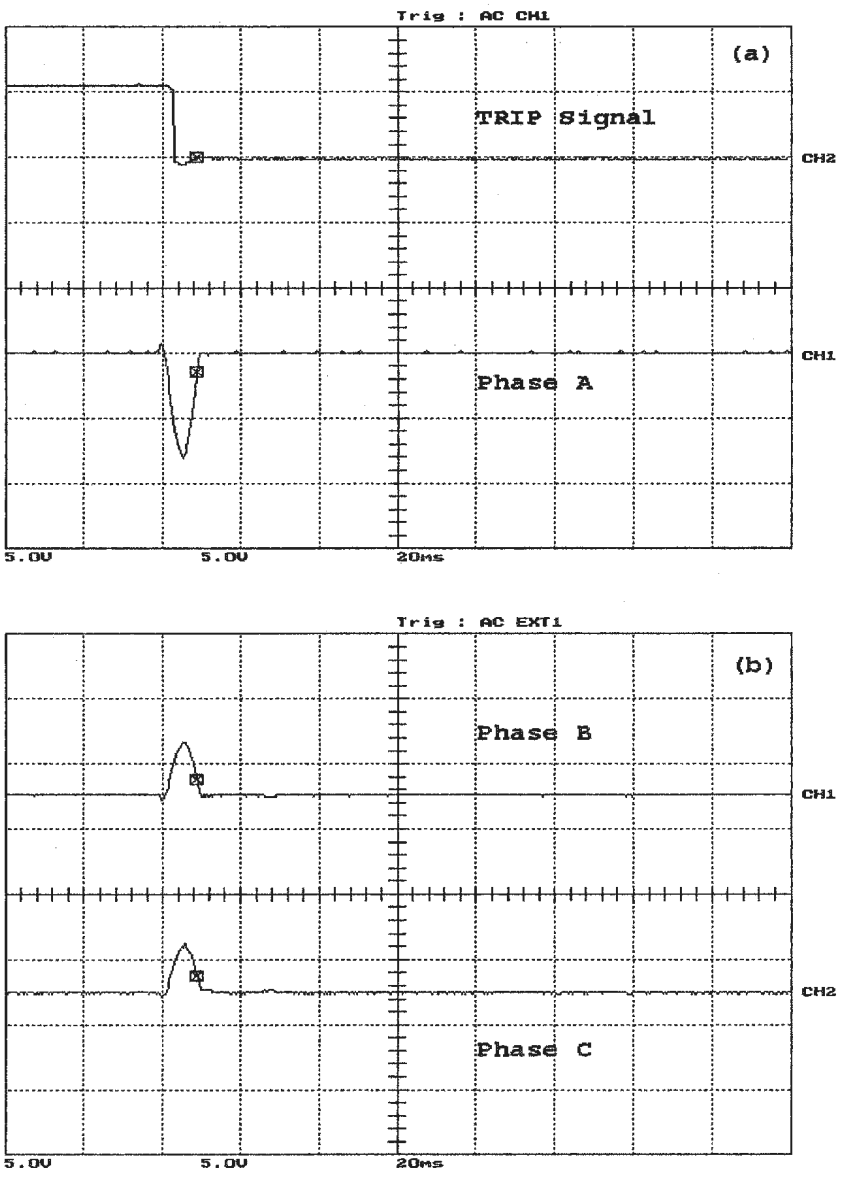

Figure 5.6: Unloaded phase A to ground fault, occurred before energization on the primary side, (a) the WPT response and phase A differential current,(b) phase B and phase C differential currents. Y-scale is 1 Div. = 11.67 A

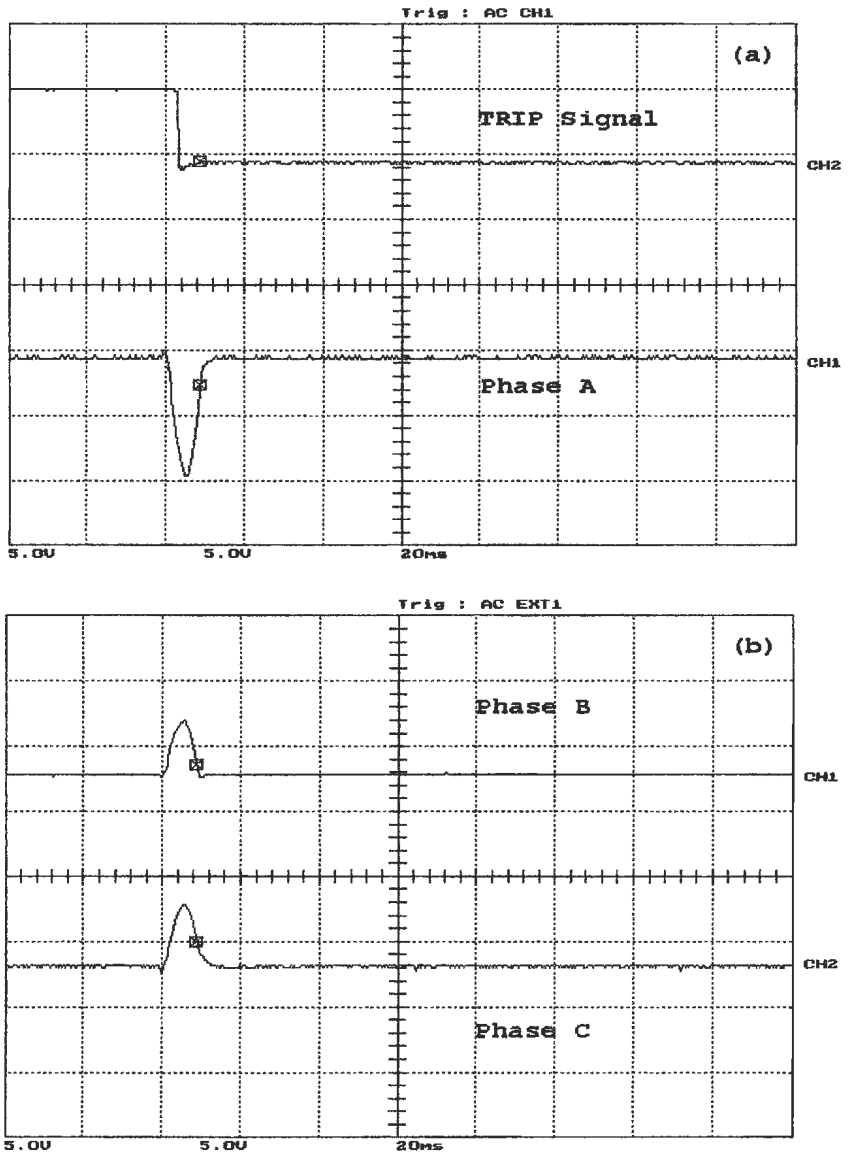

Figure 5.8: Loaded phase A to ground fault, occurred before energization on the primary side, (a) the WPT response and phase A differential current,(b) phase B and phase C differential currents. Y-scale is 1 Div. = 11.67 A

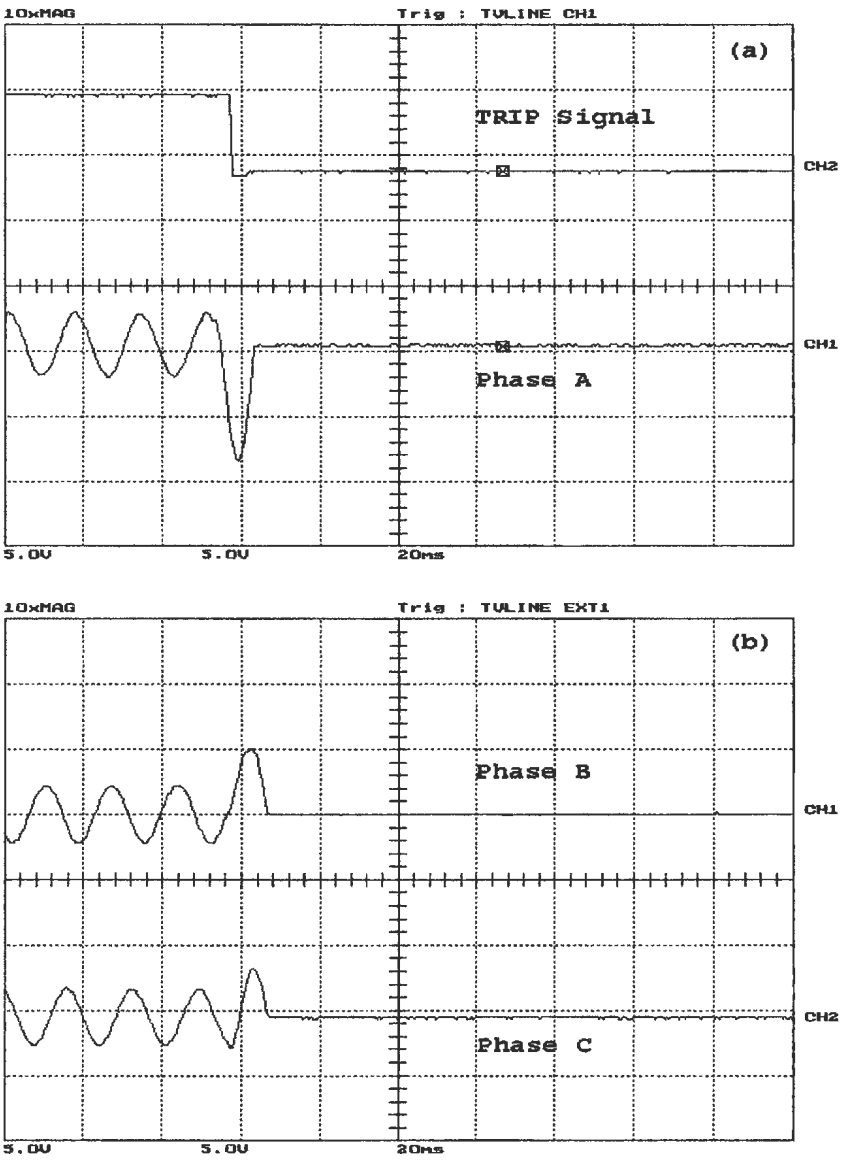

Figure 5.9: Loaded phase A to ground fault, occurred after energization on the primary side, (a) the WPT response and phase A differential current,(b) phase B and phase C differential currents. Y-scale is 1 Div. = 11.67 A

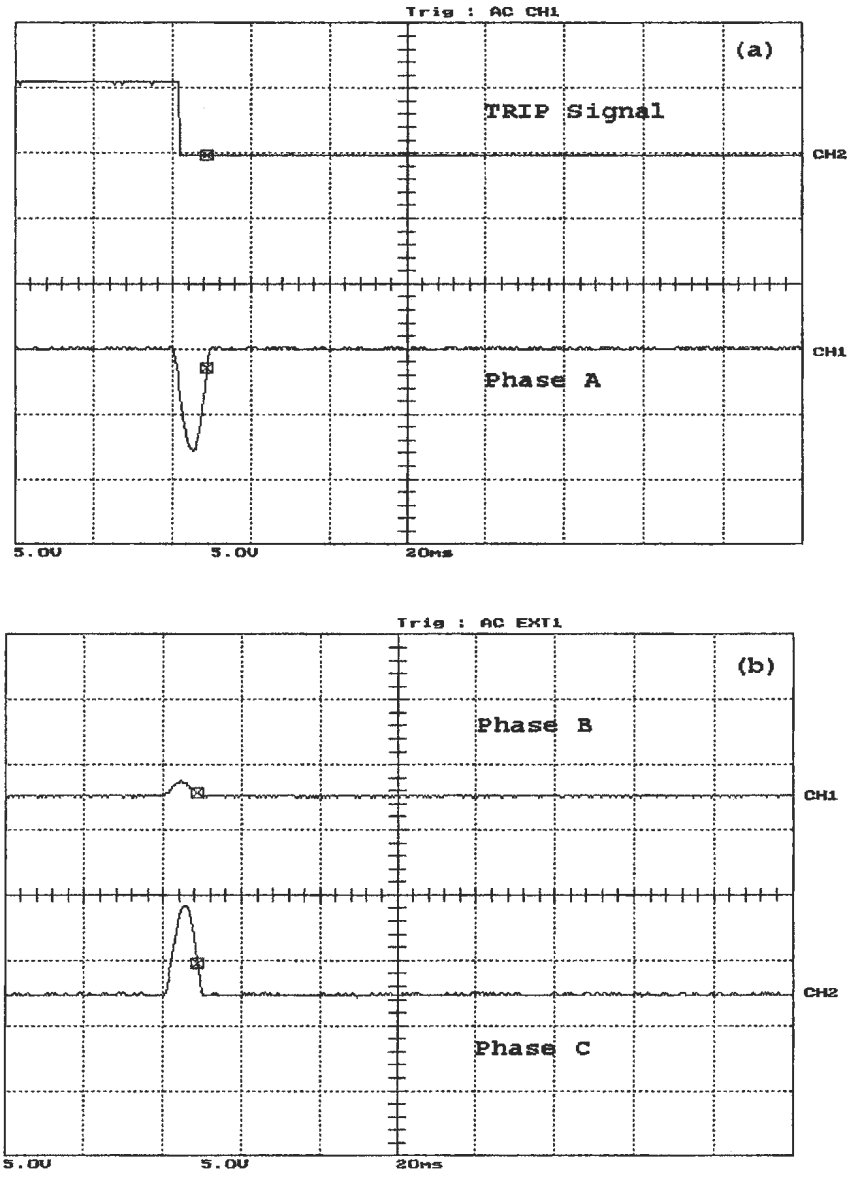

Figure 5.10: Unloaded phase A to ground fault, occurred before energization on the secondary side, (a) the WPT response and phase A differential current,(b) phase B and phase C differential currents. Y-scale is 1 Div. = 11.67 A

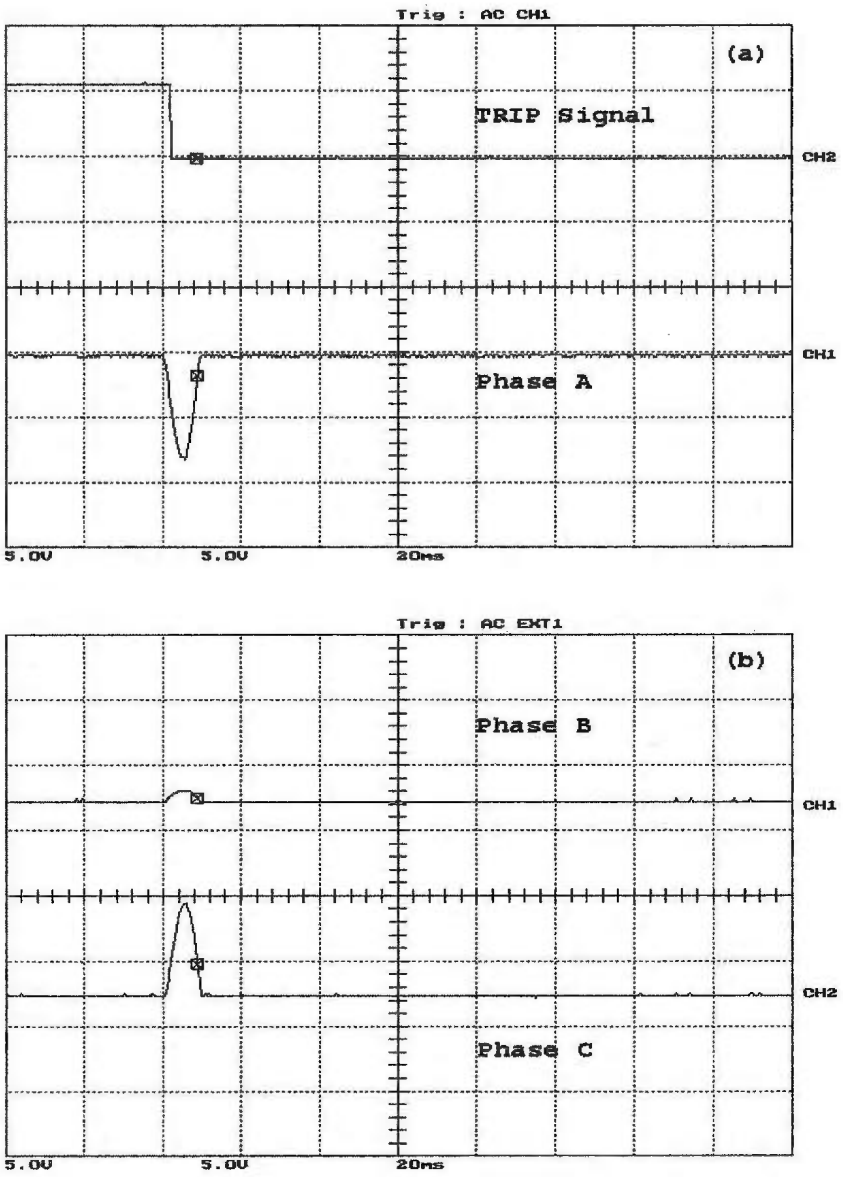

Figure 5.11: Unloaded phase A to ground fault, occurred after energization on the secondary side, (a) the WPT response and phase A differential current,(b) phase B and phase C differential currents. Y-scale is 1 Div. = 11.67 A

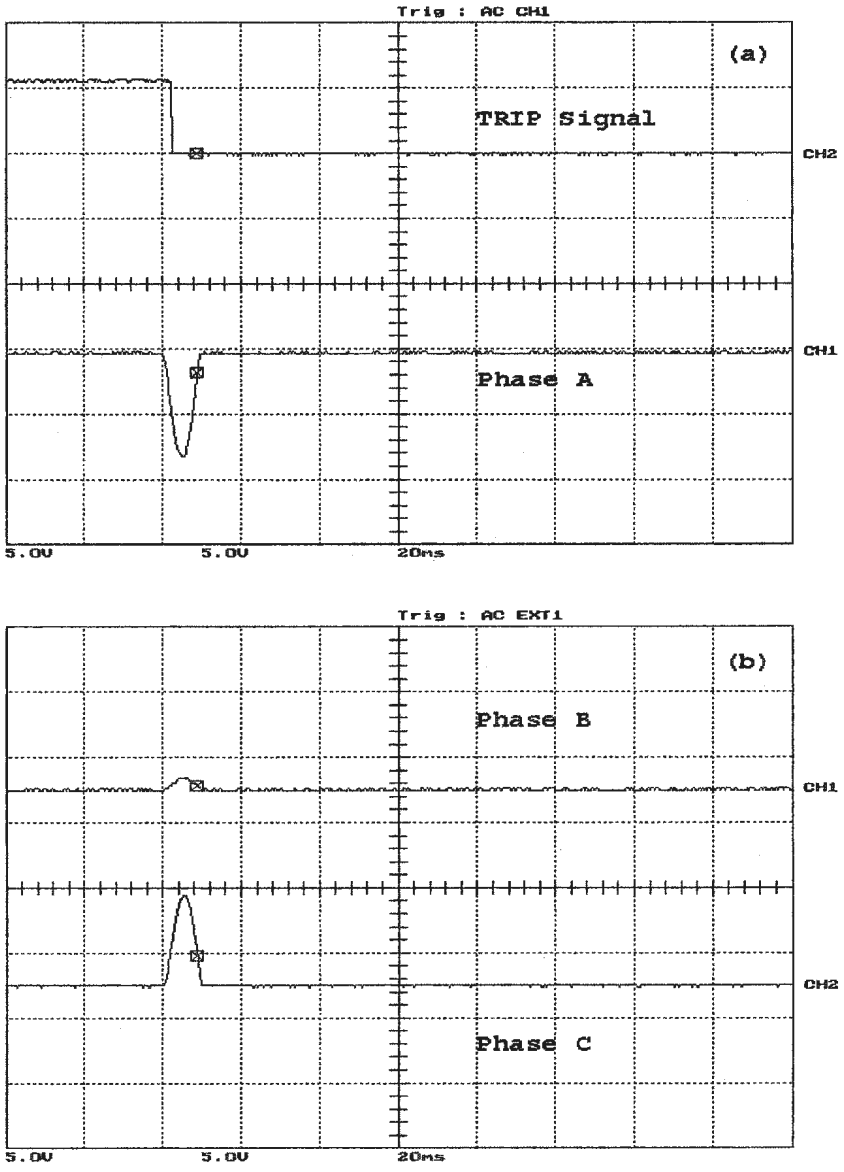

Figure 5.12: Loaded phase A to ground fault, occurred before energization on the secondary side, (a) the WPT response and phase A differential current,(b) phase B and phase C differential currents. Y-scale is 1 Div. = 11.67 A

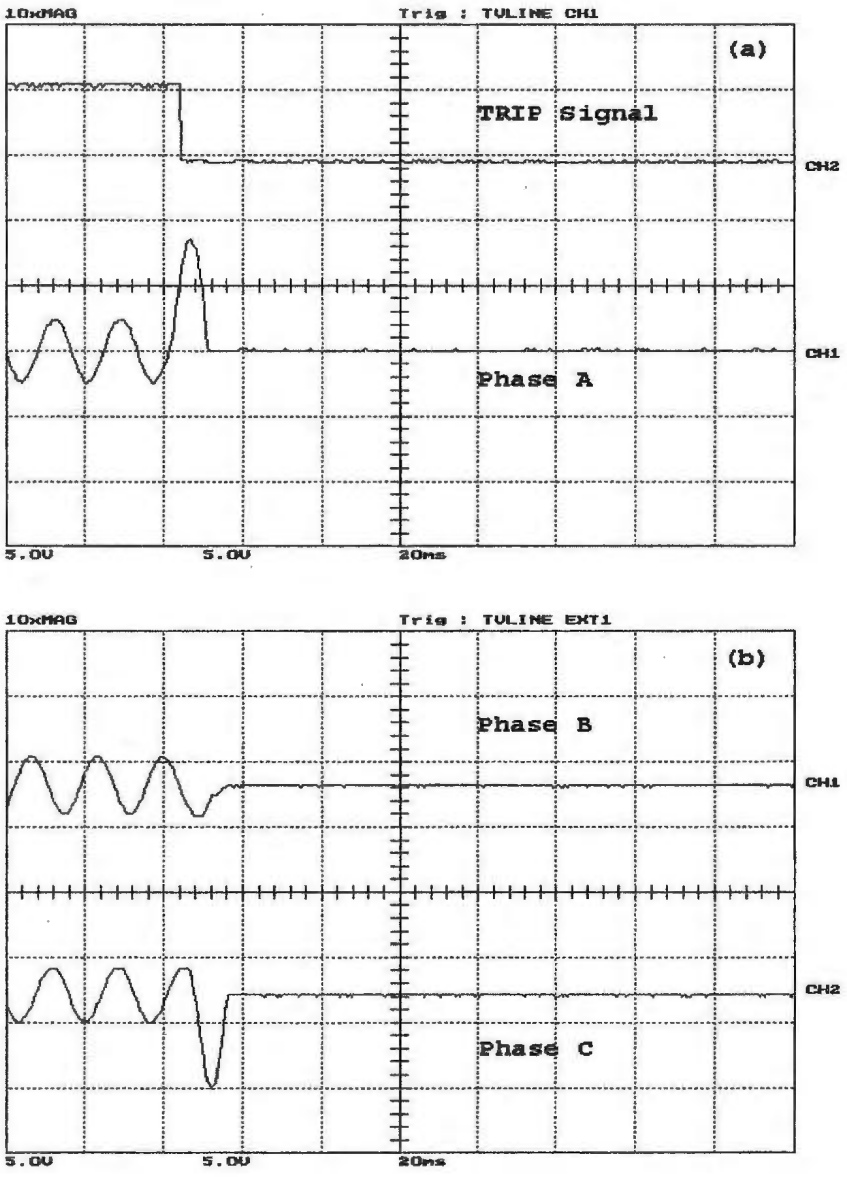

Figure 5.13: Loaded phase A to ground fault, occurred after energization on the secondary side, (a) the WPT response and phase A differential current,(b) phase B and phase C differential currents. Y-scale is 1 Div. = 11.67 A

ure 5.21 shows the phase A to Phase B fault occurring after energizing the power transformer with the inductive load connected. It should be mentioned here that in all the unsymmetrical fault tested, the primary line-to-line voltage was 75V.

Three-phase to ground fault

This test was carried out by connecting the three phases to the grounded neutral point. This fault was tested under the four aforementioned conditions of energization and loading on both the primary and the secondary sides of the power transformer. In Figures 5.22 and 5.23, the results of two cases are presented, while the remaining results are provided in Appendix A4. When the three-phase to ground fault occurred on the primary side before energizing the power transformer without a load, the result is shown in Figure 5.22. Figure 5.23 shows the three-phase to ground fault taking place on the secondary side after energizing the power transformer without a load. It should be noted that all three-phase to ground faults were tested with primary side line to line voltage of 75V, to avoid the high fault currents, which may damage the testing equipment or saturate the CTs.

Special cases

These cases include unbalanced loading of the power transformer, and the effects on the WPT response to faults occurring after the power transformer is energized. All the tests are done with primary side line to line voltage of 100V. Two cases of loading are considered, which are:

1. Unbalance loading with

   $Z_a = 20 + j11.9129\ \Omega$

   $Z_b = 20 + j0\ \Omega$

   $Z_c = 35 + j7.012\ \Omega$

2. Two Phases loading

   $Z_a = 20 + j11.9129\ \Omega$

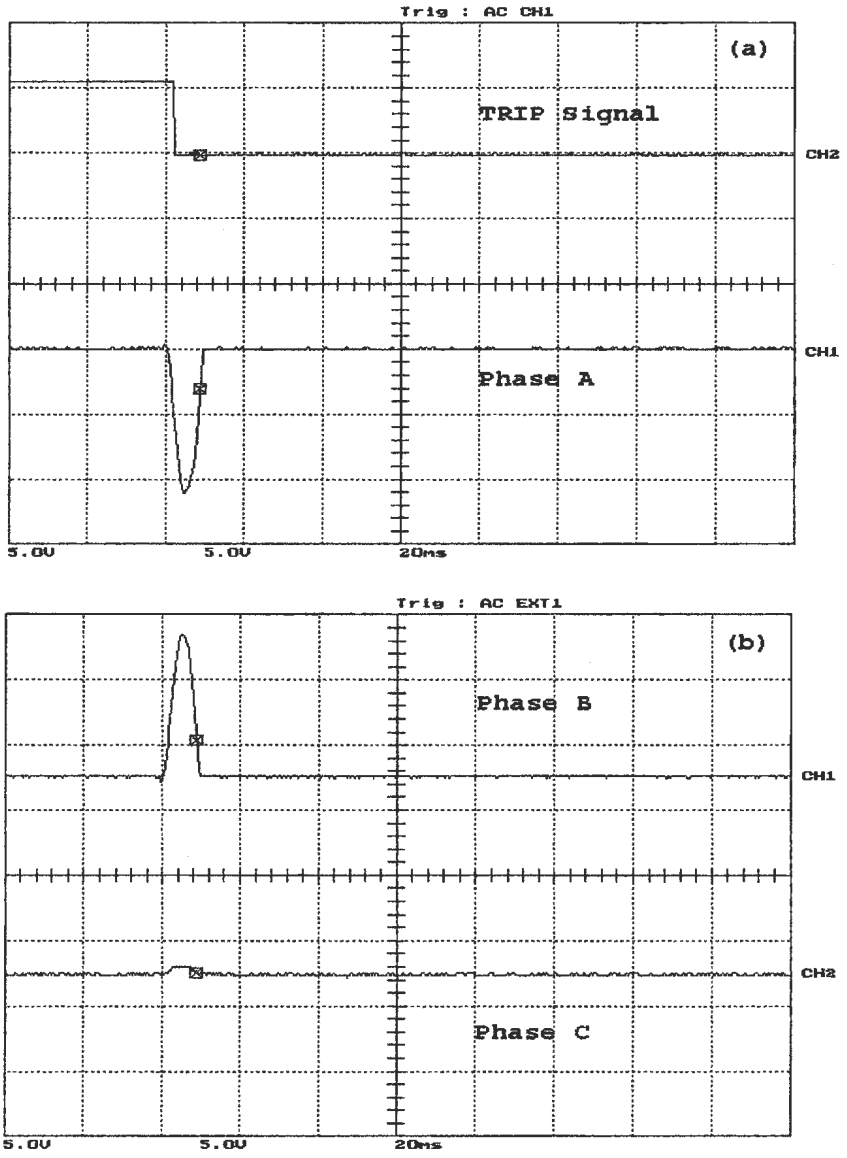

Figure 5.14: Unloaded phase A to phase B fault, occurred before energization on the primary side, (a) the WPT response and phase A differential current,(b) phase B and phase C differential currents. Y-scale is 1 Div. = 11.67 A

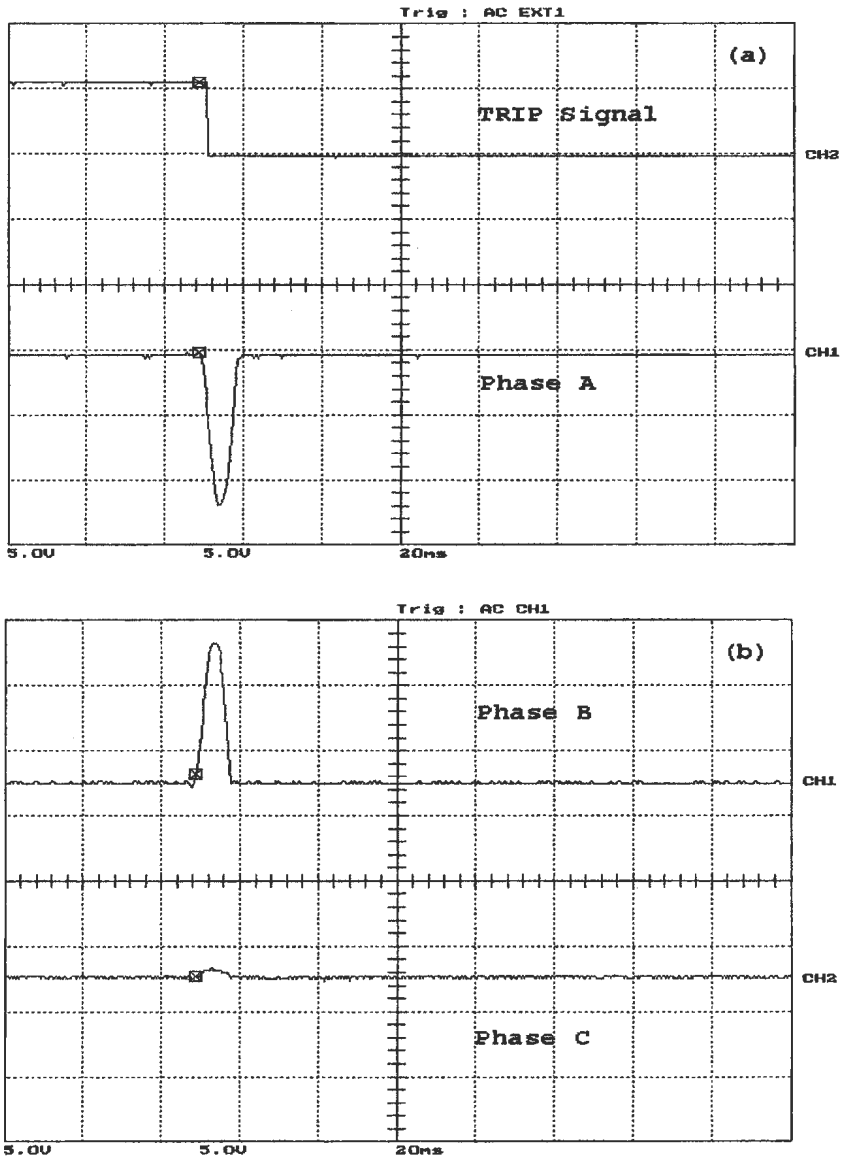

Figure 5.15: Unloaded phase A to phase B fault, occurred after energization on the primary side, (a) the WPT response and phase A differential current,(b) phase B and phase C differential currents. Y-scale is 1 Div. = 11.67 A

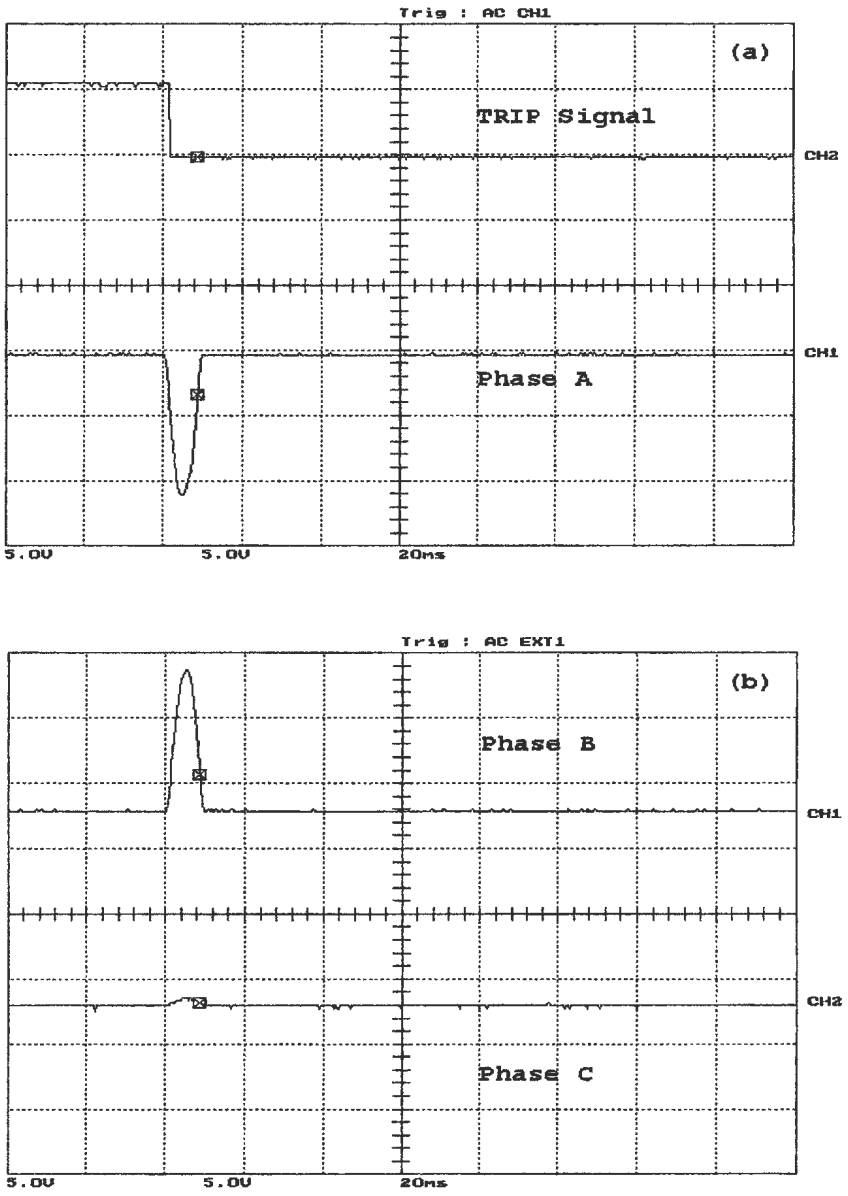

Figure 5.16: Loaded phase A to phase B fault, occurred before energization on the primary side, (a) the WPT response and phase A differential current,(b) phase B and phase C differential currents. Y-scale is 1 Div. = 11.67 A

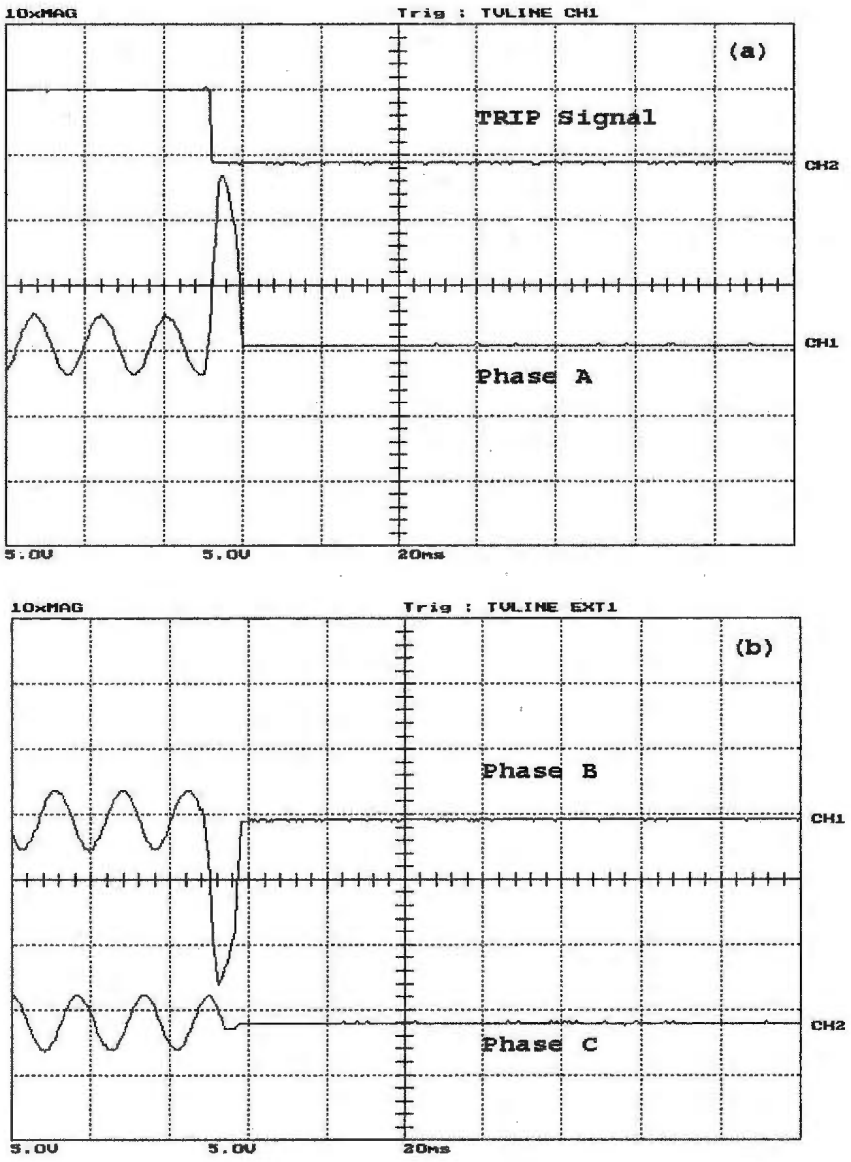

Figure 5.17: Loaded phase A to phase B fault, occurred after energization on the primary side, (a) the WPT response and phase A differential current,(b) phase B and phase C differential currents. Y-scale is 1 Div. = 11.67 A

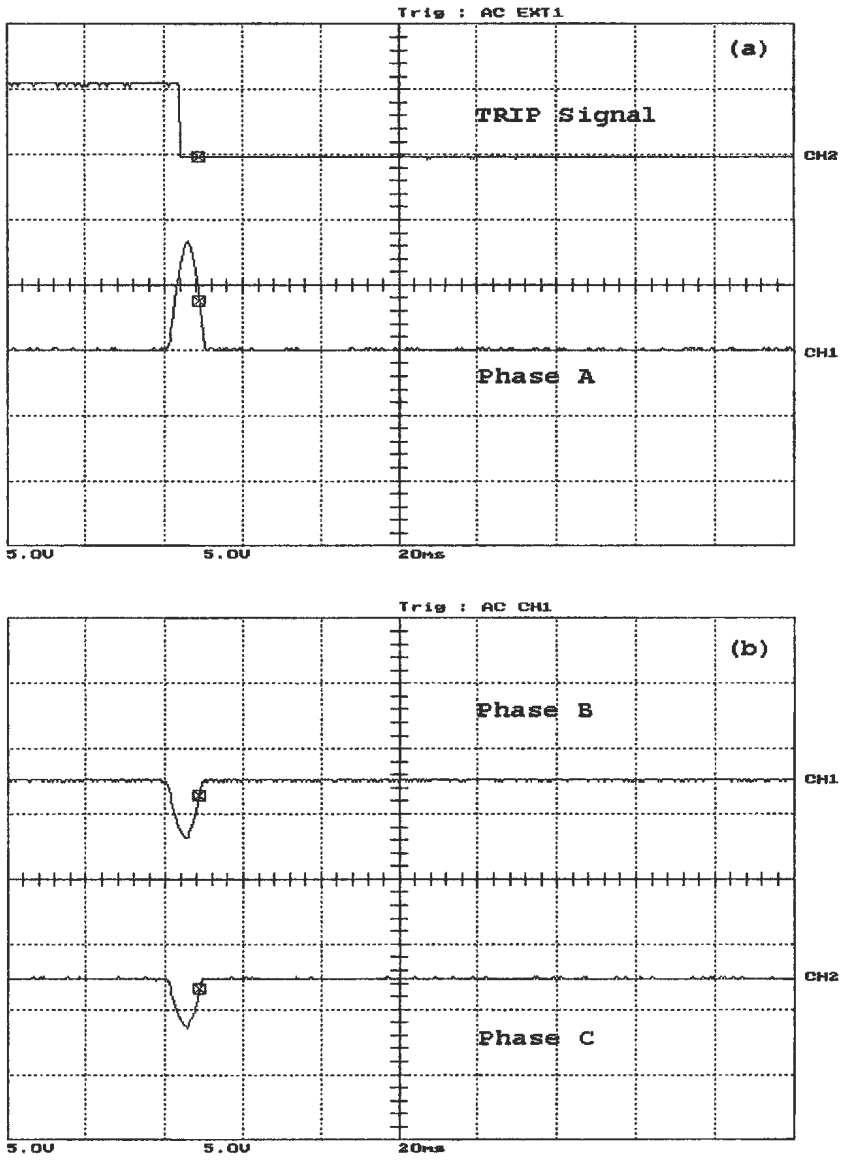

Figure 5.18: Unloaded phase A to phase B fault, occurred before energization on the secondary side, (a) the WPT response and phase A differential current,(b) phase B and phase C differential currents. Y-scale is 1 Div. = 11.67 A

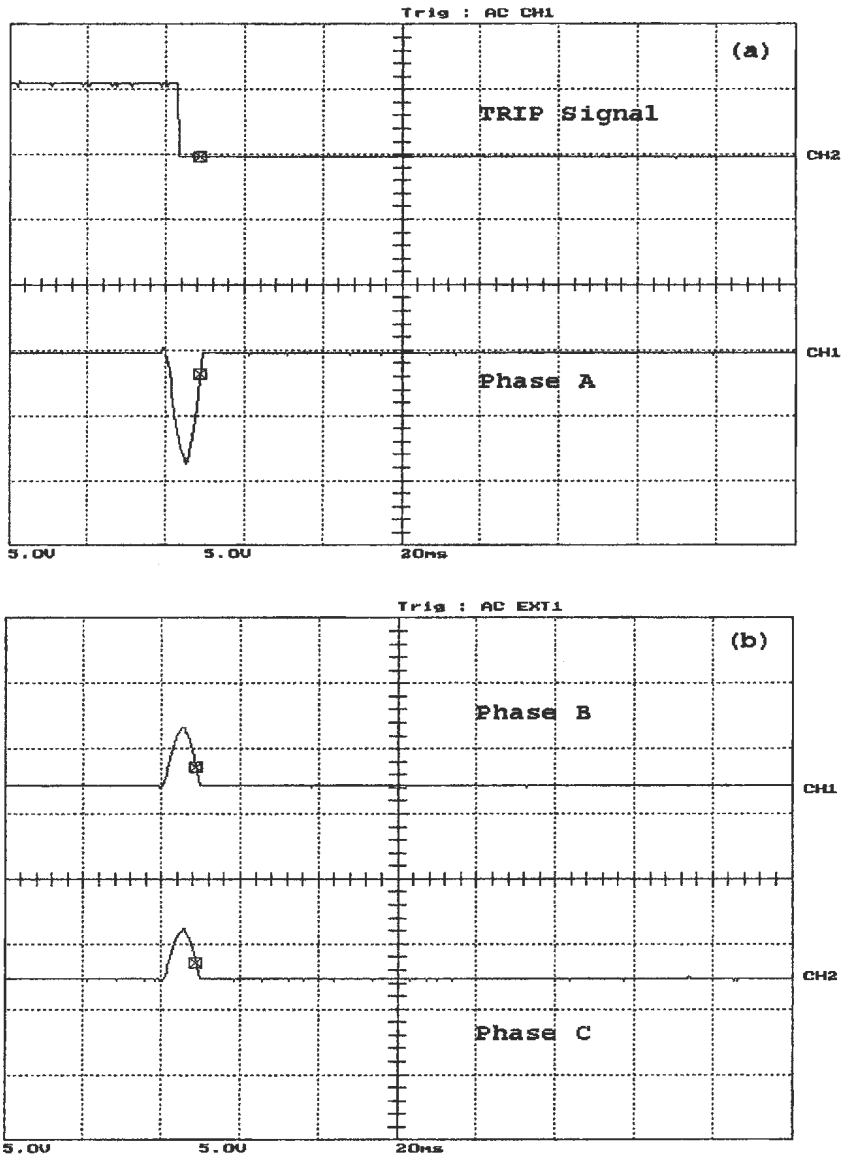

Figure 5.19: Unloaded phase A to phase B fault, occurred after energization on the secondary side, (a) the WPT response and phase A differential current,(b) phase B and phase C differential currents. Y-scale is 1 Div. = 11.67 A

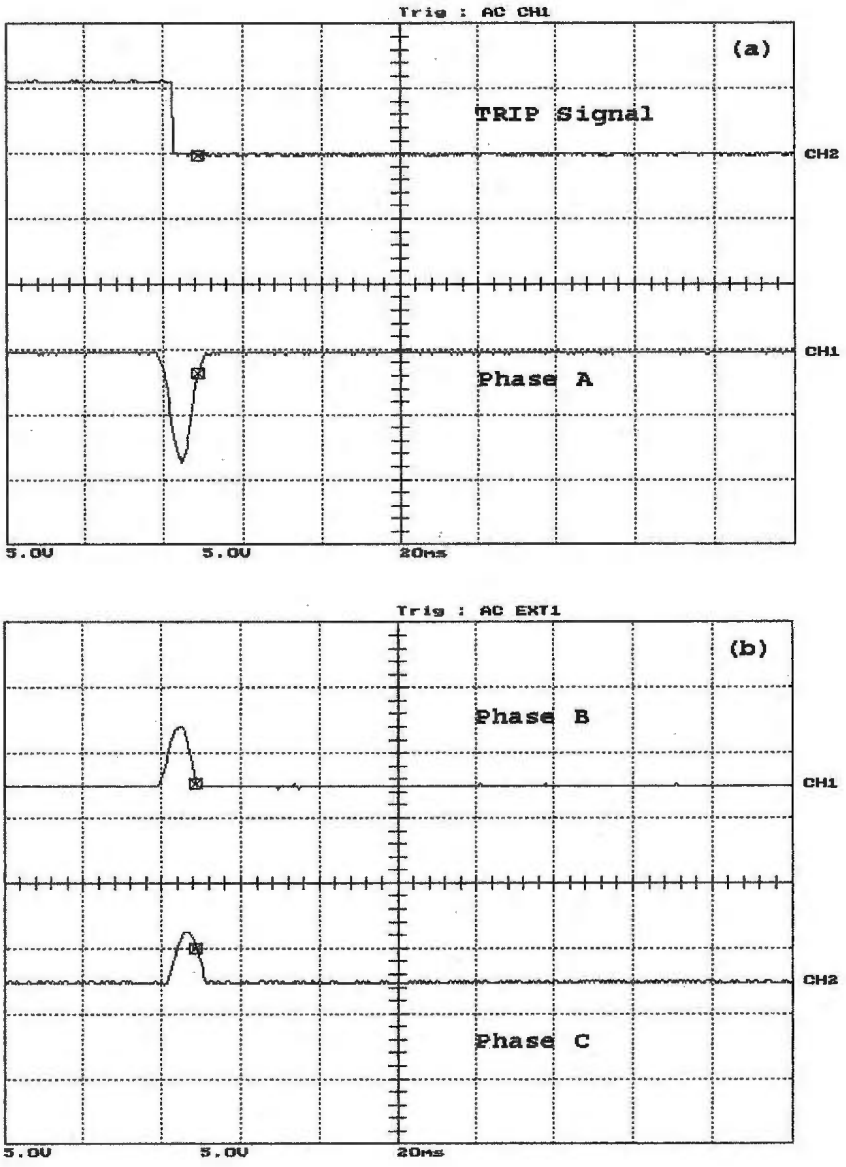

Figure 5.20: Loaded phase A to phase B fault, occurred before energization on the secondary side, (a) the WPT response and phase A differential current,(b) phase B and phase C differential currents. Y-scale is 1 Div. = 11.67 A

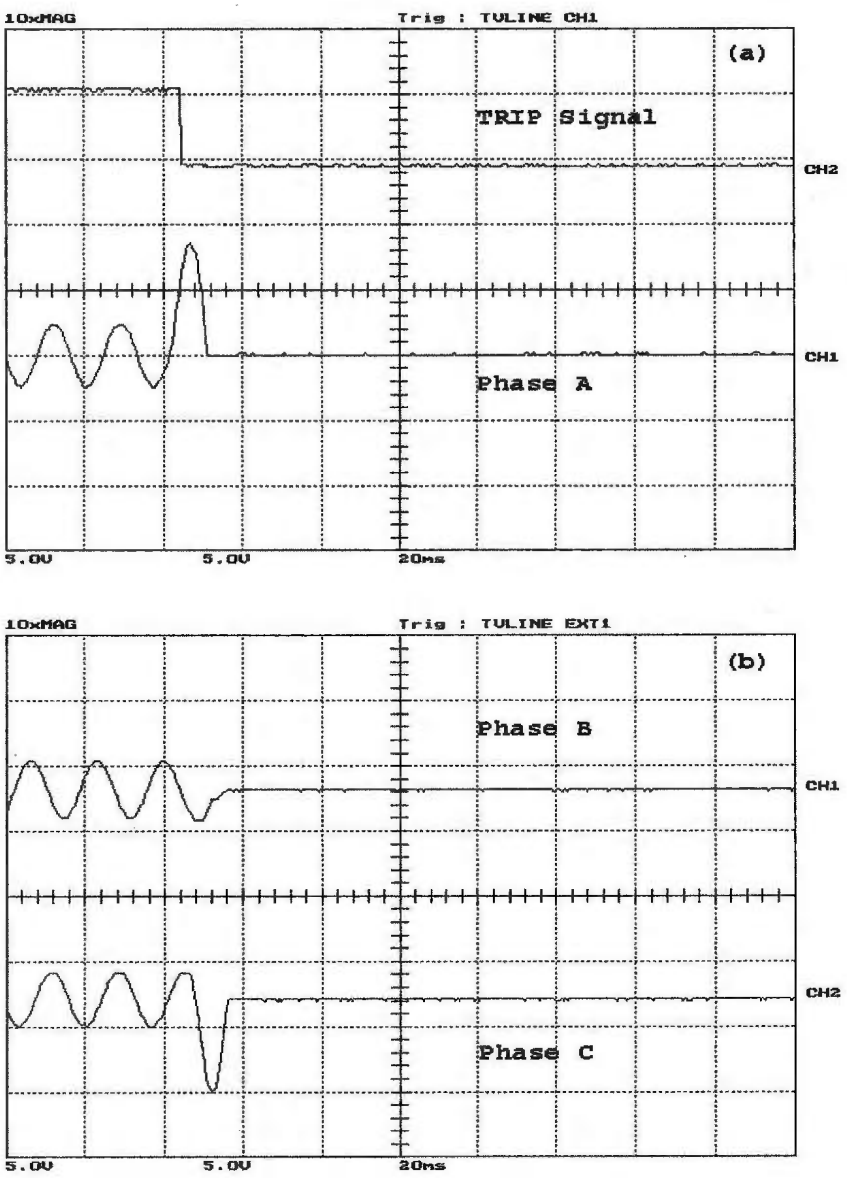

Figure 5.21: Loaded phase A to phase B fault, occurred after energization on the secondary side, (a) the WPT response and phase A differential current,(b) phase B and phase C differential currents. Y-scale is 1 Div. = 11.67 A

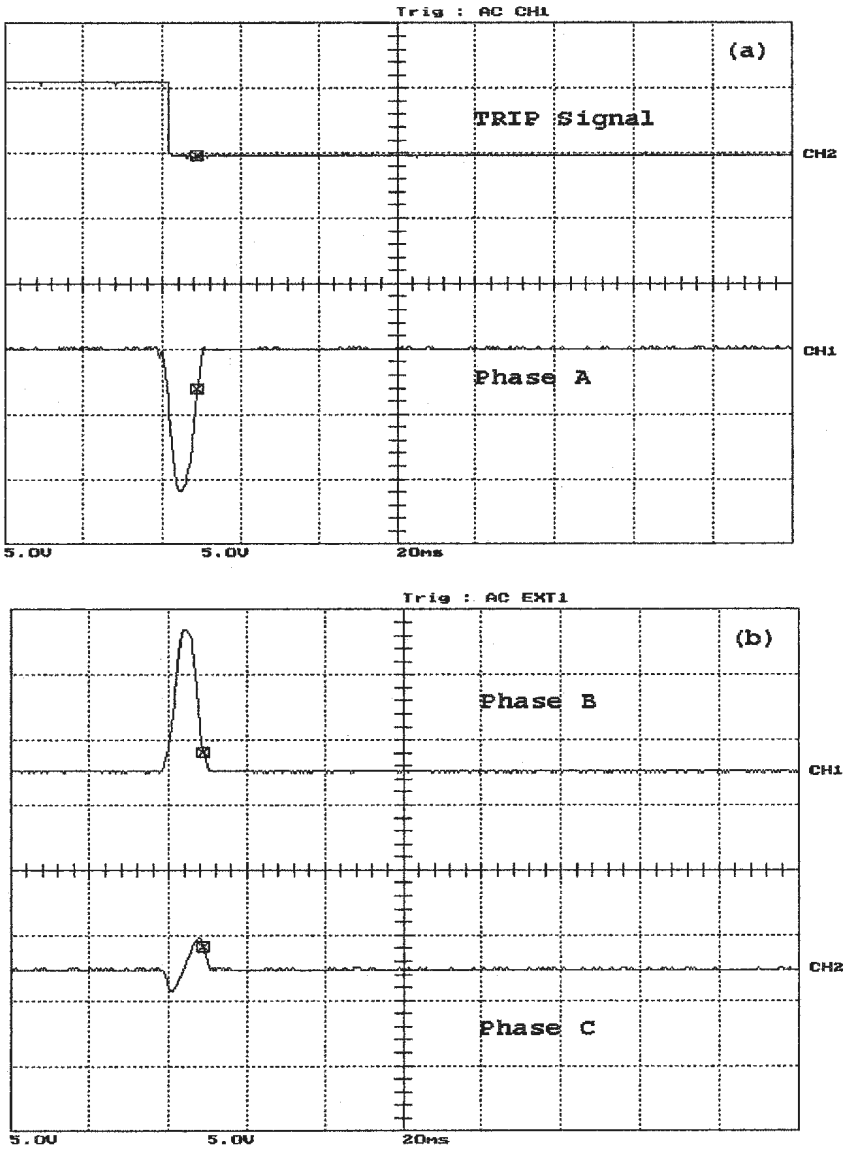

Figure 5.22: Unloaded three-phase to ground fault, occurred before energization on the primary side, (a) the WPT response and phase A differential current,(b) phase B and phase C differential currents. Y-scale is 1 Div. = 11.67 A

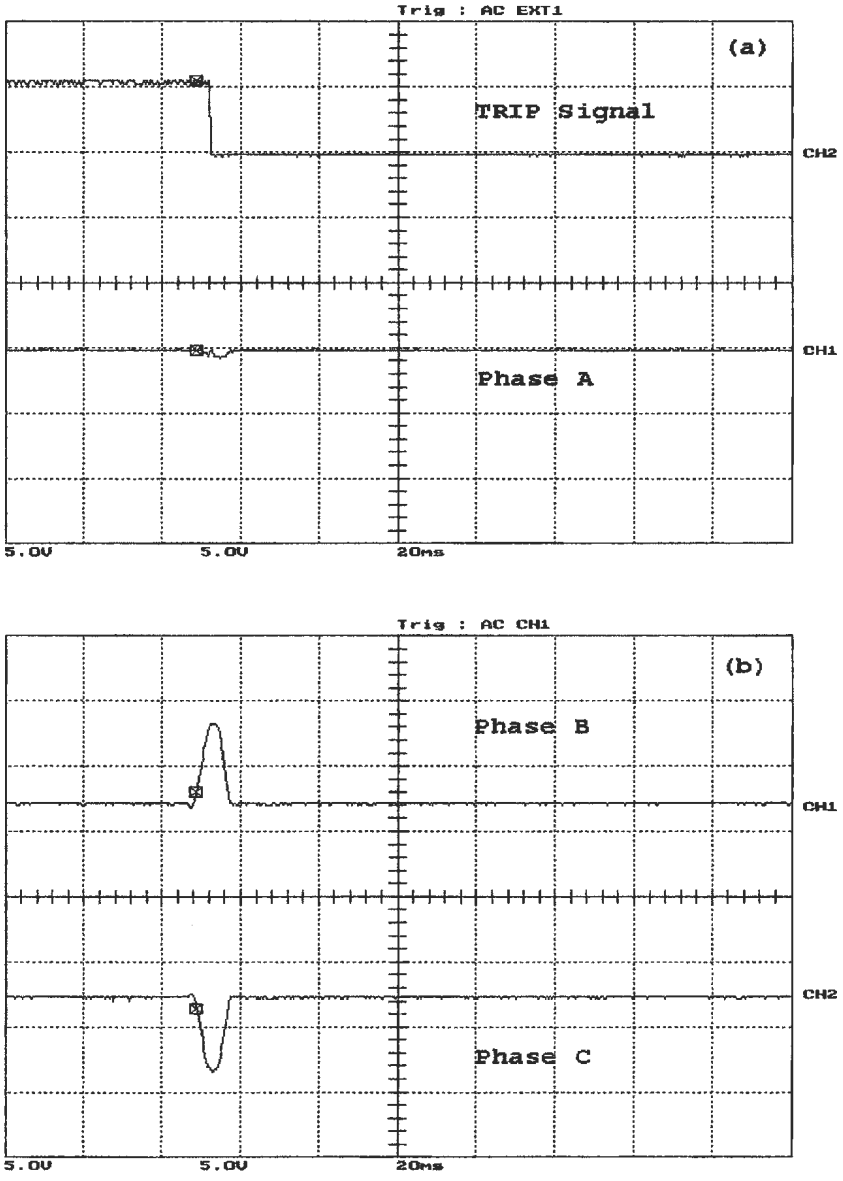

Figure 5.23: Unloaded three-phase to ground fault, occurred after energization on the secondary side, (a) the WPT response and phase A differential current,(b) phase B and phase C differential currents. Y-scale is 1 Div. = 11.67 A

$Z_b = 11.9129\ \Omega$

$Z_c = \infty$

The tests were carried out for the unbalanced loading case for the primary phase A to phase B fault, primary phase C to ground fault, secondary phase B to phase C fault and secondary phase A to ground fault. All these faults were tested after the power transformer is energized. Some of the results are presented in this chapter, while the rest are provided in Appendix A5.

Figure 5.24 shows phase A to phase B fault occurring on the primary side of the power transformer after energizing with the unbalanced loading case. The result of the case when phase B to phase C fault took place on the secondary side is shown in Figure 5.25. For the case of two phases loading (phase C is open circuit), different unsymmetrical faults were tested on both sides of the power transformer. Figures 5.26 and 5.27 show some of the results obtained, while the rest of the results are provided in Appendix A5.

Figure 5.26 shows the test results for phase C to ground fault on the primary side of the power transformer occurred after energization. The result of the case when the same type of fault took place on the secondary side is shown in Figure 5.27.

The proposed WPT-based algorithm is successfully implemented on-line using the digital signal processor board DS1102. The real time tests showed a consistent results with the off-line results obtained using a data collected from the 5 kVA three-phase core type step up laboratory power transformer. Also, the results presented an accurate, prompt and fast response of the WPT based algorithm in all cases, even with special cases of unbalanced loading conditions as well as one phase open. These special cases showed the complete independence of the protected power transformer parameters and loading conditions. The WPT trip signal was delivered in all cases of faults in less than quarter a cycle, even with

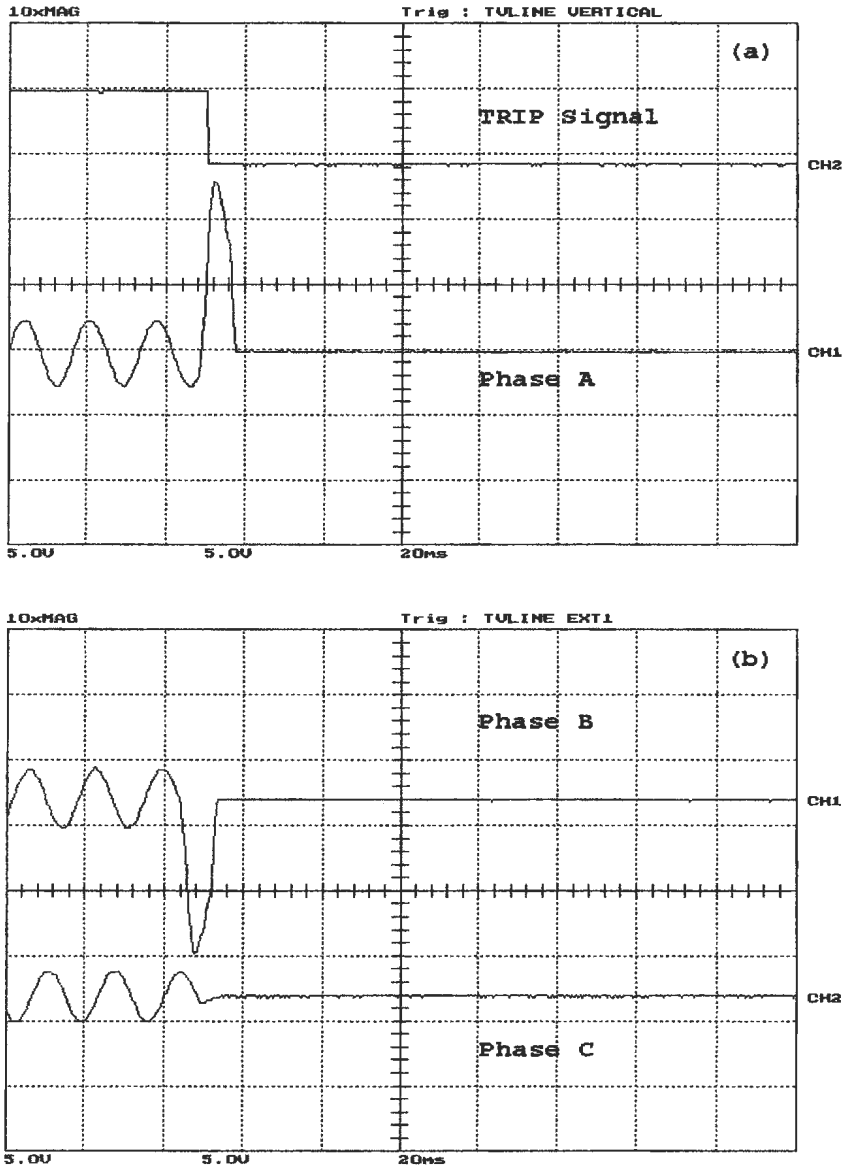

Figure 5.24: Unbalanced loaded phase A to phase B fault, occurred after energization on the primary side, (a) the WPT response and phase A differential current,(b) phase B and phase C differential currents. Y-scale is 1 Div. = 11.67 A

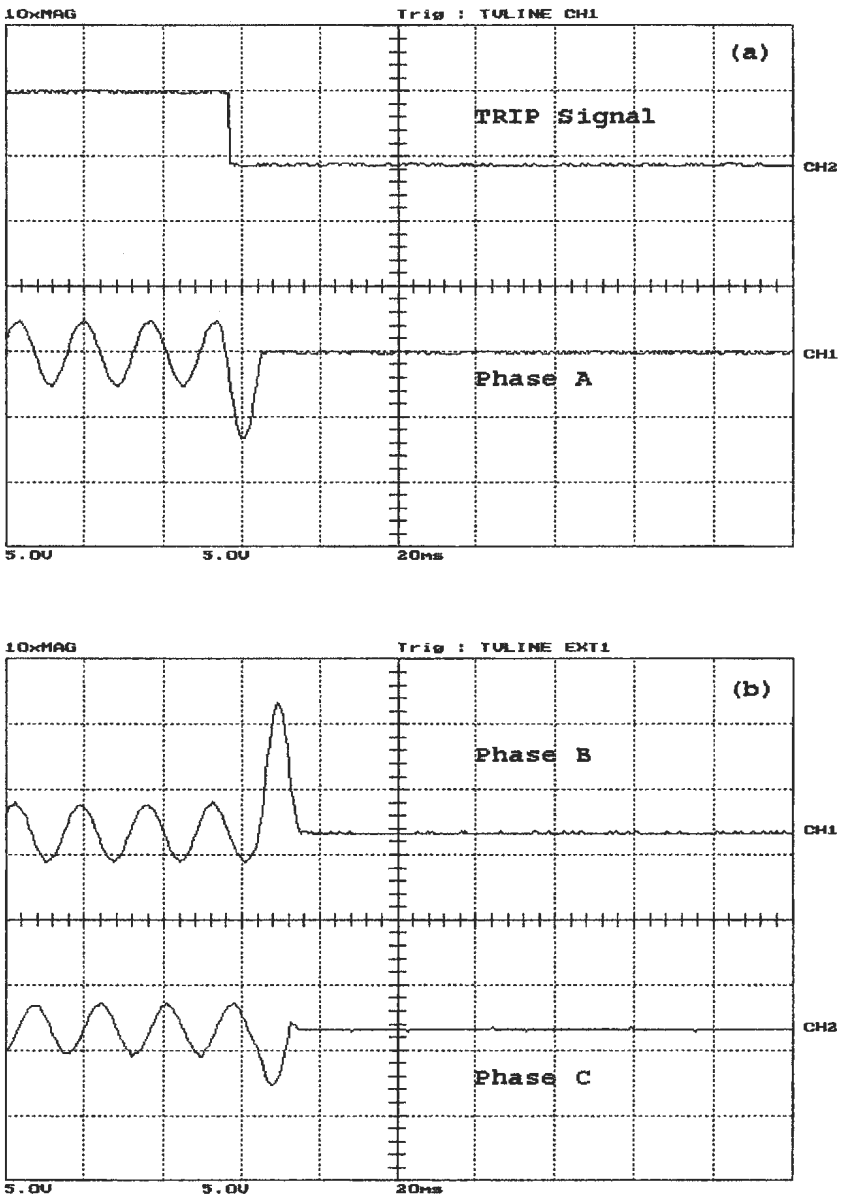

Figure 5.25: Unbalanced loaded phase B to phase C fault, occurred after energization on the secondary side, (a) the WPT response and phase A differential current,(b) phase B and phase C differential currents. Y-scale is 1 Div. = 11.67 A

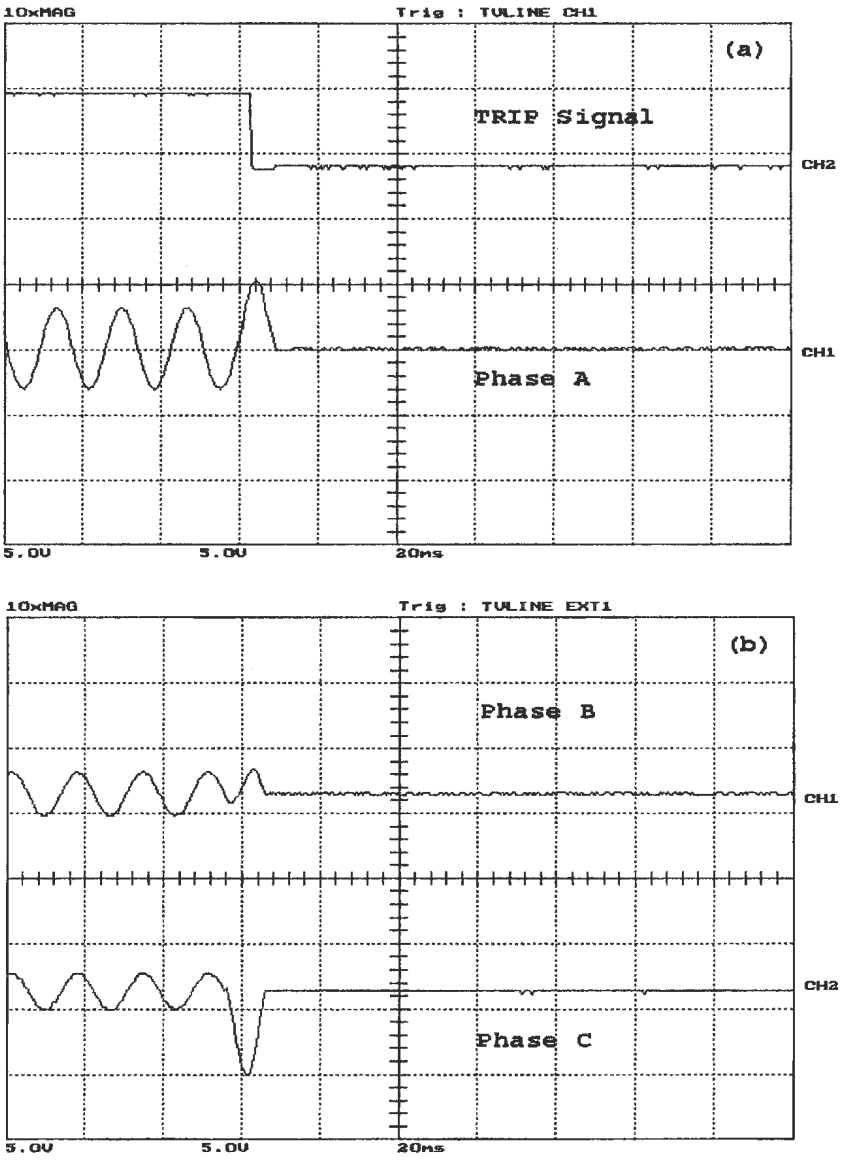

Figure 5.26: Two phases loaded phase C ground fault, occurred after energization on the primary side, (a) the WPT response and phase A differential current,(b) phase B and phase C differential currents. Y-scale is 1 Div. = 11.67 A

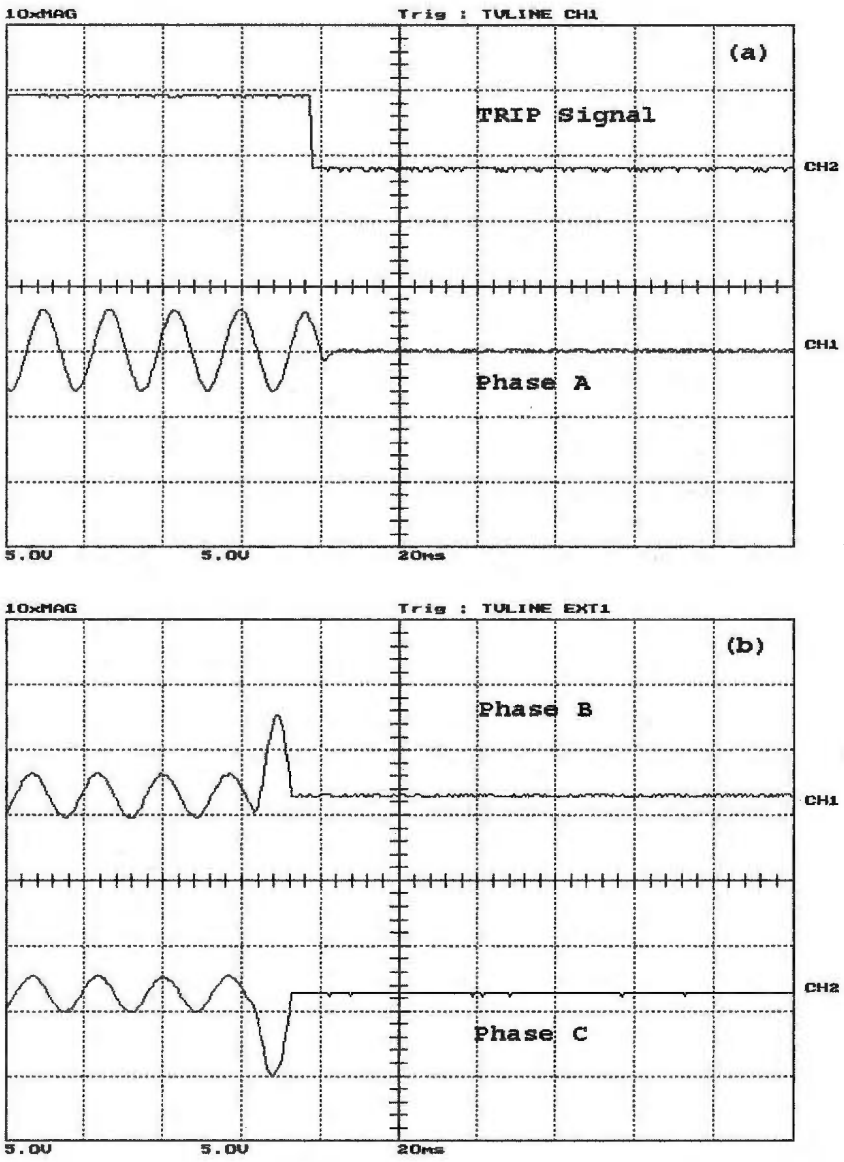

Figure 5.27: Two phases loaded phase C ground fault, occurred after energization on the secondary side, (a) the WPT response and phase A differential current,(b) phase B and phase C differential currents. Y-scale is 1 Div. = 11.67 A

the existence of some distortion in current waveforms due to CT saturation and DC offsets, the WPT was able to identify different fault currents and initiate the trip signal to open the circuit breaker.

The next chapter provides more real time testing on another three-phase 2 kVA three-phase multi-tap power transformer configured as a step down transformer.

Chapter 6

Extending The Real-Time Testing

In chapter 5, the real-time testing of the wavelet packet transform (WPT)-based differential protection algorithm has shown a powerful ability and a fast response in distinguishing between the magnetizing inrush and different internal fault currents under various conditions of energizing and loading. This chapter extends the real-time testing of the WPT-based differential protection algorithm using another power transformer, which has a quite different configuration in terms of voltage ratio, configuration of the windings, core type material and rating values. The second power transformer is to be tested using the same algorithm developed previously along with the same experimental setup described in chapter 5 as shown in Figure 5.2. Moreover, the same tests under the various conditions of loading and energizing are to be investigated. The real-time testing is extended mainly to demonstrate the universality of the proposed WPT-based differential protection algorithm for all types of power transformers. The second power transformer configuration is illustrated first. Then the real-time test results are presented. Finally, a comparison between the results obtained from both power transformers is made.

6.1 Transformer configuration

The power transformer to be used for the extended real-time testings in this chapter is a 2kVA, 127-220/31.8-42-63.5 V, 50Hz, multi-tap three-phase power transformer, and is configured as Δ-Y 127/63.5 V double secondary. The configuration is shown in Figure 6.1.

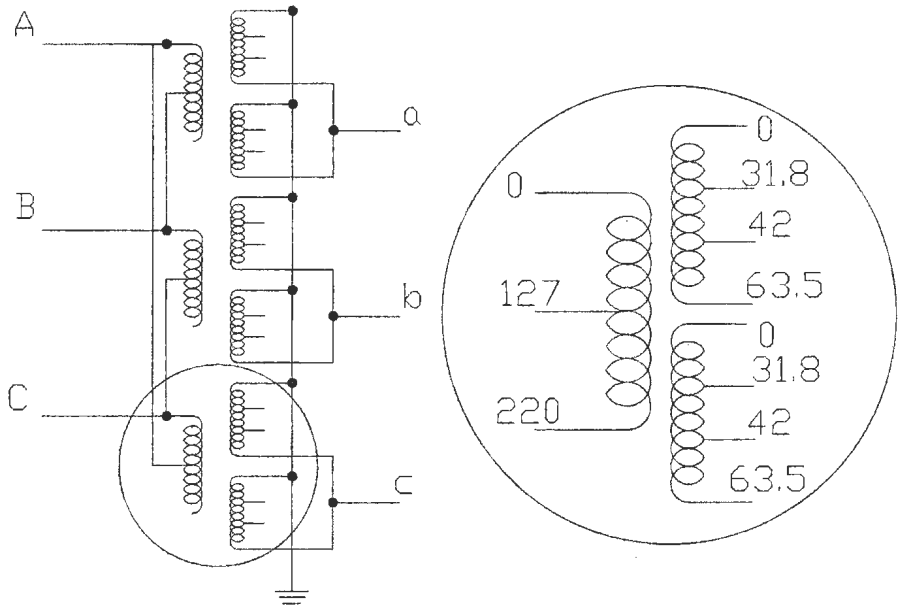

Figure 6.1: The configuration of the step down, Δ-Y, 2kVA, 127-220/31.8-42-63.5 V, 50Hz, multi-tap three-phase power transformer

This multi-tap power transformer is rated at 50Hz, which adds more complexities to the testing due to the saturation of the core and/or the saturation of the current transformers (CTs). The following section provides the test results of different magnetizing inrush currents switched on at random as well as the testing results of various internal faults under different conditions of energizing and loading.

6.2 On-line Test Results

The results of the real-time tests obtained from the core type step up power transformer in chapter 5 showed an excellent ability to identify and respond to the different types of currents flowing through the tested power transformer regardless of the saturation and distortion in the current waveforms. The test results confirmed that the proposed algorithm is independent of both the transformer parameters and any loading condition. This motivates the application of the same algorithm using the same experimental setup to test another power transformer, which has a different winding configuration, core material and rating values.

6.2.1 Magnetizing inrush current

The tests involving the magnetizing inrush current are carried out through random switching for both loaded and unloaded conditions. It is found that the WPT never provided a trip signal. Figures 6.2-6.5 show some of the magnetizing inrush current test results, while the remaining results are provided in Appendix B1. Figures 6.2-6.3 show the unloaded condition. It is evident that the WPT encountered no problem in identifying the inrush currents, and thus never initiated any trip signal (the WPT response) to open the circuit breaker. The same results of identifying the inrush conditions have been obtained for the loaded condition shown in Figures 6.4-6.5. These tests were carried out with the primary line to line voltage of 100 V.

It is worth mentioning that the magnetizing inrush current of this 2 kVA multi-tap power transformer has a higher amplitude than the magnetizing inrush current of the 5 kVA core type power transformer, and takes a longer time to decay as shown in Figures 6.2 through 6.5. In addition, the waveform of the magnetizing inrush current in the multi-tap power transformer has some distortion, which is

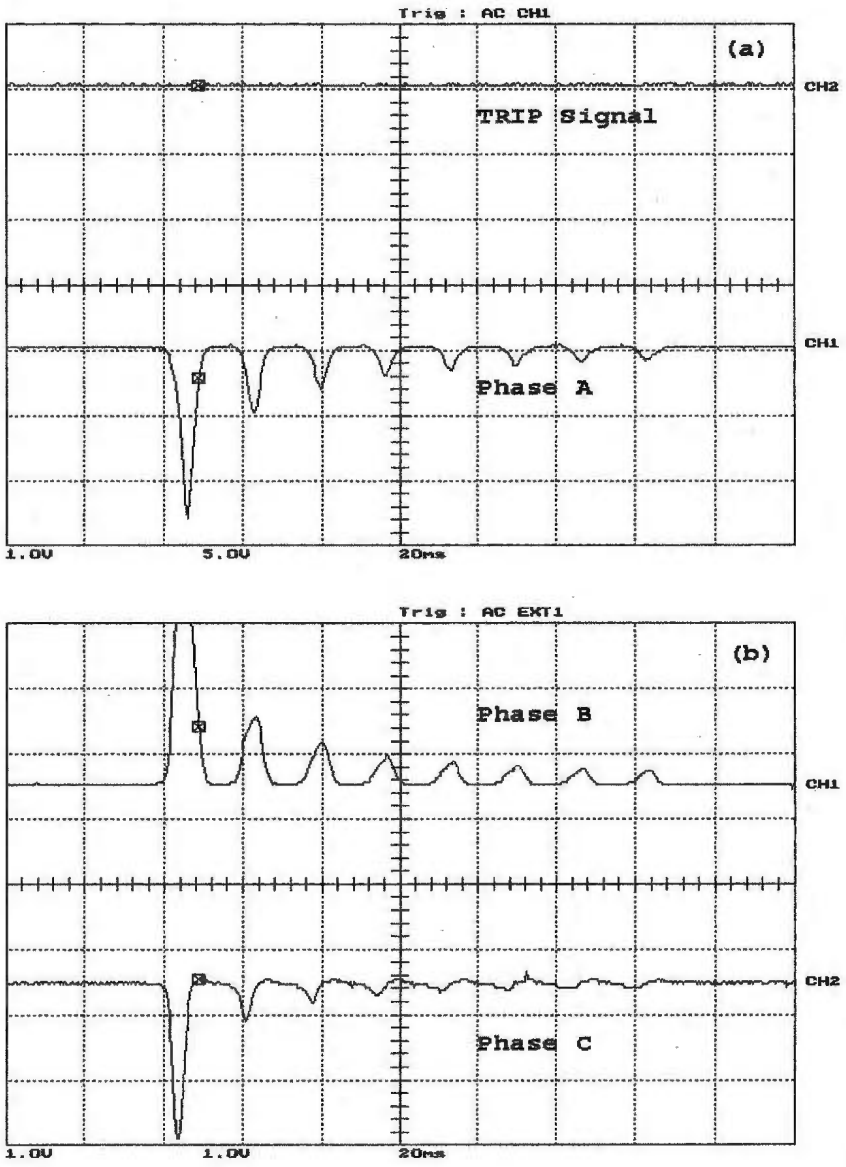

Figure 6.2: Unloaded magnetizing inrush current, (a) the WPT response and phase A differential current, (b) phase B and phase C differential currents. Y-scale is 1 Div. = 11.67 A

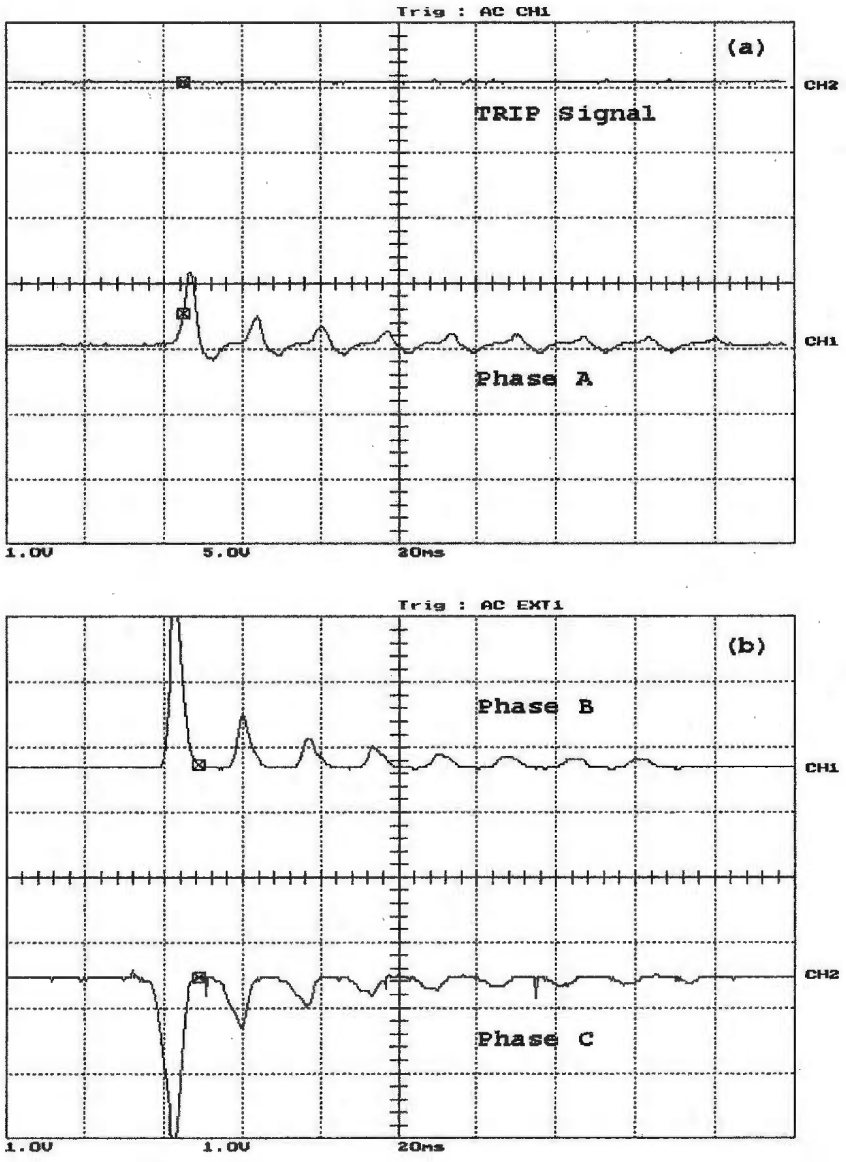

Figure 6.3: Unloaded magnetizing inrush current, (a) the WPT response and phase A differential current, (b) phase B and phase C differential currents. Y-scale is 1 Div. = 11.67 A

due to the saturation of the CTs.

6.2.2 Internal fault currents

Many internal faults are investigated to test the WPT-based algorithm response for different internal faults under various conditions of energizing and loading. All the fault tests were performed for the same four combinations mentioned in chapter 5(**(i)** for fault occurrence without a load before energizing,**(ii)** without a load after energizing, **(iii)** with a load before energizing and **(iv)** with a load after energizing). These different fault conditions were tested for each phase of the three phases on both the primary side and the secondary side of the power transformer. The results showed that the fault is distinguished and the trip signal is initiated to open the circuit breaker in less than quarter a cycle (2-3 ms) based on 60 Hz system in all cases.

Single phase to ground fault

This test was carried out by connecting one phase to the ground under the four aforementioned combinations of energizing and loading on both sides of the power transformer for each phase. It should be noted that in all cases of loading conditions, a balanced inductive (R-L) load of $Z = 20 + j11.9129\ \Omega$/phase is used. Figures 6.6-6.12 show the results of the single phase to ground fault tested on phase B. The test results for both phase A and phase C are provided in Appendix B2. These figures show the differential current in the three phases as well as the WPT trip signal. In all tests carried out, the fault was identified and the trip signal was initiated to isolate the fault by opening the circuit breaker in less than quarter a cycle based on 60 Hz system.

1- Primary side faults

Figure 6.6 shows the primary side phase B to ground fault occurring before energizing the power transformer without a load. The results of the same type of

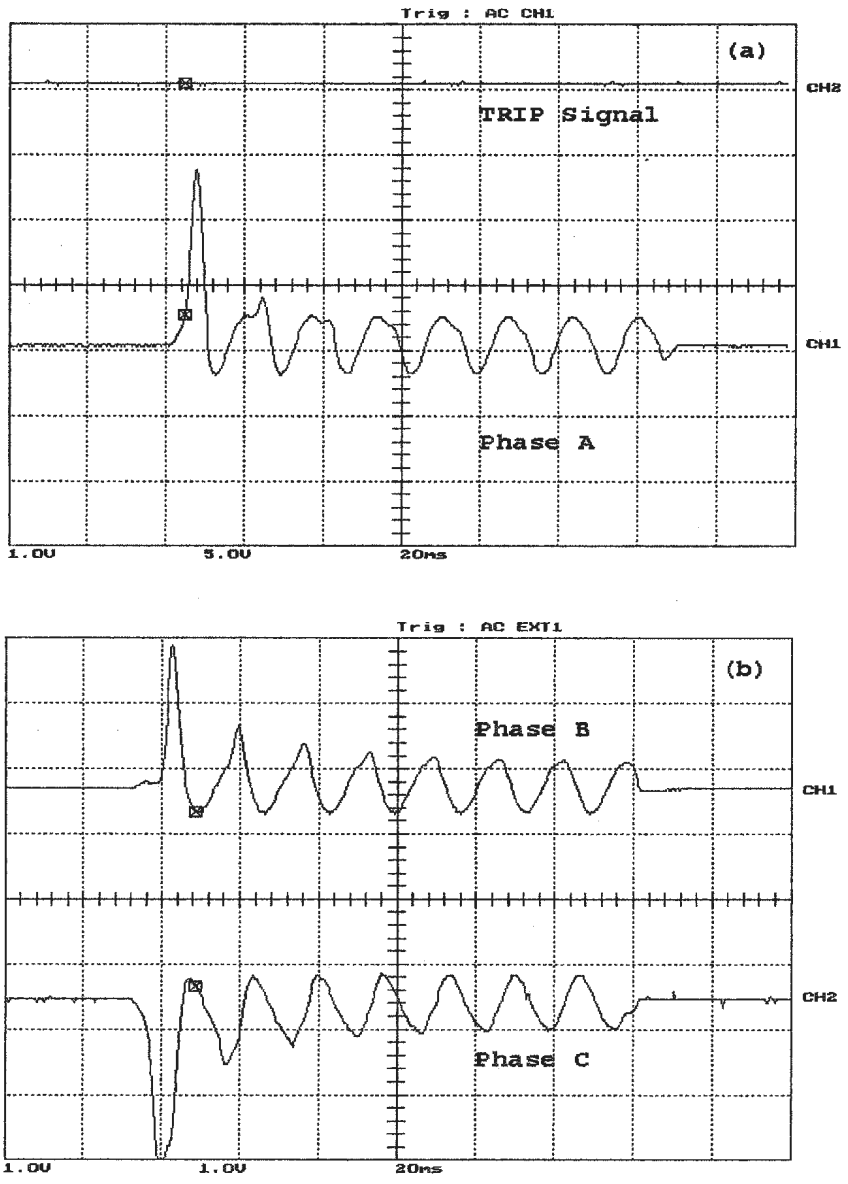

Figure 6.4: Loaded magnetizing inrush current, (a) the WPT response and phase A differential current, (b) phase B and phase C differential currents. Y-scale is 1 Div. = 11.67 A

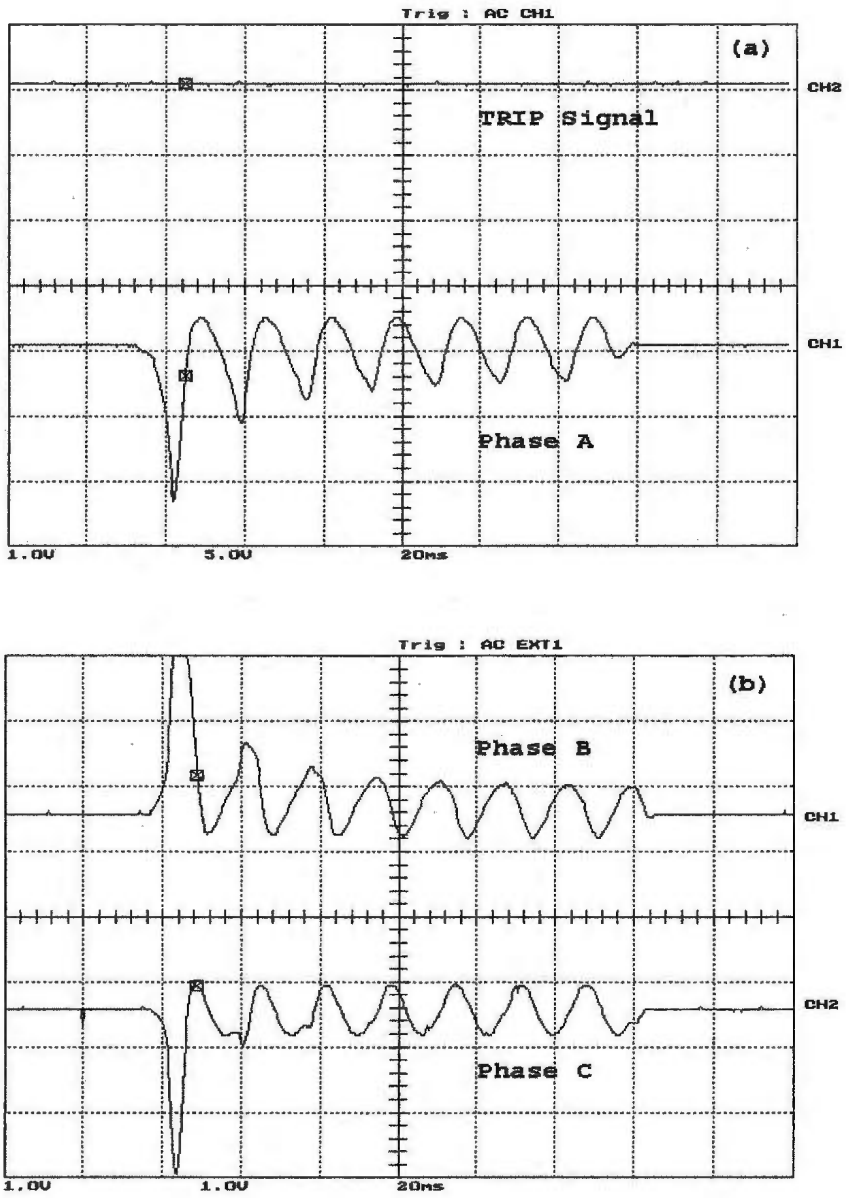

Figure 6.5: Loaded magnetizing inrush current, (a) the WPT response and phase A differential current, (b) phase B and phase C differential currents. Y-scale is 1 Div. = 11.67 A

faults occurring after energizing the power transformer without a load is shown in Figure 6.7. The result of the phase B to ground fault on the primary side occurring before energizing the power transformer when the balanced inductive load is connected on the secondary side of the power transformer is shown in Figure 6.8. The result of the case when the phase B to ground fault occurred on the primary side after energizing the power transformer for the same loading condition is shown in Figure 6.9.

2-Secondary Side faults

Figure 6.10 shows the phase B to ground fault on the secondary side before energizing the power transformer without connecting a load. The results when the same type of faults occurred after energizing the power transformer with out a load is shown in Figure 6.11. The condition of phase B to ground fault with the balanced inductive load connected before energizing the transformer is shown in Figure 6.12.

Phase to phase fault

Tests for this fault were carried out by connecting two phases for the four aforementioned conditions of energization and loading on both sides of the three-phase power transformer. Figures 6.13 through 6.19 show the phase A to phase C fault, while the remaining fault results for phase A with phase B and phase B with phase C are provided in Appendix B3. In all these figures, the differential three-phase current and the WPT trip signal are shown. Again, the WPT identified the fault and initiated a trip signal in less than quarter a cycle.

1- Primary side faults

The result of the case when the phase A to phase C fault occurred before energizing the power transformer without connecting a load is shown in Figure 6.13. Figure 6.14 shows the result of the same type of faults occurring after energizing

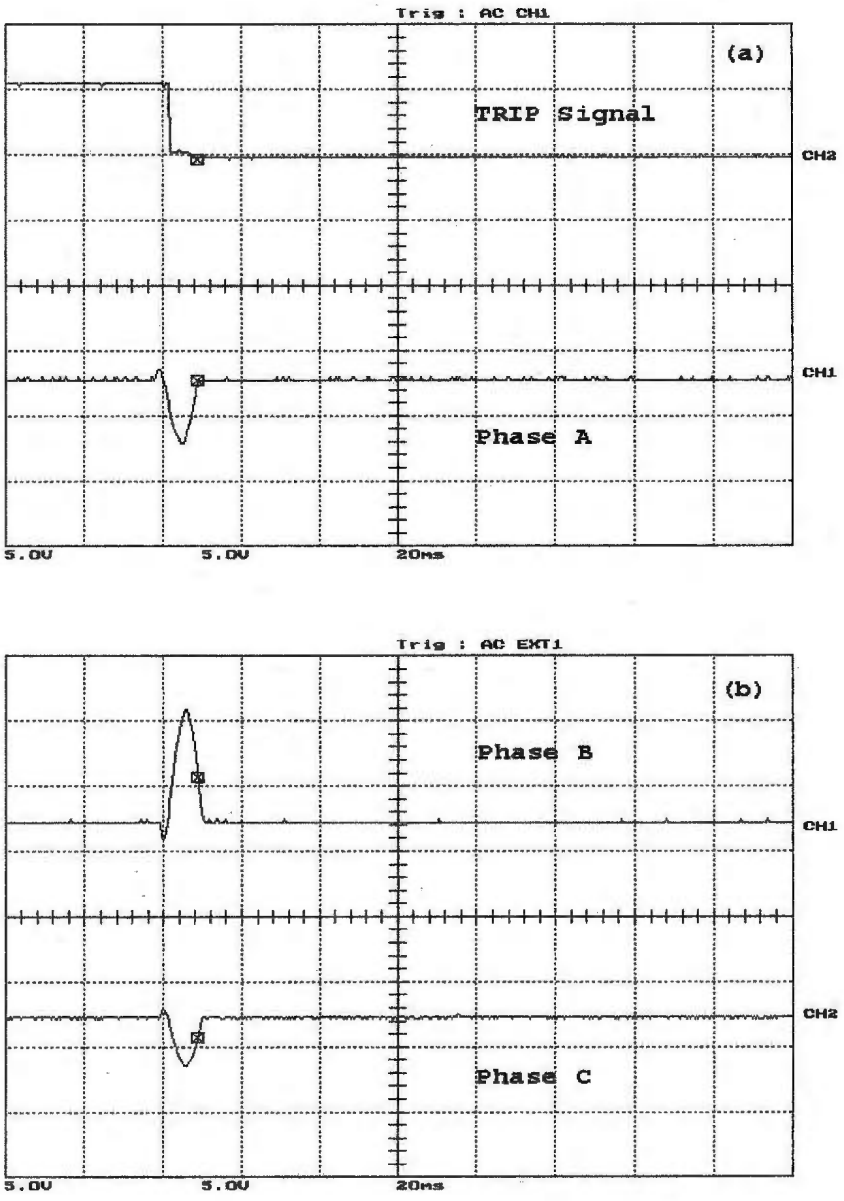

Figure 6.6: Unloaded phase B to ground fault, occurred before energization on the primary side, (a) the WPT response and phase A differential current and (b) phase B and phase C differential currents. Y-scale is 1 Div. = 11.67 A

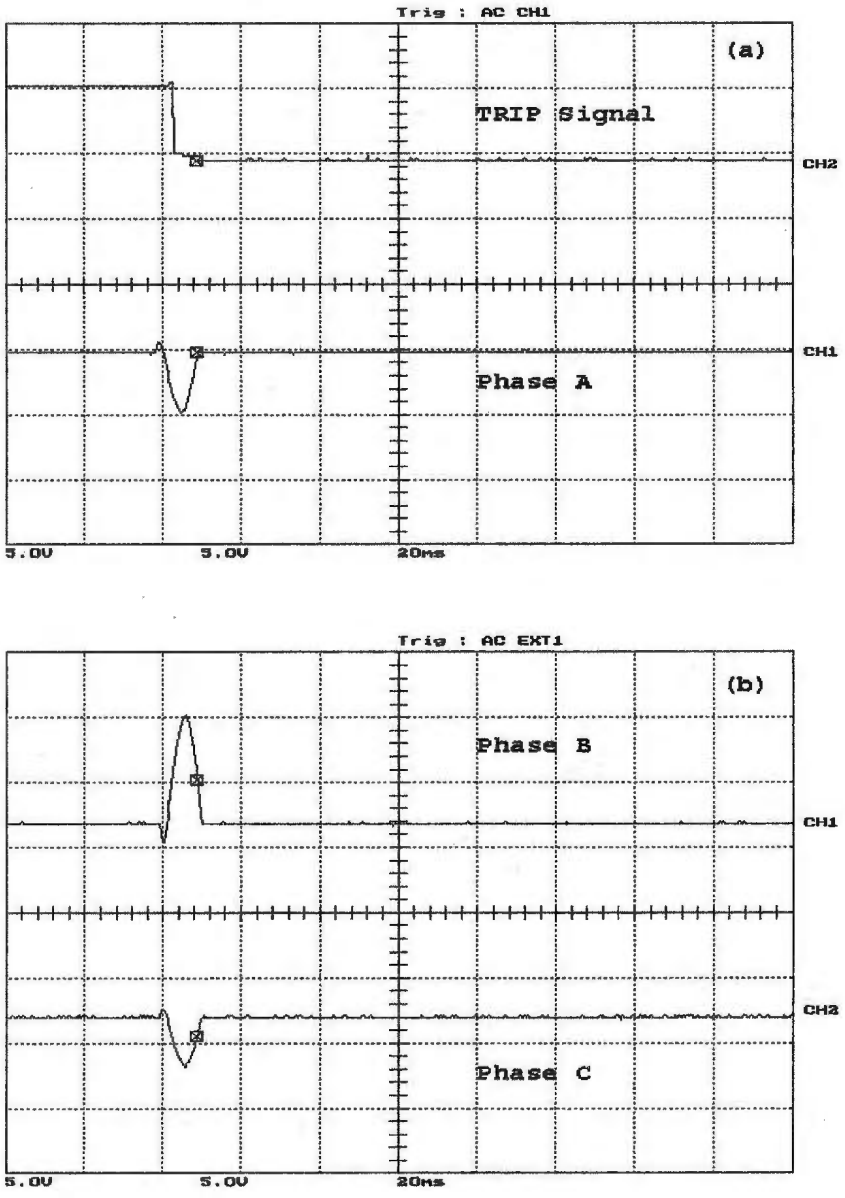

Figure 6.7: Unloaded phase B to ground fault, occurred after energization on the primary side, (a) the WPT response and phase A differential current, (b) phase B and phase C differential currents. Y-scale is 1 Div. = 11.67 A

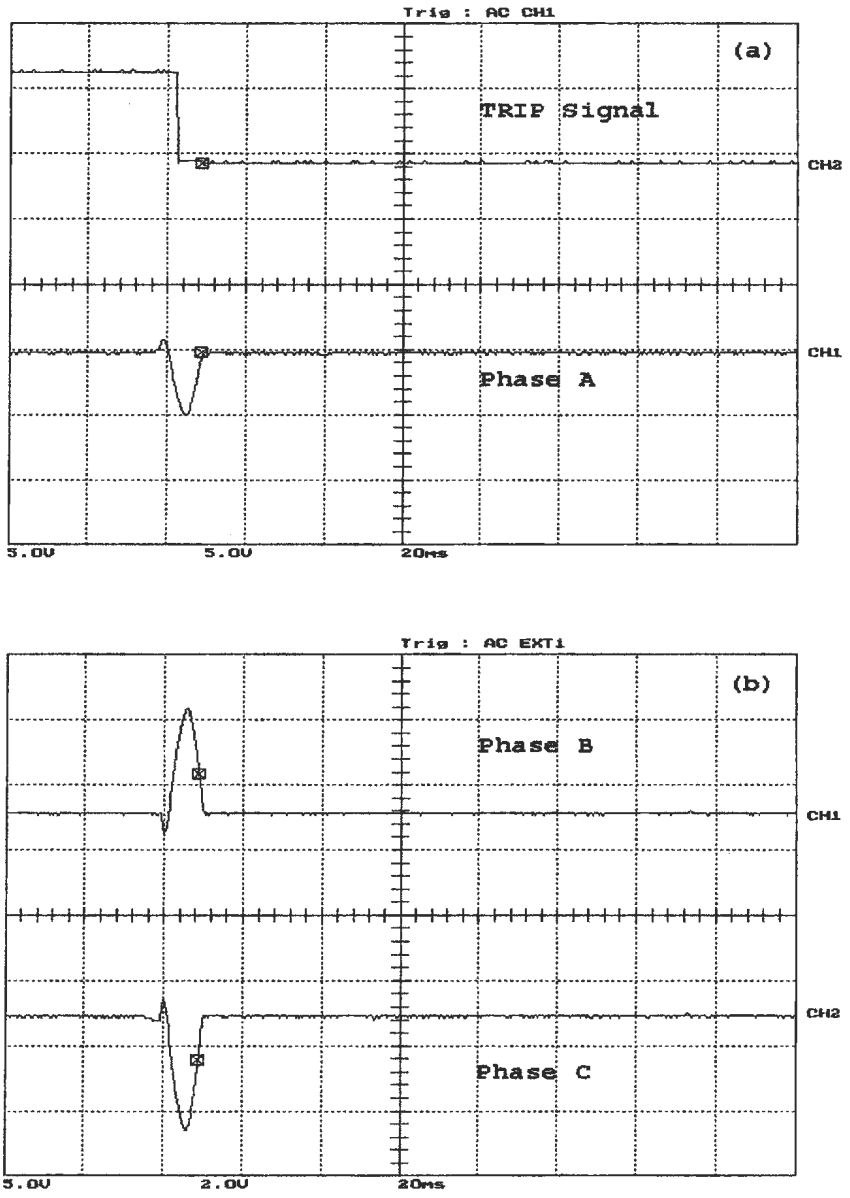

Figure 6.8: Loaded phase B to ground fault, occurred before energization on the primary side, (a) the WPT response and phase A differential current, (b) phase B and phase C differential currents. Y-scale is 1 Div. = 11.67 A

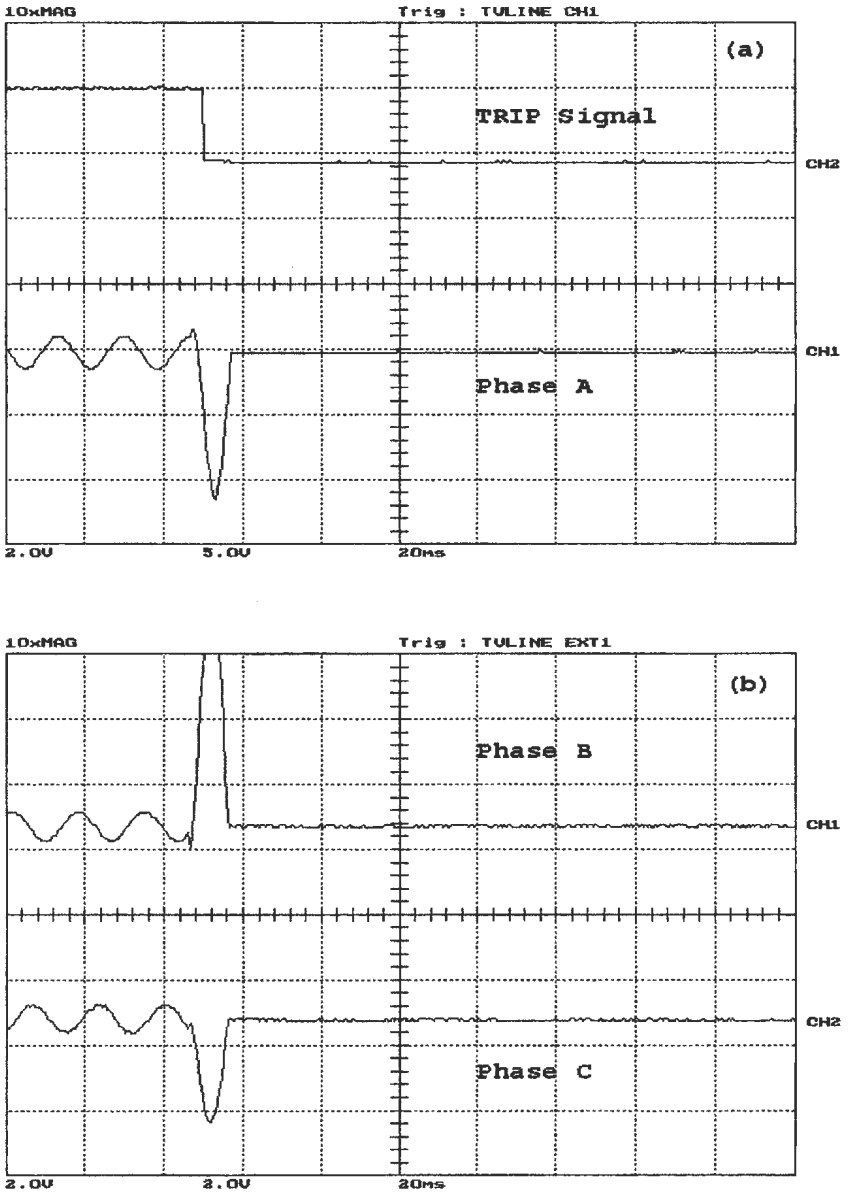

Figure 6.9: Loaded phase B to ground fault, occurred after energization on the primary side, (a) the WPT response and phase A differential current, (b) phase B and phase C differential currents. Y-scale is 1 Div. = 11.67 A

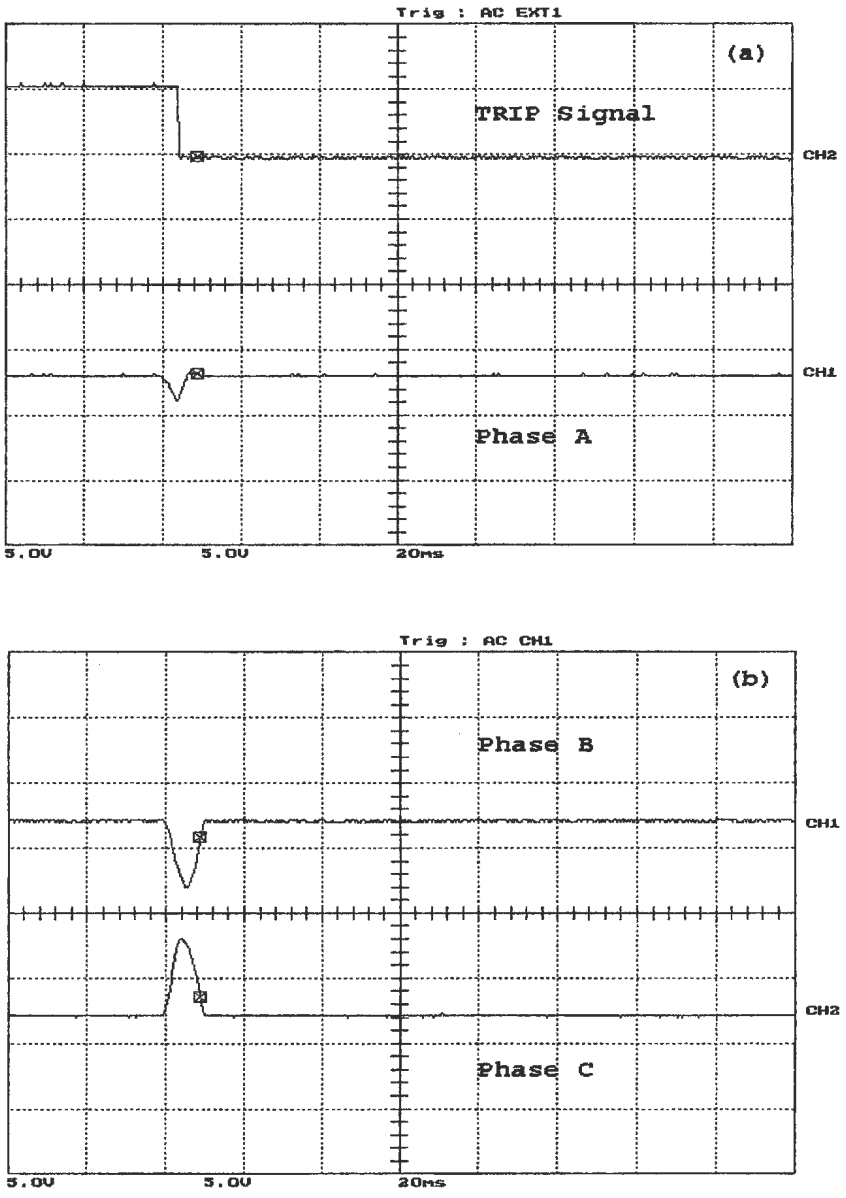

Figure 6.10: Unloaded phase B to ground fault, occurred before energization on the secondary side, (a) the WPT response and phase A differential current, (b) phase B and phase C differential currents. Y-scale is 1 Div. = 11.67 A

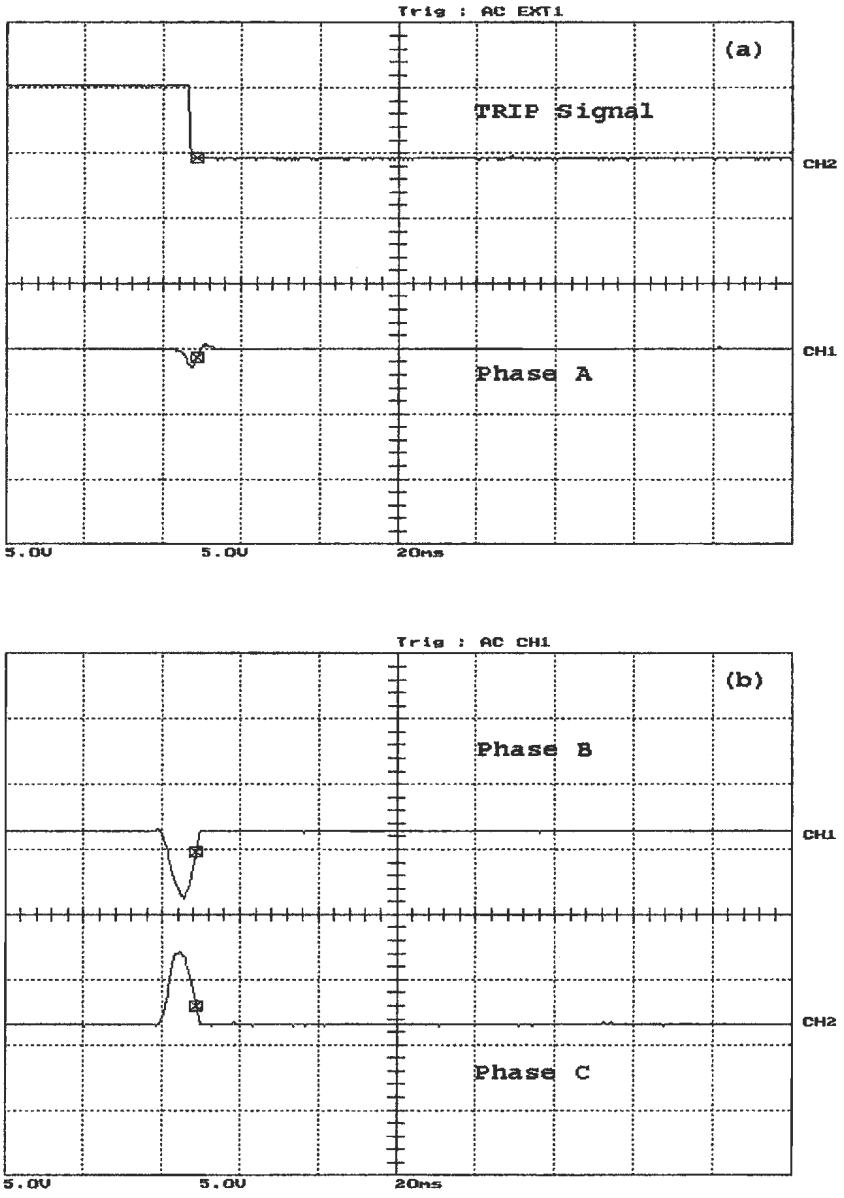

Figure 6.11: Unloaded phase B to ground fault, occurred after energization on the secondary side, (a) the WPT response and phase A differential current, (b) phase B and phase C differential currents. Y-scale is 1 Div. = 11.67 A

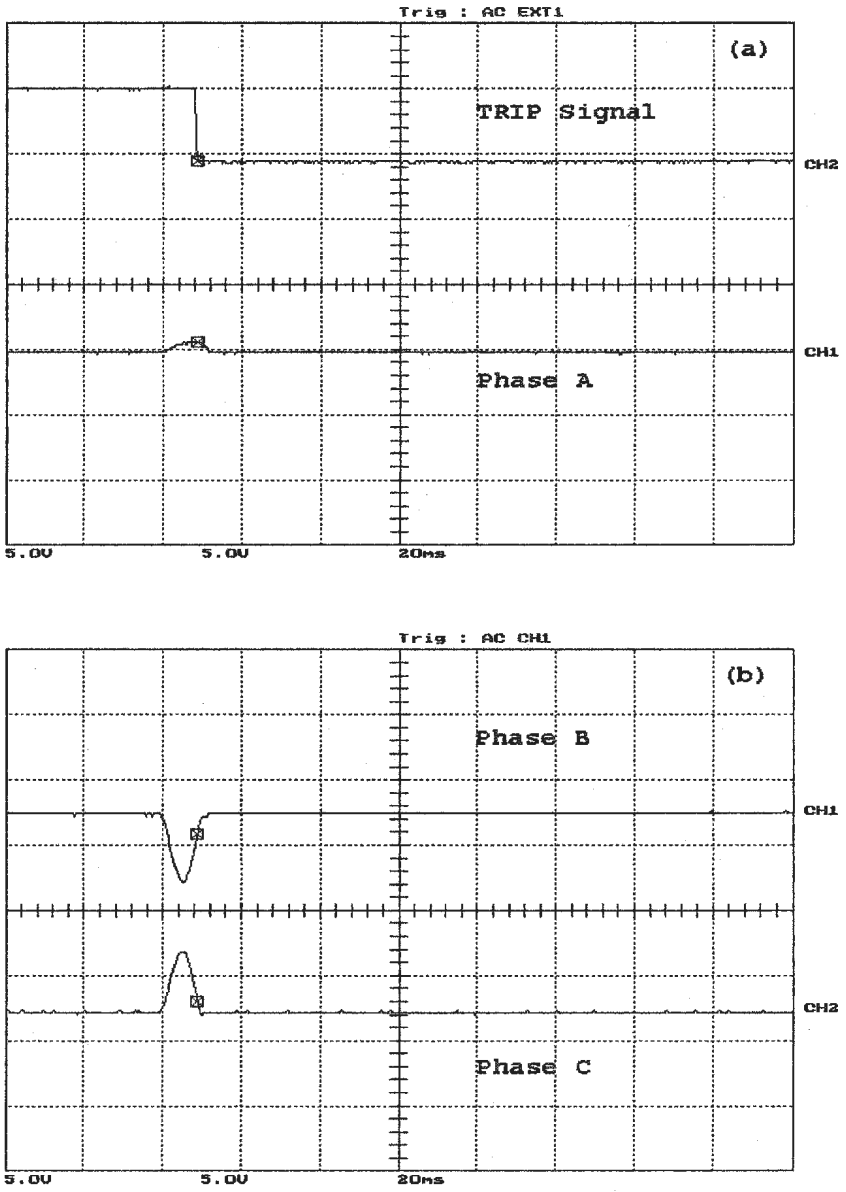

Figure 6.12: Loaded phase B to ground fault, occurred before energization on the secondary side, (a) the WPT response and phase A differential current, (b) phase B and phase C differential currents. Y-scale is 1 Div. = 11.67 A

the power transformer. For the case of connecting the balanced inductive load, Figure 6.15 shows the results when the same fault occurred before energizing the power transformer. Figure 6.16 shows the case when the fault occurred after the power transformer is energized with a load.

2- Secondary side faults

For the case of phase A to phase C fault occurring before energizing the power transformer at no load, the result is shown in Figure 6.17. The result of the case when the same type of faults occurred after the power transformer was energized is shown in Figure 6.18. The result of connecting the balanced inductive load and the fault takes place before energizing the power transformer is shown in Figure 6.19. It should be mentioned here that in all the unsymmetrical fault tested, the primary line-to-line voltage was 100V.

Three-phase to ground fault

These tests were carried out by connecting the three phases to the grounded neutral point. This fault was tested under various conditions of energization and loading on both sides of the power transformer. In Figures 6.20-6.21 the results of the two cases are presented, while the remaining results are provided in Appendix B4. The result of the case when the three-phase to ground fault occurred on the primary side before energizing the power transformer at no load is shown in Figure 6.20. Figure 6.21 shows the three-phase to ground fault taking place on the secondary side before energizing the power transformer with the balanced inductive (R-L) load connected. It should be noted that all three-phase to ground faults were tested with primary side line to line voltage of 100 V.

The real time testing of the 2 kVA multi-tap step down power transformer is successfully carried out using the proposed WPT-based protection algorithm. The proposed experimental setup used for testing the 5 kVA three-phase core type power transformer is also used for testing the 2 kVA three-phase multi tap

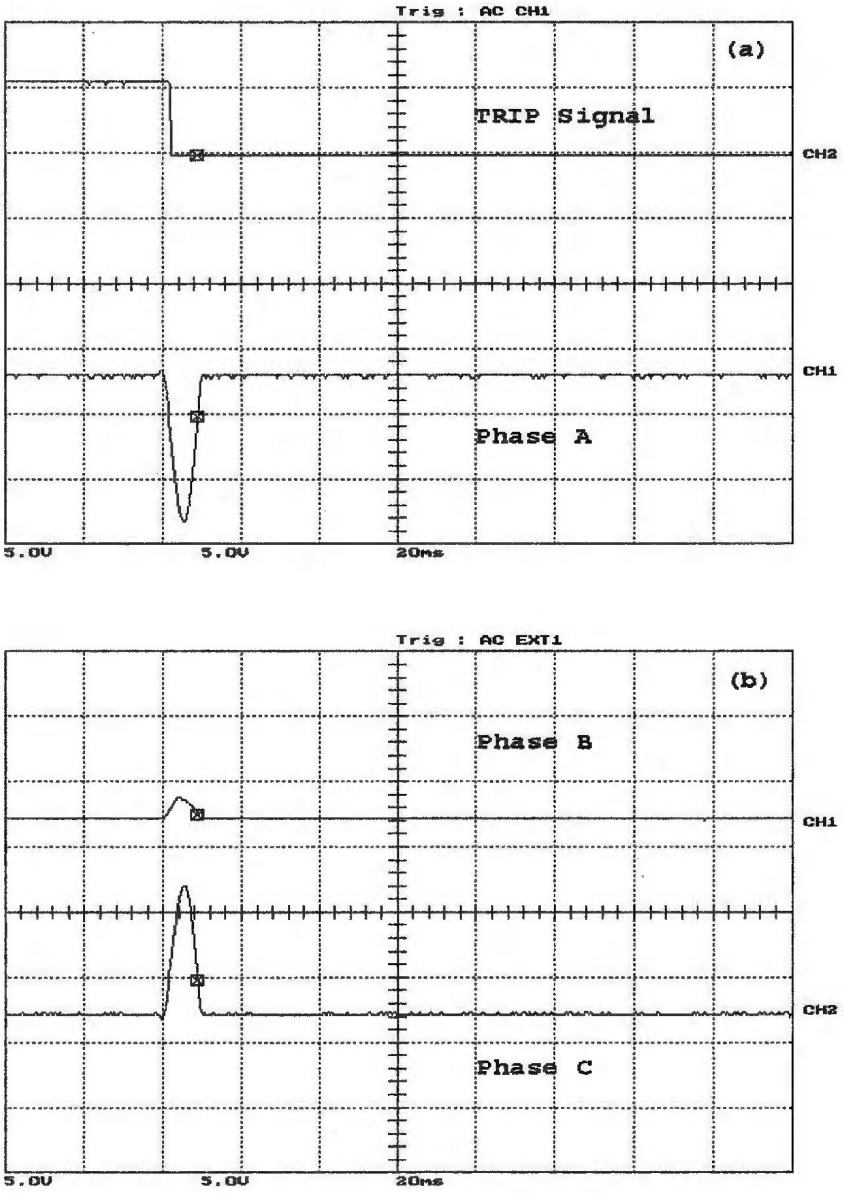

Figure 6.13: Unloaded phase A to phase C fault, occurred before energization on the primary side, (a) the WPT response and phase A differential current, (b) phase B and phase C differential currents. Y-scale is 1 Div. = 11.67 A

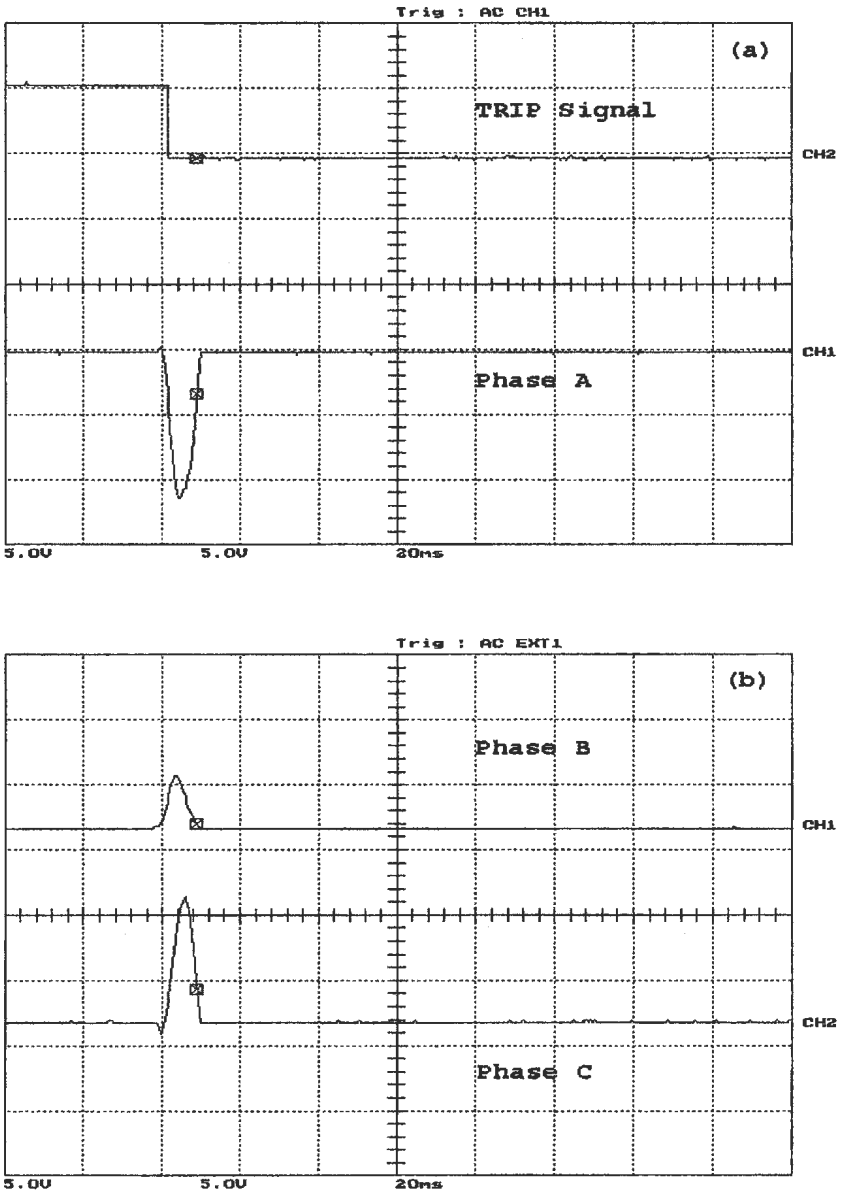

Figure 6.14: Unloaded phase A to phase C fault, occurred after energization on the primary side, (a) the WPT response and phase A differential current, (b) phase B and phase C differential currents. Y-scale is 1 Div. = 11.67 A

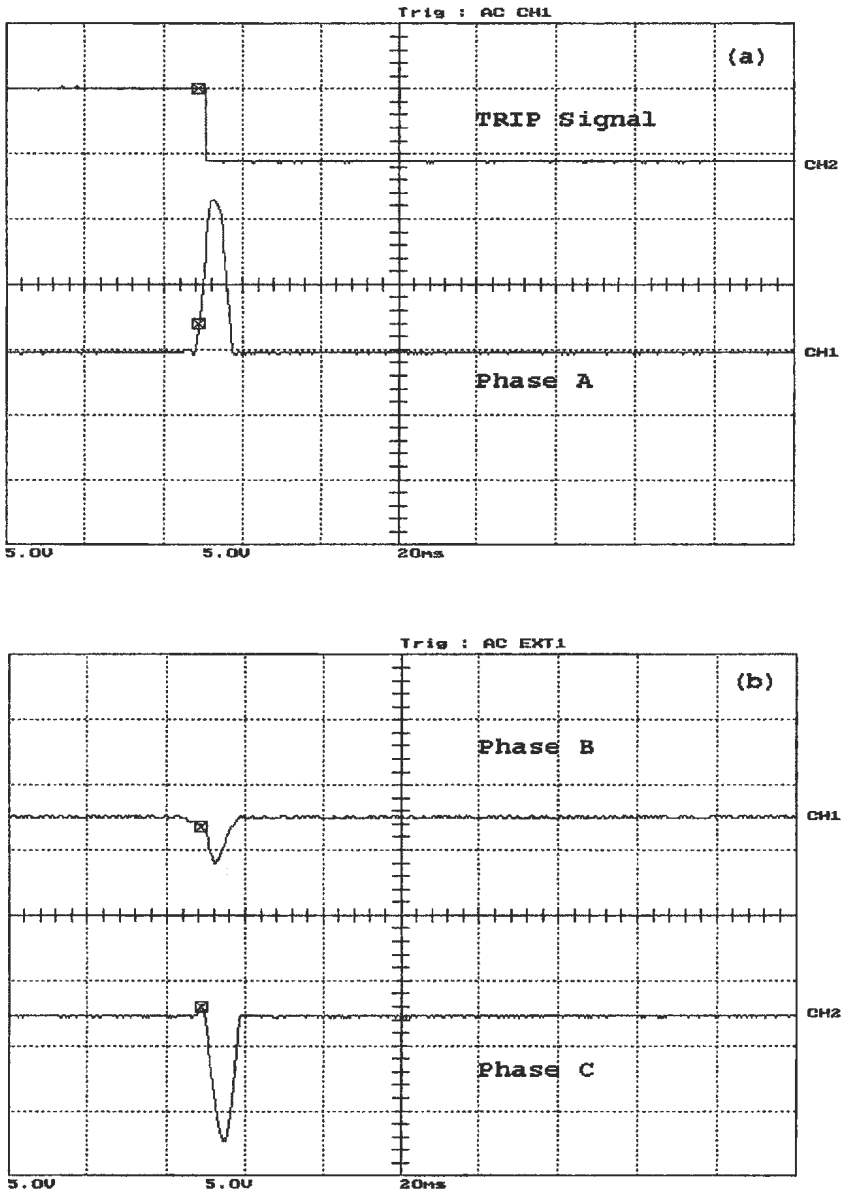

Figure 6.15: Loaded phase A to phase C fault, occurred before energization on the primary side, (a) the WPT response and phase A differential current, (b) phase B and phase C differential currents. Y-scale is 1 Div. = 11.67 A

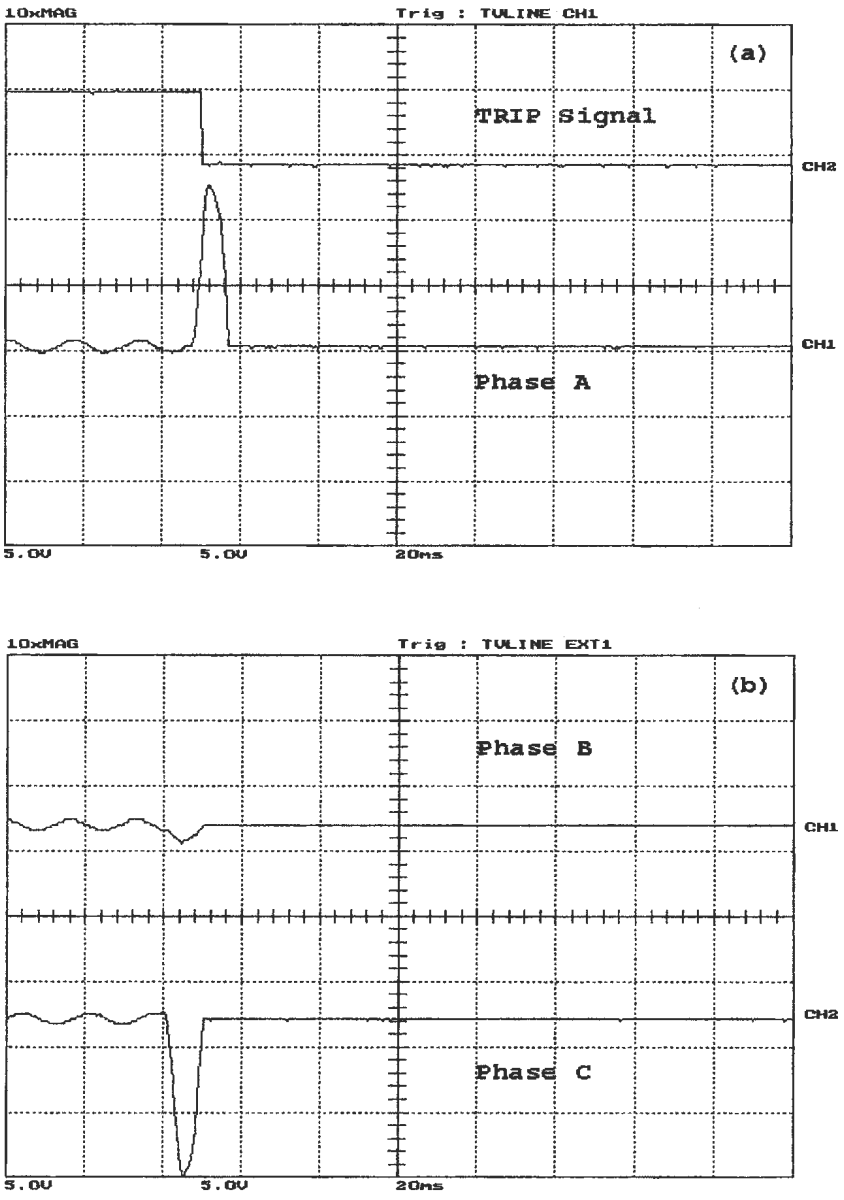

Figure 6.16: Loaded phase A to phase C fault, occurred after energization on the primary side, (a) the WPT response and phase A differential current, (b) phase B and phase C differential currents. Y-scale is 1 Div. = 11.67 A

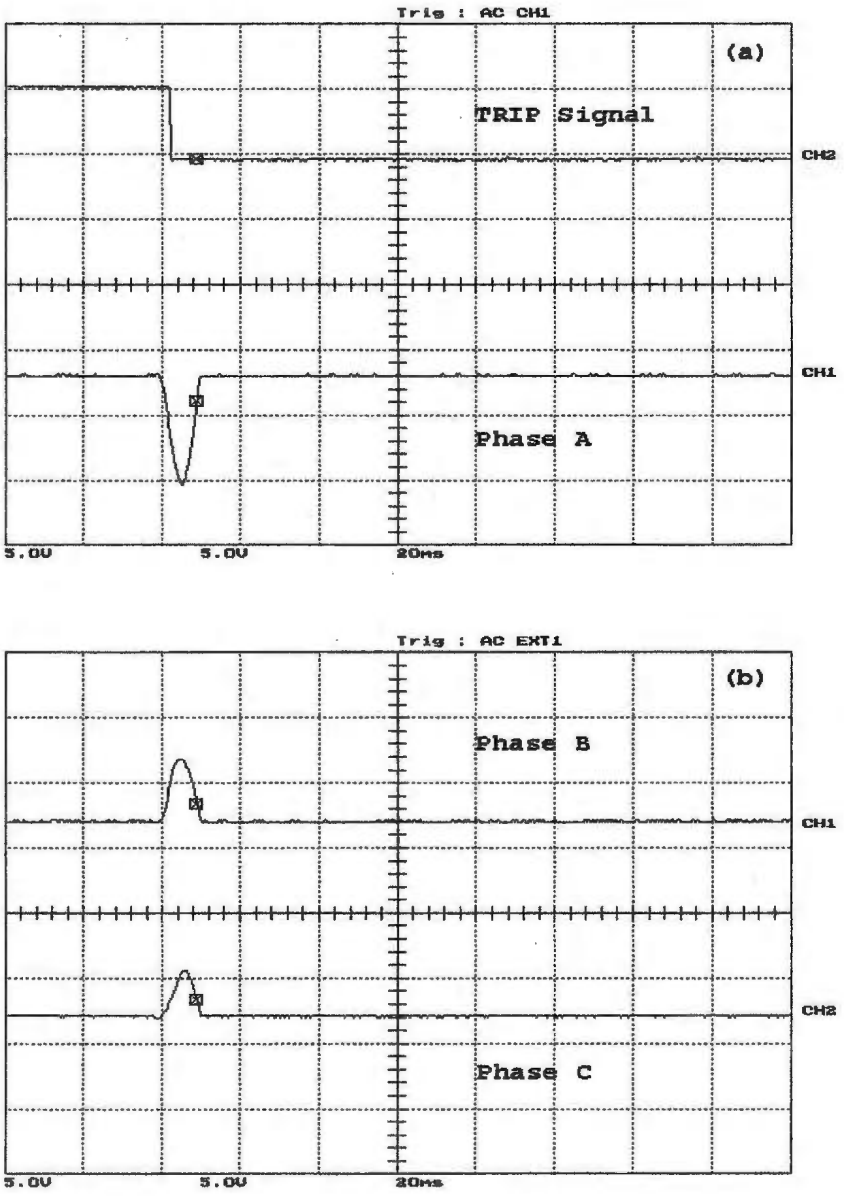

Figure 6.17: Unloaded phase A to phase C fault, occurred before energization on the secondary side, (a) the WPT response and phase A differential current, (b) phase B and phase C differential currents. Y-scale is 1 Div. = 11.67 A

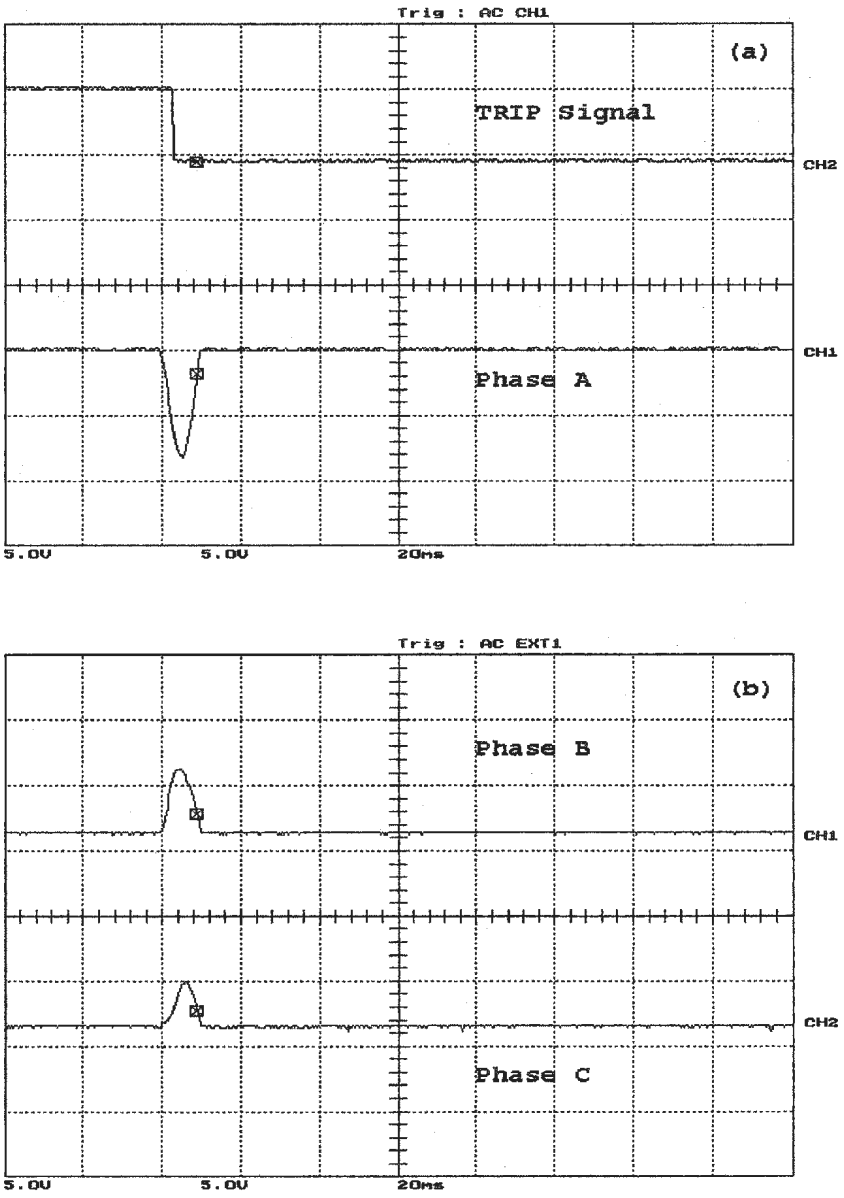

Figure 6.18: Unloaded phase A to phase C fault, occurred after energization on the secondary side, (a) the WPT response and phase A differential current, (b) phase B and phase C differential currents. Y-scale is 1 Div. = 11.67 A

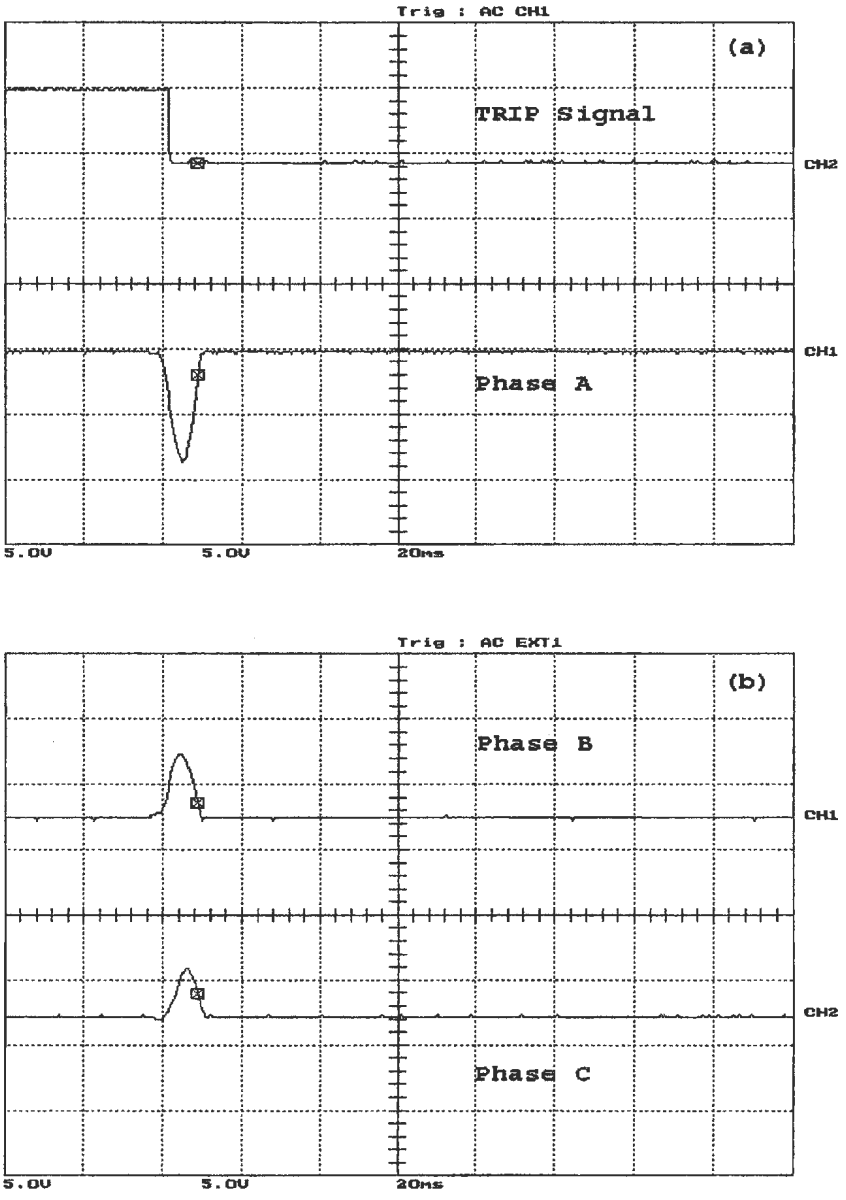

Figure 6.19: Loaded phase A to phase C fault, occurred before energization on the secondary side, (a) the WPT response and phase A differential current, (b) phase B and phase C differential currents. Y-scale is 1 Div. = 11.67 A

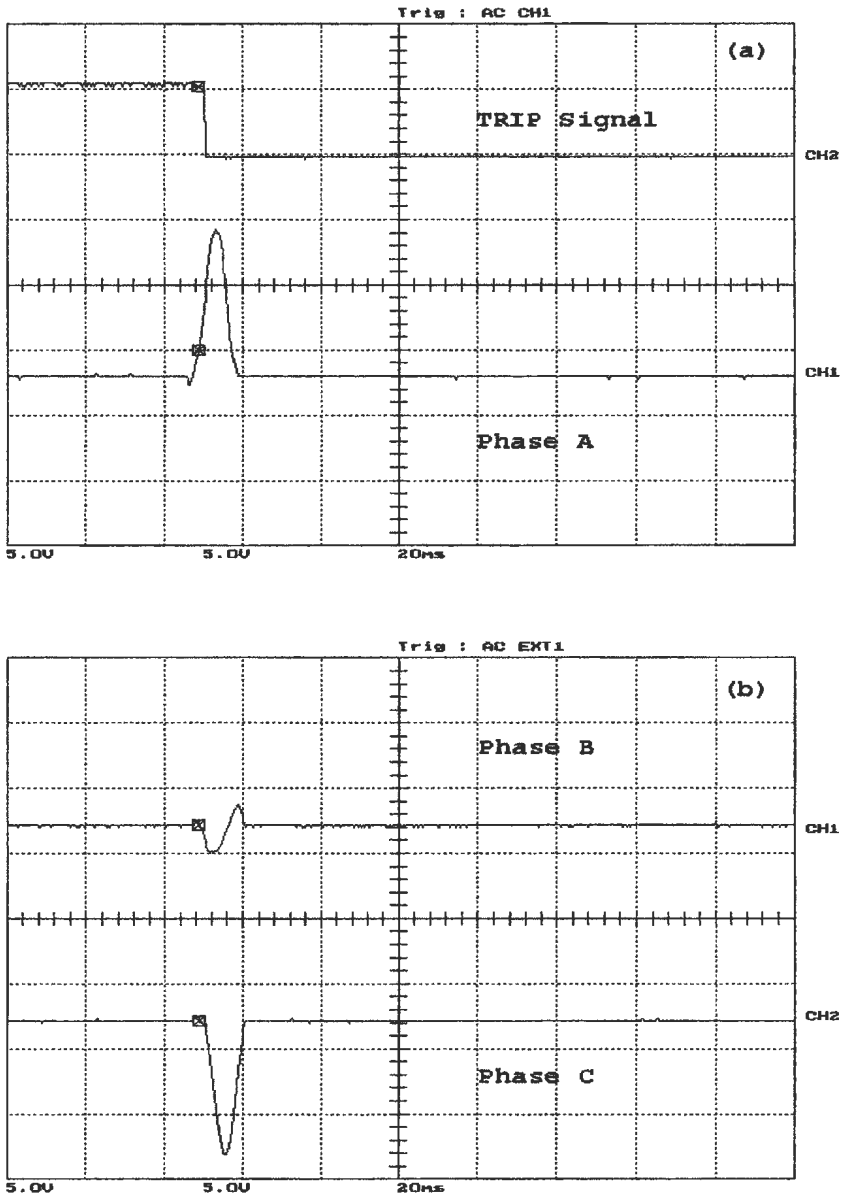

Figure 6.20: Unloaded three-phase to ground fault, occurred before energization on the primary side, (a) the WPT response and phase A differential current, (b) phase B and phase C differential currents. Y-scale is 1 Div. = 11.67 A

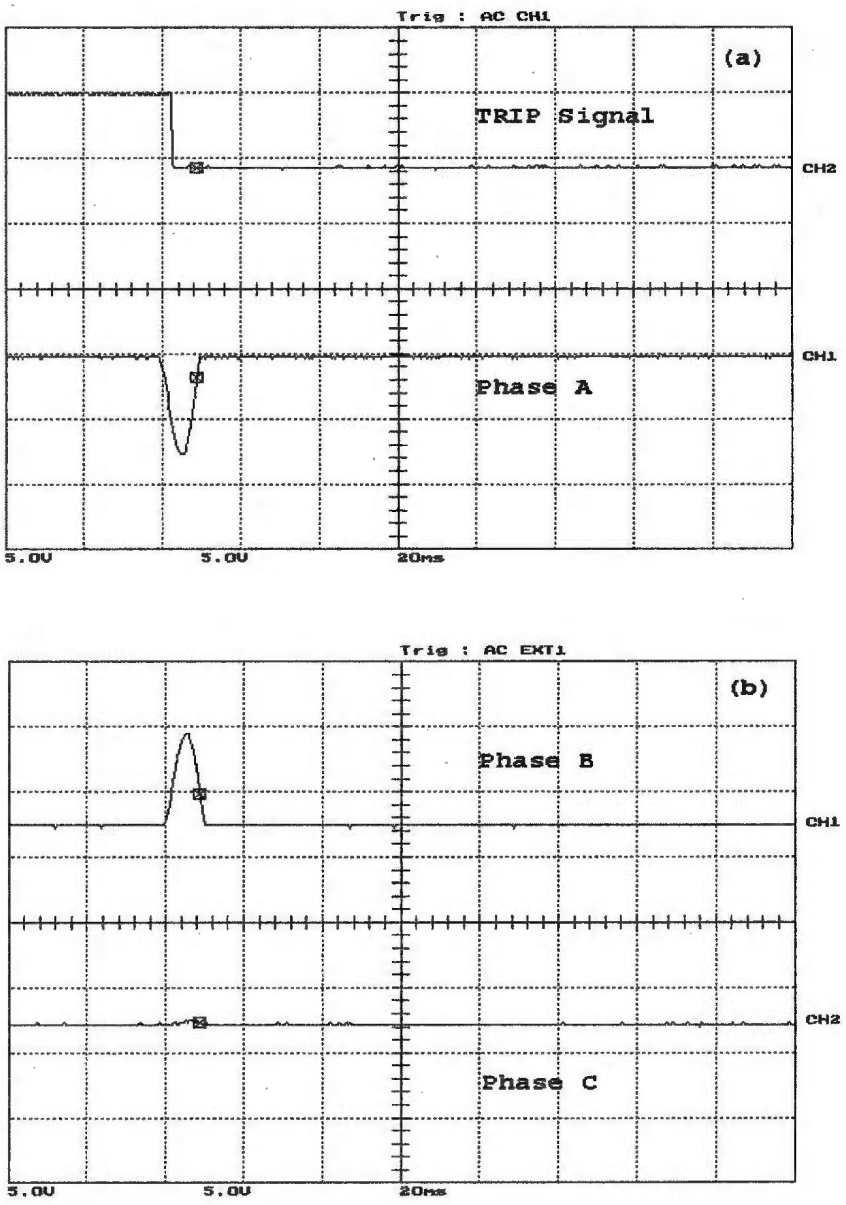

Figure 6.21: Loaded three-phase to ground fault, occurred before energization on the secondary side, (a) the WPT response and phase A differential current, (b) phase B and phase C differential currents. Y-scale is 1 Div. = 11.67 A

one. The WPT is able to detect and respond successfully to the different types of currents flowing through the tested power transformer. For all random switchings of the power transformer to investigate the magnetizing inrush current, the WPT was always able to distinguish it and issued no trip signal. In all tested internal faults, the WPT was able to detect the faults and initiate the trip signal in less than quarter a cycle (about 2-3 ms).

The results obtained for both the 5 kVA core type and 2 kVA multi-tap power transformers show that the WPT is able to distinguish accurately between the magnetizing inrush and internal fault currents. In addition, in all the fault tests carried out on both the power transformers, the trip signal is initiated in less than quarter a cycle based on 60Hz system. It is worth mentioning that the magnetizing inrush currents are quite different in both power transformers due to the differences in core material, windings configuration, parameters and/or rating values. However, the magnetizing inrush current obtained from the 2 kVA three-phase multi tap power transformer showed higher amplitude, longer time to decay and more distortion than its counter part of the 5 kVA three-phase core type power transformer.

The next chapter provides a brief summary of this work as well as the major contributions. Finally, the thesis is concluded by some future scopes of this work.

Chapter 7

Conclusions and Future Work

7.1 Summary

Power transformers have a very important function in modern power systems, and their protection represents a critical task to maintain both the stability and reliability of these systems. However, the protection of a power transformer appears to be more difficult than the protection of any other part or element of the power system. Such difficulties arise from the existence of the magnetizing inrush phenomenon, which is responsible for the occurrence of mal-functioning in the conventional protection techniques under high magnetizing inrush currents. The differential protection scheme with harmonic restraint is one of the most common techniques used for power transformer protection purposes. This technique is based on employing certain harmonics to restrain the differential relay during transformer energizing when the magnetizing inrush current is experienced to avoid mal operation. The harmonic restraint technique was implemented using digital algorithm based on evaluating the discrete Fourier transform (DFT) to extract the second harmonic and sometimes the fifth harmonic as well. The basic assumption behind this technique is that the magnetizing inrush current contains a

significant amount of the second harmonic than any typical internal fault, normal or over excitation current. However, a low-loss amorphous material has recently been used to manufacture the core in most of the modern power transformers, which is able to reduce the second harmonic content present in magnetizing inrush currents. In addition, some winding fault currents can contain a significant amount of the second harmonic. Such features of the harmonic approach affect the reliability of applying this type of protective relays for protecting modern power transformers.

The latest techniques of power transformer protection have deviated from the harmonic restraint concept and new approaches have been proposed. Among these new approaches are voltage and flux restraint, transformer equivalent circuit model, artificial neural network (ANN), etc. These approaches have shown good results in terms of speed of response and ability to diagnose the type of current flowing in the protected power transformer. Nevertheless, such approaches have a significant dependence on either the transformer parameters and/or the loading conditions. Also, power transformer parameters and loading conditions (which are subject to change due to many factors) may affect the performance of these approaches.

Taking into account the limitations of the previous approaches of protecting power transformers, an alternative method is searched for. The proposed method in this work is the wavelet packet based differential scheme. Wavelets and wavelet transforms have recently emerged as a powerful tool of signal processing, and have been successfully applied in many areas, in particular, for transient detection, classification and feature extraction. The major problem in power transformer protection is the discrimination between the magnetizing inrush and different internal fault currents, that can be categorized as a disturbance detection and classification problem. In this work, one of the wavelet transforms known as the wavelet packet

transform (WPT) is implemented and tested successfully off-line and on-line for two different types of three phase power transformers.

An extensive literature review on both the conventional and the digital differential protection techniques has been conducted in chapter 1. The problem involving the power transformer protection is stated and a solution approach using WPT is proposed.

Chapter 2 provides an illustration of the magnetizing inrush phenomenon in both single phase and three phase power transformers. Also, it gives more details about other concerns affecting the design of a differential relay, among these concerns the current transformer (CT) saturation, over excitation, etc. In addition, chapter 2 explains the basic principle of operation of the harmonic restraint differential relay along with an example of an existing relay. Finally, a pattern recognition approach implemented using artificial neural network (ANN) is explained with its basics and principles of operation.

In chapter 3, the concept of wavelets (that can be viewed as band pass filters with a dynamic bandwidths) along with different wavelet families, types, their characteristics and some examples are introduced. The different wavelet transforms and their mathematical expressions with the definition of scaling function related to some mother wavelets are presented. In recent years, the need for a signal processing tool that has the capabilities of preserving the time location for each frequency component present in the processed signal has made the wavelet analysis an adequate method for processing signals with complex frequency-time structure such as non-periodic signals with short duration and impulse superimposed features. In addition, chapter 3 presents the filter banks created by wavelets, which are known as quadrature mirror filter (QMF) banks. Each mother wavelet is capable of generating other wavelets with the same nature and characteristics through shifting and scaling. Such generated wavelets are defined as daughter

wavelets, while the shifting process is known as moving from one level of resolution to a higher one, or multi-resolution analysis (MRA). The MRA analysis begins from the highest frequency and the moves in octaves till the frequency of the next level of resolution is the same as the current one. Finally, chapter 3 introduces a selection criteria of both the optimal mother wavelet and the optimal number of levels of resolution for certain application using a technique called the minimum description length (MDL) data.

The experimental setup for data acquisition is introduced in chapter 4, where a three-phase 5 kVA,60 Hz, Δ-Y, core type, 230/550-575-600 V laboratory power transformer is used. The collected data included many magnetizing inrush, normal operating current (for a Y balanced resistive load) and different internal fault current waveforms. It is ensured that in all cases of data collection, the current was not allowed to flow for more than a few number of cycles (within 5 cycles at max.) to avoid any damage to the experimental transformer and measuring equipment. The collected data are used for off-line testing of the WPT algorithm and for selecting the optimal mother wavelet as well as selecting the optimal number of levels of resolution using the MDL criteria. The application of the MDL criteria on the acquired data has resulted in selecting the Daubechies (db4) mother wavelet as an optimal mother wavelet, and the second level of resolution as an optimal level of resolution to construct an effective, fast and reliable current disturbance classifier.

Chapter 5 presents the real time implementation and testing of the proposed WPT-based differential protection algorithm using a digital signal processor board (DSP) DS1102. All the real time testings in chapter 5 are carried out on a 5 kVA three-phase core type power transformer. The on-line test results are consistent with the off-line test results in terms of the high ability to diagnose the type of the current flowing through the power transformer and the very fast response to

any internal fault. The on-line testings are carried out for a balanced inductive (R-L) load, then extended to different unbalanced loading conditions. In all test cases, the responses of the WPT are found to be accurate, prompt and reliable. In all cases of internal faults, the fault is detected and the trip signal is initiated in less than quarter a cycle based on 60 Hz system (in about 2-3 ms).

The testing of the WPT based protection algorithm is extended to another three-phase, 2 kVA, 50 Hz, Δ-Y, 127-220/31.8-42-63.5 V multi tap power transformer. The results of the on-line testings along with its configuration are presented in chapter 6. It is ensured that these on-line tests are carried out using the same experimental setup to demonstrate the insensitivity of the WPT algorithm to the loading conditions as well as the power transformer parameters. The last results also show accurate, prompt and reliable responses. In all cases of the tested internal faults, the fault is detected and the trip signal is initiated in less than quarter a cycle based on 60 Hz system (in about 1-3 ms).

7.2 Contributions

The major contributions of this work are

- A novel algorithm for differential protection of power transformer using the wavelet packet transform (WPT) is developed.
- Real time implementation of the WPT with a proper sampling frequency:- has been carried out for the first time.
- An innovative disturbance detection and classification technique is successfully developed, implemented and tested on-line.
- A successful application of the minimum description length (MDL) data criteria for selecting the optimal wavelet as well as the optimal number

of levels of resolution of a multiresolution analysis for power transformer protection purpose has been established.

- The proposed innovative WPT algorithm is successfully implemented on-line and tested for two different power transformers under different types of balanced and unbalanced loading conditions, which has been used in testing for the first time.

7.3 Conclusions

- The wavelet transformation is a fairly new concept in different power system applications, in particular, for protection purposes. In this work, an innovative application of the wavelet packet transform for differential protection of two different three phase power transformers is successfully implemented on-line for the first time.

- Unlike other relaying algorithms, the WPT does not need any kind of a training, thresholding or harmonic content analysis of the differential current waveform. Therefore, the different and unpredicted characteristics of magnetizing inrush currents do not affect the ability of the WPT-based algorithm to diagnose them as non-fault current disturbances. Also, the CT saturation throughout all the on-line testing does not create any noticeable effect, delay in response or misidentification of the tested current waveform. The WPT-based algorithm successfully distinguished the magnetizing inrush current and restrained the relay from mal operation for all the investigated magnetizing inrush current cases.

- The optimal selection of both the mother wavelet and the number of levels of resolution using the MDL criterion is successfully applied for purposes

of power transformer protection for the first time. In addition, the selected mother wavelet and number of levels of resolution are implemented for real time application, where they show excellent results.

- The consistent results obtained from two different power transformers demonstrate the realistic applicability of the WPT-based algorithm for power transformers protection independent of their ratings, voltage ratio, core material and/or loading conditions.

- The WPT is quite simple to implement and easy to be coded with a small amount of needed memory for storage and compilation. However, it is accurate, prompt and reliable. There is not a case in which the WPT response took more than quarter a cycle based on 60Hz system (3 ms at max.).

7.4 Future Works

This algorithm can be applied to other types of protection, which may need some modifications in hardware equipments according to the desired protected elements such as adding PTs. Such applications in power systems may include:

- Power quality assessment and improvement, where different types of voltage fluctuation, sags, swells, under voltage, harmonic distortion and over voltage can be detected and classified and suitable actions can be taken to restore and improve the power quality.

- Other types of protection applications, which may include distance relaying, directional relaying, generator differential protection, etc. In addition, locating different types of faults can be an important application of the WPT-based disturbance classifier for protection purposes.

Appendix A

5 kVA Core Type Three-Phase Power Transformer

A.1 The Magnetizing Inrush Current

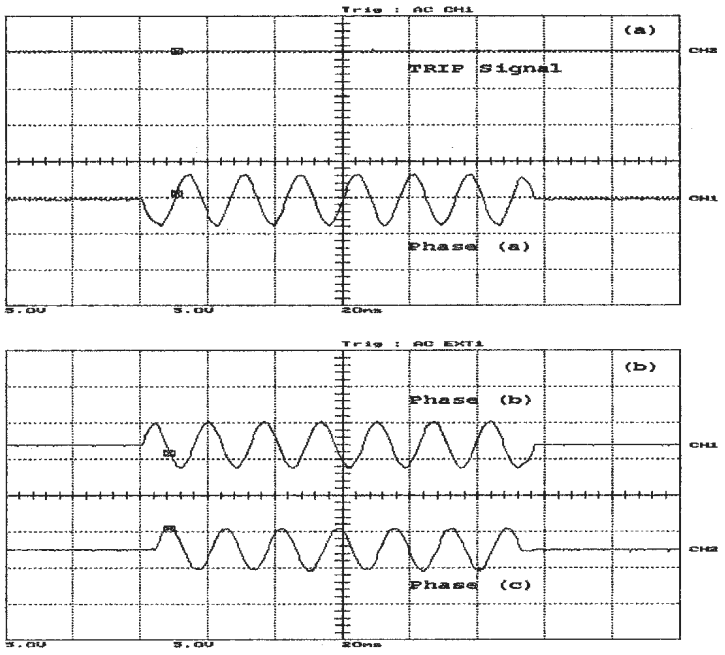

Figure A.1: Magnetizing inrush current for resistive balanced load of Z=20 Ω/phase, (a) the WPT response and phase (a) differential current , (b) phase (b) and phase (c) differential currents. Y-scale is 1 Div. = 11.67 A

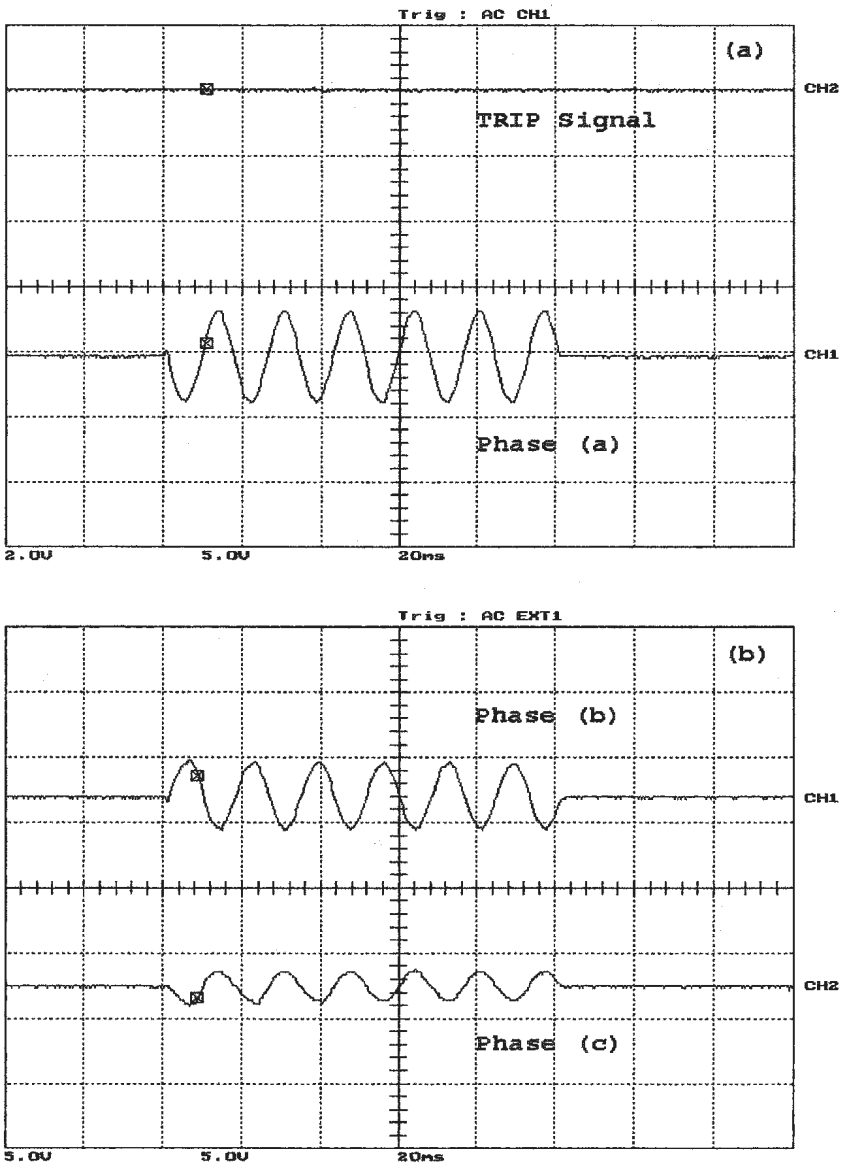

Figure A.2: Magnetizing inrush current for resistive unbalanced load of $Z_a=\infty$, $Z_b=$ 20 Ω and Z_c=35 Ω/phase, (a) the WPT response and phase (a) differential current , (b) phase (b) and phase (c) differential currents. Y-scale is 1 Div. = 11.67 A

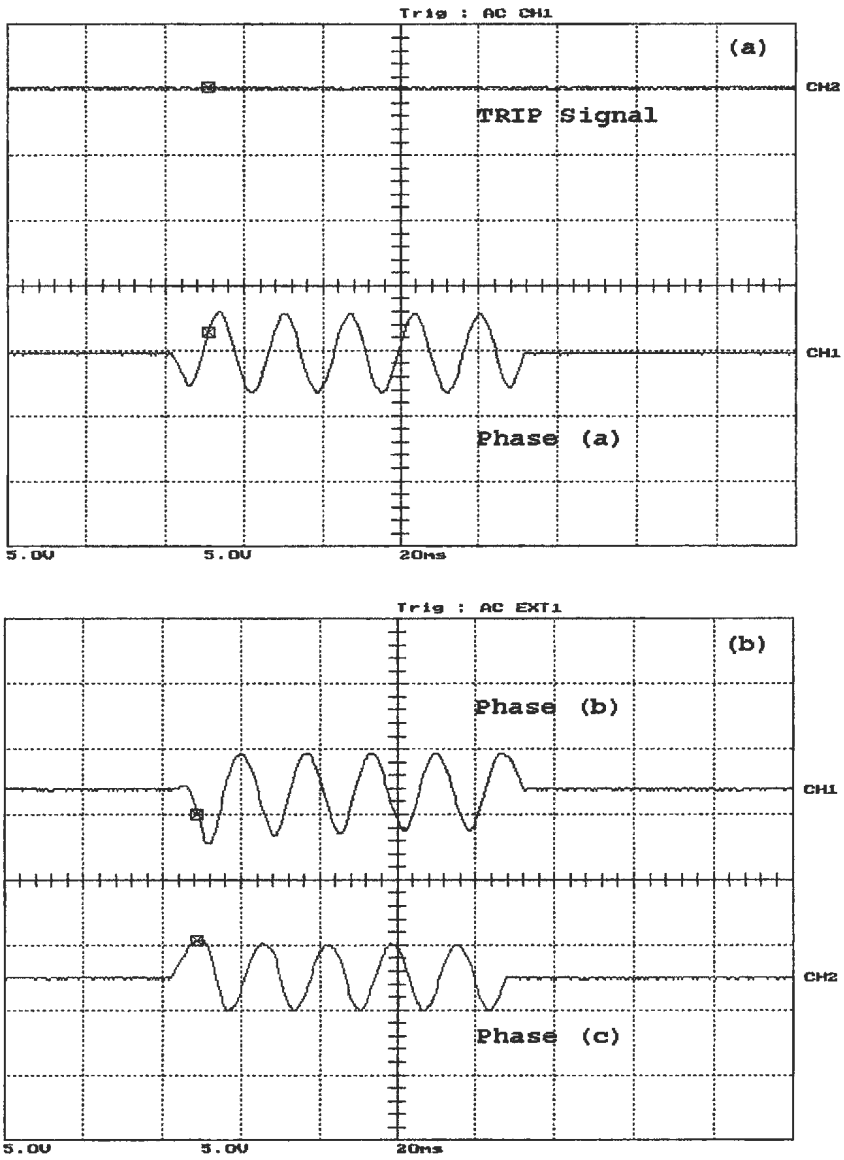

Figure A.3: Magnetizing inrush current for inductive balanced load of Z=20+j11.9129 Ω/phase, (a) the WPT response and phase (a) differential current , (b) phase (b) and phase (c) differential currents. Y-scale is 1 Div. = 11.67 A

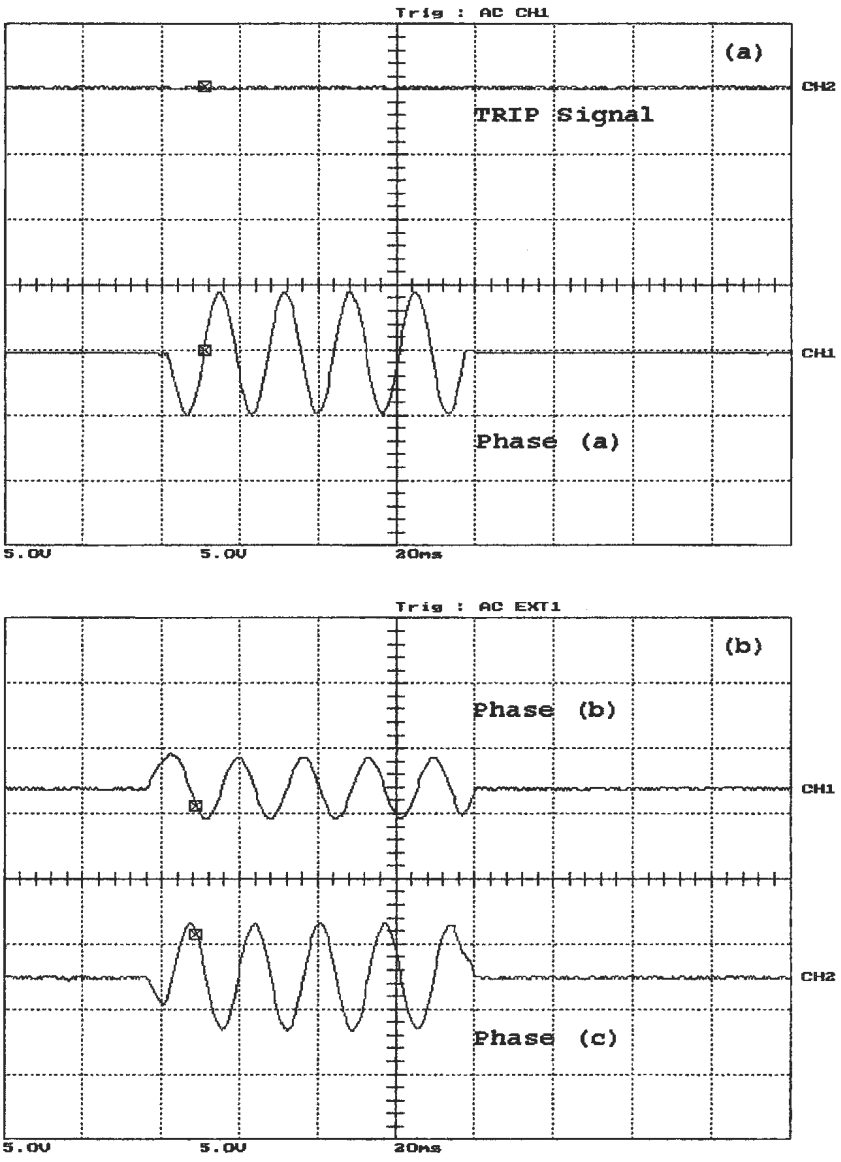

Figure A.4: Magnetizing inrush current for inductive unbalanced load of Z_a=j11.9129, Z_b= 20+j11.9129 Ω and Z_c=20 Ω/phase, (a) the WPT response and phase (a) differential current , (b) phase (b) and phase (c) differential currents. Y-scale is 1 Div. = 11.67 A

A.2 Single Phase to Ground Fault

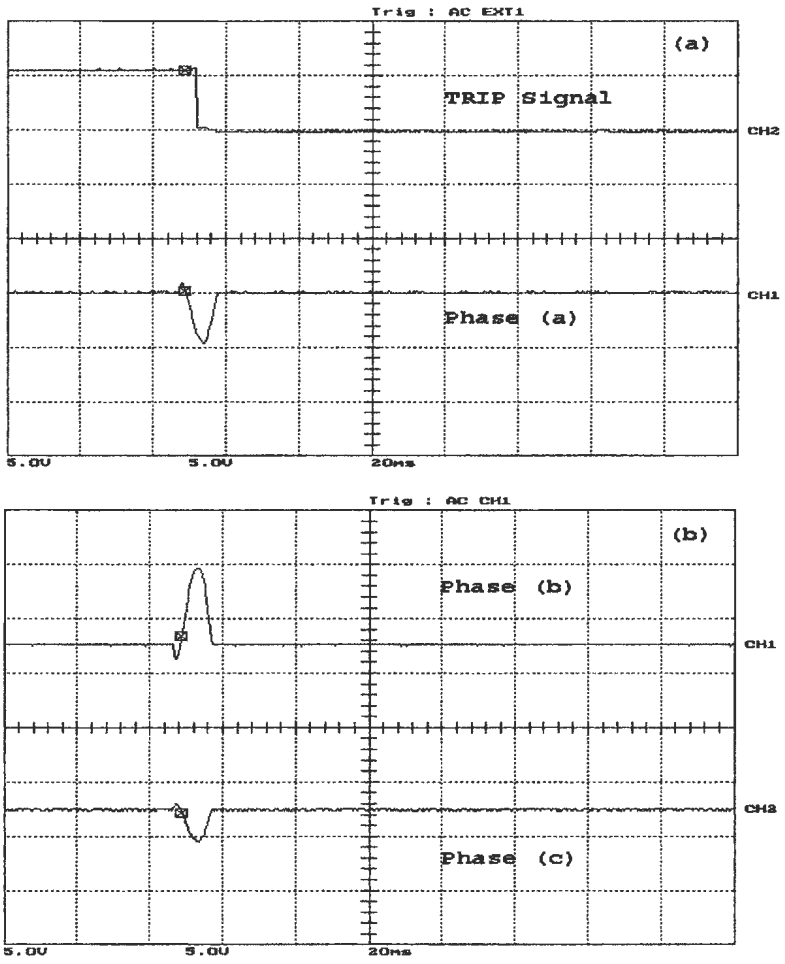

Figure A.5: Unloaded phase (b) to ground fault, occurred before energization on the primary side, (a) the WPT response and phase (a) differential current , (b) phase (b) and phase (c) differential currents. Y-scale is 1 Div. = 11.67 A

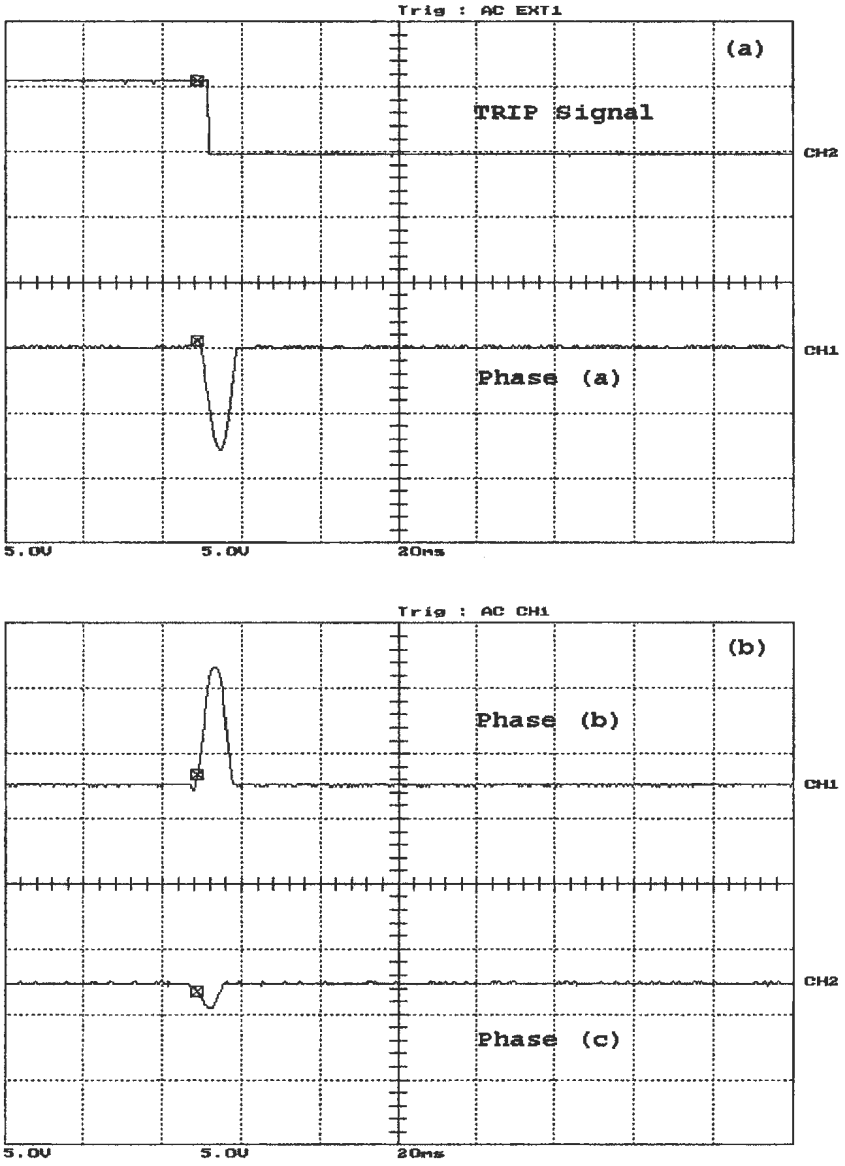

Figure A.6: Unloaded phase (b) to ground fault, occurred before energization on the secondary side, (a) the WPT response and phase (a) differential current , (b) phase (b) and phase (c) differential currents. Y-scale is 1 Div. = 11.67 A

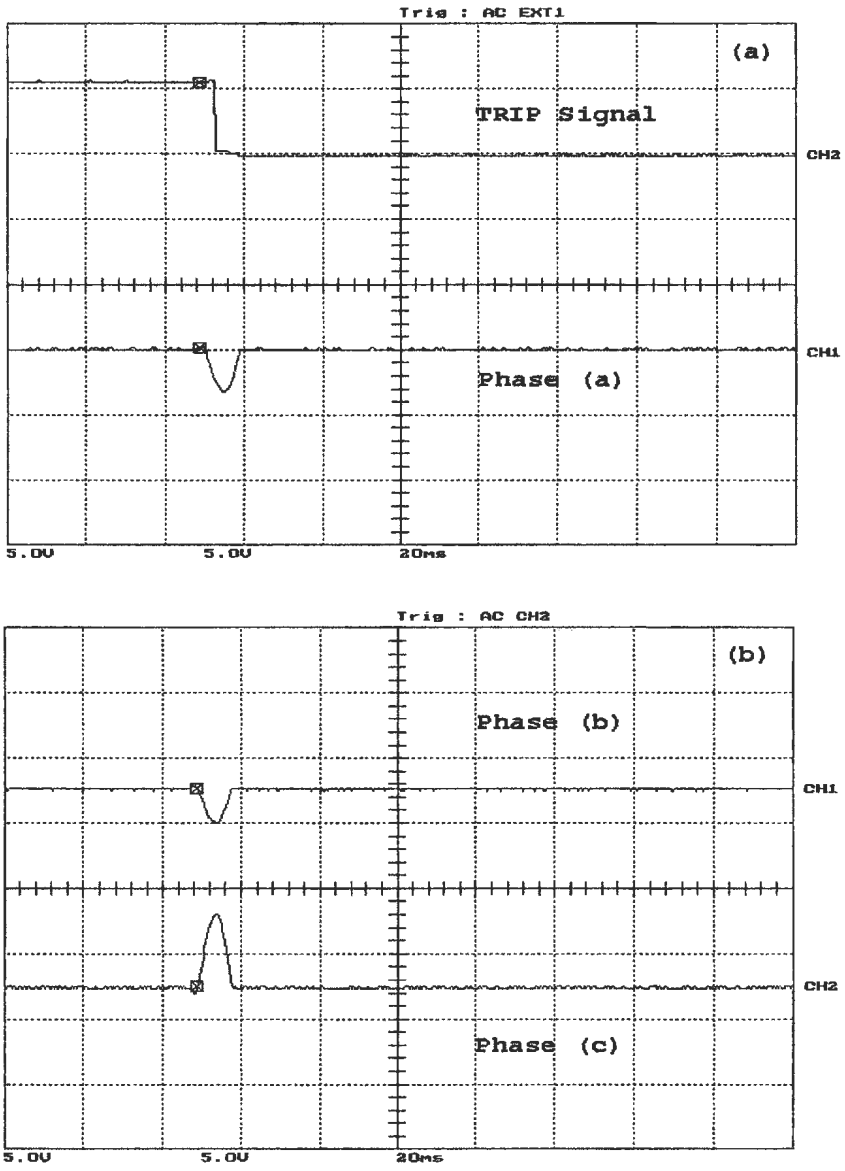

Figure A.7: Unloaded phase C to ground fault, occurred before energization on the primary side, (a) the WPT response and phase (a) differential current , (b) phase (b) and phase (c) differential currents. Y-scale is 1 Div. = 11.67 A

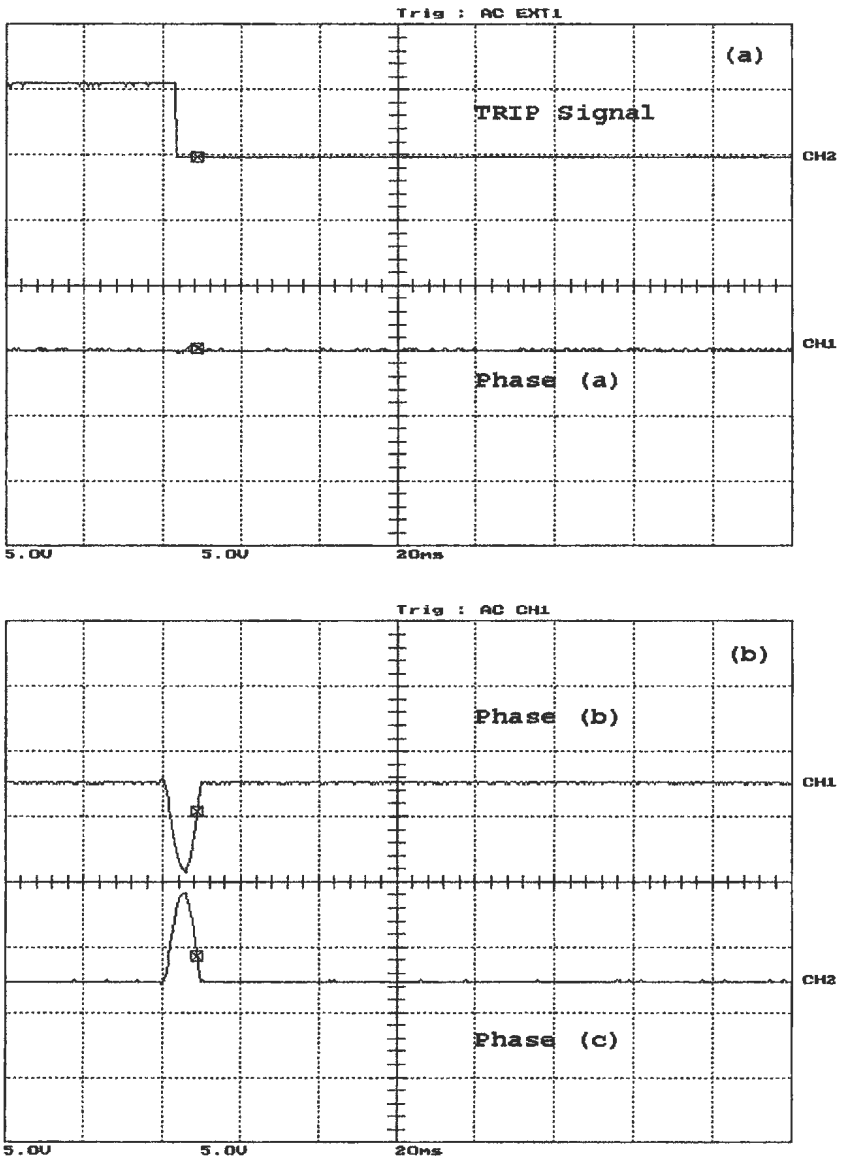

Figure A.8: Unloaded phase C to ground fault, occurred before energization on the secondary side, (a) the WPT response and phase (a) differential current , (b) phase (b) and phase (c) differential currents. Y-scale is 1 Div. = 11.67 A

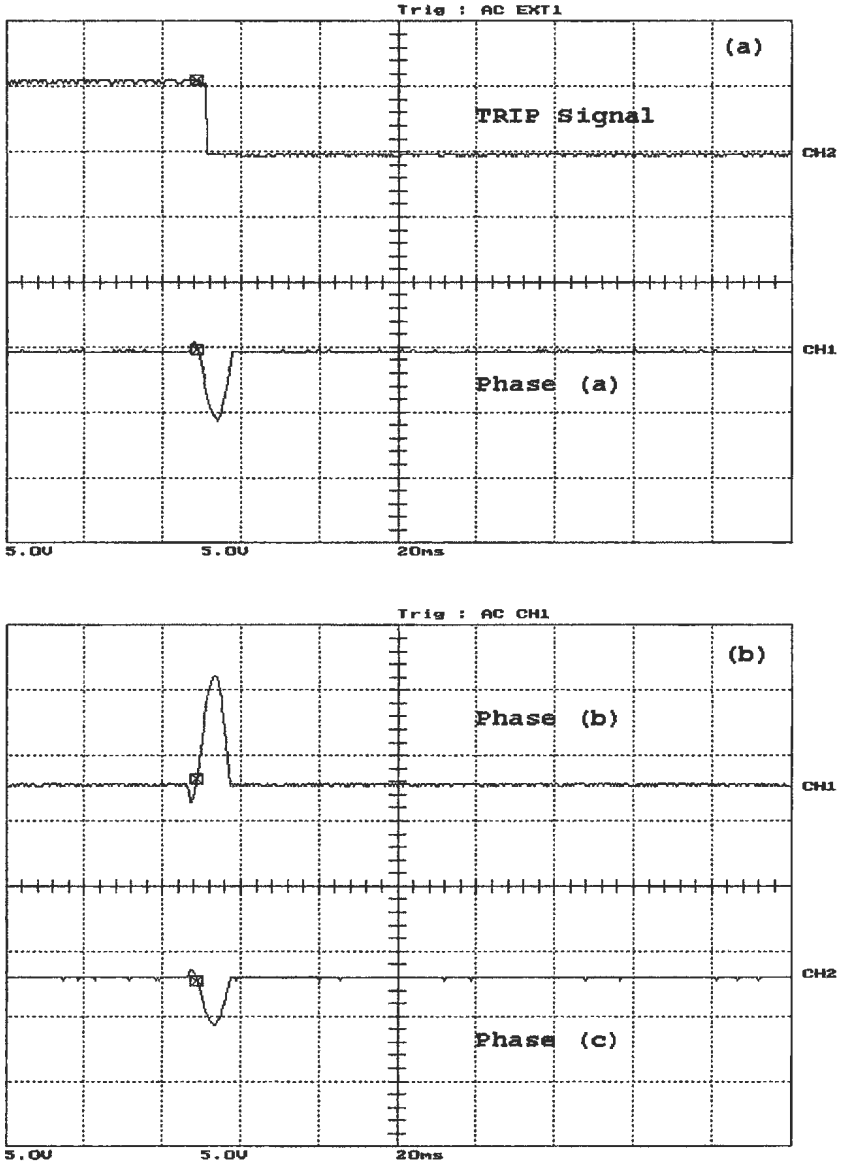

Figure A.9: Unloaded phase (b) to ground fault, occurred after energization on the primary side, (a) the WPT response and phase (a) differential current , (b) phase (b) and phase (c) differential currents. Y-scale is 1 Div. = 11.67 A

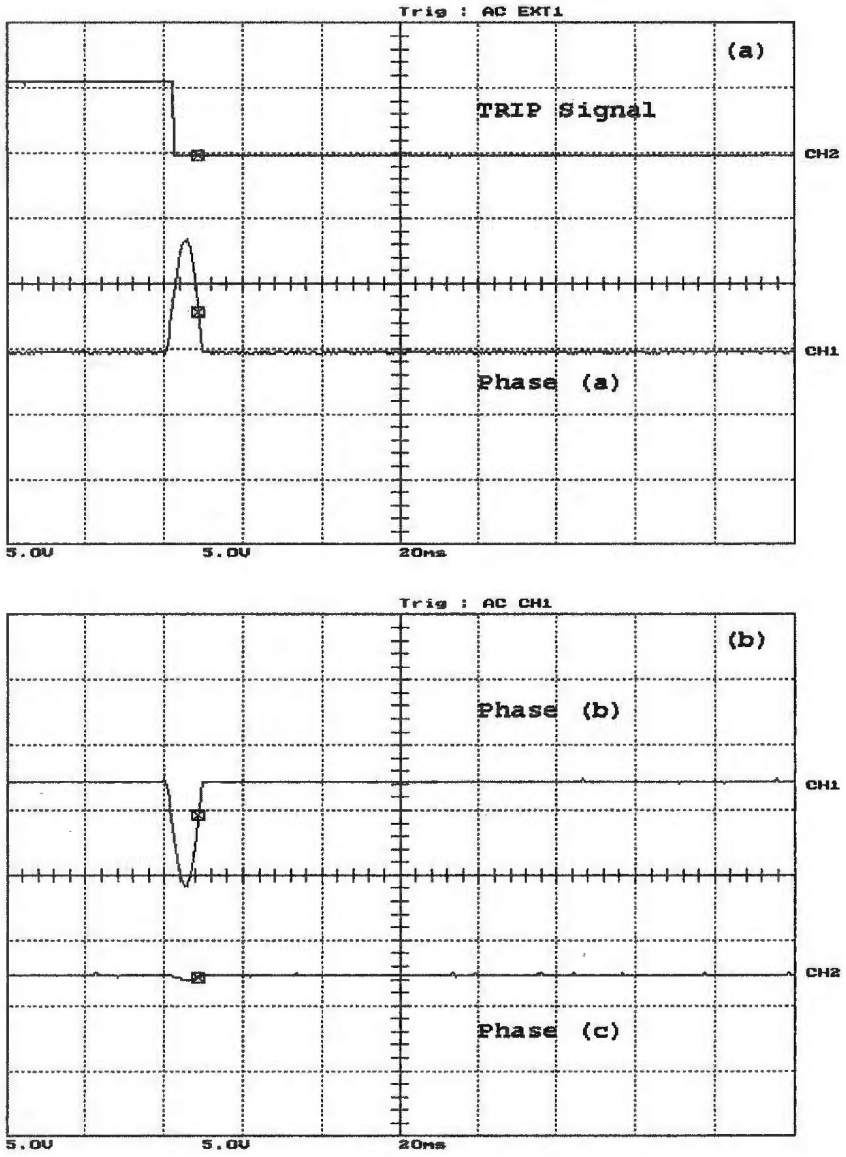

Figure A.10: Unloaded phase (b) to ground fault, occurred after energization on the secondary side, (a) the WPT response and phase (a) differential current , (b) phase (b) and phase (c) differential currents. Y-scale is 1 Div. = 11.67 A

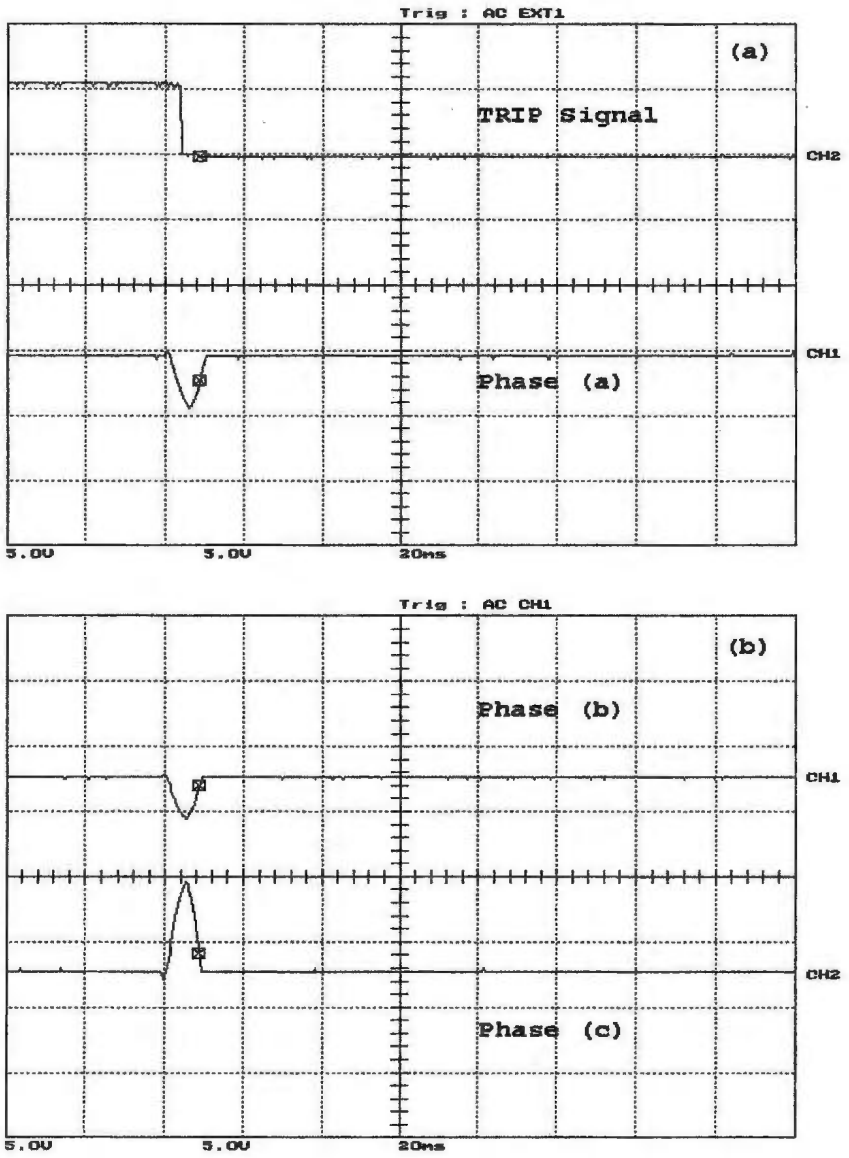

Figure A.11: Unloaded phase C to ground fault, occurred after energization on the primary side, (a) the WPT response and phase (a) differential current , (b) phase (b) and phase (c) differential currents. Y-scale is 1 Div. = 11.67 A

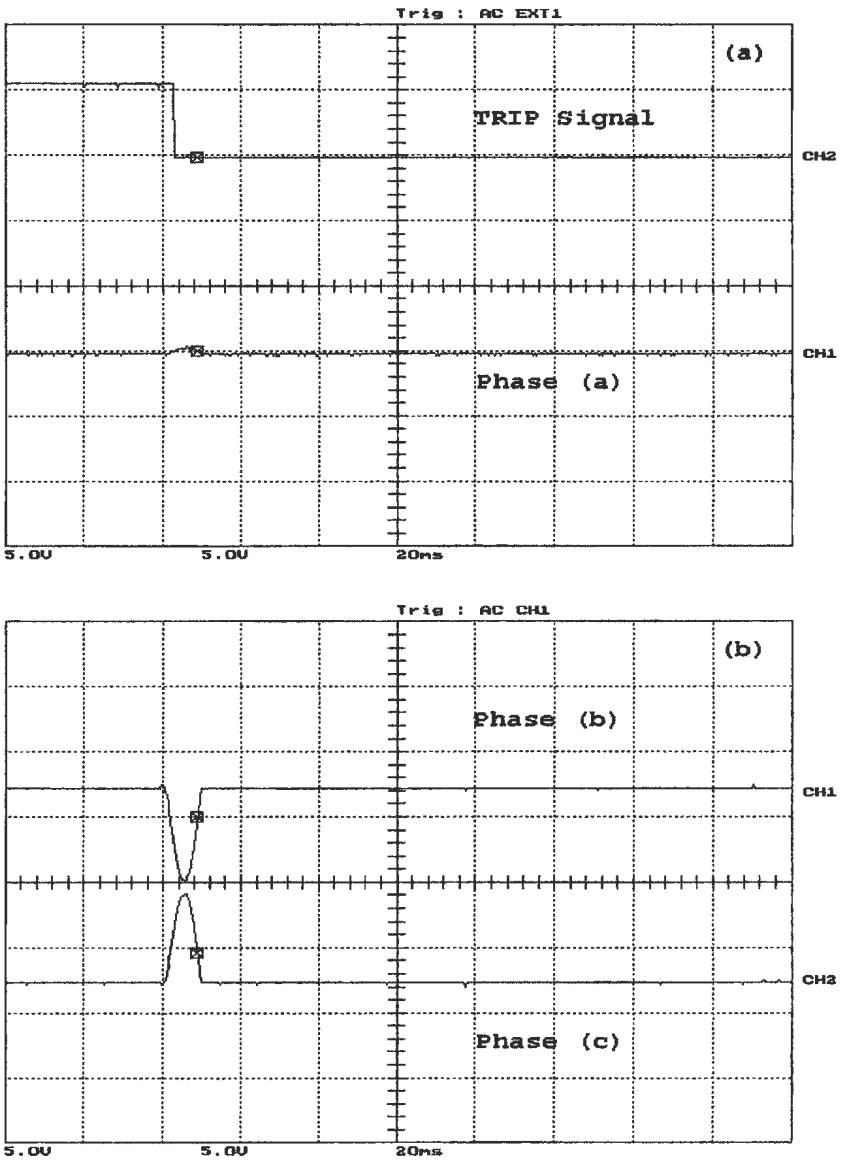

Figure A.12: Unloaded phase C to ground fault, occurred after energization on the secondary side, (a) the WPT response and phase (a) differential current , (b) phase (b) and phase (c) differential currents. Y-scale is 1 Div. = 11.67 A

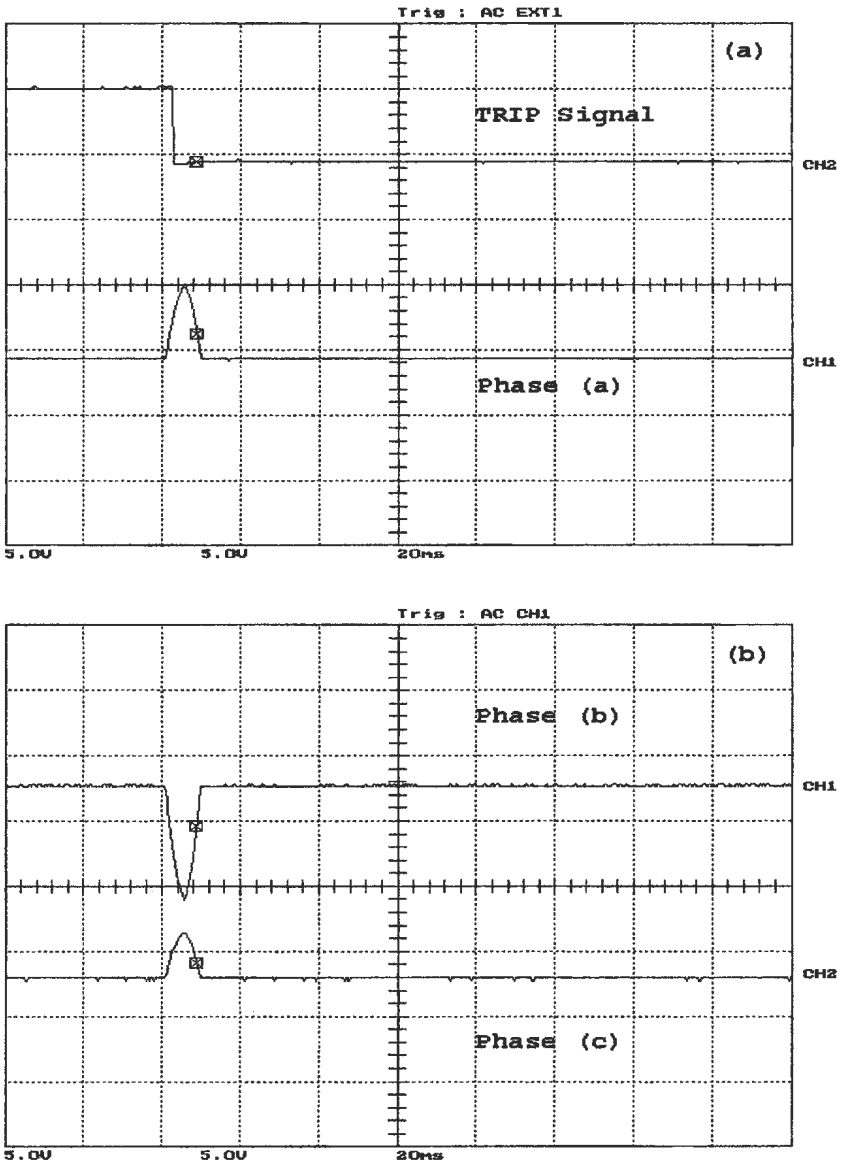

Figure A.13: Loaded phase (b) to ground fault, occurred before energization on the primary side, (a) the WPT response and phase (a) differential current , (b) phase (b) and phase (c) differential currents. Y-scale is 1 Div. = 11.67 A

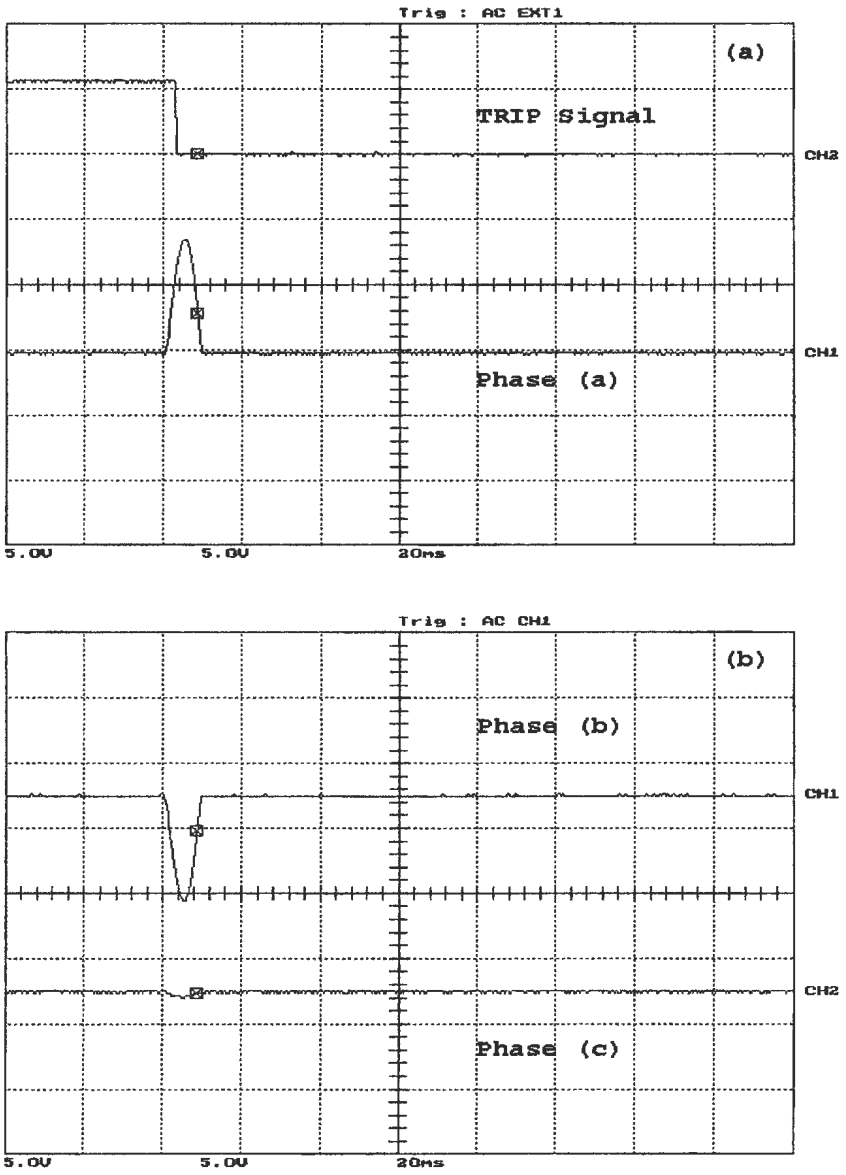

Figure A.14: Loaded phase (b) to ground fault, occurred before energization on the secondary side, (a) the WPT response and phase (a) differential current , (b) phase (b) and phase (c) differential currents. Y-scale is 1 Div. = 11.67 A

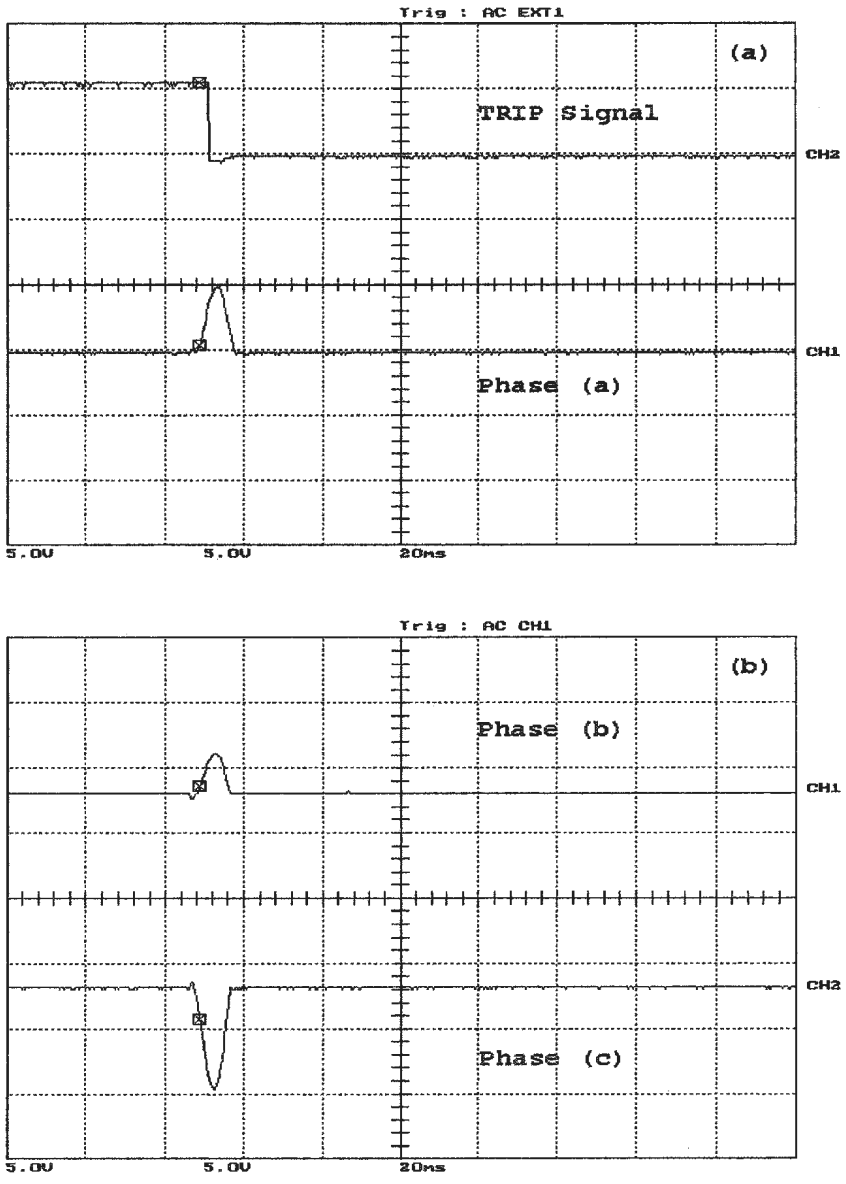

Figure A.15: Loaded phase C to ground fault, occurred before energization on the primary side, (a) the WPT response and phase (a) differential current , (b) phase (b) and phase (c) differential currents. Y-scale is 1 Div. = 11.67 A

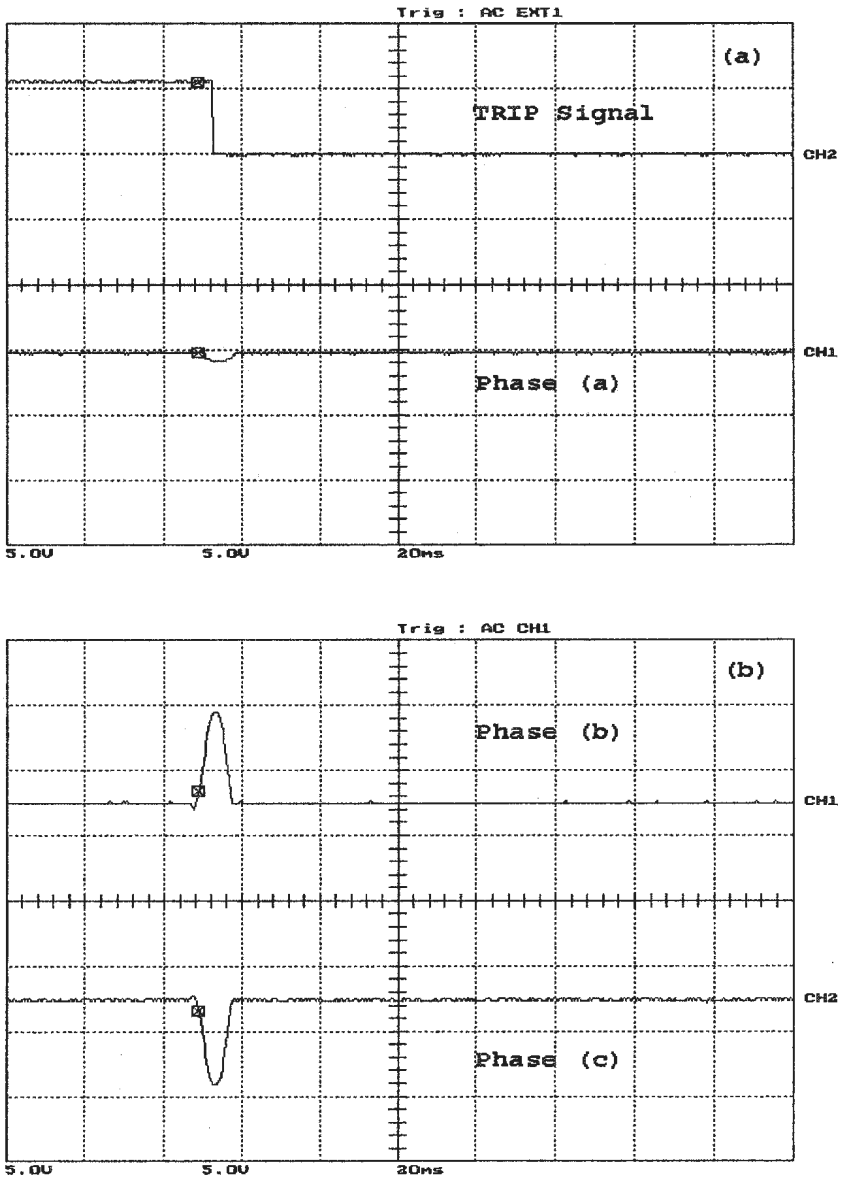

Figure A.16: Loaded phase C to ground fault, occurred before energization on the secondary side, (a) the WPT response and phase (a) differential current , (b) phase (b) and phase (c) differential currents. Y-scale is 1 Div. = 11.67 A

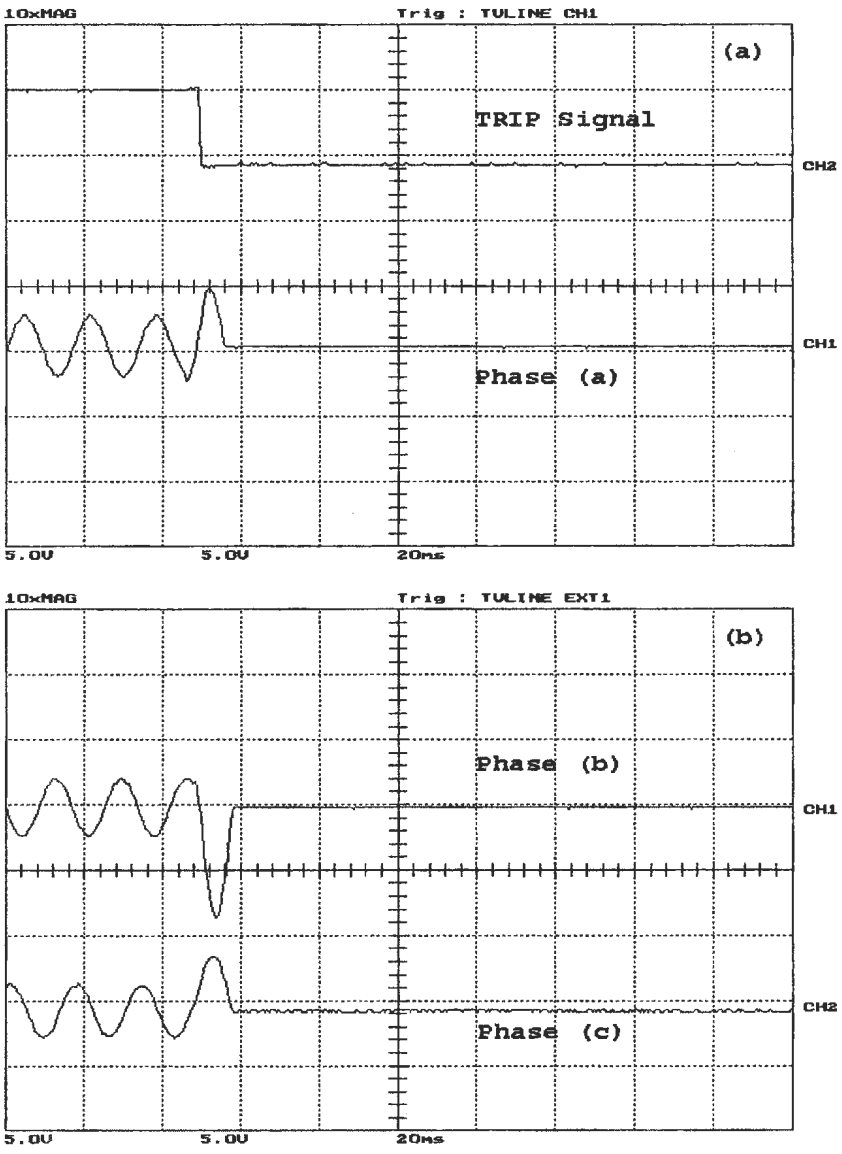

Figure A.17: Loaded phase (b) to ground fault, occurred after energization on the primary side, (a) the WPT response and phase (a) differential current , (b) phase (b) and phase (c) differential currents. Y-scale is 1 Div. = 11.67 A

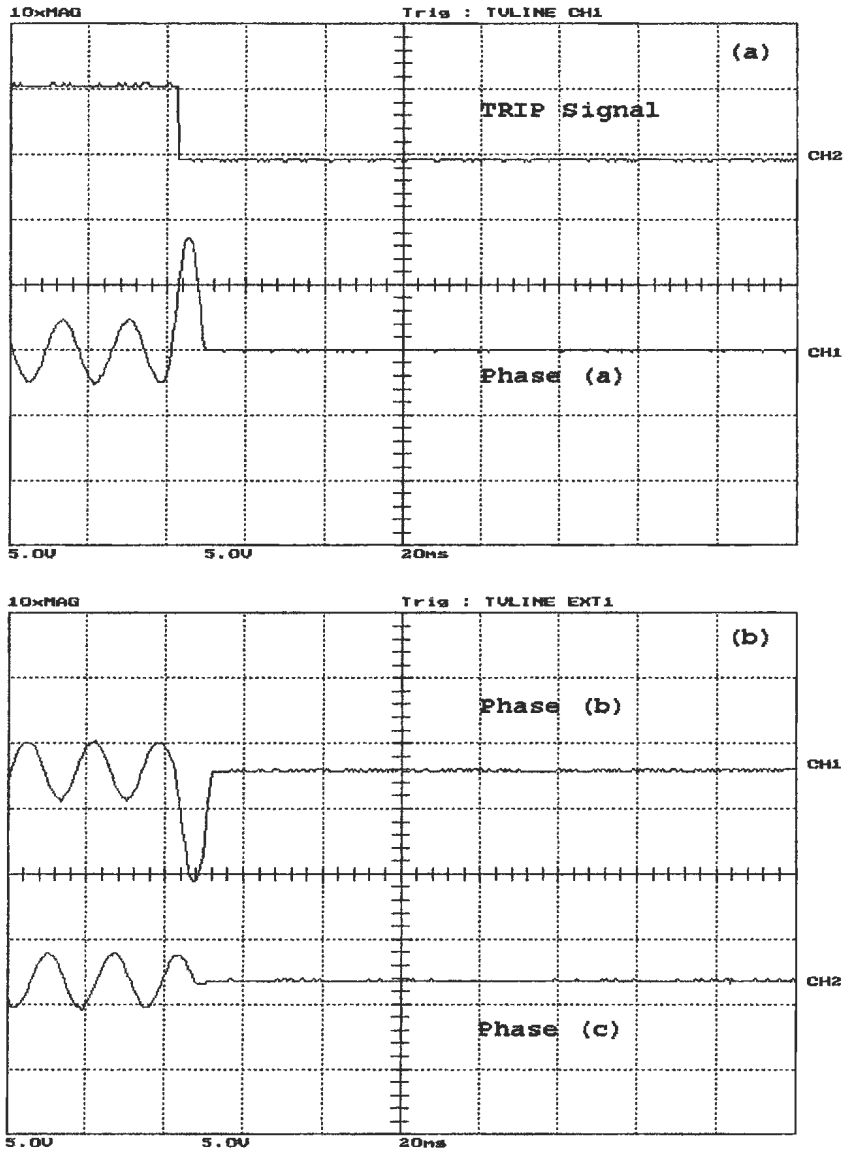

Figure A.18: Loaded phase (b) to ground fault, occurred after energization on the secondary side, (a) the WPT response and phase (a) differential current , (b) phase (b) and phase (c) differential currents. Y-scale is 1 Div. = 11.67 A

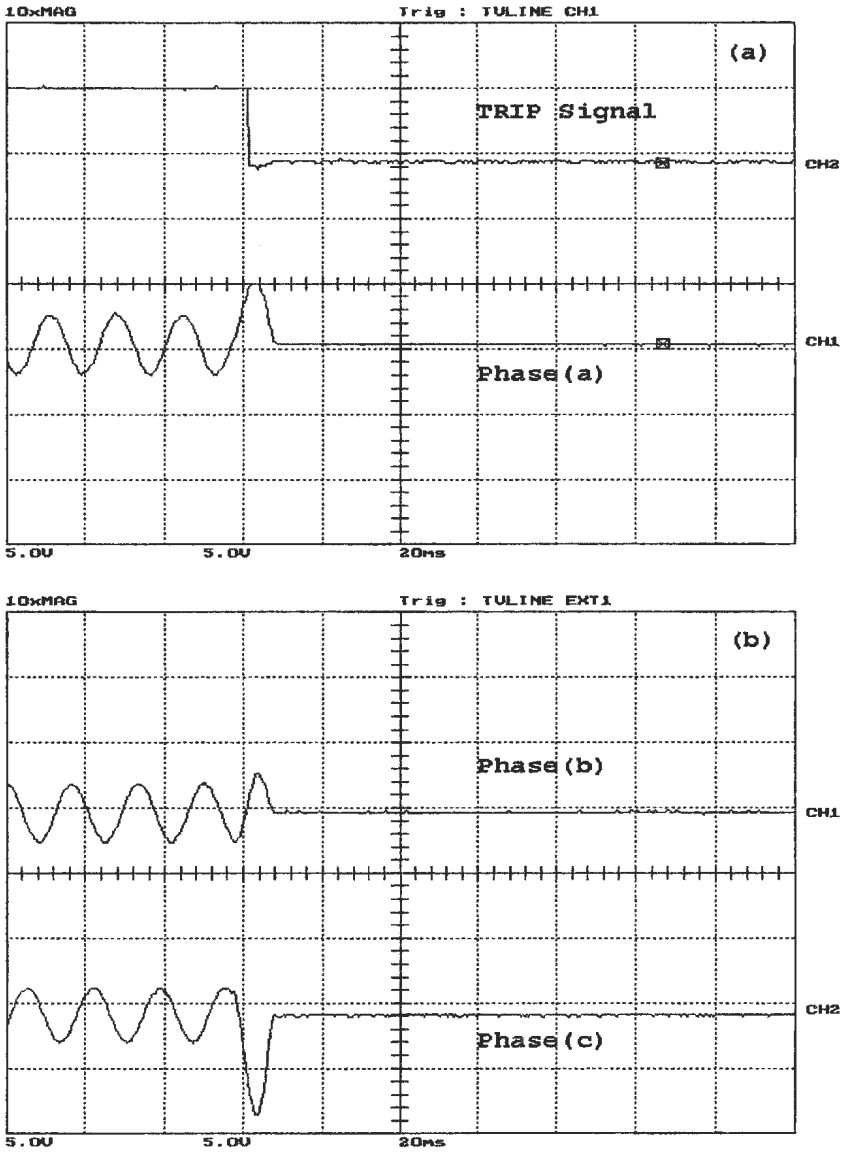

Figure A.19: Loaded phase C to ground fault, occurred after energization on the primary side, (a) the WPT response and phase (a) differential current , (b) phase (b) and phase (c) differential currents. Y-scale is 1 Div. = 11.67 A

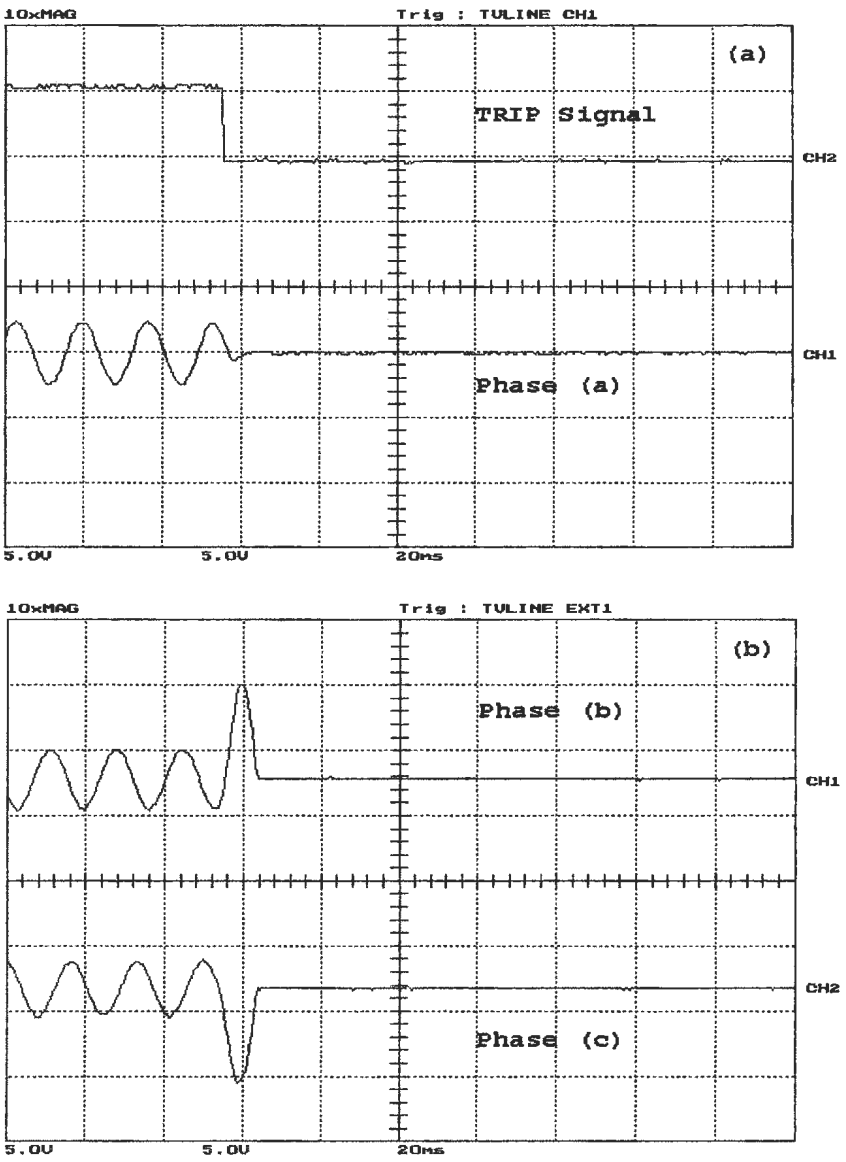

Figure A.20: Loaded phase C to ground fault, occurred after energization on the secondary side, (a) the WPT response and phase (a) differential current , (b) phase (b) and phase (c) differential currents. Y-scale is 1 Div. = 11.67 A

A.3 Phase to Phase Fault

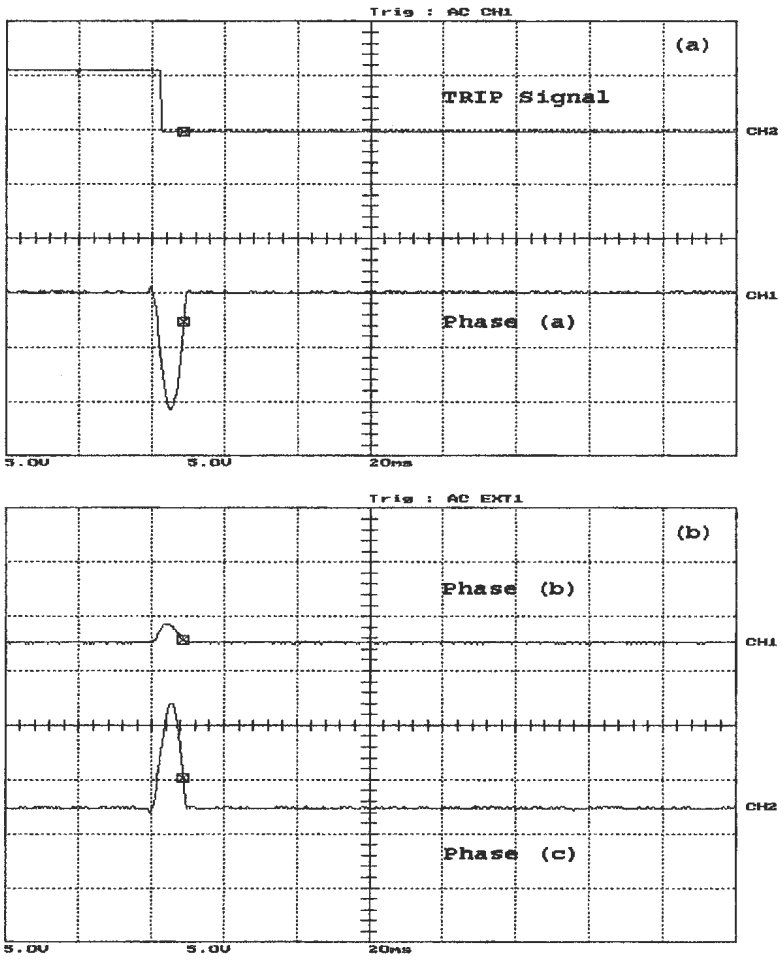

Figure A.21: Unloaded phase (a) to phase C fault, occurred before energization on the primary side, (a) the WPT response and phase (a) differential current , (b) phase (b) and phase (c) differential currents. Y-scale is 1 Div. = 11.67 A

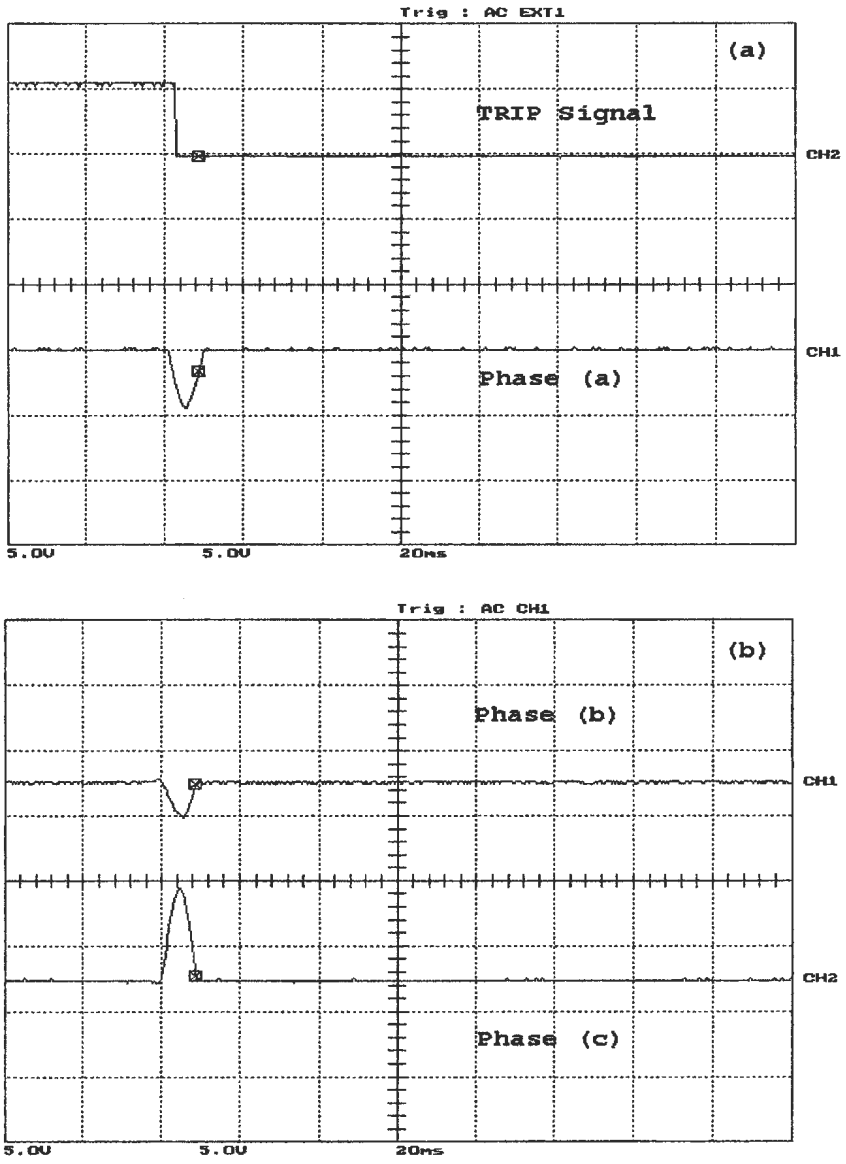

Figure A.22: Unloaded phase (a) to phase C fault, occurred before energization on the secondary side, (a) the WPT response and phase (a) differential current , (b) phase (b) and phase (c) differential currents. Y-scale is 1 Div. = 11.67 A

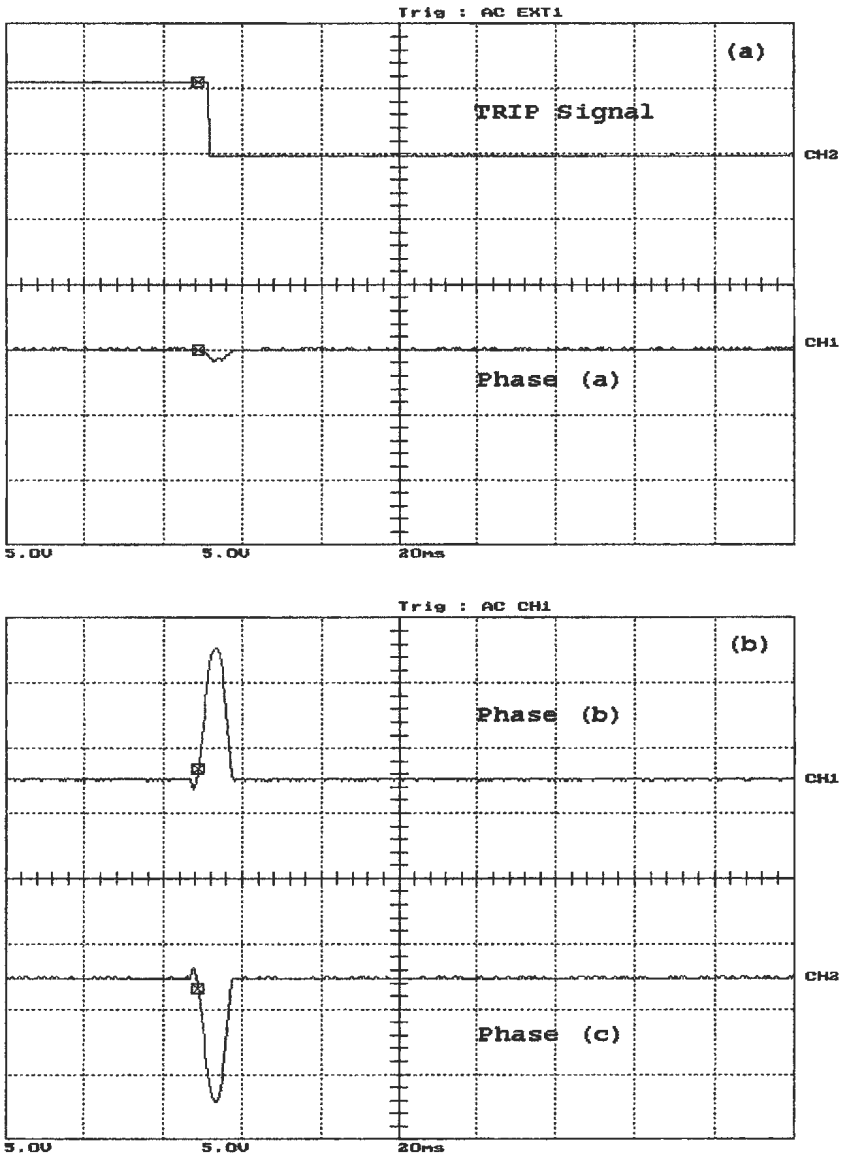

Figure A.23: Unloaded phase (b) to to phase C fault, occurred before energization on the primary side, (a) the WPT response and phase (a) differential current , (b) phase (b) and phase (c) differential currents. Y-scale is 1 Div. = 11.67 A

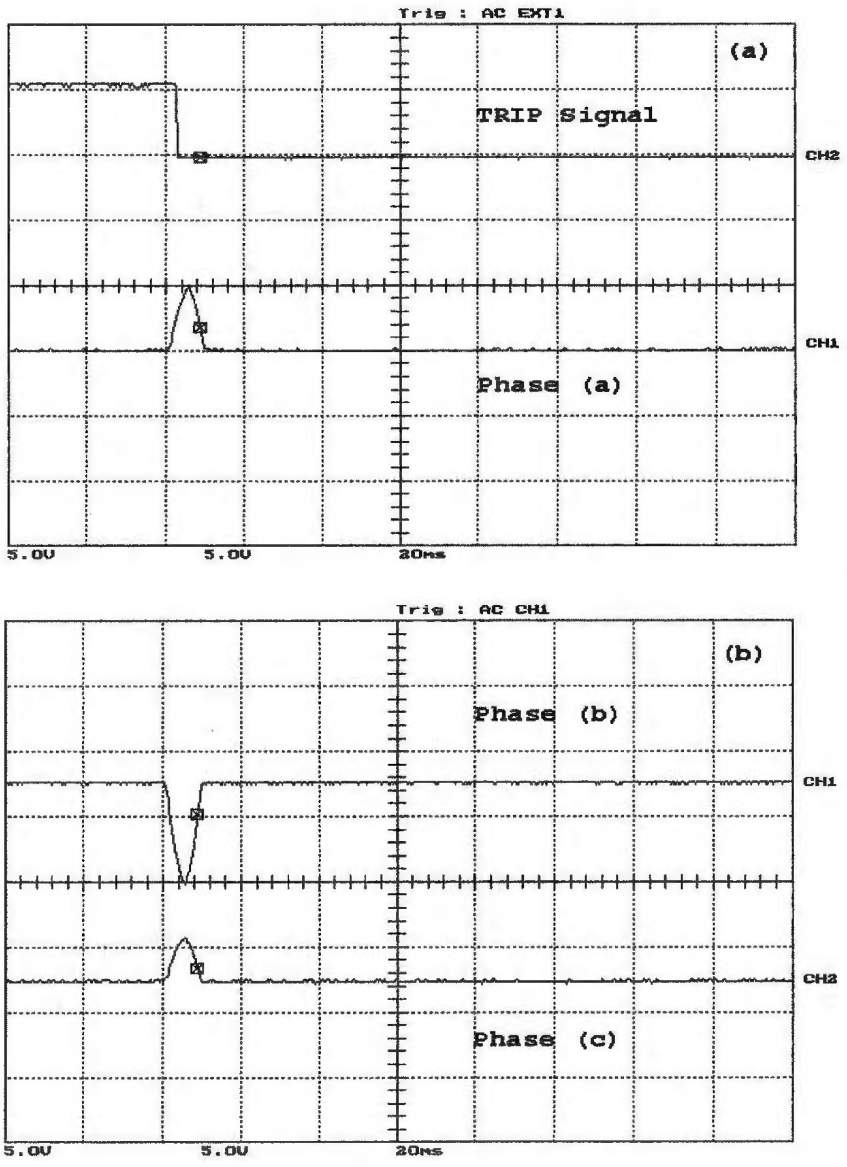

Figure A.24: Unloaded phase (b) to to phase C fault, occurred before energization on the secondary side, (a) the WPT response and phase (a) differential current , (b) phase (b) and phase (c) differential currents. Y-scale is 1 Div. = 11.67 A

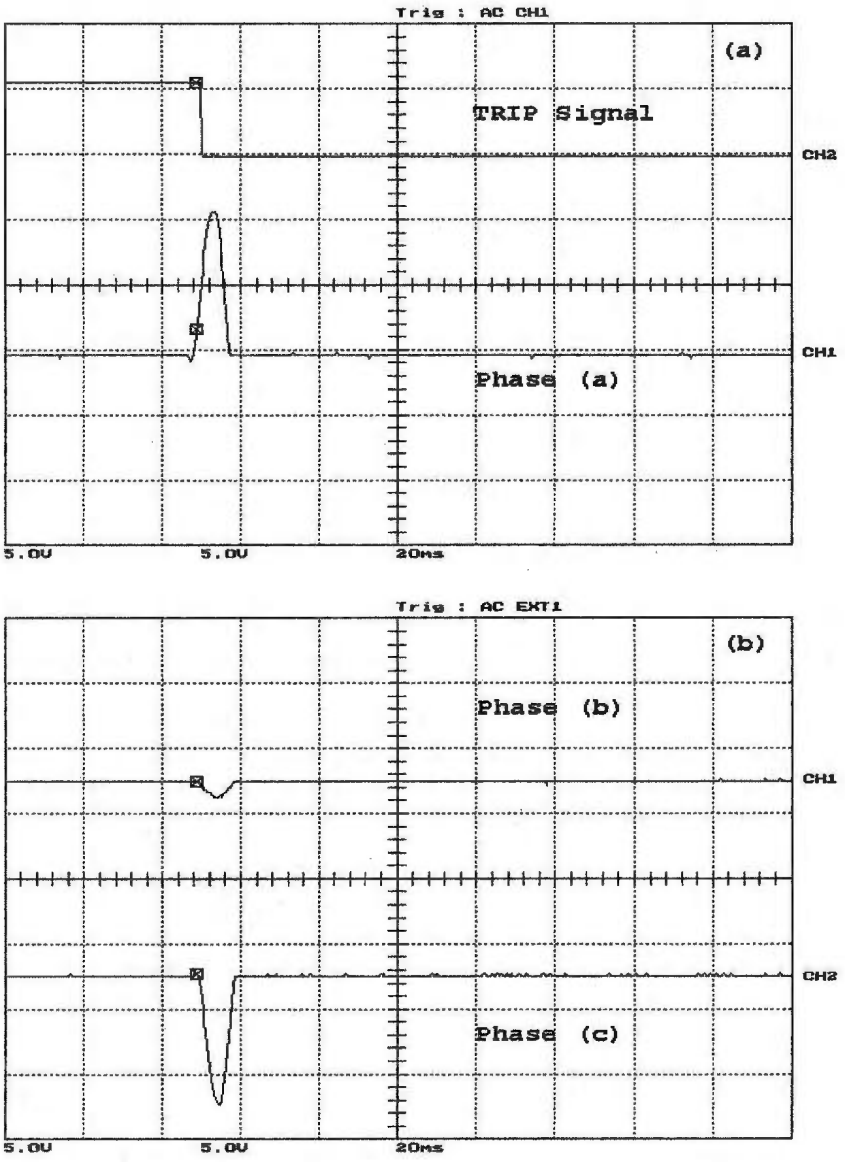

Figure A.25: Unloaded phase (a) to phase C fault, occurred after energization on the primary side, (a) the WPT response and phase (a) differential current , (b) phase (b) and phase (c) differential currents. Y-scale is 1 Div. = 11.67 A

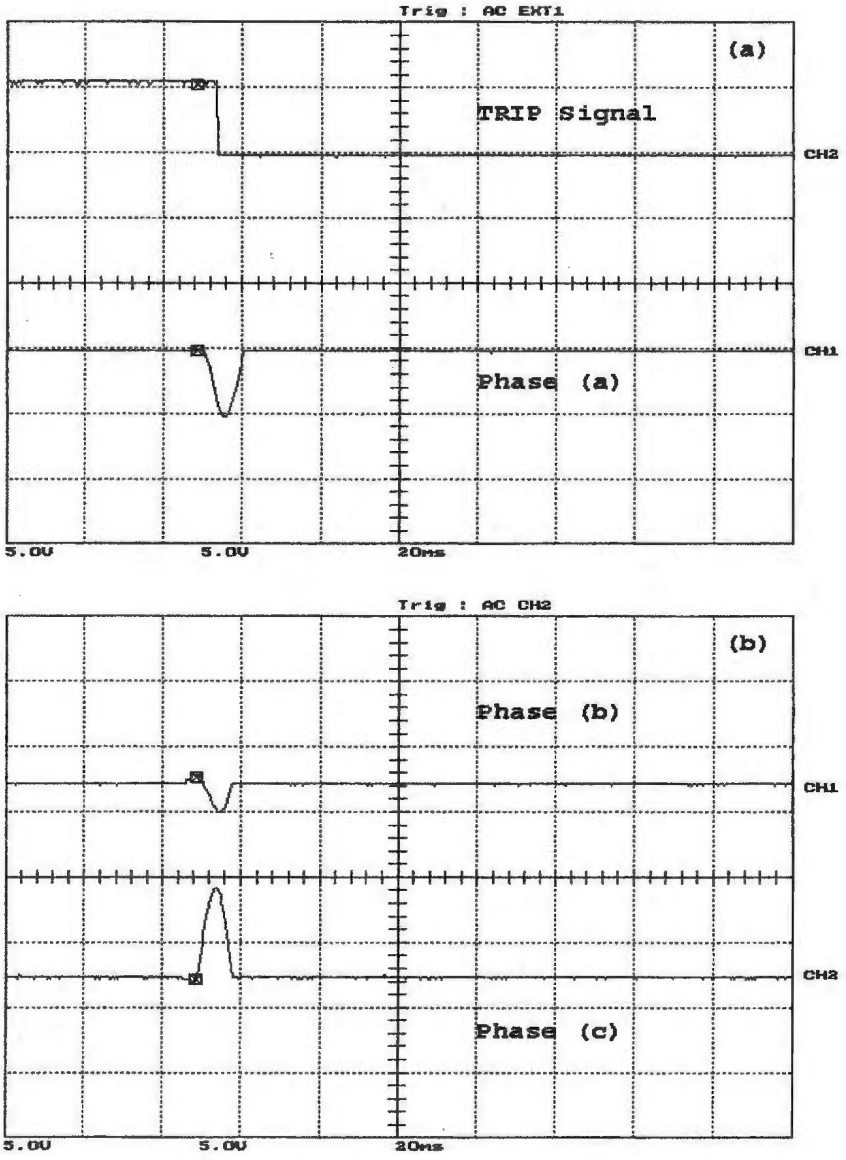

Figure A.26: Unloaded phase (a) to phase C fault, occurred after energization on the secondary side, (a) the WPT response and phase (a) differential current , (b) phase (b) and phase (c) differential currents. Y-scale is 1 Div. = 11.67 A

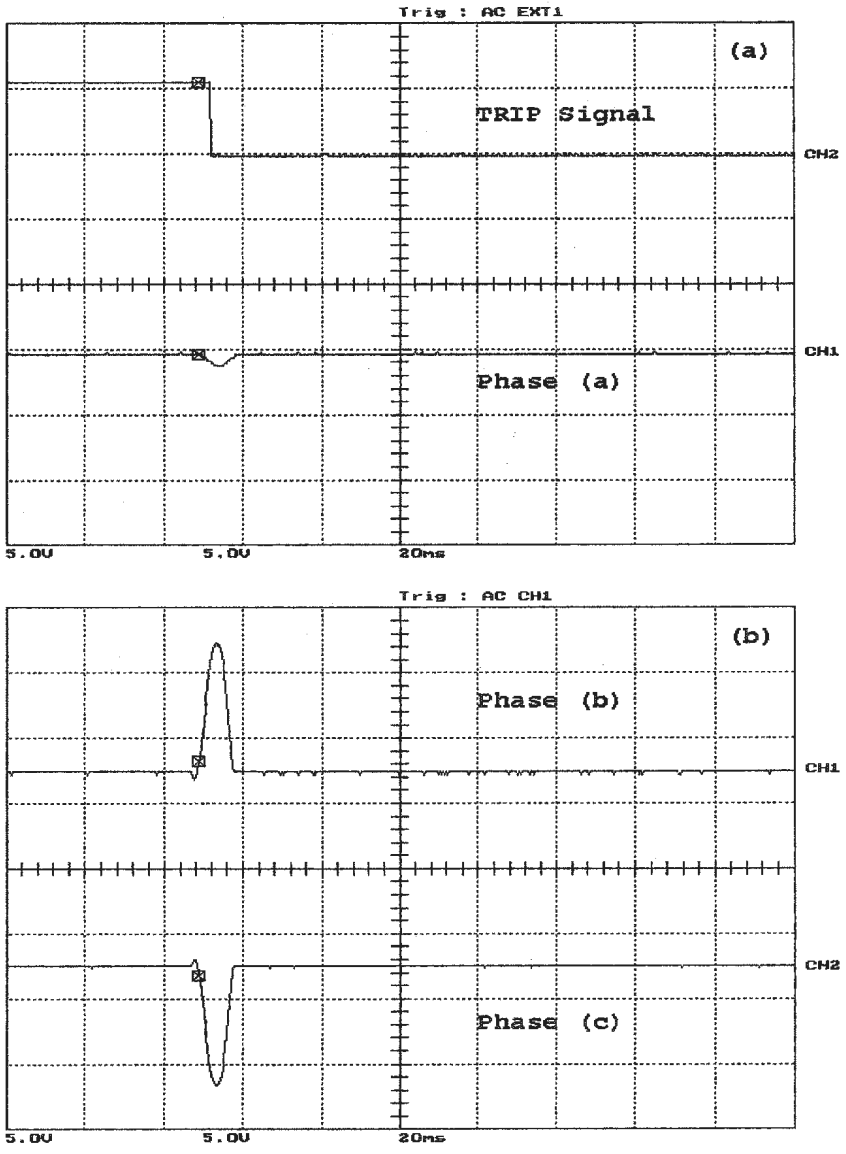

Figure A.27: Unloaded phase (b) to to phase C fault, occurred after energization on the primary side, (a) the WPT response and phase (a) differential current , (b) phase (b) and phase (c) differential currents. Y-scale is 1 Div. = 11.67 A

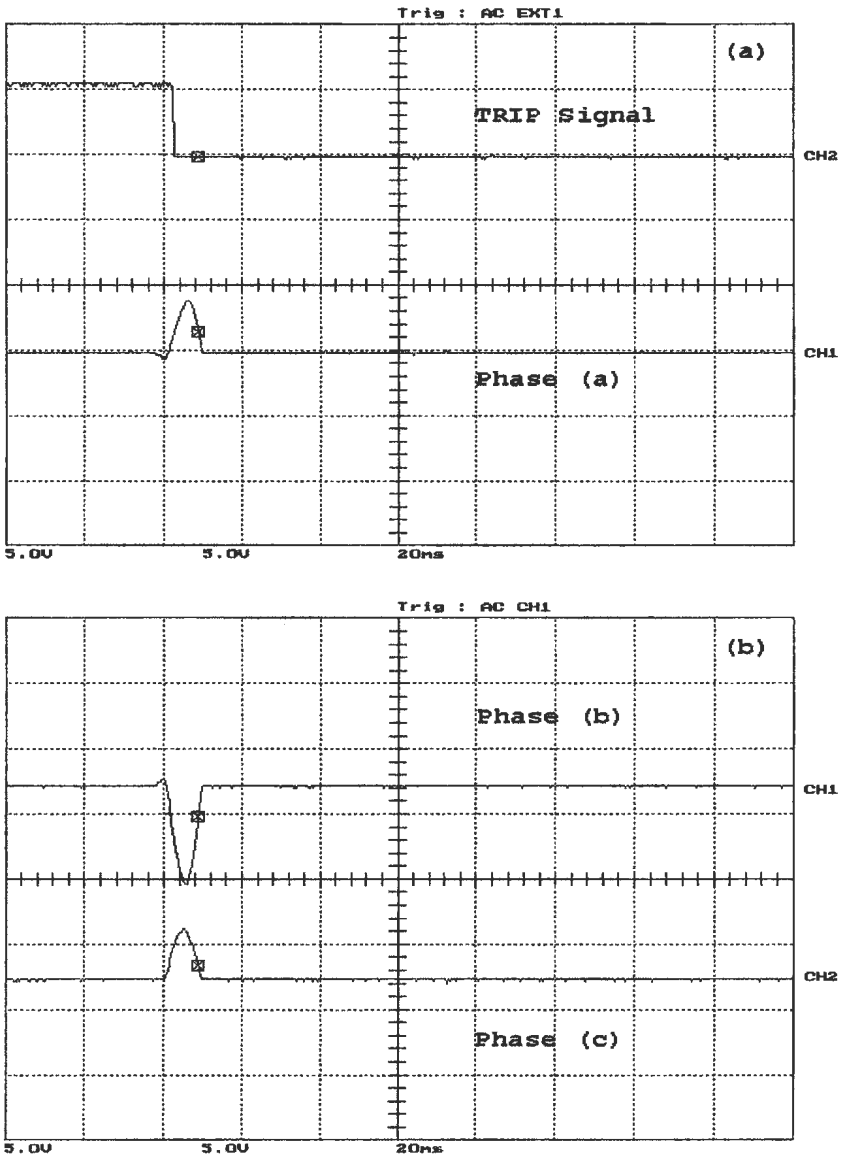

Figure A.28: Unloaded phase (b) to to phase C fault, occurred after energization on the secondary side, (a) the WPT response and phase (a) differential current , (b) phase (b) and phase (c) differential currents. Y-scale is 1 Div. = 11.67 A

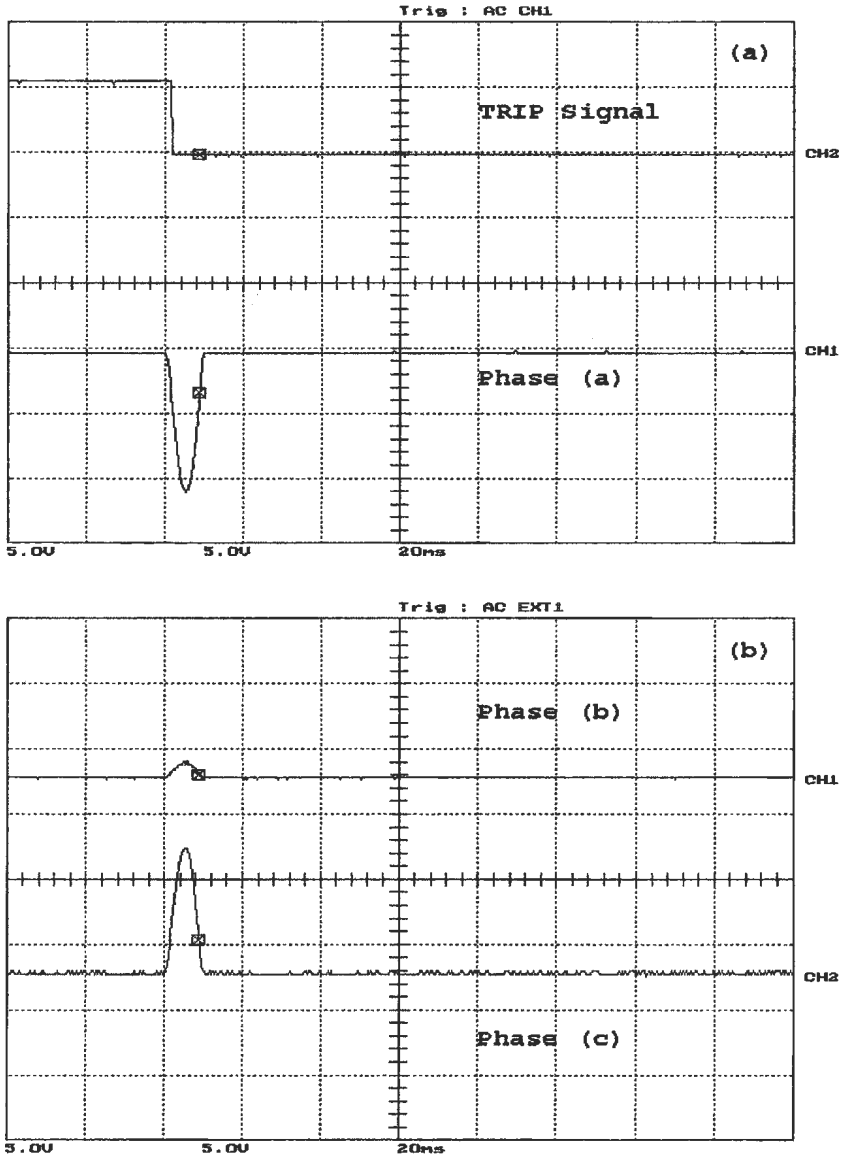

Figure A.29: Loaded phase (a) to phase C fault, occurred before energization on the primary side, (a) the WPT response and phase (a) differential current , (b) phase (b) and phase (c) differential currents. Y-scale is 1 Div. = 11.67 A

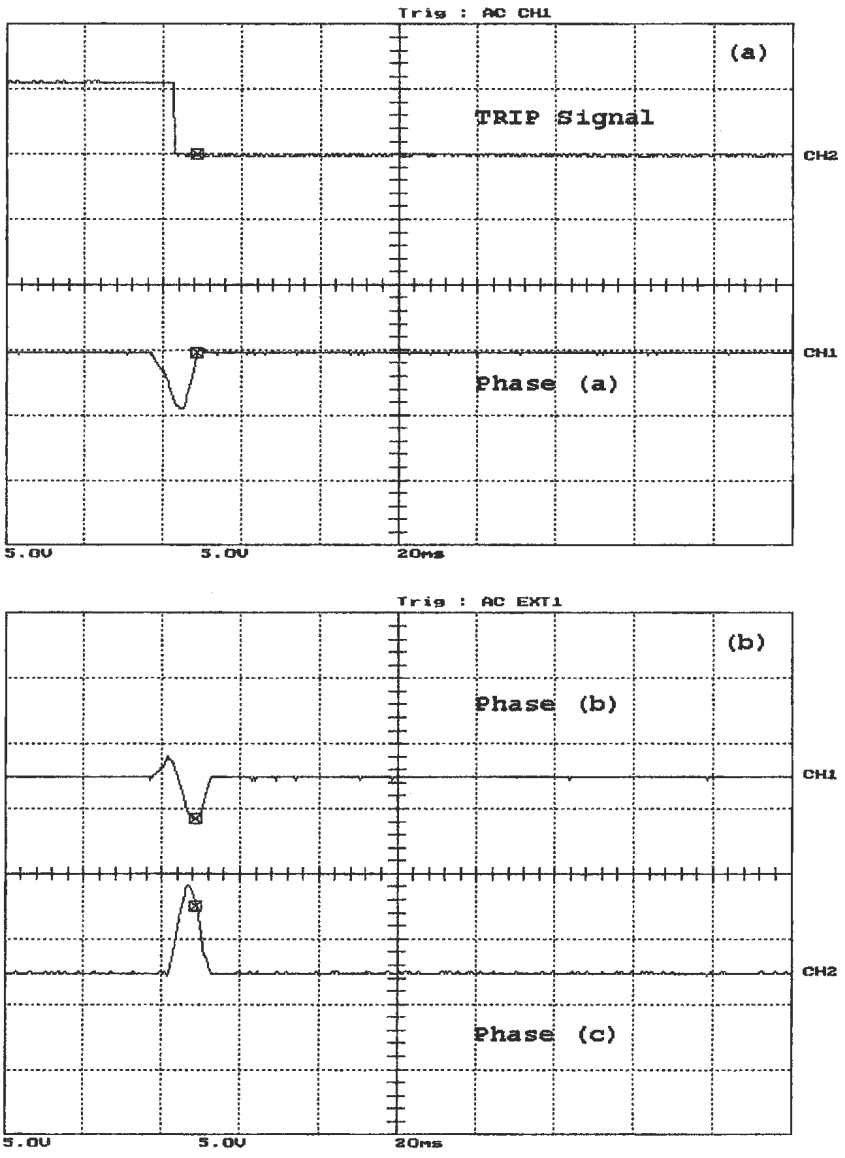

Figure A.30: Loaded phase (a) to phase C fault, occurred before energization on the secondary side, (a) the WPT response and phase (a) differential current , (b) phase (b) and phase (c) differential currents. Y-scale is 1 Div. = 11.67 A

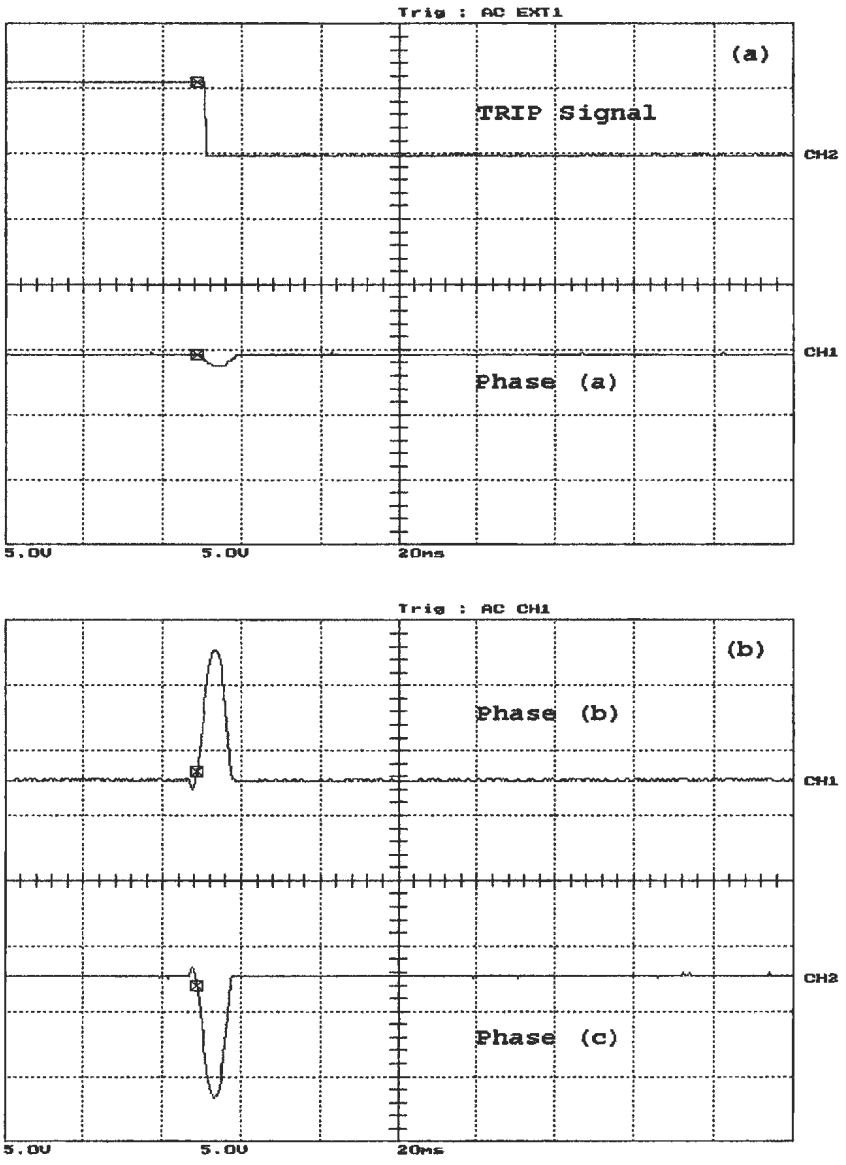

Figure A.31: Loaded phase (b) to to phase C fault, occurred before energization on the primary side, (a) the WPT response and phase (a) differential current , (b) phase (b) and phase (c) differential currents. Y-scale is 1 Div. = 11.67 A

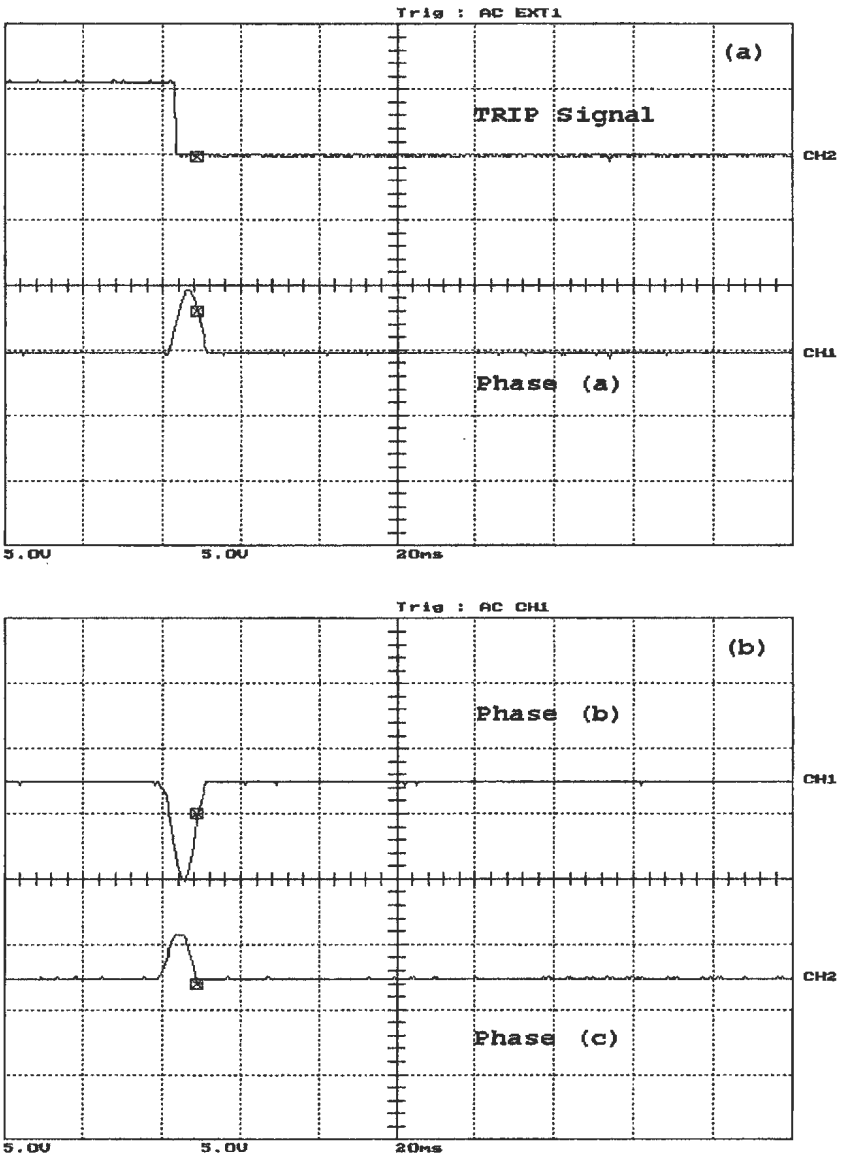

Figure A.32: Loaded phase (b) to to phase C fault, occurred before energization on the secondary side, (a) the WPT response and phase (a) differential current , (b) phase (b) and phase (c) differential currents. Y-scale is 1 Div. = 11.67 A

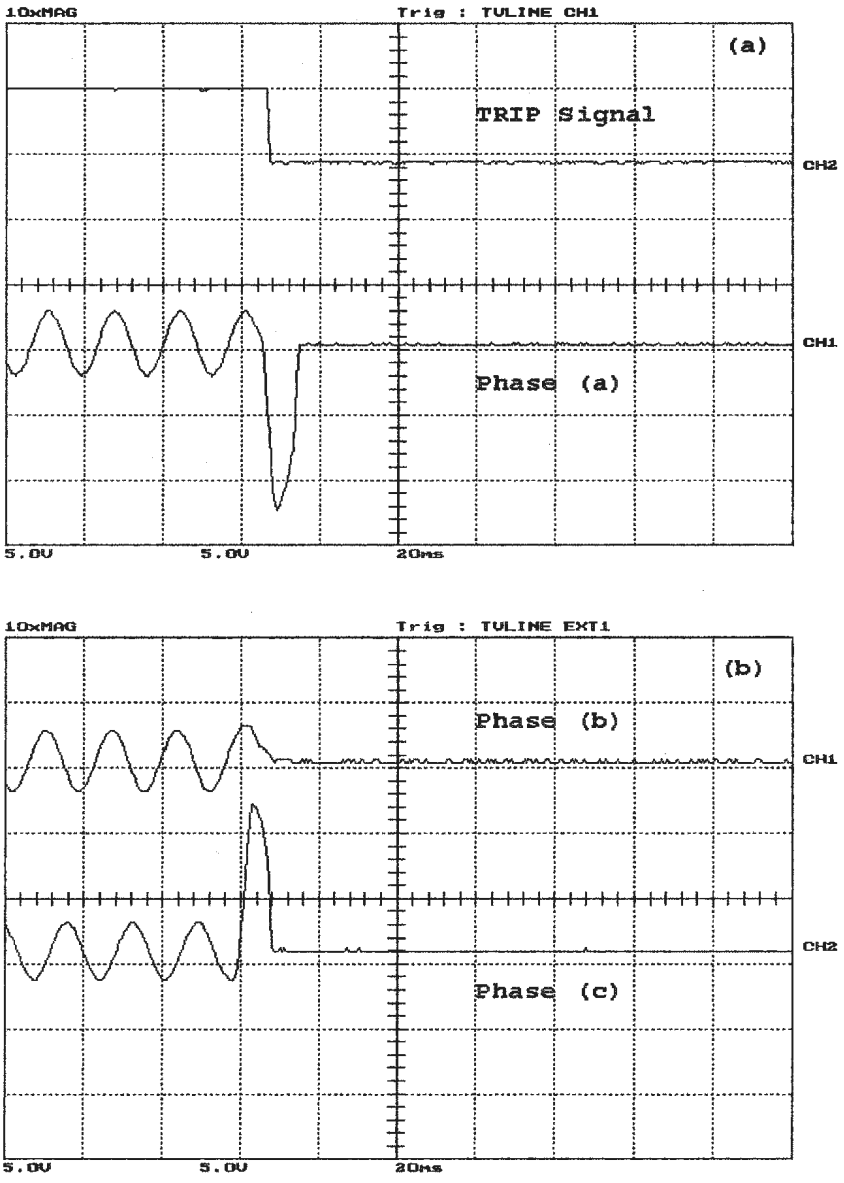

Figure A.33: Loaded phase (a) to phase C fault, occurred after energization on the primary side, (a) the WPT response and phase (a) differential current , (b) phase (b) and phase (c) differential currents. Y-scale is 1 Div. = 11.67 A

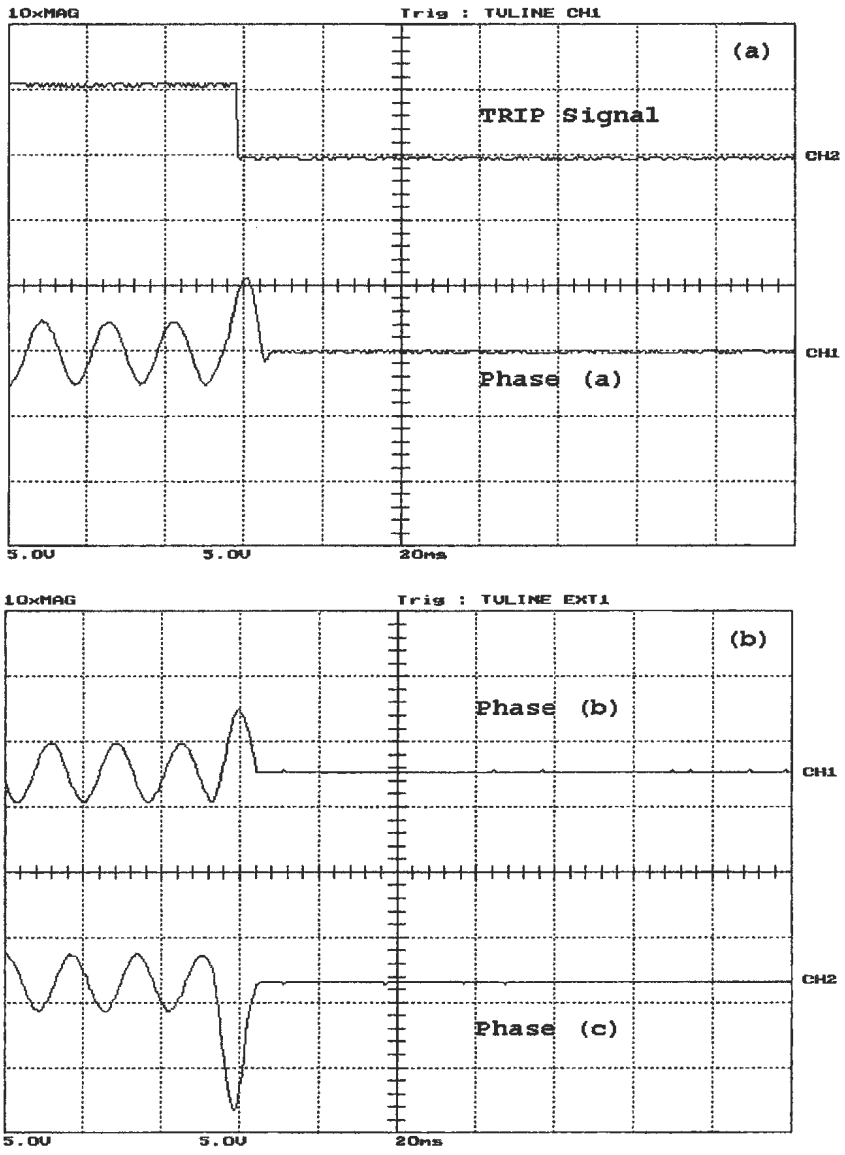

Figure A.34: Loaded phase (a) to phase C fault, occurred after energization on the secondary side, (a) the WPT response and phase (a) differential current , (b) phase (b) and phase (c) differential currents. Y-scale is 1 Div. = 11.67 A

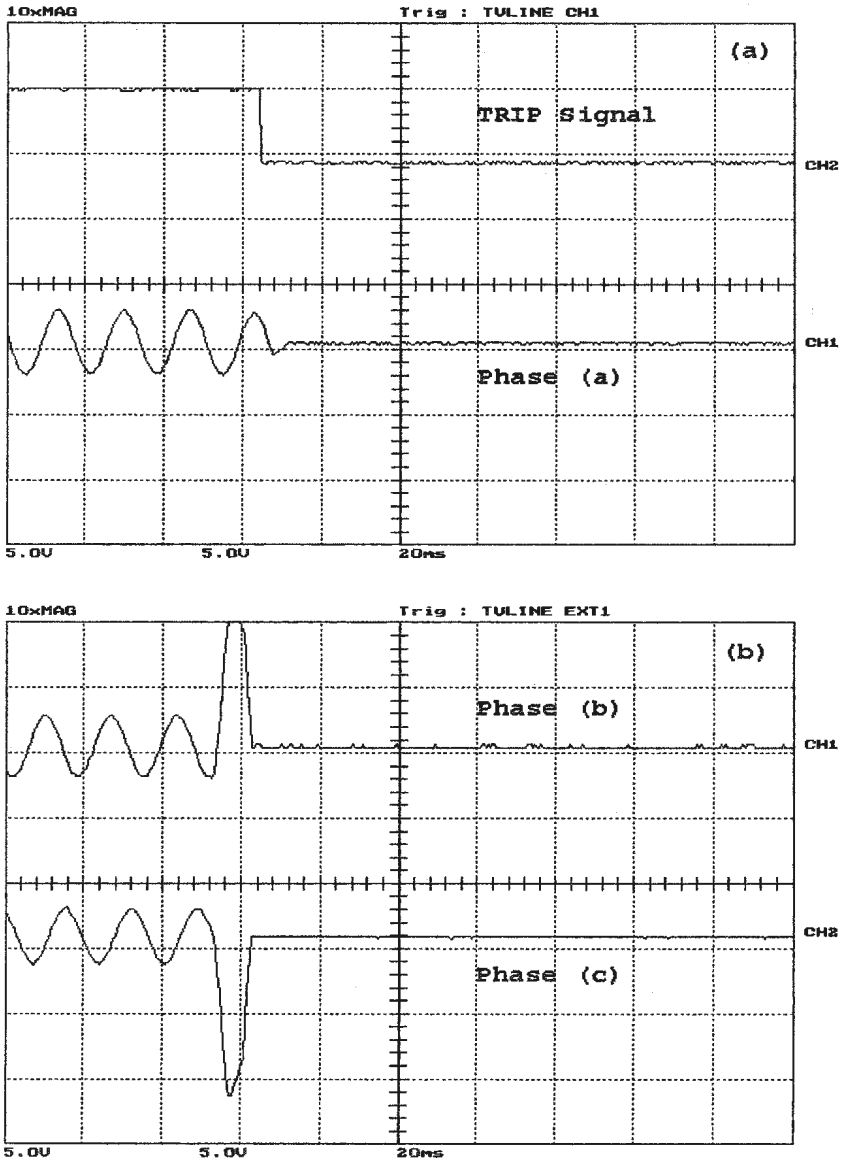

Figure A.35: Loaded phase (b) to to phase C fault, occurred after energization on the primary side, (a) the WPT response and phase (a) differential current , (b) phase (b) and phase (c) differential currents. Y-scale is 1 Div. = 11.67 A

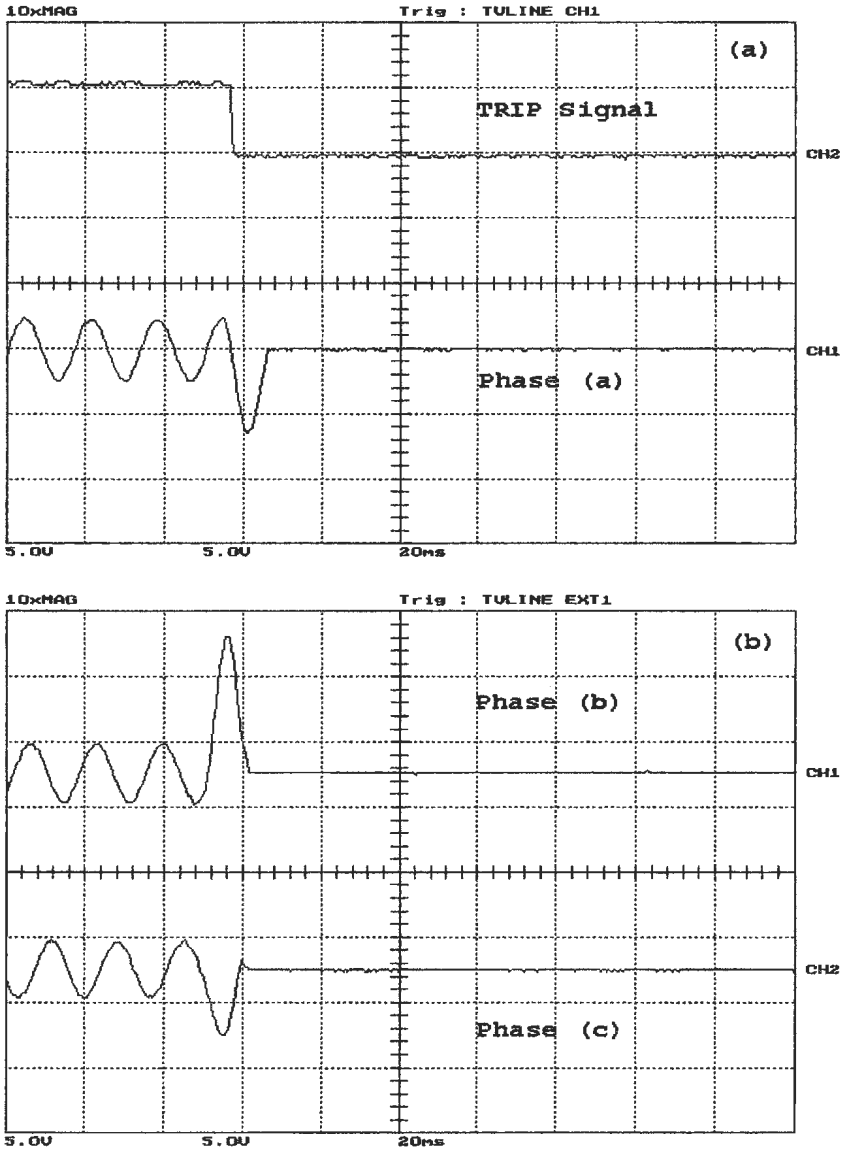

Figure A.36: Loaded phase (b) to to phase C fault, occurred after energization on the secondary side, (a) the WPT response and phase (a) differential current , (b) phase (b) and phase (c) differential currents. Y-scale is 1 Div. = 11.67 A

A.4 Three-Phase to Ground Fault

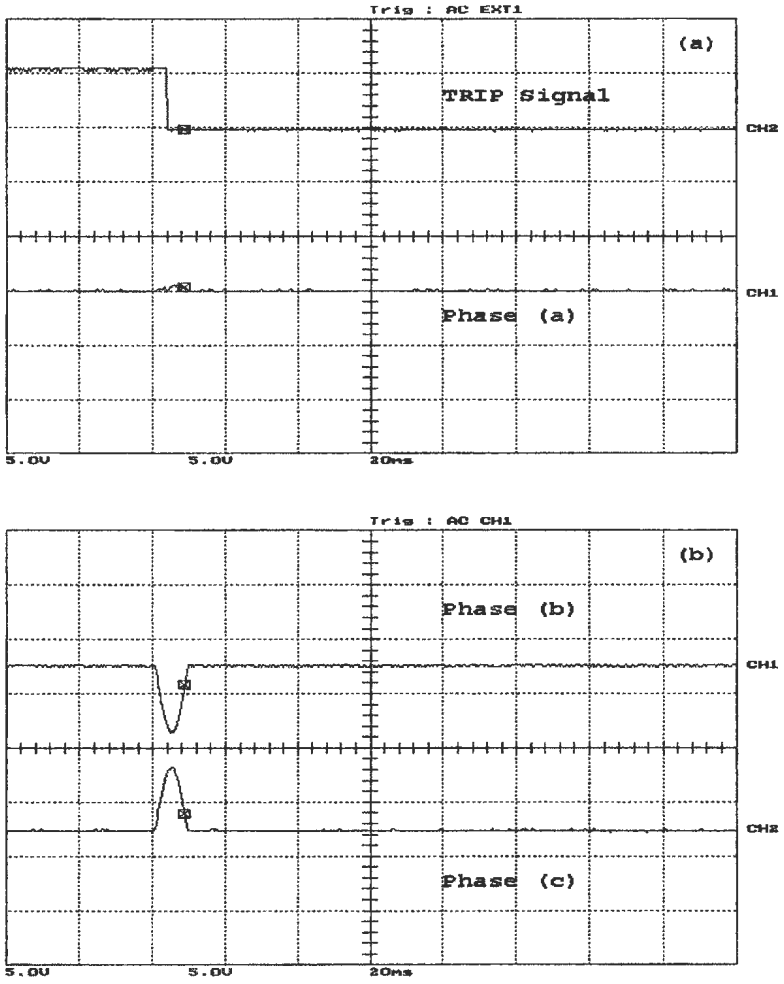

Figure A.37: Unloaded three-phase to ground fault, occurred before energization on the secondary side, (a) the WPT response and phase (a) differential current , (b) phase (b) and phase (c) differential currents. Y-scale is 1 Div. = 11.67 A

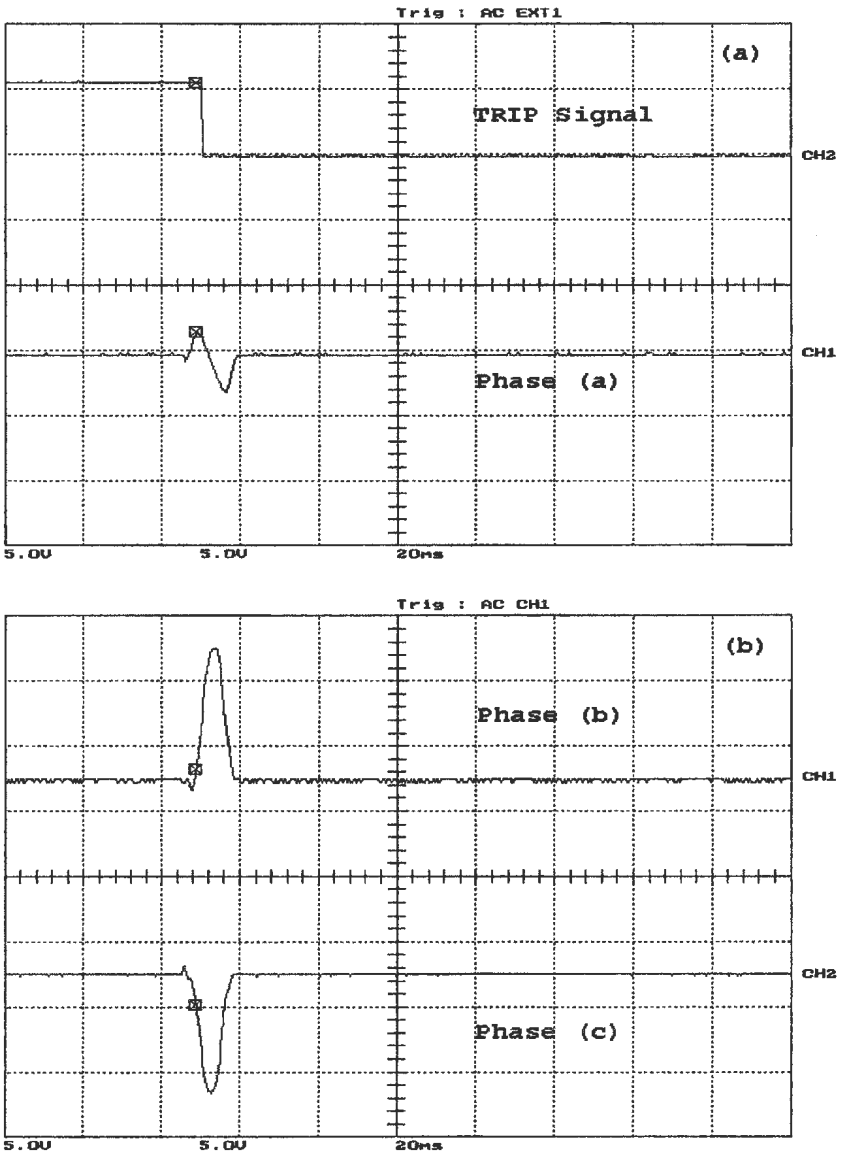

Figure A.38: Unloaded three-phase fault, occurred after energization on the primary side, (a) the WPT response and phase (a) differential current , (b) phase (b) and phase (c) differential currents. Y-scale is 1 Div. = 11.67 A

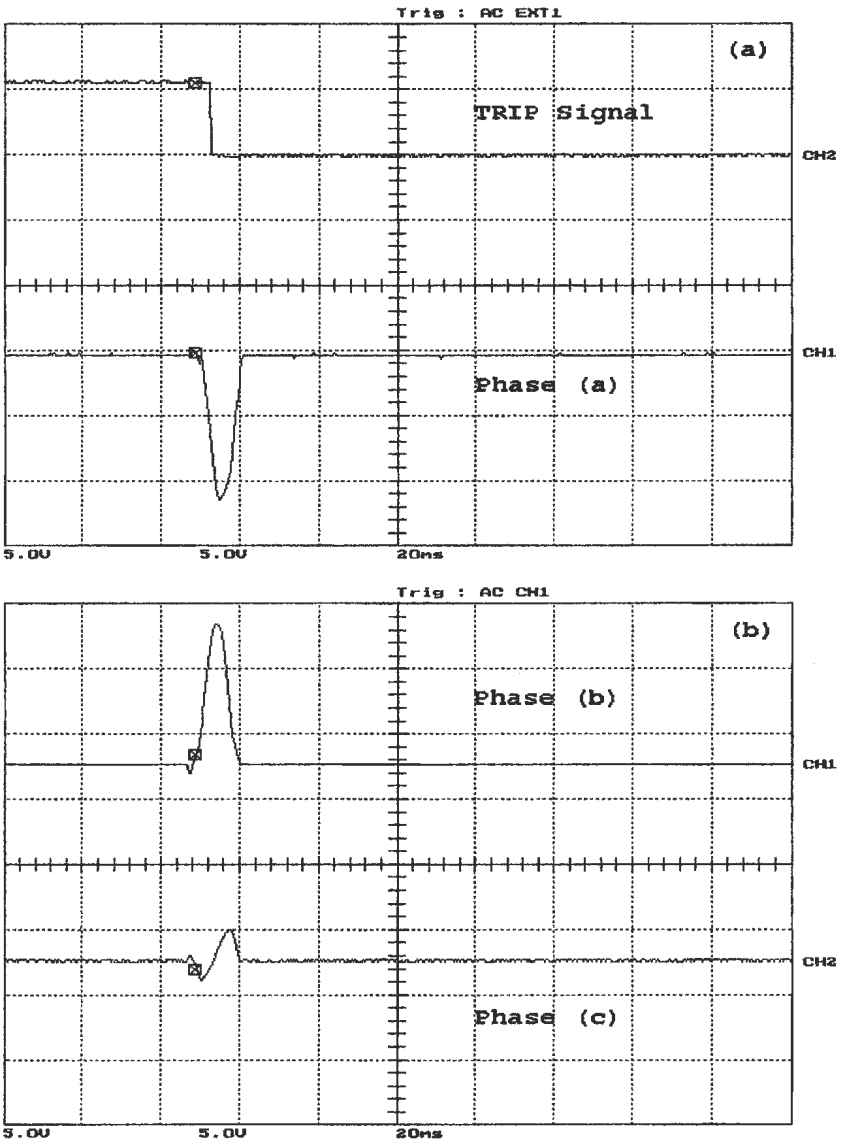

Figure A.39: Loaded three-phase fault, occurred before energization on the primary side, (a) the WPT response and phase (a) differential current , (b) phase (b) and phase (c) differential currents. Y-scale is 1 Div. = 11.67 A

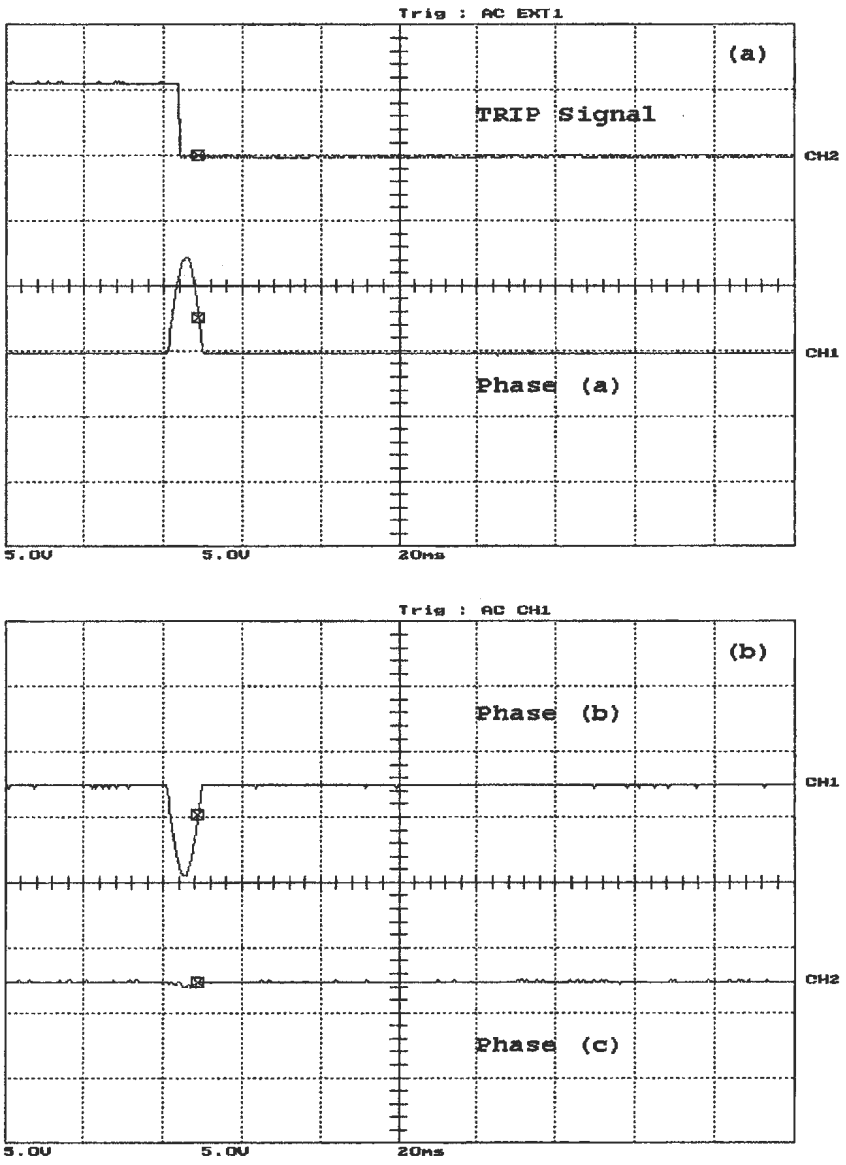

Figure A.40: Loaded three-phase fault, occurred before energization on the secondary side, (a) the WPT response and phase (a) differential current , (b) phase (b) and phase (c) differential currents. Y-scale is 1 Div. = 11.67 A

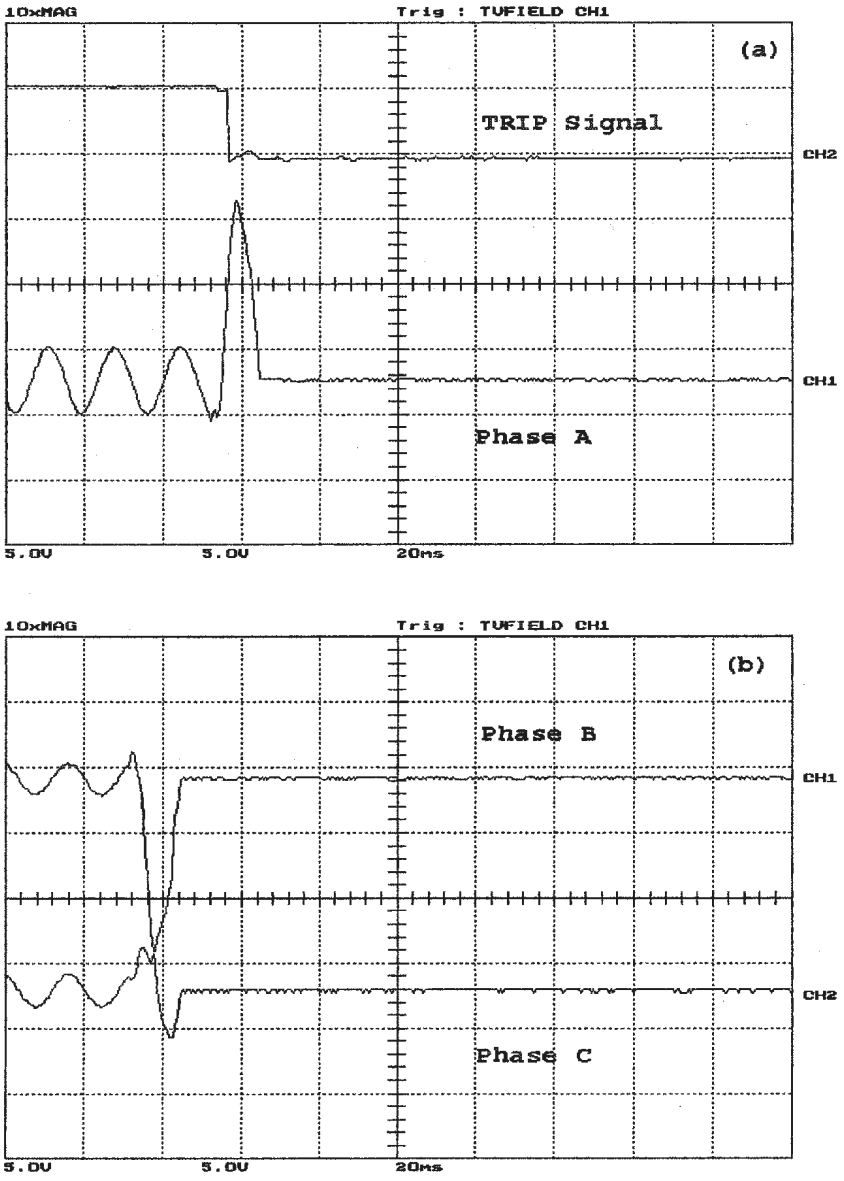

Figure A.41: Loaded three-phase fault, occurred after energization on the primary side, (a) the WPT response and phase (a) differential current , (b) phase (b) and phase (c) differential currents. Y-scale is 1 Div. = 11.67 A

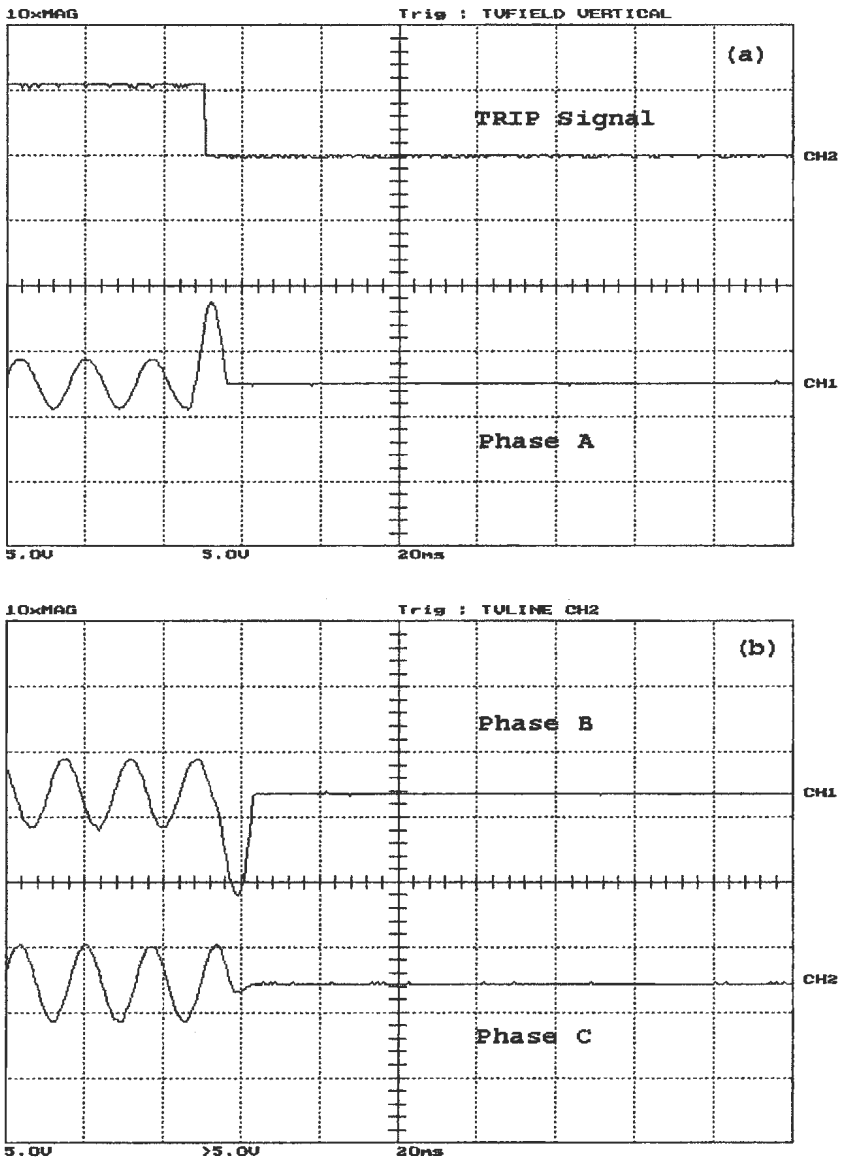

Figure A.42: Loaded three-phase fault, occurred after energization on the secondary side, (a) the WPT response and phase (a) differential current , (b) phase (b) and phase (c) differential currents. Y-scale is 1 Div. = 11.67 A

A.5 Different Faults Under Unbalaced Loading Conditions

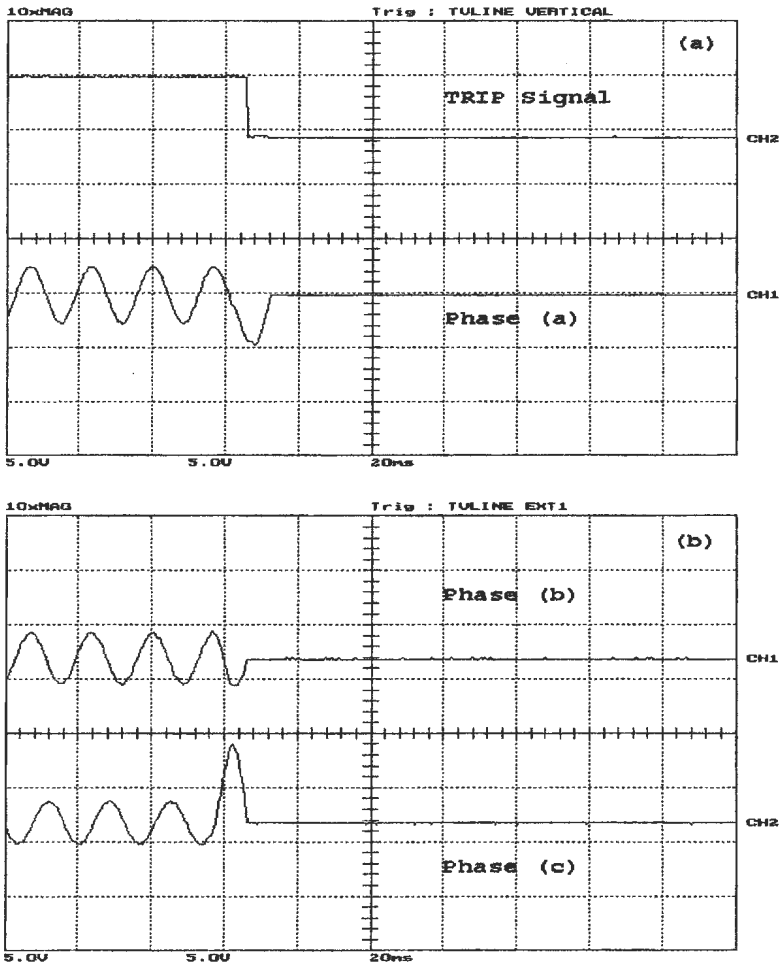

Figure A.43: Phase C to ground fault, occurred after energization with Z_a= 20 + j11.9129, Z_b= 20 + j0, Z_c= 35 + j7.012 Ω on the primary side, (a) the WPT response and phase (a) differential current , (b) phase (b) and phase (c) differential currents. Y-scale is 1 Div. = 11.67 A

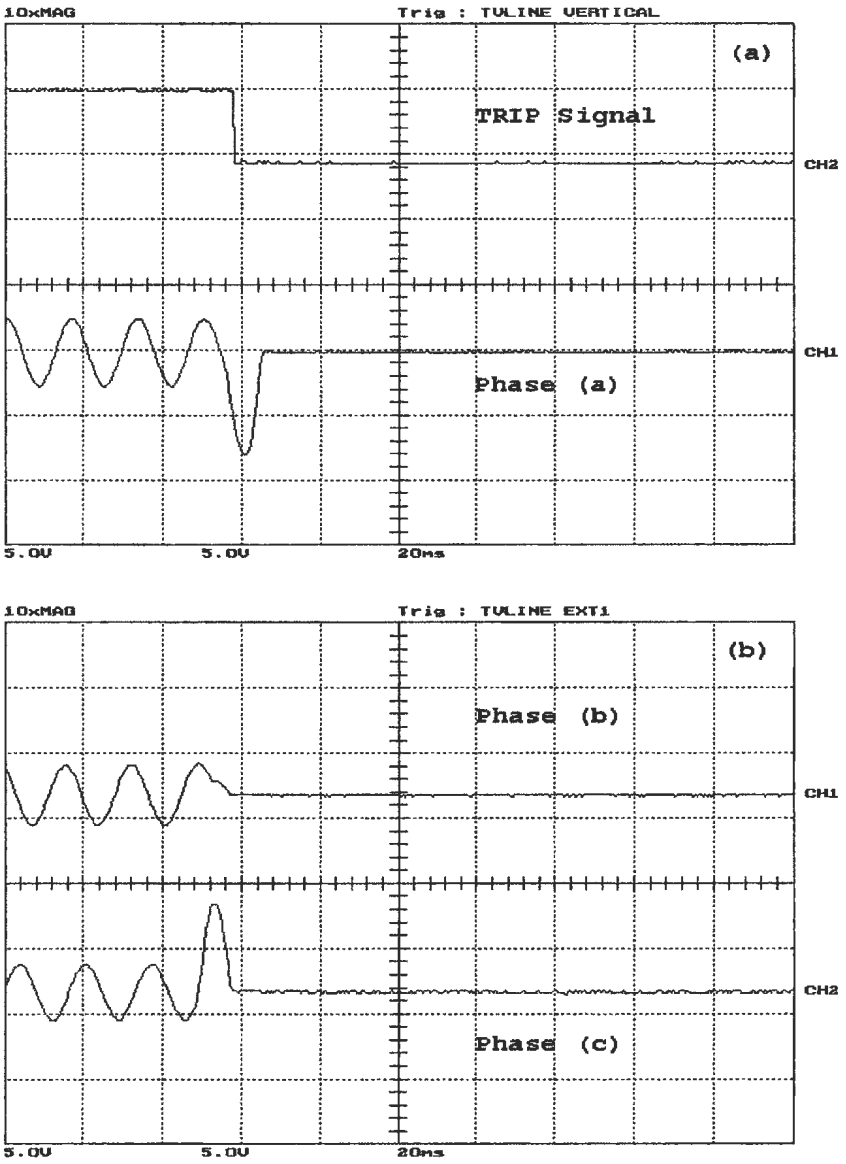

Figure A.44: phase (a) to ground fault, occurred after energization with Z_a= 20 + j11.9129, Z_b= 20 + j0, Z_c= 35 + j7.012 Ω on the secondary side, (a) the WPT response and phase (a) differential current , (b) phase (b) and phase (c) differential currents. Y-scale is 1 Div. = 11.67 A

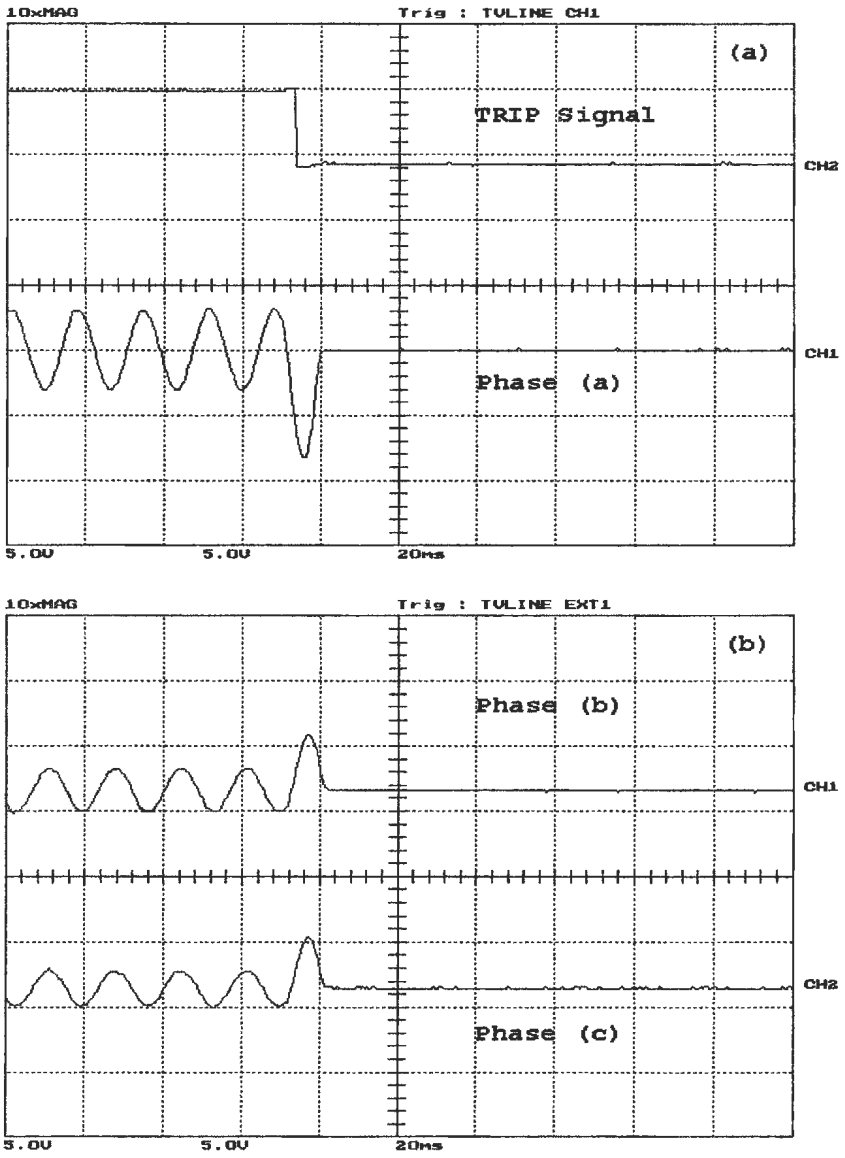

Figure A.45: phase (a) to ground fault, occurred after energization with $Z_a = 20 + j11.9129$, $Z_b = 11.9129$, $Z_c = \infty\ \Omega$ on the primary side, (a) the WPT response and phase (a) differential current , (b) phase (b) and phase (c) differential currents. Y-scale is 1 Div. = 11.67 A

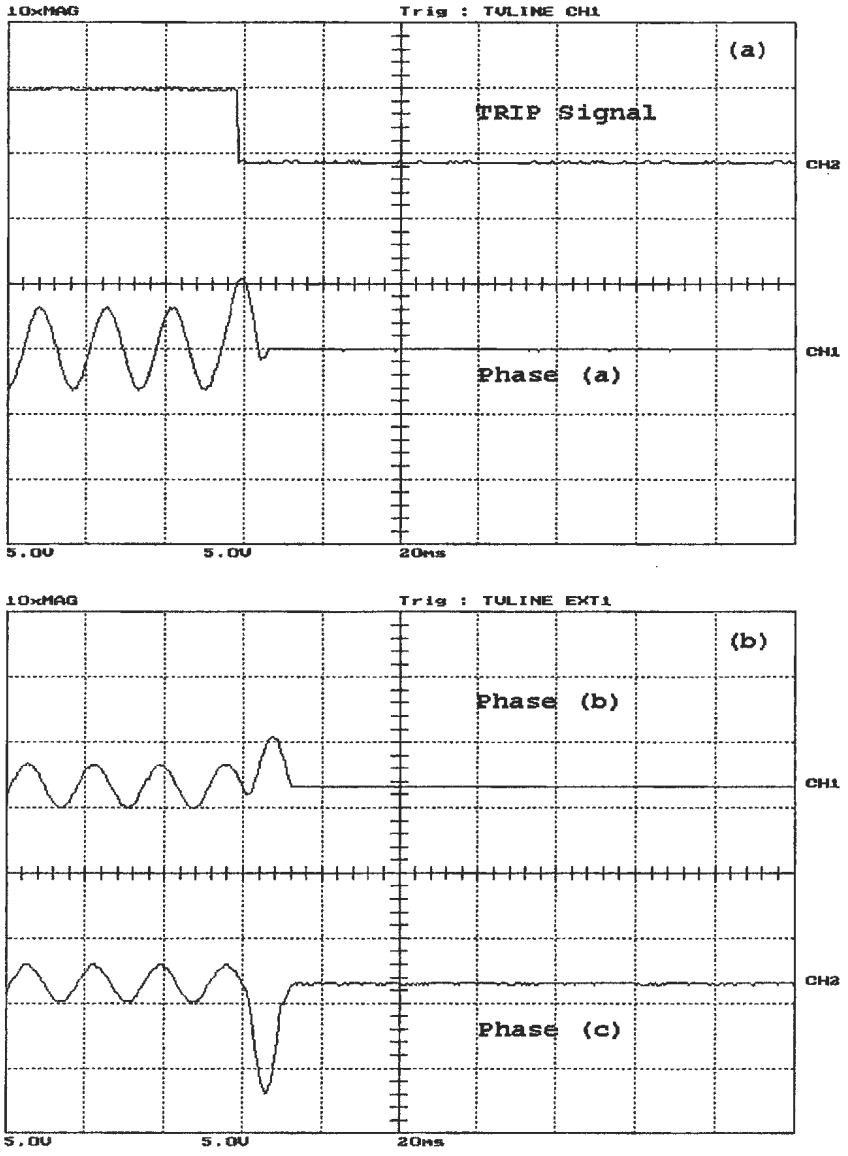

Figure A.46: phase (a) phase C fault, occurred after energization with $Z_a = 20 + j11.9129$, $Z_b = 11.9129$, $Z_c = \infty\ \Omega$ on the secondary side, (a) the WPT response and phase (a) differential current , (b) phase (b) and phase (c) differential currents. Y-scale is 1 Div. = 11.67 A

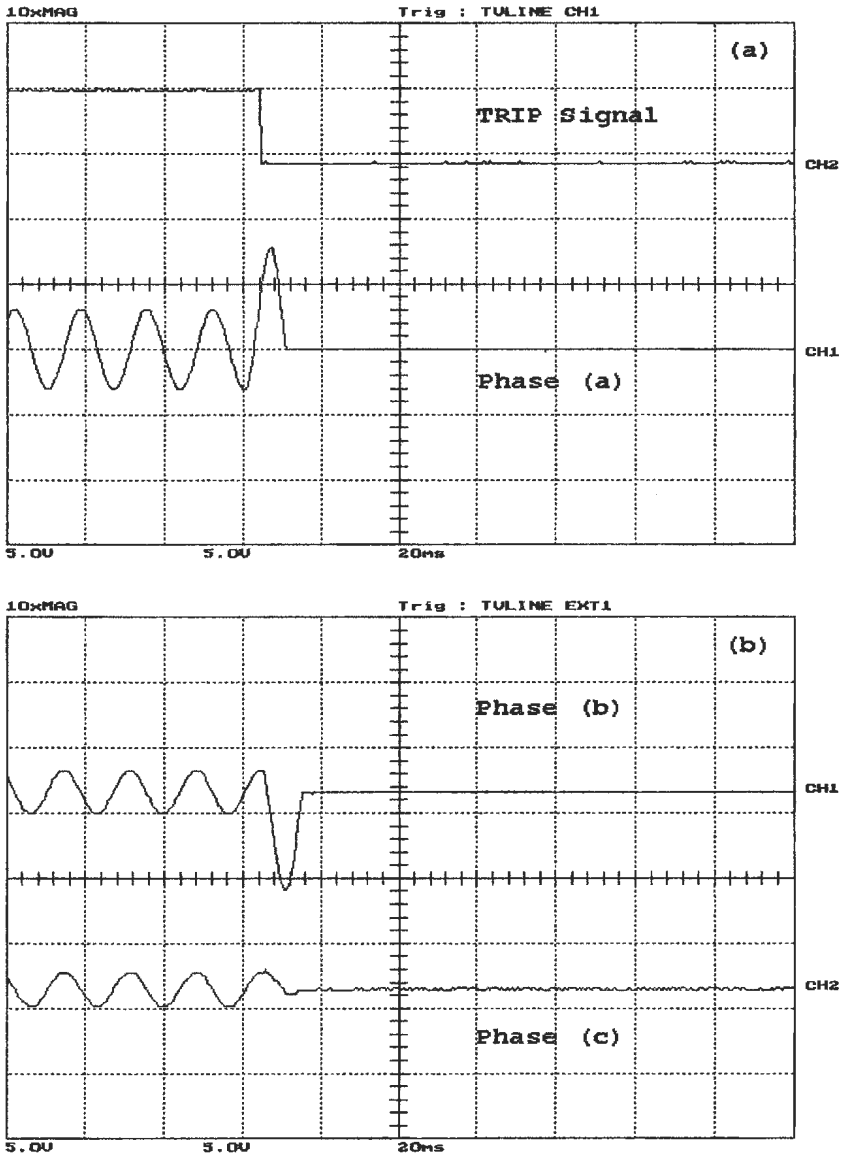

Figure A.47: phase (b) to ground fault, occurred after energization with $Z_a = 20 + j11.9129$, $Z_b = 11.9129$, $Z_c = \infty\ \Omega$ on the secondary side, (a) the WPT response and phase (a) differential current , (b) phase (b) and phase (c) differential currents. Y-scale is 1 Div. = 11.67 A

Appendix B

2 kVA Multi Tap Three-Phase Power Transformer

B.1 Magnetizing Inrush Currents

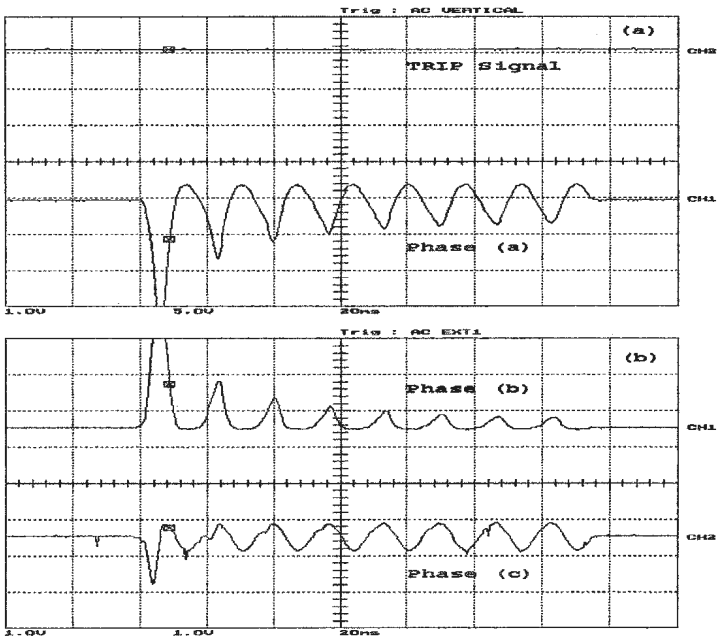

Figure B.1: Magnetizing inrush current for unbalanced inductive load of Z_a=20+j11.9129, Z_b= j11.9129 and Z_c=20 Ω, (a) the WPT response and phase (a) differential current , (b) phase (b) and phase (c) differential currents. Y-scale is 1 Div. = 11.67 A

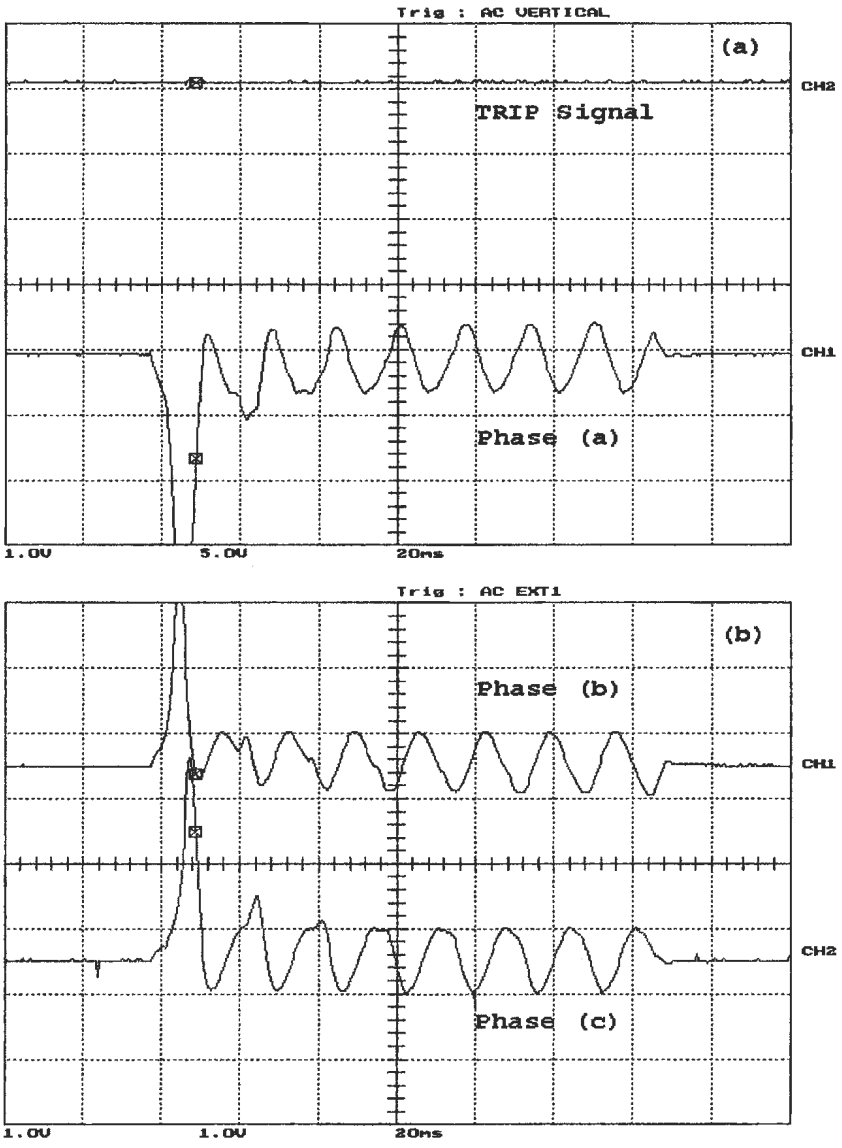

Figure B.2: Magnetizing inrush current for balanced resistive load of Z=20 Ω/phase, (a) the WPT response and phase (a) differential current , (b) phase (b) and phase (c) differential currents. Y-scale is 1 Div. = 11.67 A

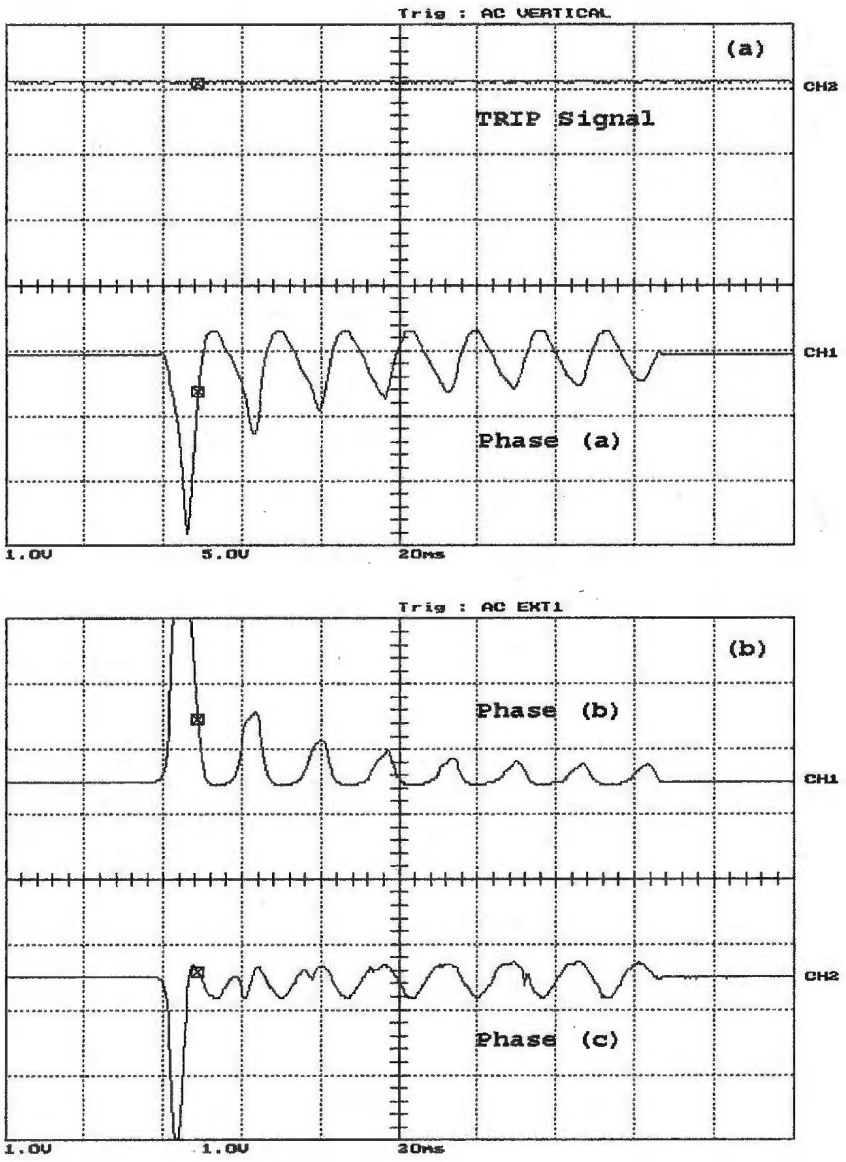

Figure B.3: Magnetizing inrush current for unbalanced resistive load of Z_a=20, Z_b=∞ and Z_c=35 Ω, (a) the WPT response and phase (a) differential current , (b) phase (b) and phase (c) differential currents. Y-scale is 1 Div. = 11.67 A

B.2 Single Phase to Ground Fault

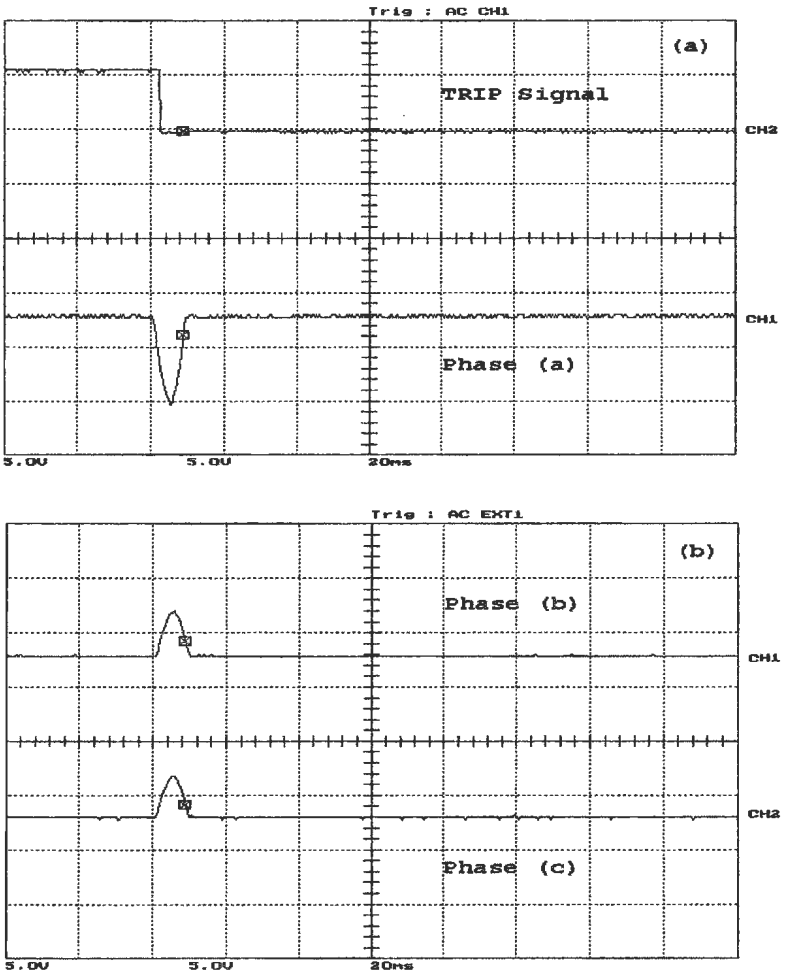

Figure B.4: Unloaded phase (a) to ground fault, occurred before energization on the primary side, (a) the WPT response and phase (a) differential current , (b) phase (b) and phase (c) differential currents. Y-scale is 1 Div. = 11.67 A

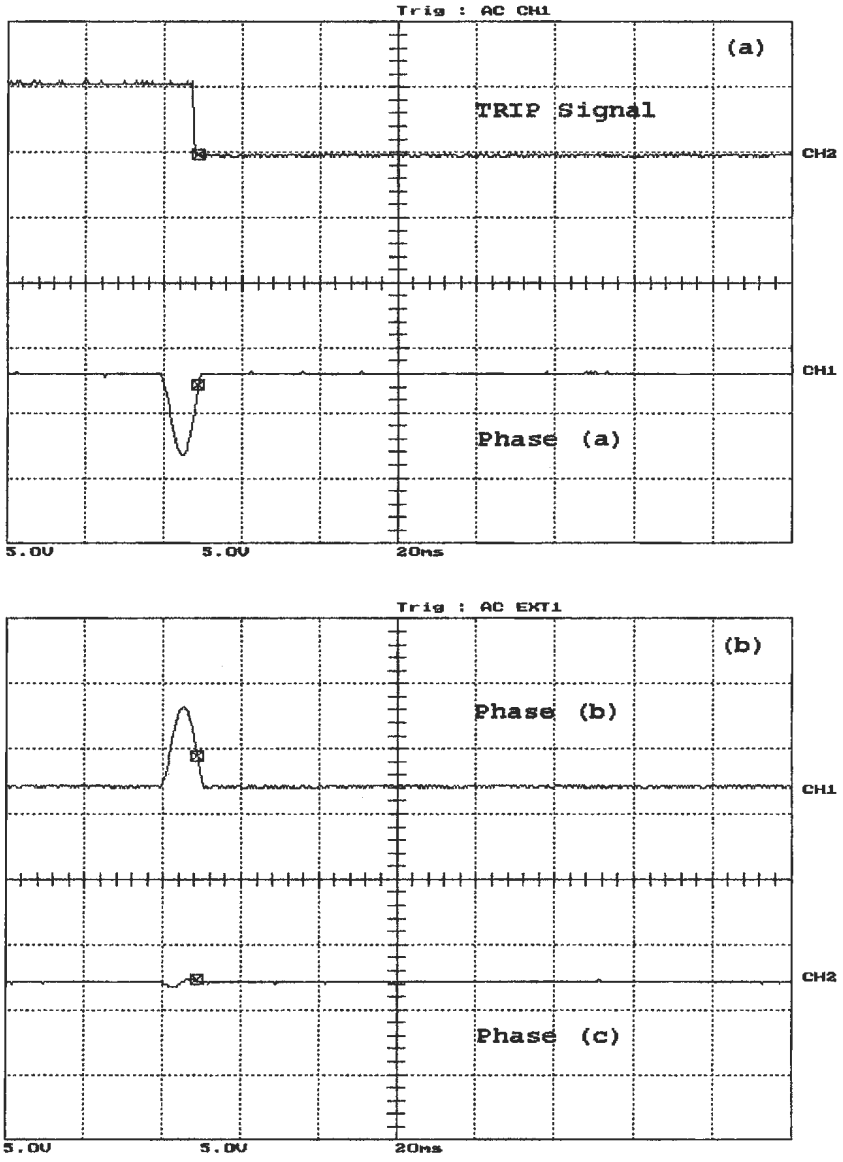

Figure B.5: Unloaded phase (a) to ground fault, occurred before energization on the secondary side, (a) the WPT response and phase (a) differential current , (b) phase (b) and phase (c) differential currents. Y-scale is 1 Div. = 11.67 A

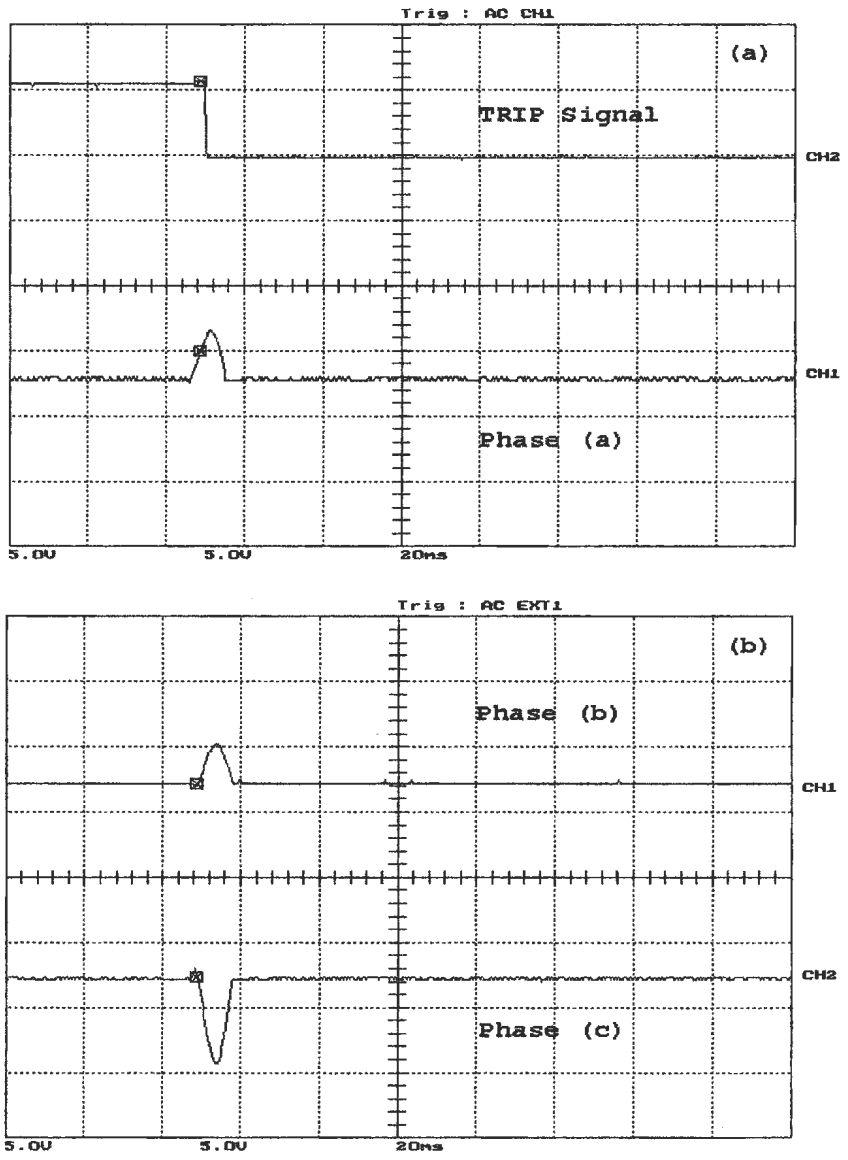

Figure B.6: Unloaded phase C to ground fault, occurred before energization on the primary side, (a) the WPT response and phase (a) differential current , (b) phase (b) and phase (c) differential currents. Y-scale is 1 Div. = 11.67 A

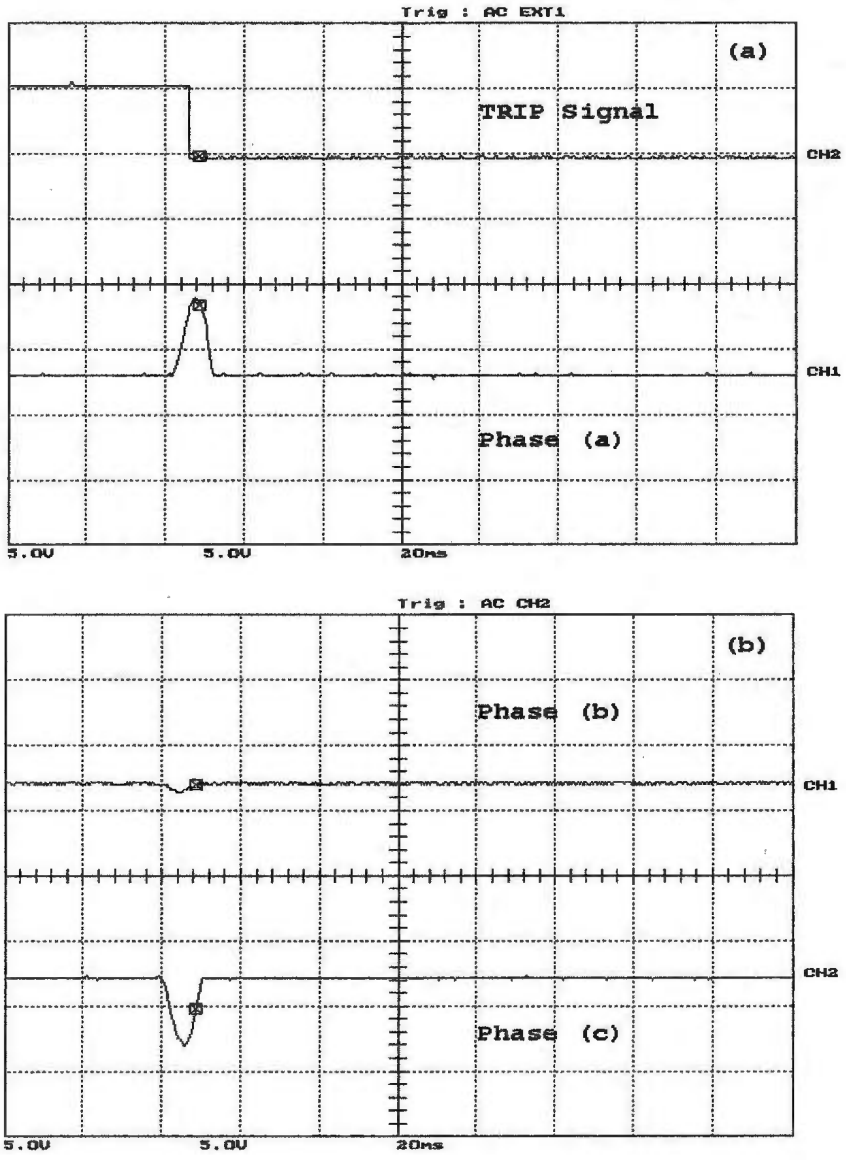

Figure B.7: Unloaded phase C to ground fault, occurred before energization on the secondary side, (a) the WPT response and phase (a) differential current , (b) phase (b) and phase (c) differential currents. Y-scale is 1 Div. = 11.67 A

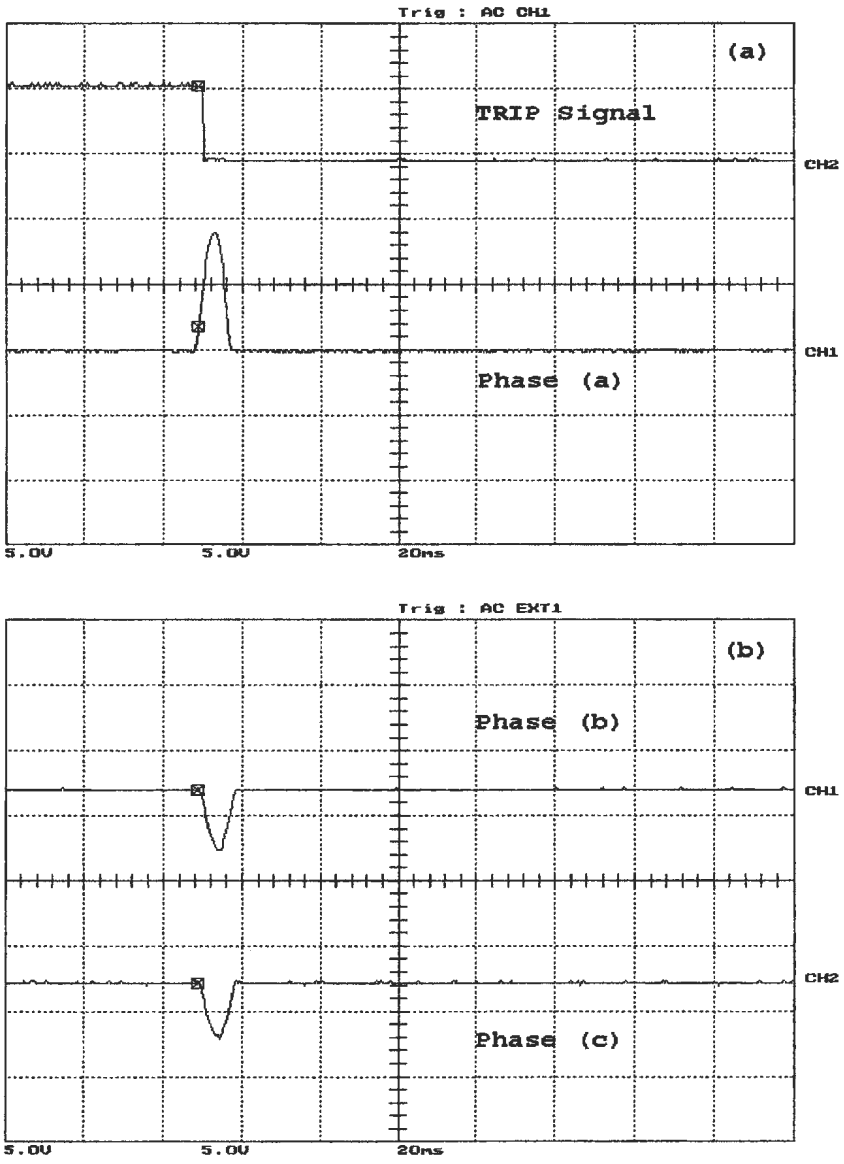

Figure B.8: Unloaded phase (a) to ground fault, occurred after energization on the primary side, (a) the WPT response and phase (a) differential current , (b) phase (b) and phase (c) differential currents. Y-scale is 1 Div. = 11.67 A

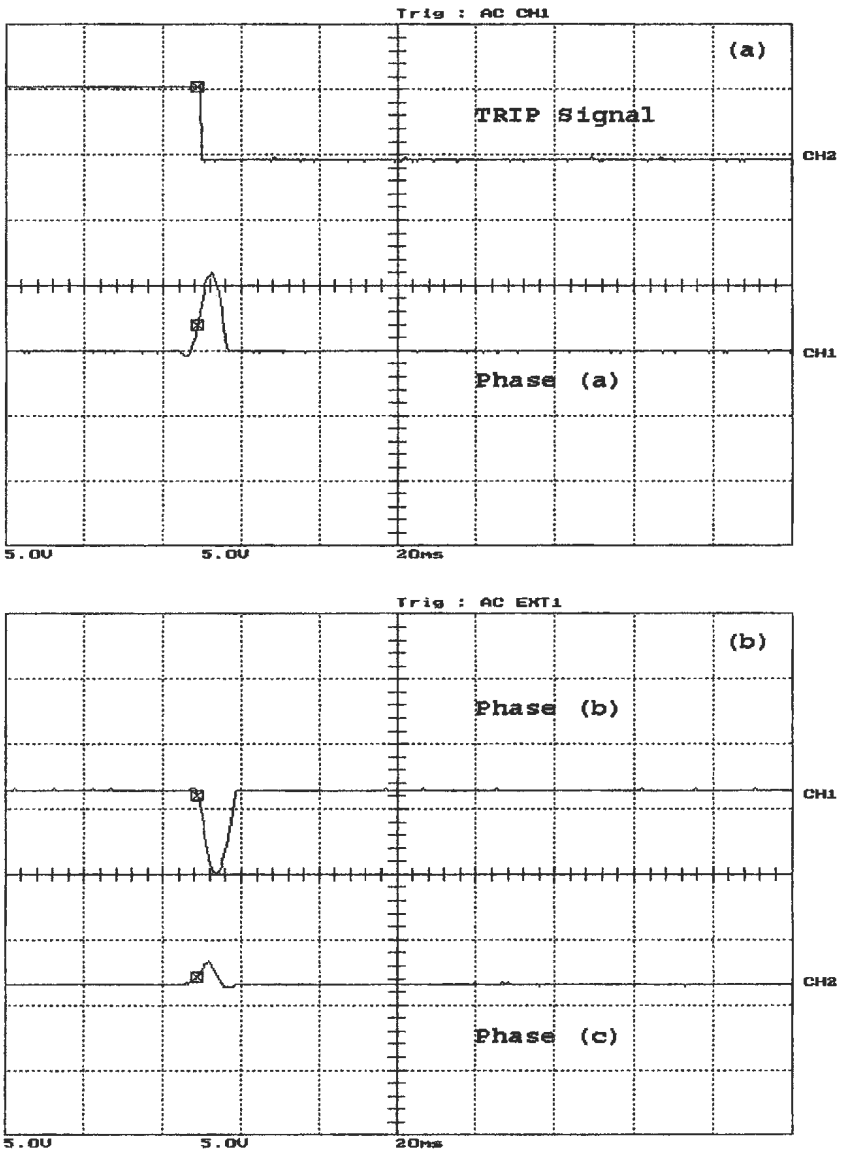

Figure B.9: Unloaded phase (a) to ground fault, occurred after energization on the secondary side, (a) the WPT response and phase (a) differential current , (b) phase (b) and phase (c) differential currents. Y-scale is 1 Div. = 11.67 A

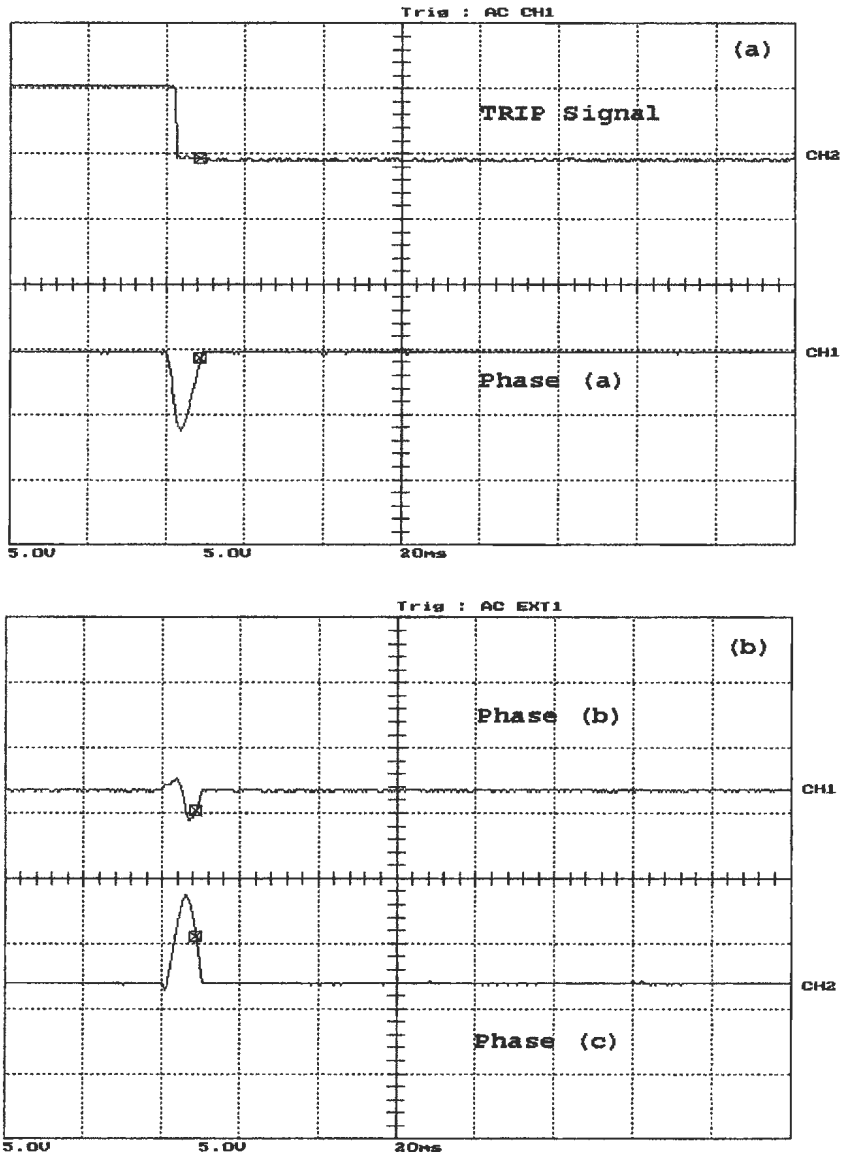

Figure B.10: Unloaded phase C to ground fault, occurred after energization on the primary side, (a) the WPT response and phase (a) differential current , (b) phase (b) and phase (c) differential currents. Y-scale is 1 Div. = 11.67 A

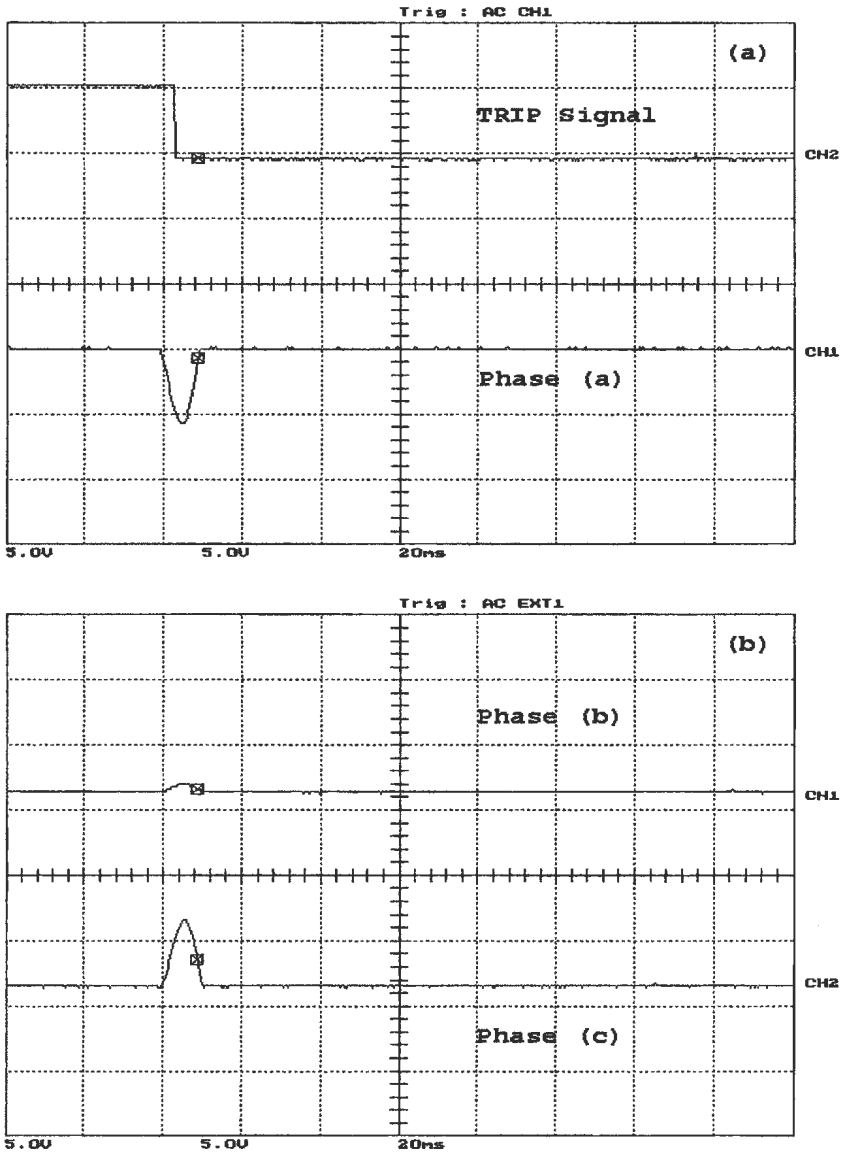

Figure B.11: Unloaded phase C to ground fault, occurred after energization on the secondary side, (a) the WPT response and phase (a) differential current , (b) phase (b) and phase (c) differential currents. Y-scale is 1 Div. = 11.67 A

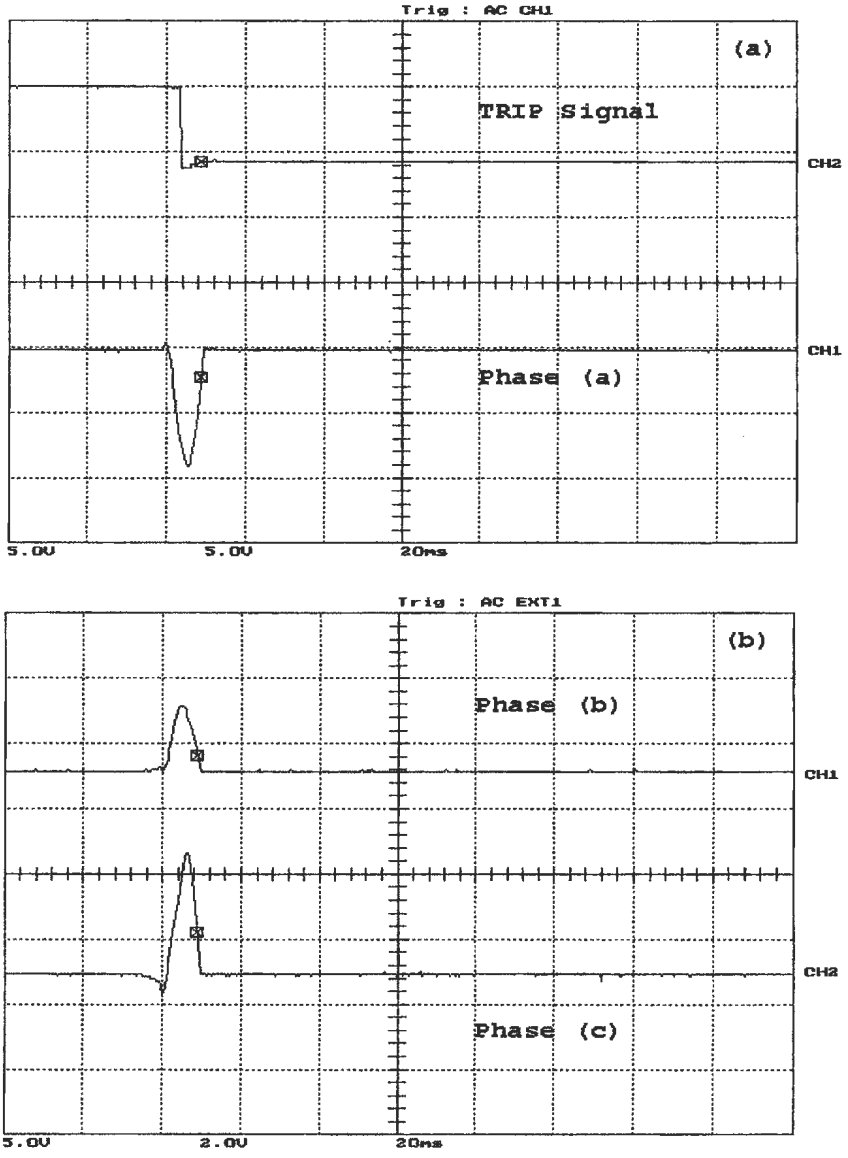

Figure B.12: Loaded phase (a) to ground fault, occurred before energization on the primary side, (a) the WPT response and phase (a) differential current , (b) phase (b) and phase (c) differential currents. Y-scale is 1 Div. = 11.67 A

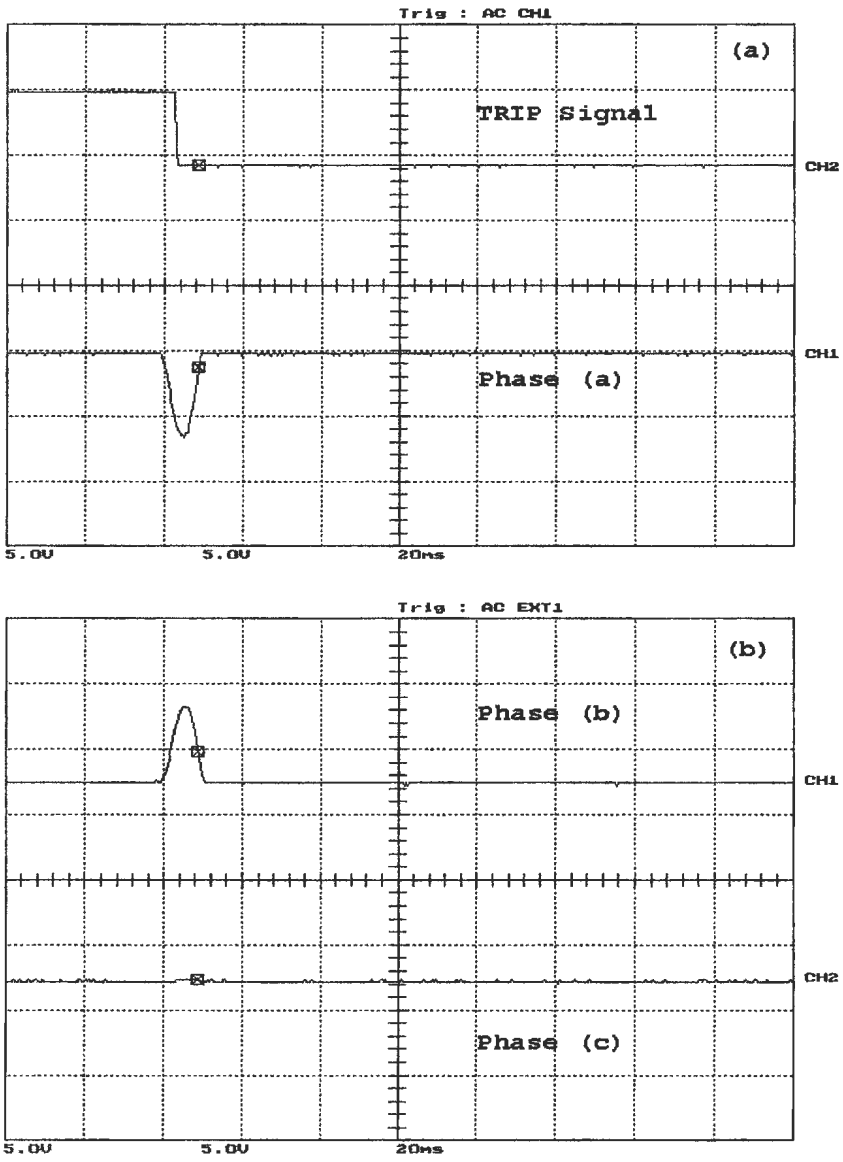

Figure B.13: Loaded phase (a) to ground fault, occurred before energization on the secondary side, (a) the WPT response and phase (a) differential current , (b) phase (b) and phase (c) differential currents. Y-scale is 1 Div. = 11.67 A

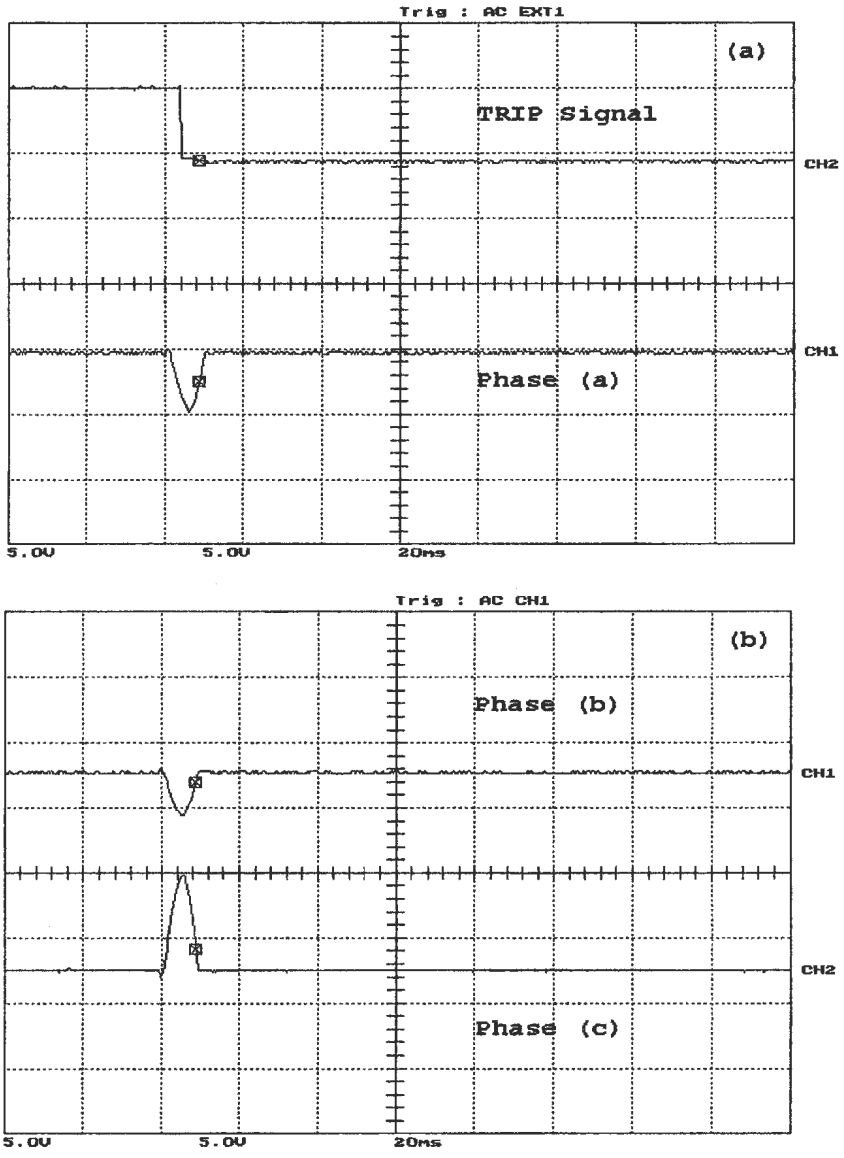

Figure B.14: Loaded phase C to ground fault, occurred before energization on the primary side, (a) the WPT response and phase (a) differential current , (b) phase (b) and phase (c) differential currents. Y-scale is 1 Div. = 11.67 A

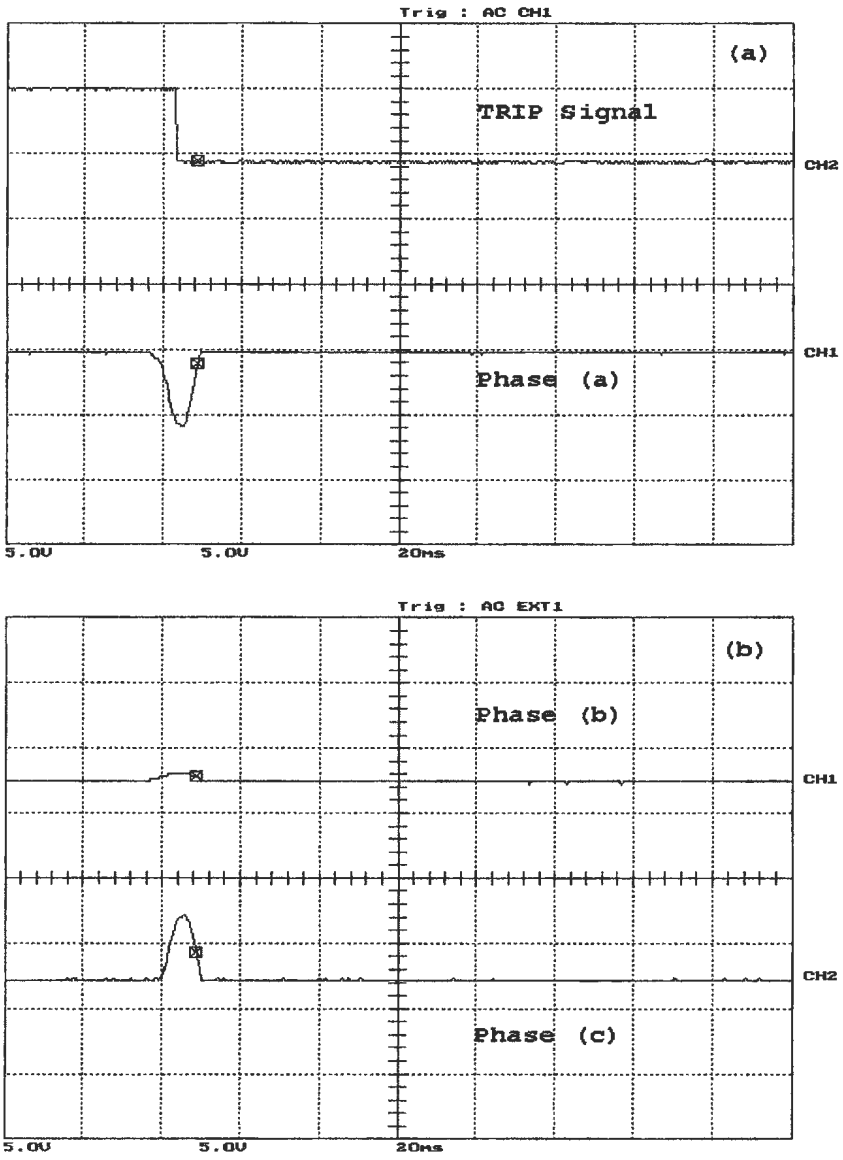

Figure B.15: Loaded phase C to ground fault, occurred before energization on the secondary side, (a) the WPT response and phase (a) differential current , (b) phase (b) and phase (c) differential currents. Y-scale is 1 Div. = 11.67 A

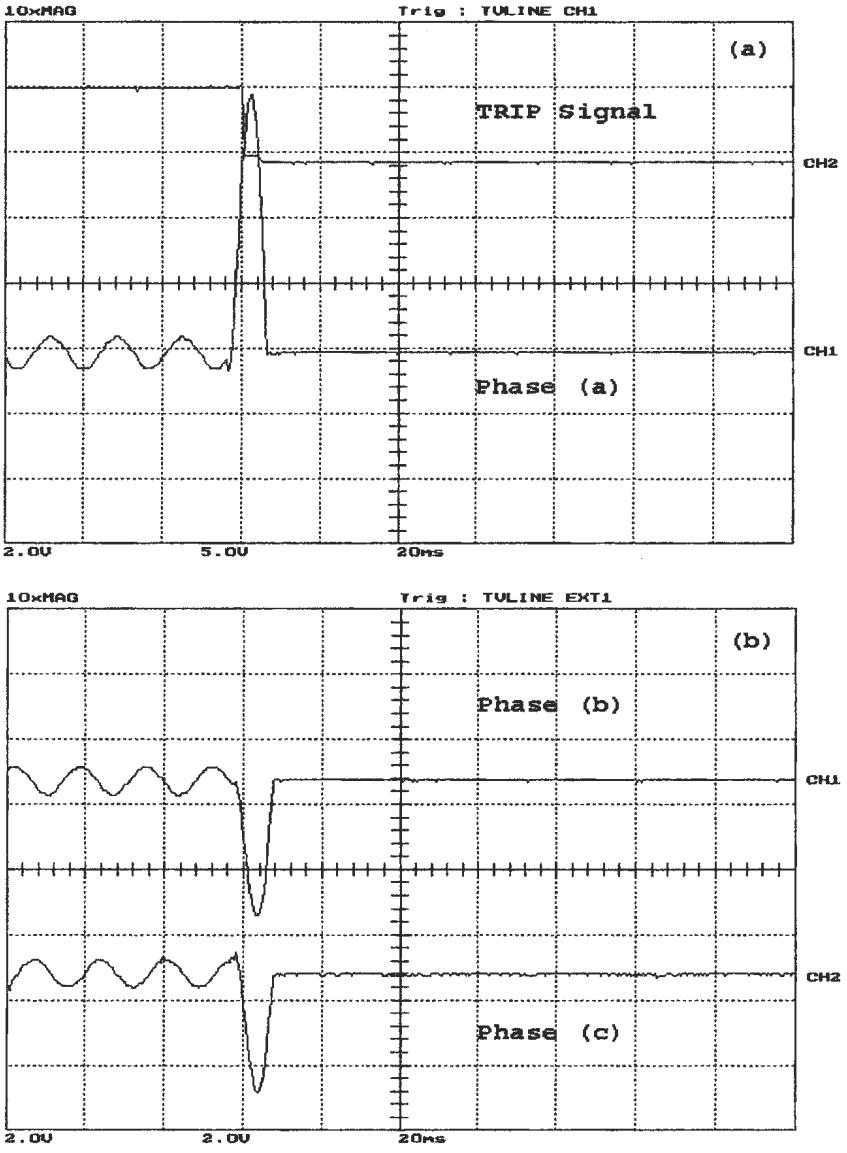

Figure B.16: Loaded phase (a) to ground fault, occurred after energization on the primary side, (a) the WPT response and phase (a) differential current , (b) phase (b) and phase (c) differential currents. Y-scale is 1 Div. = 11.67 A

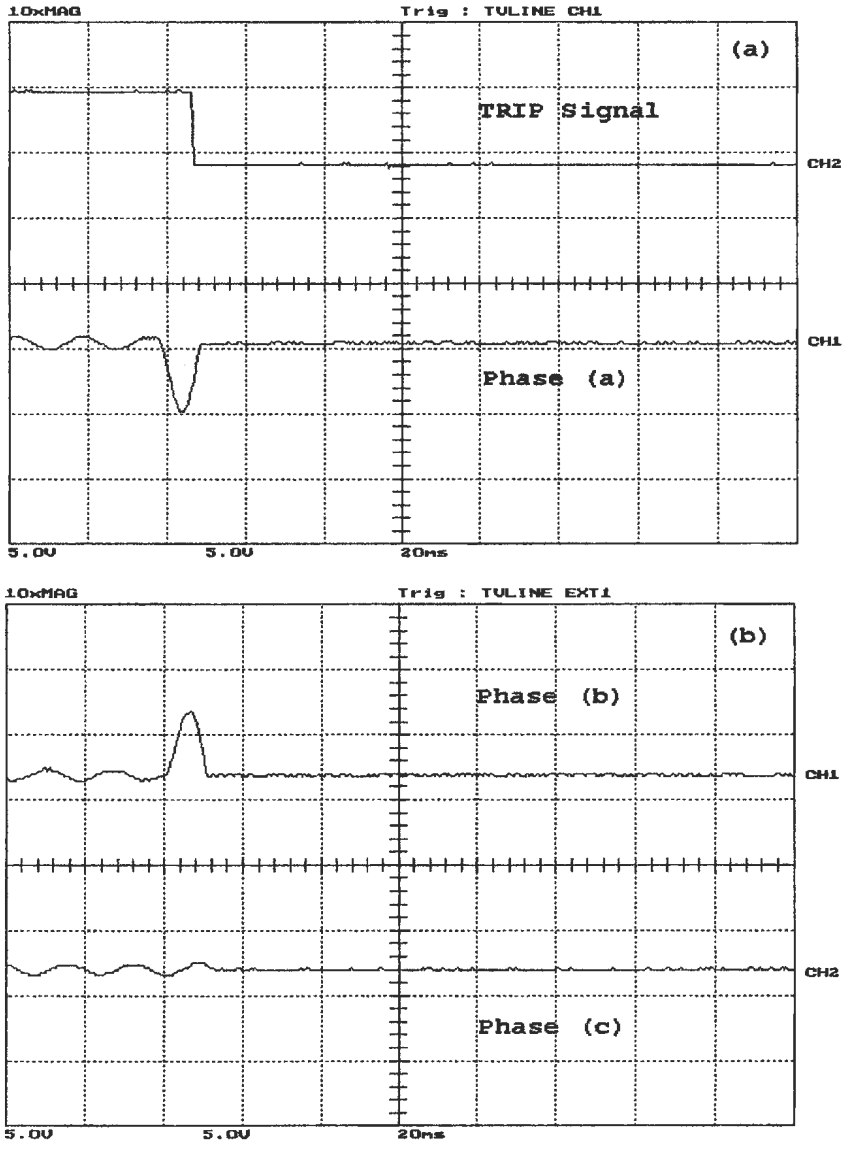

Figure B.17: Loaded phase (a) to ground fault, occurred after energization on the secondary side, (a) the WPT response and phase (a) differential current , (b) phase (b) and phase (c) differential currents. Y-scale is 1 Div. = 11.67 A

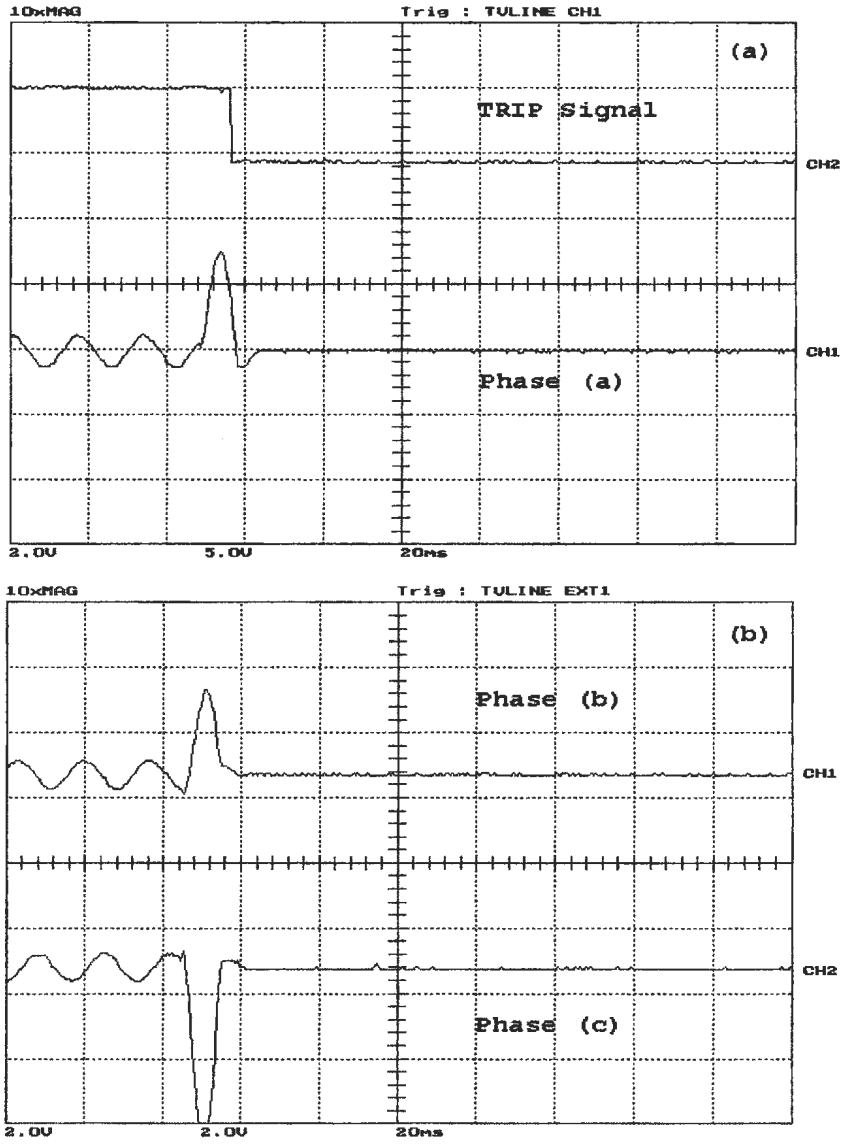

Figure B.18: Loaded phase C to ground fault, occurred after energization on the primary side, (a) the WPT response and phase (a) differential current , (b) phase (b) and phase (c) differential currents. Y-scale is 1 Div. = 11.67 A

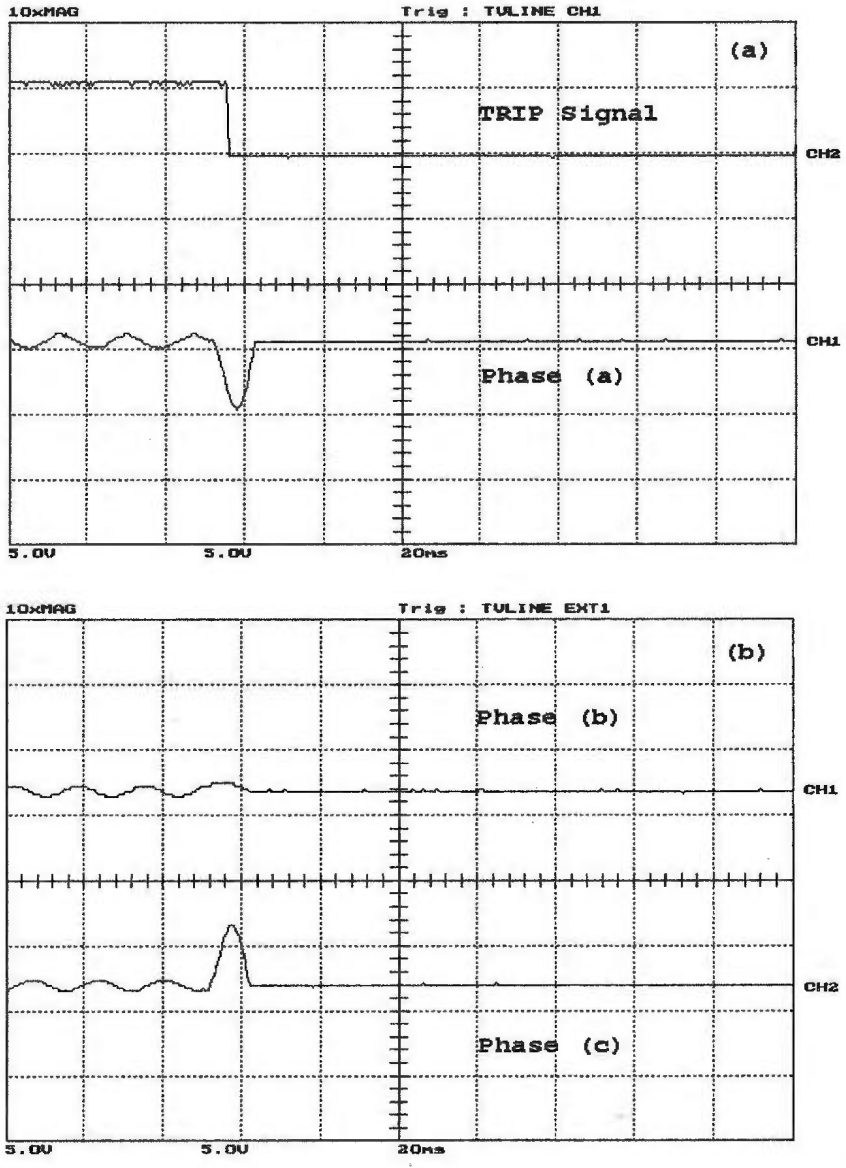

Figure B.19: Loaded phase C to ground fault, occurred after energization on the secondary side, (a) the WPT response and phase (a) differential current , (b) phase (b) and phase (c) differential currents. Y-scale is 1 Div. = 11.67 A

B.3 Phase to Phase Fault

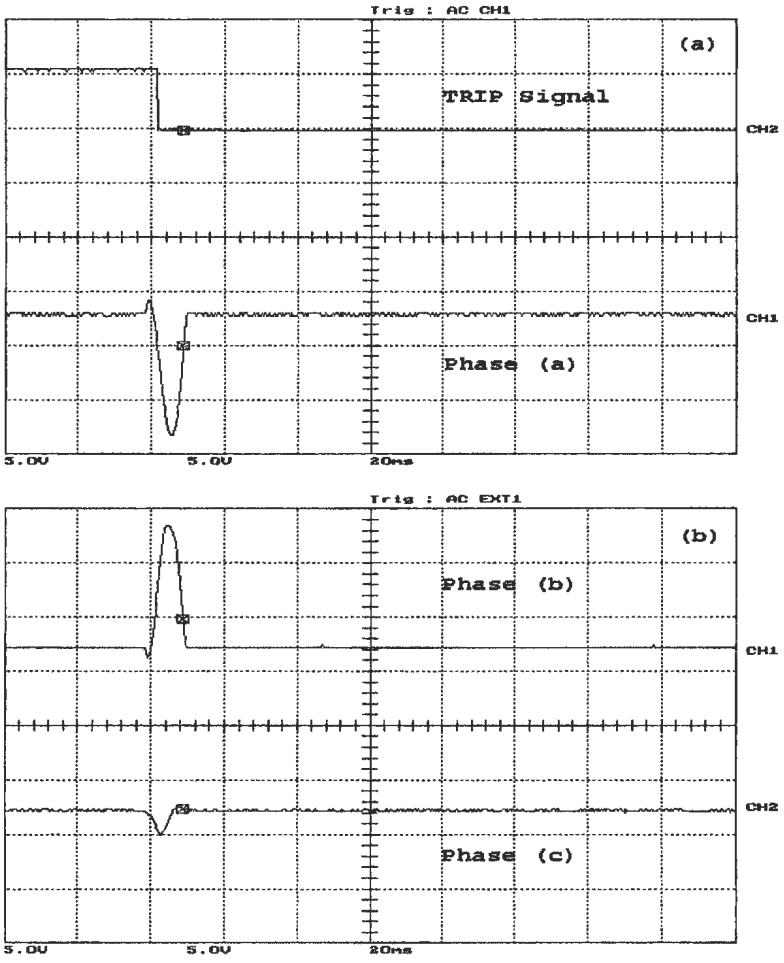

Figure B.20: Unloaded phase (a) to phase (b) fault, occurred before energization on the primary side, (a) the WPT response and phase (a) differential current , (b) phase (b) and phase (c) differential currents. Y-scale is 1 Div. = 11.67 A

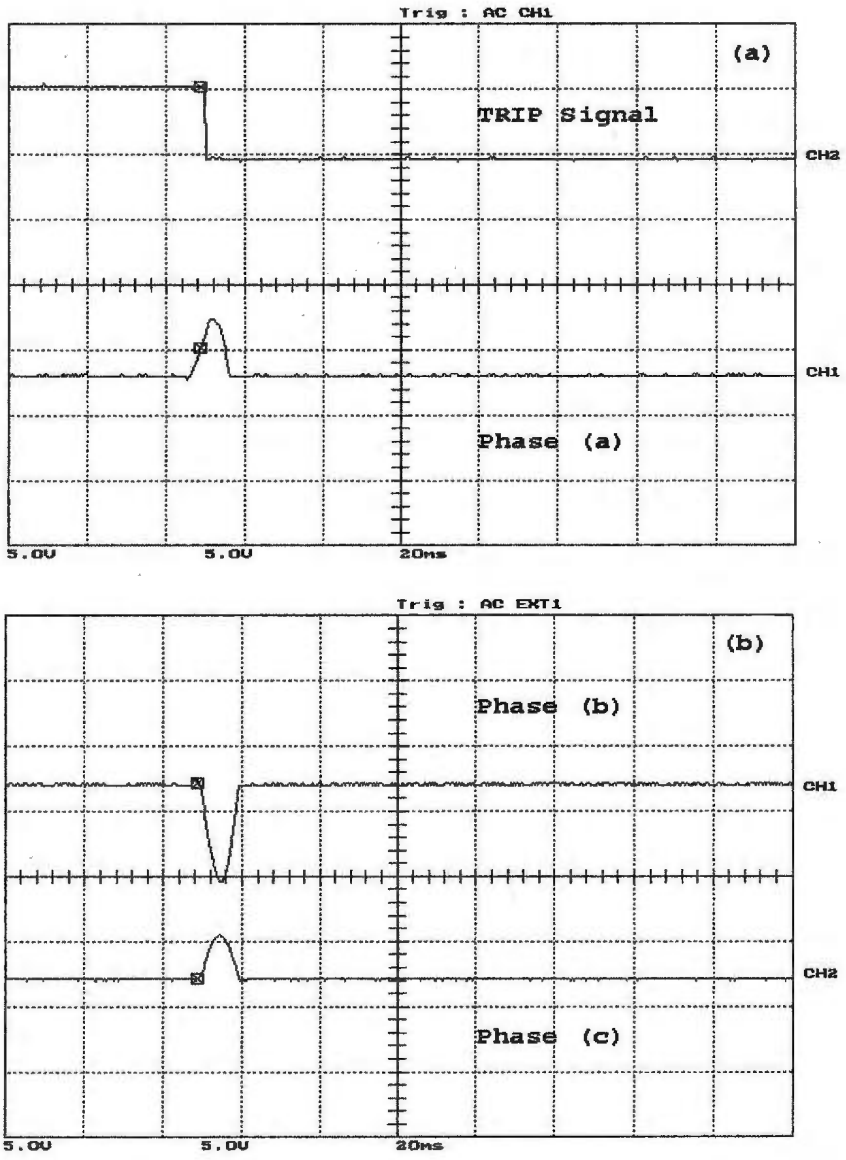

Figure B.21: Unloaded phase (a) to phase (b) fault, occurred before energization on the secondary side, (a) the WPT response and phase (a) differential current , (b) phase (b) and phase (c) differential currents. Y-scale is 1 Div. = 11.67 A

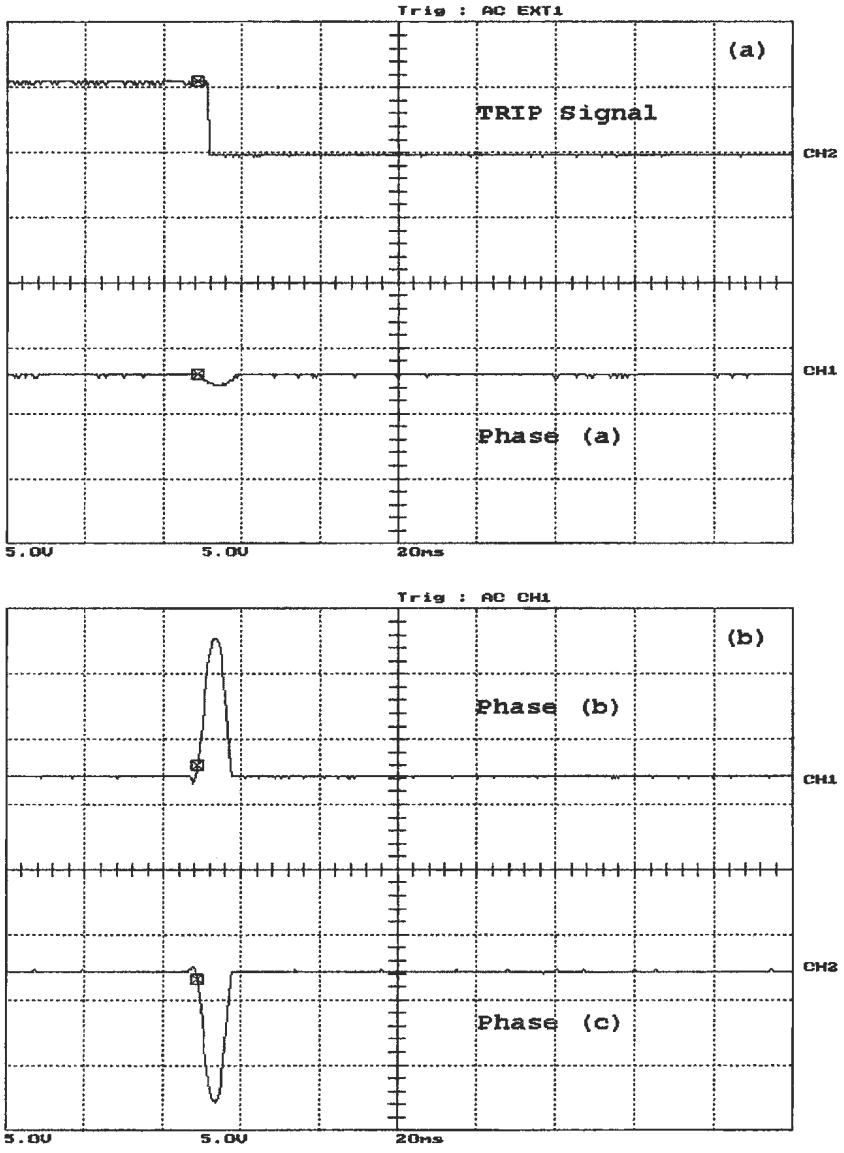

Figure B.22: Unloaded phase (b) to to phase C fault, occurred before energization on the primary side, (a) the WPT response and phase (a) differential current , (b) phase (b) and phase (c) differential currents. Y-scale is 1 Div. = 11.67 A

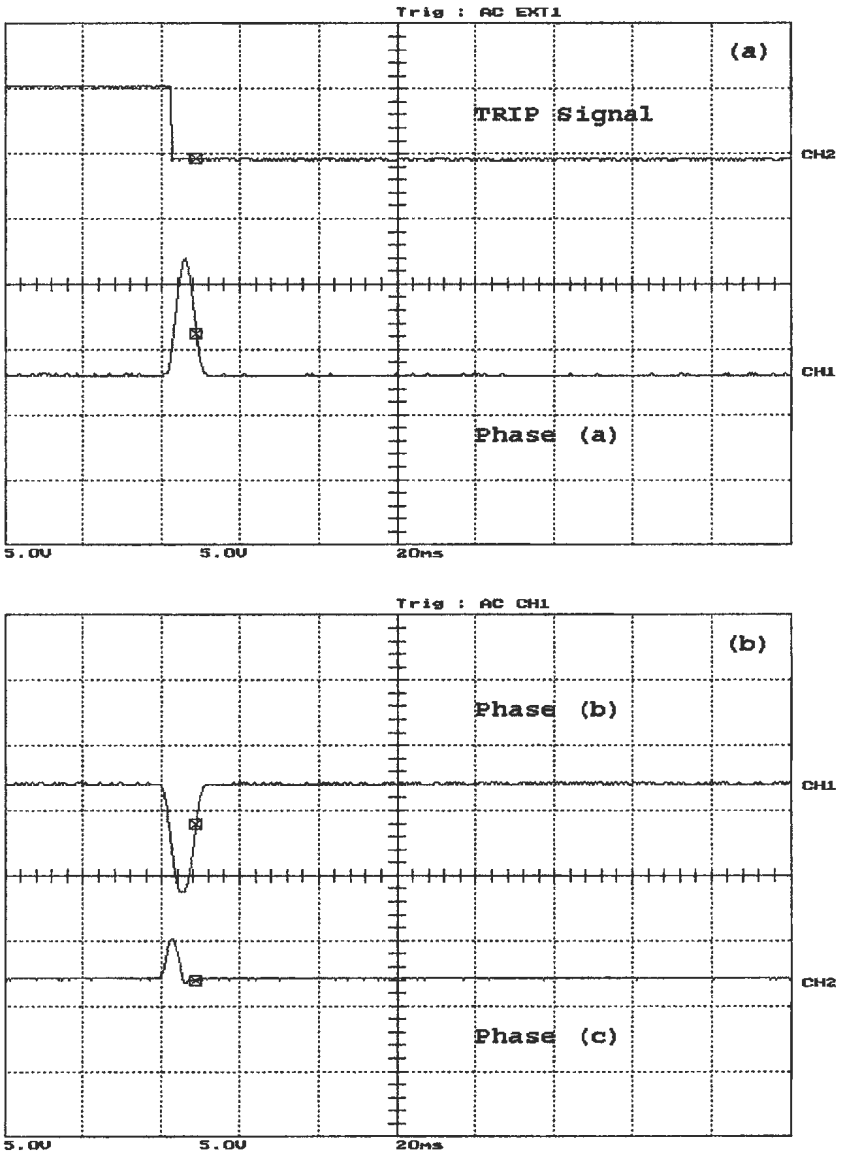

Figure B.23: Unloaded phase (b) to to phase C fault, occurred before energization on the secondary side, (a) the WPT response and phase (a) differential current , (b) phase (b) and phase (c) differential currents. Y-scale is 1 Div. = 11.67 A

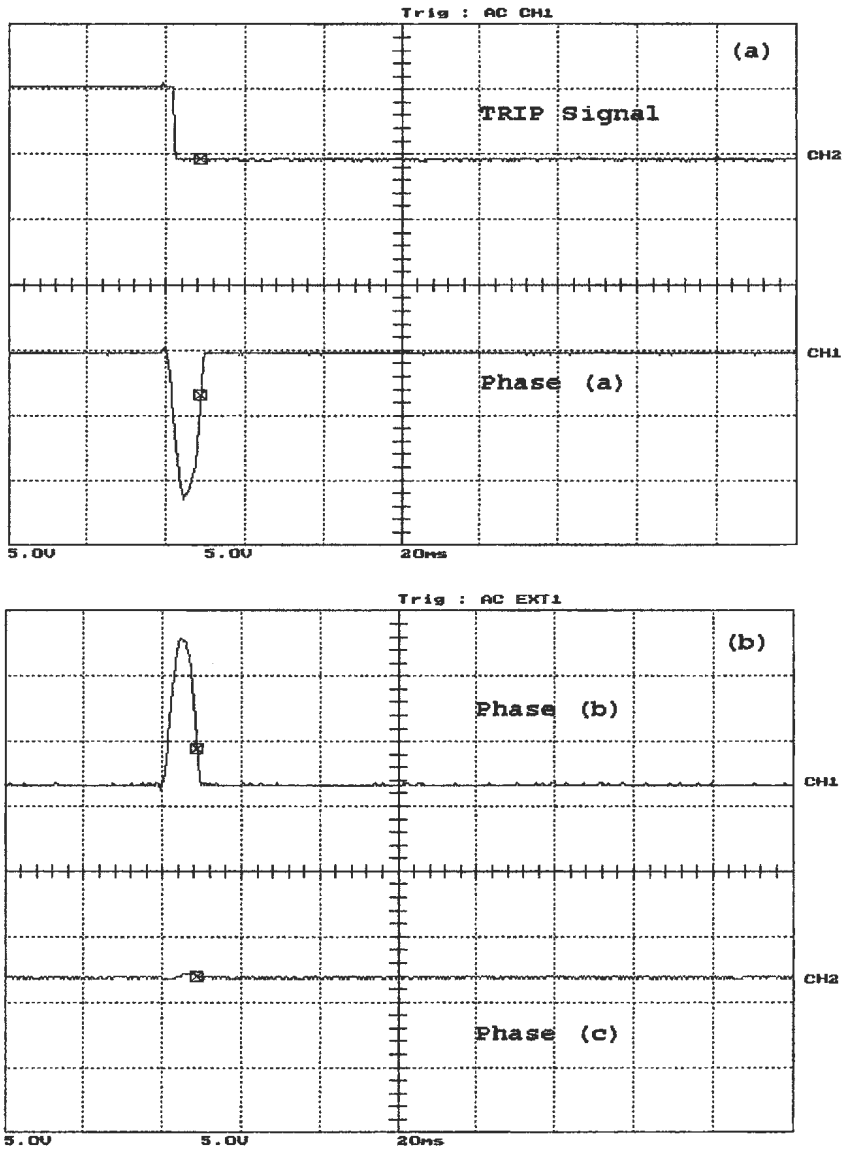

Figure B.24: Unloaded phase (a) to phase (b) fault, occurred after energization on the primary side, (a) the WPT response and phase (a) differential current , (b) phase (b) and phase (c) differential currents. Y-scale is 1 Div. = 11.67 A

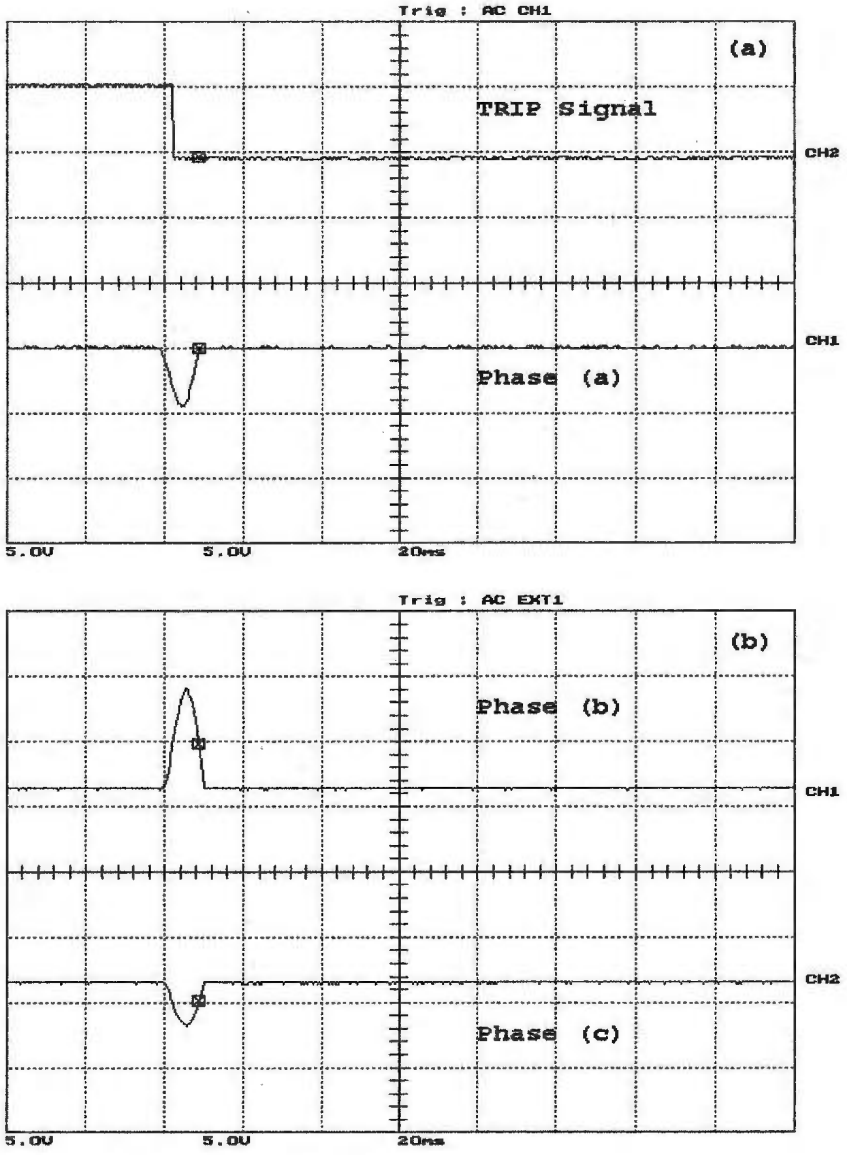

Figure B.25: Unloaded phase (a) to phase (b) fault, occurred after energization on the secondary side, (a) the WPT response and phase (a) differential current , (b) phase (b) and phase (c) differential currents. Y-scale is 1 Div. = 11.67 A

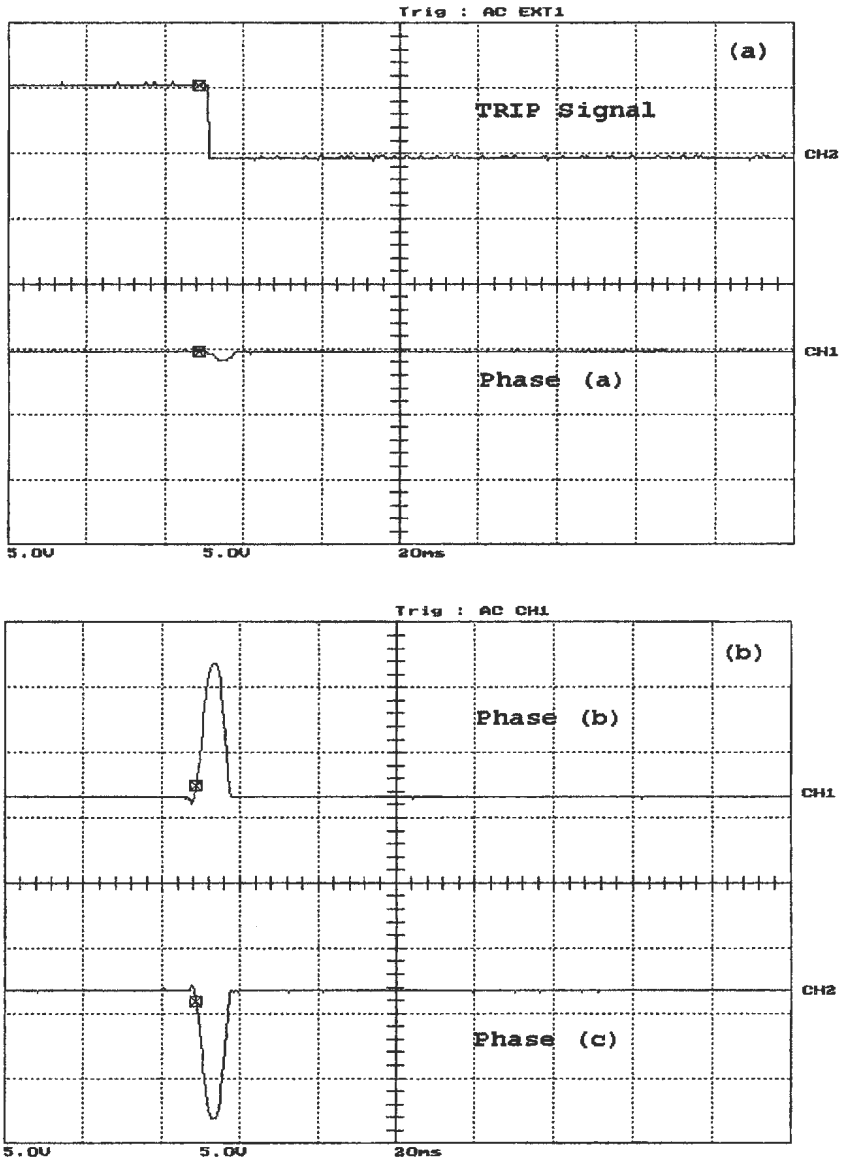

Figure B.26: Unloaded phase (b) to to phase C fault, occurred after energization on the primary side, (a) the WPT response and phase (a) differential current , (b) phase (b) and phase (c) differential currents. Y-scale is 1 Div. = 11.67 A

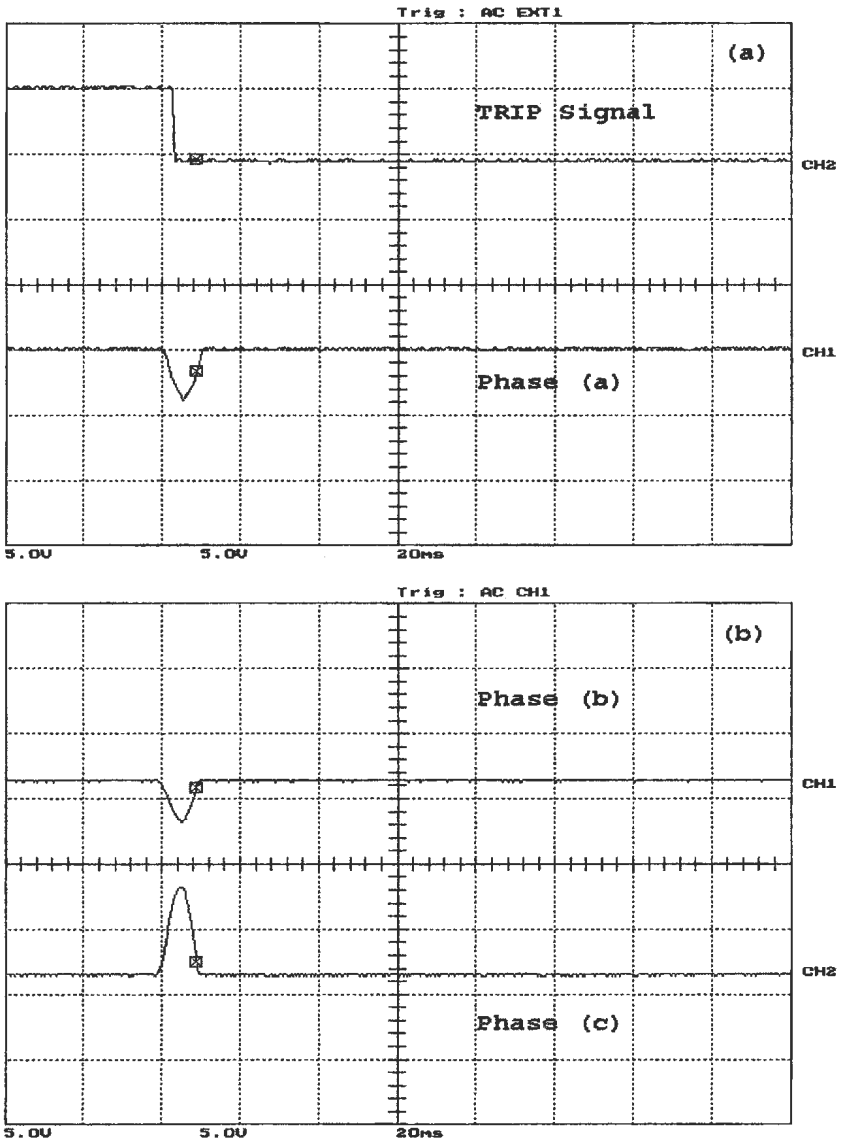

Figure B.27: Unloaded phase (b) to to phase C fault, occurred after energization on the secondary side, (a) the WPT response and phase (a) differential current , (b) phase (b) and phase (c) differential currents. Y-scale is 1 Div. = 11.67 A

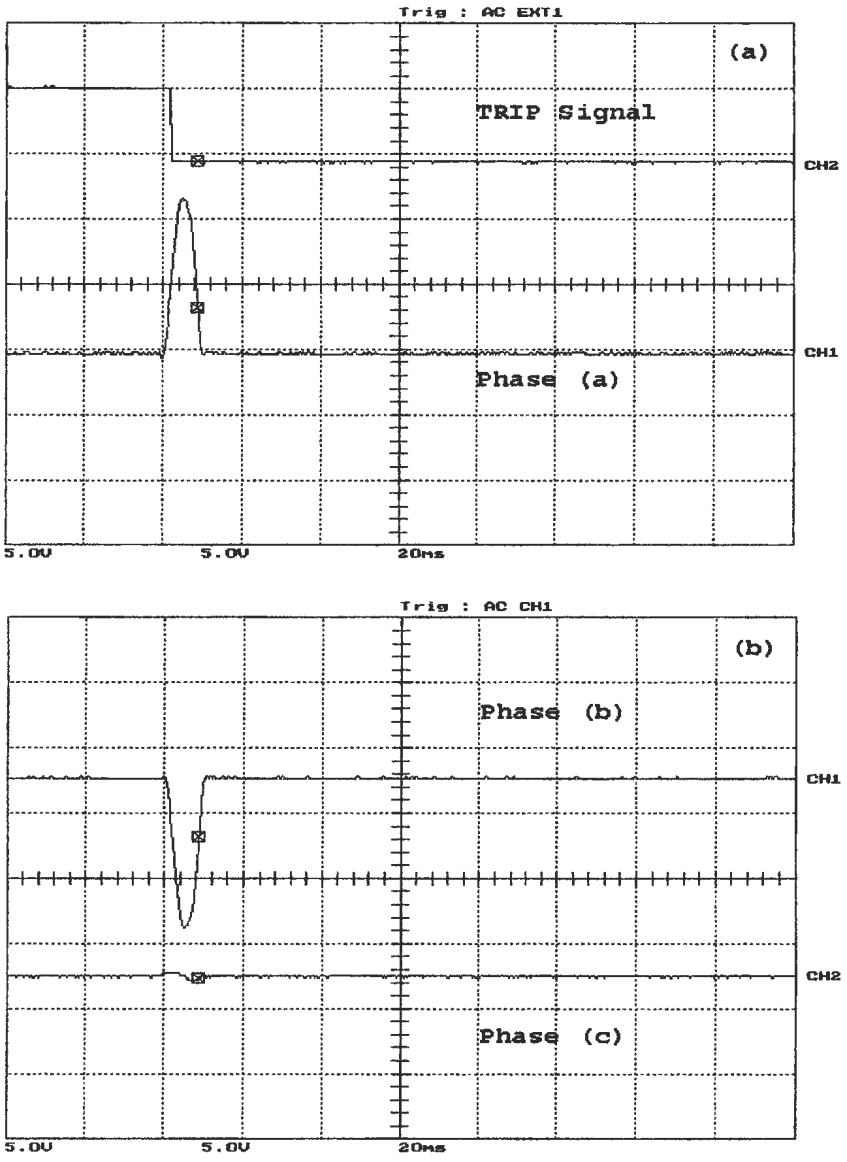

Figure B.28: Loaded phase (a) to phase (b) fault, occurred before energization on the primary side, (a) the WPT response and phase (a) differential current , (b) phase (b) and phase (c) differential currents. Y-scale is 1 Div. = 11.67 A

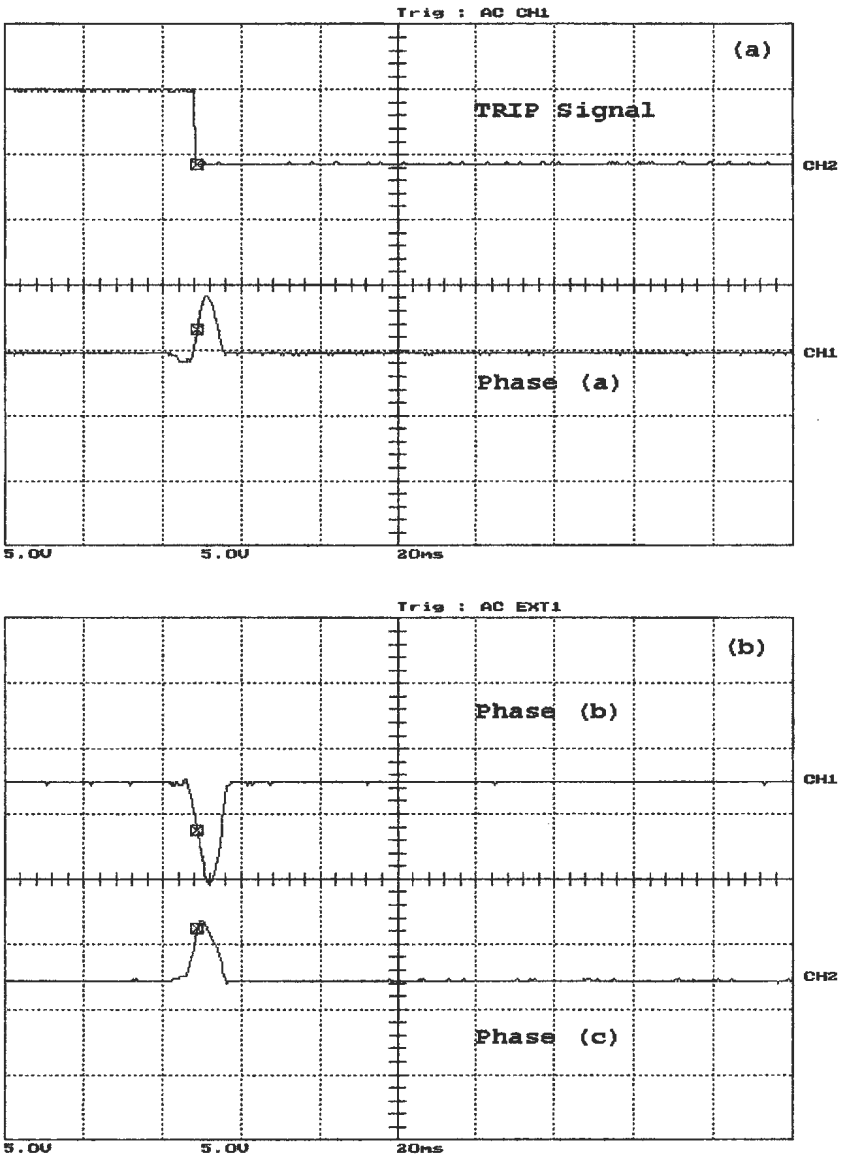

Figure B.29: Loaded phase (a) to phase (b) fault, occurred before energization on the secondary side, (a) the WPT response and phase (a) differential current , (b) phase (b) and phase (c) differential currents. Y-scale is 1 Div. = 11.67 A

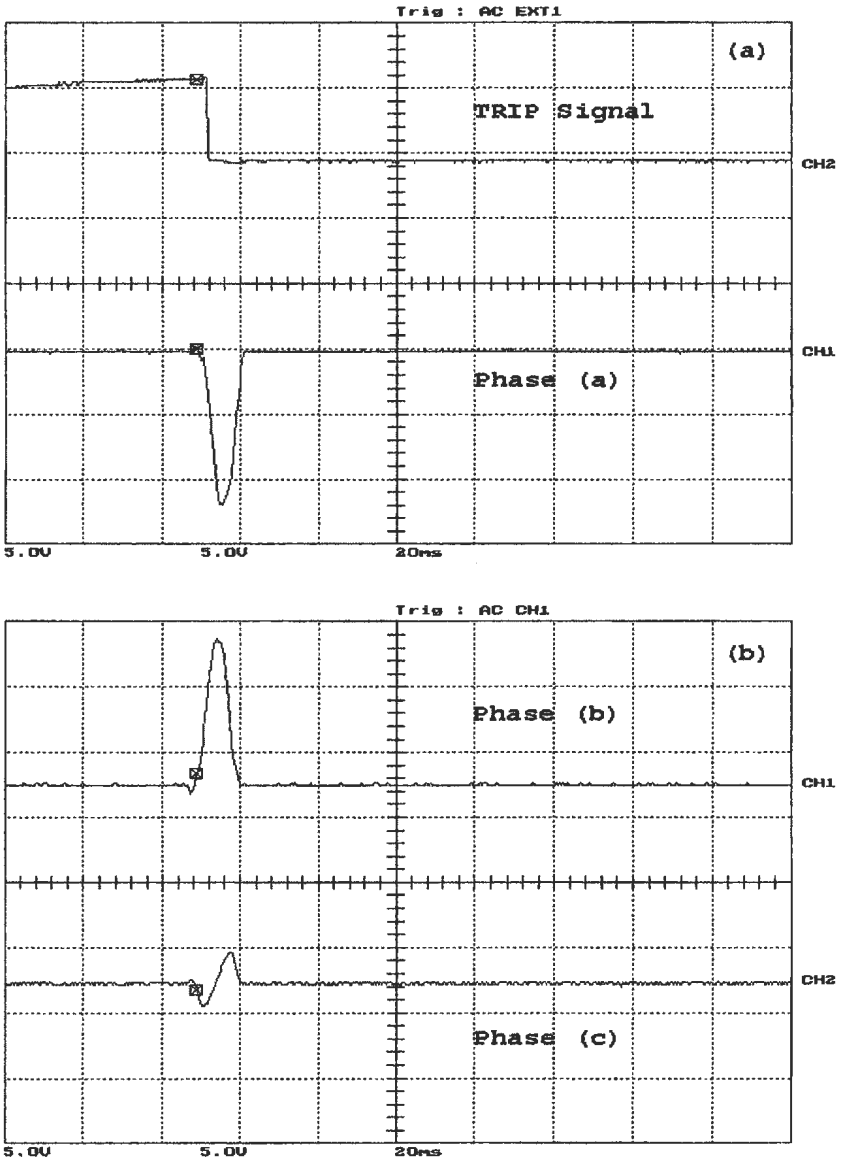

Figure B.30: Loaded phase (b) to to phase C fault, occurred before energization on the primary side, (a) the WPT response and phase (a) differential current , (b) phase (b) and phase (c) differential currents. Y-scale is 1 Div. = 11.67 A

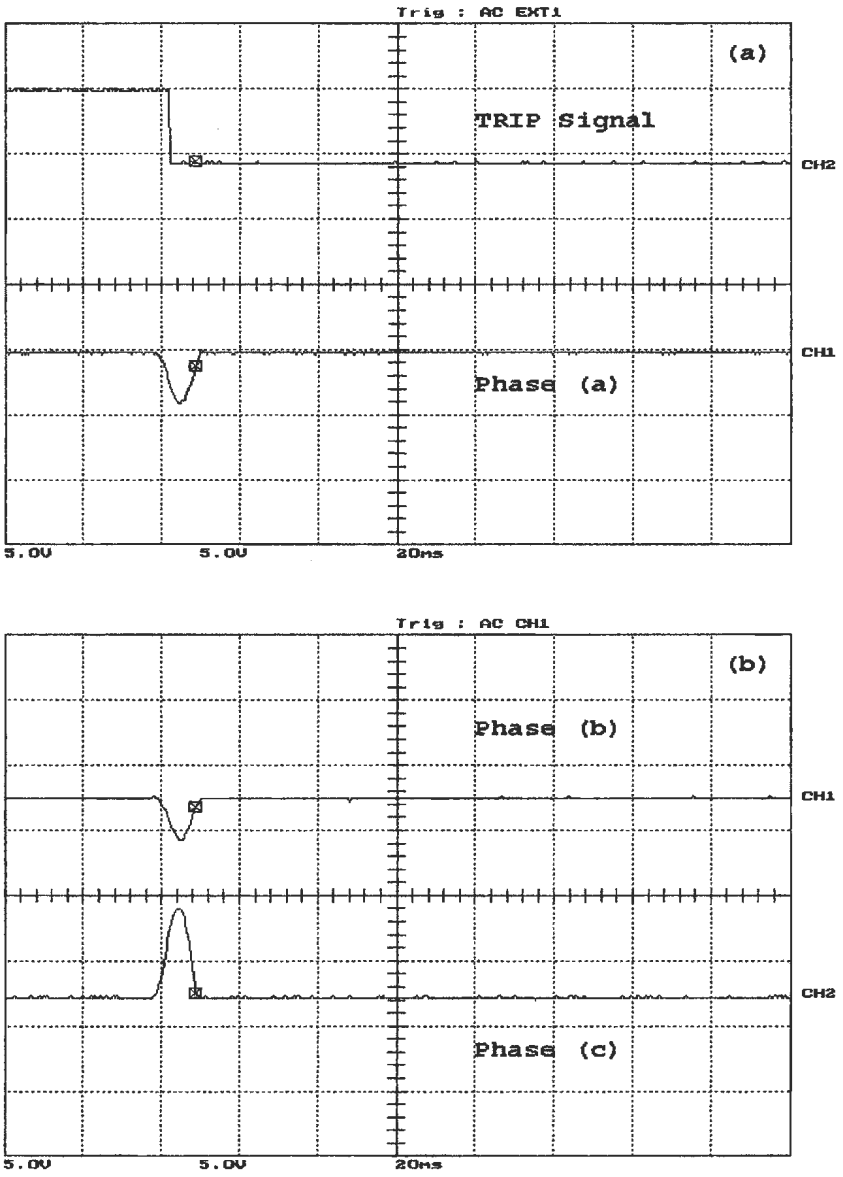

Figure B.31: Loaded phase (b) to to phase C fault, occurred before energization on the secondary side, (a) the WPT response and phase (a) differential current , (b) phase (b) and phase (c) differential currents. Y-scale is 1 Div. = 11.67 A

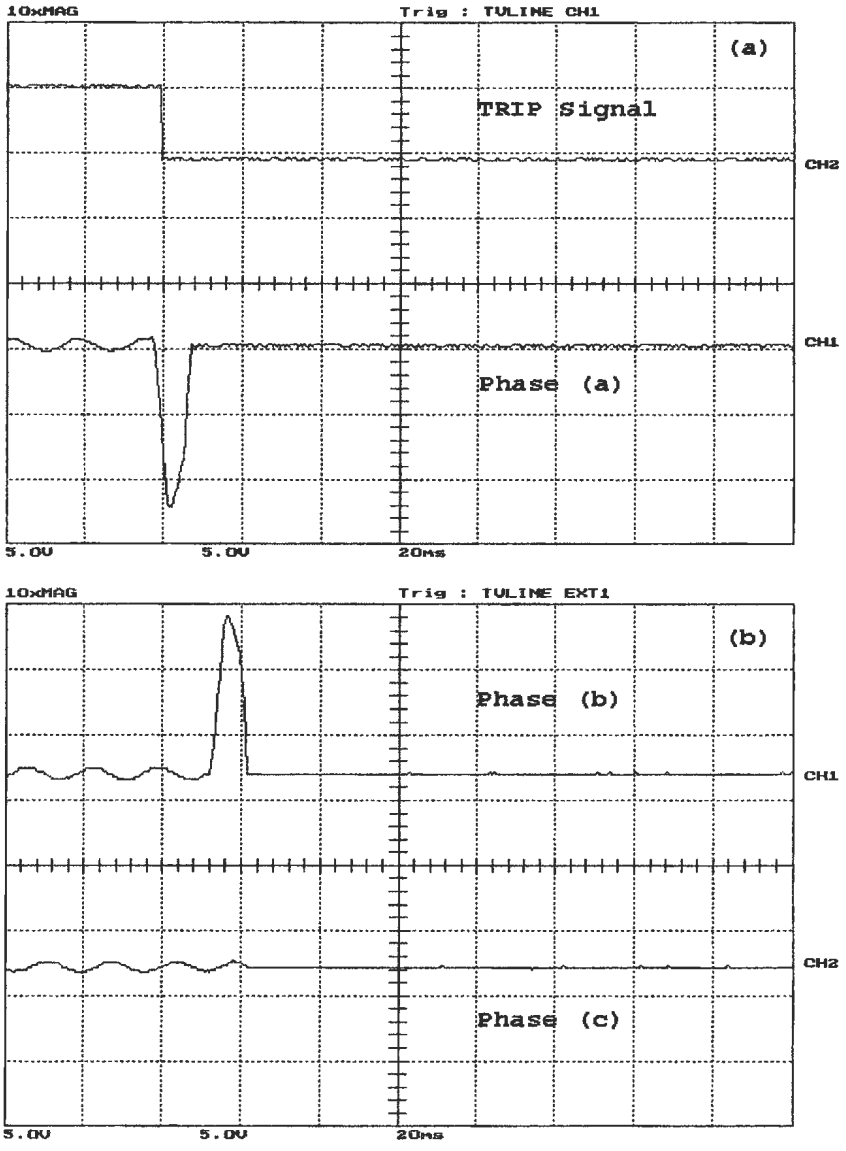

Figure B.32: Loaded phase (a) to phase (b) fault, occurred after energization on the primary side, (a) the WPT response and phase (a) differential current , (b) phase (b) and phase (c) differential currents. Y-scale is 1 Div. = 11.67 A

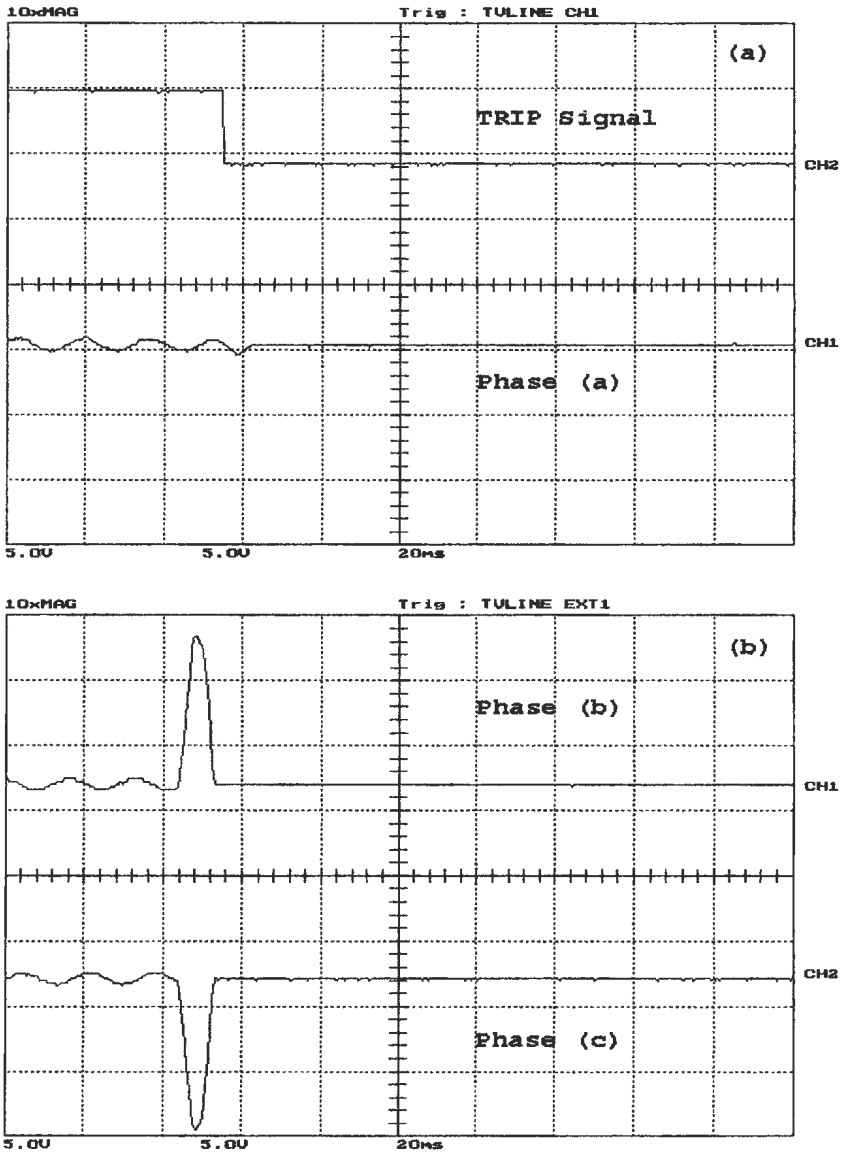

Figure B.33: Loaded phase (b) to to phase C fault, occurred after energization on the primary side, (a) the WPT response and phase (a) differential current , (b) phase (b) and phase (c) differential currents. Y-scale is 1 Div. = 11.67 A

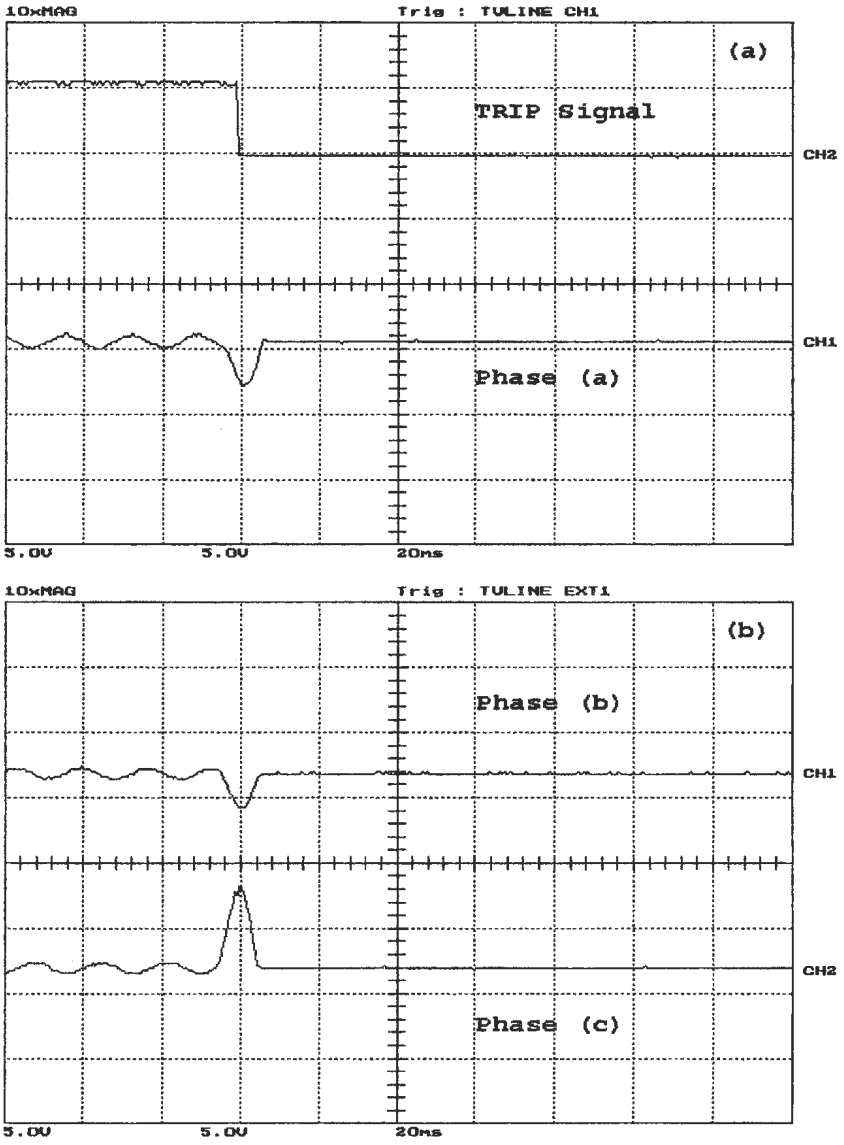

Figure B.34: Loaded phase (b) to to phase C fault, occurred after energization on the secondary side, (a) the WPT response and phase (a) differential current , (b) phase (b) and phase (c) differential currents. Y-scale is 1 Div. = 11.67 A

B.4 Three-Phase to Ground Fault

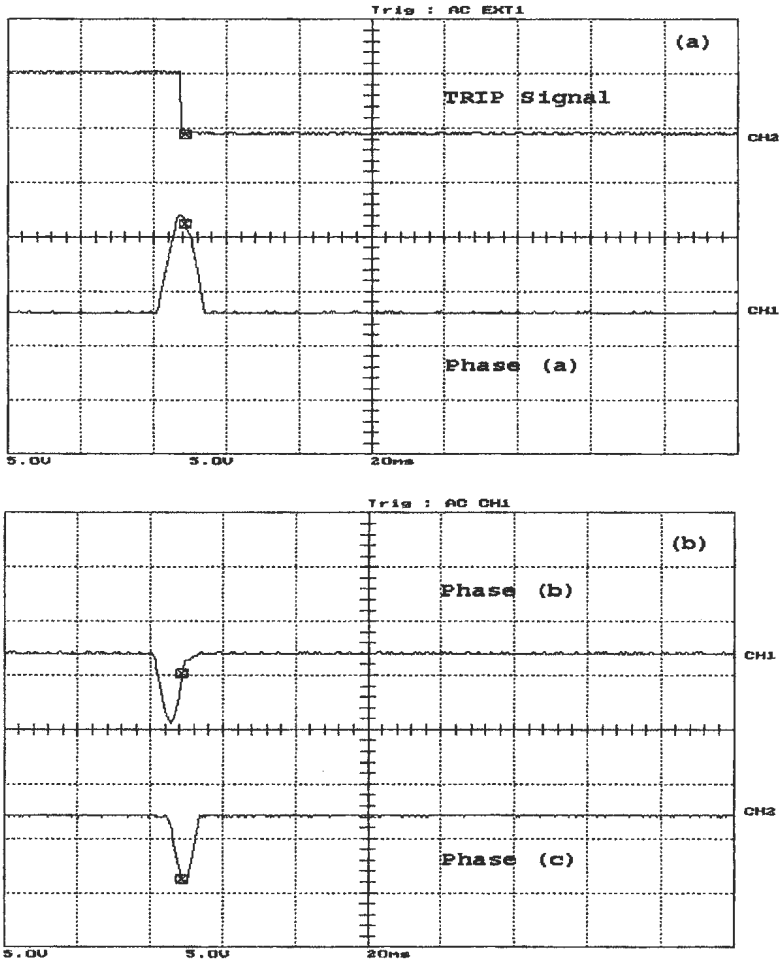

Figure B.35: Unloaded three-phase to ground fault, occurred before energization on the secondary side, (a) the WPT response and phase (a) differential current , (b) phase (b) and phase (c) differential currents. Y-scale is 1 Div. = 11.67 A

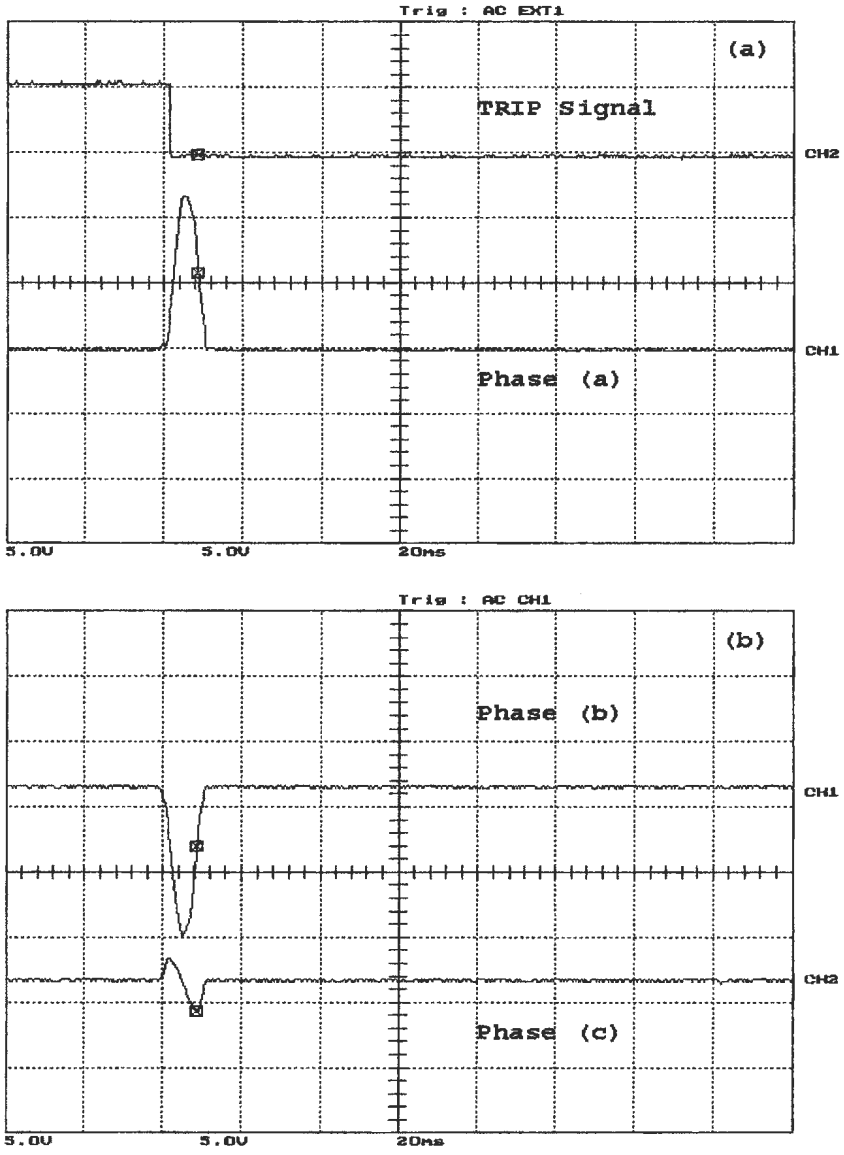

Figure B.36: Unloaded three-phase fault, occurred after energization on the primary side, (a) the WPT response and phase (a) differential current , (b) phase (b) and phase (c) differential currents. Y-scale is 1 Div. = 11.67 A

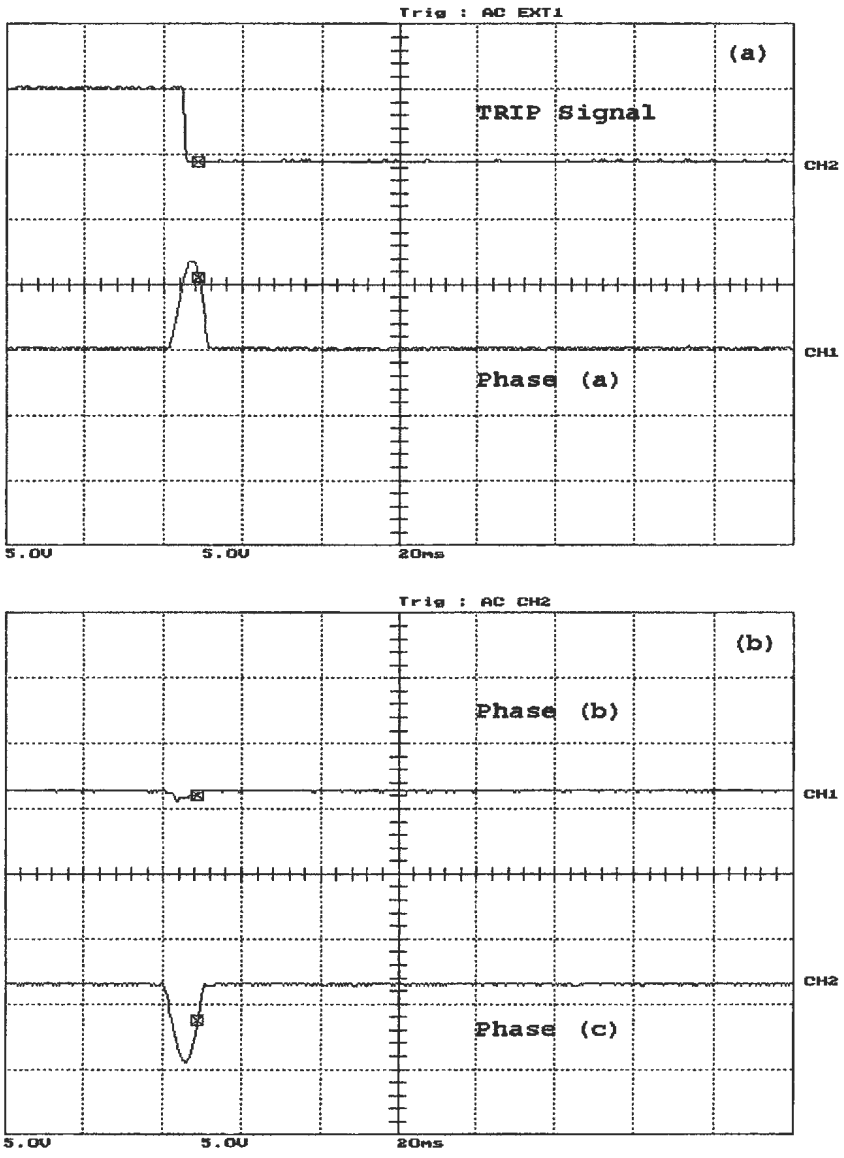

Figure B.37: Unloaded three-phase fault, occurred after energization on the secondary side, (a) the WPT response and phase (a) differential current , (b) phase (b) and phase (c) differential currents. Y-scale is 1 Div. = 11.67 A

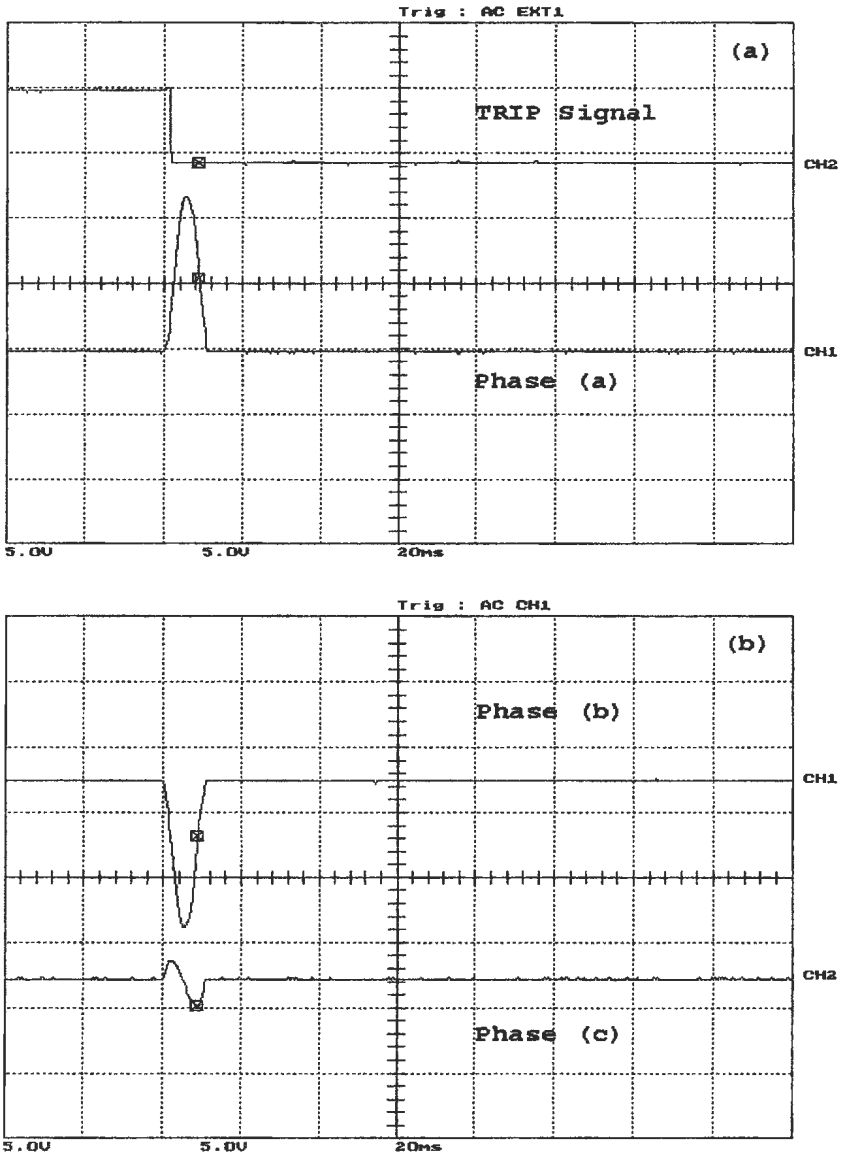

Figure B.38: Loaded three-phase fault, occurred before energization on the primary side, (a) the WPT response and phase (a) differential current , (b) phase (b) and phase (c) differential currents. Y-scale is 1 Div. = 11.67 A

Bibliography

[1] Applied Protective Relaying,Westinghouse Electric Co., Newark, N.J, 1976.

[2] Zaman, M. R., Artificial Neural Network Based Protection of Power Transformer. *Ph.D thesis*, Memorial University of Newfoundland, St. John's, NF, Canada, 1996.

[3] Rahman, M. A. and Gangopandhy, A., "Digital Simulation of Magnetizing Inrush Current in Three-Phase Transformers", *IEEE Trans. on Power Delivery*, Vol. PWRD-1, No. 4, 1986, pp. 232–242.

[4] Specht, T. R., "Transformer Inrush and Rectifier Transient Current", *IEEE Trans. on Power Apparatus and Systems*, Vol. PAS-88, No. 4,1969, pp. 269–276.

[5] Blume, L. F., Camilli, G., Farnham, S.B. and Peterson, H.A. , "Transformer Magnetizing Inrush Currents and Influence on System Operation", *AIEE Transaction*, Vol. 63, 1944, pp. 366–375.

[6] Finzi, L. A. and Mutschler, W. H., "The Inrush Magnetizing Current in Single-Phase Transformers", *AIEE Transaction*, Vol. 70, 1951, pp. 1436–1438.

[7] Sonnemann, W. K. , Wanger, C. L. and Rockfeller, G. D., "Magnetizing Inrush Phenomenon in Transformer Banks", *AIEE Transaction*, Vol. 77, 1958, pp. 884–892.

[8] Vaessen, P.M. and Hanique, E., "A New Frequency Response Analysis Method for Power Transformer", *IEEE Trans. on Power Delivery*, Vol. 7, No. 1, 1992, pp. 384–391.

[9] Leon, F. and Semylen, A., "Efficient Calculation of Electromagnetic Parameters of Transformer", *IEEE Trans. on Power Delivery*, Vol. 7, 1992, No. 1, pp. 376–383.

[10] Leon, F. and Semylen, A., "Complete Transformer Model for Electromagnetic Transients", *IEEE Trans. on Power Delivery*, Vol. 7, No. 1, 1992, pp. 361–369.

[11] Leon, F. and Semylen, A., "Reduced Order Model of Transformer Transients", *IEEE Trans. on Power Delivery*, Vol. 9, No. 1, 1994, pp. 231–239.

[12] Saleh, S. A. and Rahman, M. A., "Transient Model for Power Transformer Using Wavelet-Filter-Bank", in *LESCOPE02 Proceedings*, Halifax, NS, Canada, 2002, pp. 47–54.

[13] Kennedy, L. F. and Hayward, C. D., "Harmonic−Current Restrained Relays for Differential Protection", *AIEE Transaction*, Vol. 57, 1938, pp. 262–271.

[14] Mathews, C. A., "Improved Transformer Differential Relay", *AIEE Transaction*, Vol. 73, 1954, pp. 645–649.

[15] Sharp,R. L. and Glassburn, W. E., "A Transformer Differential Relay with Second Harmonic Restraint", *AIEE Transaction*, Vol. 77, 1958, pp. 913–918.

[16] Einval, C. H. and Linders, J. R., "A Three-Phase Differential Relay for Power Transformer Protection", *IEEE Trans. on Power Apparatus and Systems*, Vol. PAS-94, No. 6, 1975, pp. 1971–1980.

[17] Rockfeller, G. D., "Fault Protection with a Digital Computer", *IEEE Trans. on Power Apparatus and Systems*, Vol. PAS-88, No. 4, 1969, pp. 438–461.

[18] Mann, B. J. and Morrison, I. F., "Digital Calculation of Impedance for Transmission Line Protection", *IEEE Trans. on Power Apparatus and Systems*, Vol. PAS-90, No. 1, 1971, pp. 270–279.

[19] Mann, B. J. and Morrison, I. F., "Relaying a Three-Phase Transmission Line with a Digital Computer", *IEEE Trans. on Power Apparatus and Systems*, Vol. PAS-90, No. 2, 1971, pp. 742–750.

[20] Zaman, M. R., Houque, M. A. and Rahman, M. A., "On-Line Implementation of the Artificial Neural Network Based Protection for Power Transformers", in *NECEC'96 Proceedings*, St. John's, NF, Canada, 1996, pp. 5–11.

[21] Sykes, J. A. and Morrison, I. F., "A Proposed Method for Harmonic restraint Differential Protection Relay for Power Transformers", *IEEE Trans. on Power Apparatus and Systems*, Vol. PAS-91, No. 3, 1972, pp. 1266–1272.

[22] Malik, O. P., Dask, P. K. and Hope, G. S., "Digital protection of power transformer", in *IEEE Power Engineering Society Winter Meeting*, Paper A 76 191-7, New York, 1976.

[23] Scheweitzer, E. O., Larson, R. R. and Flechisg, A. J., "An efficient inrush current-detection algorithm for digital computer relay protection of transformers", in *IEEE Power Engineering Society Summer Meeting*, Paper A 77 510-1, Mexico City, Mexico, 1977.

[24] Scheweitzer, E. O., Larson, R. R. and Flechisg, A. J., "The Design and Test of a Digital Relay for Transformer Protection", *IEEE Trans. on Power Apparatus and Systems*, Vol. PAS-98, No. 3, 1979, pp. 795–804.

[25] Ramamoorty, M., "Applications of Digital Computers to Power System Protection", *Journal of Institute of Engineering (India)*, Vol. 52, No. 10, 1972, pp. 235–238.

[26] Throp, J. S. and Phadke, A. G., "A Microprocessor Based Three-Phase Transformer Differential Relay", *IEEE Trans. on Power Apparatus and Systems*, Vol. PAS-101, No. 2, 1982, pp. 426–432.

[27] Rahman, M. A. and Dash, P. K., "Fast Algorithm for Digital Protection of Power Transformer", *IEE Proceedings.*, Vol. 129, Part C, No. 2, 1982, pp. 79–85.

[28] Horton, J. H., "Walsh function for digital impedance relay for power lines", in *IEEE Power Engineering Society Summer Meeting*, San Fransisco, CA, pp. 530–541, 1975.

[29] Jayasurya, B. and Rahman, M. A., "Applications Of Walsh Functions for Microprocessor-Based Transformer Protection", *IEEE Trans. on Electromagnetic Compatibility*, Vol. EMC-27, No. 4, 1985, pp. 221–225.

[30] Fakruddin, D. B., Parthasarathy, K., Jenkins, L. and Hogg, B. W., "Applications of Haar Functions for Transmission Line and Transformer Differential Protection", *Electrical Power and Energy Systems*, Vol. 6, No. 3, 1984, pp. 169–180.

[31] Murty, Y. V. V. S. and Somlinski, W. J., "Design and Implementation of Digital Differential Relay for 3-Phase Power Transformer Based on Kalman Filtering Theory", *IEEE Trans. on Power Delivery*, Vol. 3, No. 2, 1988, pp. 525–533.

[32] Murty, Y. V. V. S. and Somlinski, W. J., "A Kalman Filter Based Digital Percentage Differential and Ground Fault Relay for 3-Phase Power Transformer", *IEEE Trans. on Power Delivery*, Vol. 5, No. 3, 1990, pp. 1299–1308.

[33] Degens, A. J., "Algorithm for a Digital Transformer Differential Protection Based on a Least-Square-Curve-Fitting", *IEE Proceedings*, Vol. 128, Part C, 1981, pp. 155–161.

[34] Degens, A. J., "Microprocessor-Implemented Digital Filters for Inrush Current Detection", *Electrical Power and Energy Systems*, Vol. 4, No. 3, 1982, pp. 196–205.

[35] Rahman, M. A., Dash, P. K. and Downton, E. R., "Digital Protection of Power Transformer Based on Weighted Least Square Algorithm", *IEEE Trans. on Power Apparatus and Systems*, Vol. PAS-101, No. 11, 1982, pp. 4204–4210.

[36] Sachdev, M. S. and Sidhu, T. S., "A Least Squares Technique and Differential Protection of Three-Phase Transformers", *Transaction of The Engineering and Operating Division of Canadian Electrical Association, Power System Planning and Operation Section*, Vol. 90-sp-158, 1990.

[37] Lihua, H., Yilin, Y., Rahman, M. A., Chan, D. T. W. and Ong, P. K. S., "A Novel Algorithm for Digital Protection of Power Transformers", *Transaction of The Engineering and Operating Division of Canadian Electrical Association Power System Planning and Operation Section*, Vol. 92-sp-165, 1992.

[38] Hermanto, I., Murty, Y. V. V. S. and Rahman, M. A., "A Stand Alone Digital Protective Relay for Power Transformers", *IEEE Trans. on Power Delivery*, Vol. 6, No. 1, 1991, pp. 85–95.

[39] Habib, M. and Martin, M. A., "A Comparative Analysis of Digital Relaying Algorithms for Differential Protection of Three-Phase Power Transformer", *IEEE Trans. on Power Systems*, Vol. 3, No. 3, 1988, pp. 1378–1384.

[40] Rahman, M. A. and Jayasurya, B., "A State of-Art Review of Transformer Protection Algorithms", *IEEE Trans. on Power Power Delivery*, Vol. 3, No. 2, 1988, pp. 534–544.

[41] Liu, P., Malik, O. P., Chen, D. and Hope, G. S., "Study of Non-operation for Internal Faults of Second Harmonic Restraint Differential Protection of Power Transformers", *Transaction of The Engineering and Operating Division of Canadian Electrical Association Power System Planning and Operation Section*, Vol. 89-sp-141, 1989.

[42] Sachdev, M. S. and Sidhu, T. S., "On-Line Identification of Magnetizing Inrush and Internal Faults in Three-Phase Transformers", *IEEE Trans. on Power Power Delivery*, Vol. 7, No. 4, 1992, pp. 1885–1891.

[43] Sidhu, T. S., Sachdev, M. S. and Wood, H. C., "A Digital Relaying Algorithm for Detecting Transformer Winding Faults", *IEEE Trans. on Power Power Delivery*, Vol. 4, 1989, pp. 1638–1648.

[44] Gangopadyay, A., "An Analysis for Digital Protection of Transformers", Master's thesis, Memorial University of Newfoundland, St.John's, NF, 1984.

[45] Zaman, M. R. and Rahman, M. A., "Experimental Testing of the Artificial Neural Network Based Protection of Power Transformers", *IEEE Trans. on Power Power Delivery*, Vol. 13, No. 2, 1998, pp. 510–517.

[46] Kim, C. H. and Aggarwal, R., "Wavelet Transforms in Power Systems: Part I", *IEE Power Engineering Journal*, Vol. 14, No. 2, 2000, pp. 81–87.

[47] Saleh, S. A. and Rahman, M. A., "A Wavelet-Controlled Dynamic Voltage Restorer for Power Quality Applications", in *NECEC02 Proceedings*, St. John's, NL, Canada, 2002.

[48] Orr, J. A., Negenevitsky, M. and Nguyen, T., "A Neural-Fuzzy Calssifier for Recognition of Power Quality Disturbances", *IEEE Trans. on Power Delivery*, Vol. 17, No. 2, 2002, pp. 609–616.

[49] Poission, O., Rioual, P. and Meunier, M., "Detection and Measurement of Power Quality Disturbances Using Wavelet Transform", *IEEE Trans. on Power Delivery*, Vol. 15, No. 3, 2000, pp. 1039–1044.

[50] Karimi, M., Mokhtari, H. and Iravani, M. R., "Wavelet-Based On-Line Disturbance Detection for Power Quality Applications", *IEEE Trans. on Power Delivery*, Vol. 17, No. 4, 2002, pp. 1212–1220.

[51] H. Mokhtari, Ghartermani, M. K. and Iravani, M. R., "Experimental Performance Evaluation of a Wavelet-Based On-Line Voltage Detection Method for Power Quality Applications", *IEEE Trans. on Power Delivery*, Vol. 17, No. 1, 2002, pp. 161–172.

[52] Kim, C. H. and Aggarwal, R., "Wavelet Transforms in Power Systems: Part II", *IEE Power Engineering Journal*, Vol. 15, No. 4, 2001, pp. 193–202.

[53] Youssef, O. S., "A Wavelet-Based Technique for Discrimination Between Faults and Inrush Currents in Transformers", in *IEEE Power Engineering Society Summer Meeting*, Paper PE-027PRD (03-2002), Chicago, IL, 2002.

[54] Pandy, S. K. and Satish, L., "Multiresolution Signal Decomposition: Anew Tool for Fault Detection in Power Transformers During Impulse Tests", *IEEE Trans. on Power Delivery*, Vol. 13, No. 4, 1998, pp. 1194–1200.

[55] Hamid, E. Y. and Kawasaki, Z. I., "Wavelet-Based Data Compression for Power Disturbances Using Minimum Description Length Data", *IEEE Trans. on Power Delivery*, Vol. 17, No. 2, 1998, pp. 460–466.

[56] Stang, G. and Nguyen, T., *Wavelets and Wavelet Filter Banks.* Wellesly-Cambridge Press, 1996.

[57] Devore, R. A., and Lucier, B. J., "Introduction to Wavelets", 1992.

[58] Dogaru, T. and Carin, L., "Multiresolution Time-Domain Using CDF Biorthogonal Wavelets", *IEEE Trans. on Microwave Theory and Techniques*, Vol. 49, No. 5, 2001, pp. 902–912.

[59] Zhuang, Y. and Baras, J.S. , "Optimal Wavelet Basis Selection for Signal Representation", CSHCN T.R. 94-7, Center for Satellite and Hybrid Communication Networks, 1994.

[60] Mathworks, *Matlab: Wavelet Tool Box*, 1995. Ver.6.1.